Vents, chromosphères et activité avant la séquence principale : les étoiles Ae/Be de Herbig

Claude Catala

THESE DE DOCTORAT ES SCIENCES PHYSIQUES

Présentée
à la Faculté des Sciences
de Paris VII

par

Claude CATALA

pour obtenir
le grade de Docteur ès-Sciences Physiques

VENTS, CHROMOSPHERES ET ACTIVITE AVANT LA SEQUENCE PRINCIPALE : LES ETOILES Ae/Be DE HERBIG

Soutenue le 28 Septembre 1987 devant la commission d'Examen:

M.	J. HEYVAERTS	Président
Mme	F. PRADERIE	Directeur de la thèse
MM.	R. CAYREL	Rapporteur
	P. KUNASZ	Rapporteur
	P. DELACHE	Examinateur
	P. FELENBOK	Examinateur
	D. PEQUIGNOT	Examinateur

THESE DE DOCTORAT ES SCIENCES PHYSIQUES

Présentée
à la Faculté des Sciences
de Paris VII

par

Claude CATALA

pour obtenir
le grade de Docteur ès-Sciences Physiques

VENTS, CHROMOSPHERES ET ACTIVITE AVANT LA SEQUENCE PRINCIPALE : LES ETOILES Ae/Be DE HERBIG

Soutenue le 28 Septembre 1987 devant la commission d'Examen:

M.	J. HEYVAERTS	Président
Mme	F. PRADERIE	Directeur de la thèse
MM.	R. CAYREL	Rapporteur
	P. KUNASZ	Rapporteur
	P. DELACHE	Examinateur
	P. FELENBOK	Examinateur
	D. PEQUIGNOT	Examinateur

à mes parents,
qui ont tant donné pour qu'un
jour je puisse écrire cette thèse

REMERCIEMENTS

Je tiens à exprimer ici ma sincère reconnaissance envers tous ceux qui m'ont apporté leur aide, leur soutien et leurs encouragements pendant ces quelques années de travail.

Je remercie tout d'abord Françoise Praderie qui a su me faire profiter de toute l'étendue de son expérience et guider mes efforts dans les directions les plus appropriées.

Paul Felenbok et Jean Czarny, avec qui j'ai effectué la plupart des missions d'observation décrites dans cette thèse, m'ont appris à connaître et à maîtriser les dures lois de l'observation astronomique. Qu'ils en soient ici vivement remerciés.

Merci à Paul Kunasz pour son aide précieuse en ce qui concerne les problèmes de transfert radiatif.

Je remercie également André Mangeney pour les nombreuses discussions scientifiques que nous avons eues.

Enfin, je remercie Jean Heyvaerts, Roger Cayrel, Philippe Delache et Daniel Péquignot d'avoir accepté de faire partie de mon jury.

RESUME

VENTS, CHROMOSPHERES ET ACTIVITE AVANT LA SEQUENCE PRINCIPALE: LES ETOILES Ae/Be DE HERBIG

Les étoiles Ae/Be de Herbig sont des objets pré-séquence principale de masse intermédiaire (2 - 5 $M_{\odot}$). L'étude des vents, des chromosphères et de l'activité pour ces étoiles est essentielle et s'inscrit naturellement dans le cadre d'un effort général d'analyse de ces phénomènes à travers tout le diagramme HR.

Le premier pas vers la compréhension des mécanismes responsables des vents et des chromosphères dans ces étoiles consiste en une approche semi-empirique, c'est-à-dire que nous nous efforçons dans un premier temps de déterminer avec précision la structure de l'atmosphère étendue de ces objets. Il s'agit pour cela de contraindre les paramètres décrivant le vent et la chromosphère de ces étoiles par l'interprétation quantitative des nombreuses signatures spectrales (raies et continus) observées. Dans cette thèse, nous batissons un modèle semi-empirique à symétrie sphérique et sans rotation, représentant les propriétés moyennes de l'atmosphère de ces étoiles. Nous utilisons pour cela une analyse détaillée des raies de résonance de Mg II et de C IV, ainsi que les raies et continus de l'hydrogène. C'est ainsi que, par exemple, nous mettons en évidence l'existence d'une chromosphère étendue de température modérée (~ 17000 K) et que nous contraignons fortement le taux de perte de masse d'une de ces étoiles, qui, comme nous le montrons, peut être considérée comme un bon prototype de la classe. Ces contraintes peuvent alors servir de point de départ pour la constuction d'un modèle hydrodynamique ou magnéto-hydrodynamique de l'atmosphère des étoiles Ae/Be de Herbig.

L'activité des étoiles Ae/Be de Herbig nous est révélée par la modulation rotationnelle de certaines raies dans leur spectre. Nous présentons les observations de la modulation rotationnelle des raies de Mg II et de Ca II d'AB Aur, prototype des étoiles Ae/Be de Herbig. Un modèle qualitatif est proposé pour expliquer ce phénomène. Il fait intervenir une alternance de jets lents et de jets rapides sur la ligne de visée pendant la rotation de l'étoile. D'autres observations indiquent la présence d'un phénomène semblable dans une autre de ces étoiles, et suggèrent un troisième excellent candidat. On conclut donc

que l'activité est un phénomène présent dans la classe des étoiles Ae/Be de Herbig. La question se pose alors de savoir si cette activité est d'origine magnétique et, si oui, de quelle origine est le champ magnétique.

Enfin, quelques considérations sont présentées sur la manière de s'attaquer au problème de la description quantitative à trois dimensions des vents non axisymétriques, tels que nous les laissent entrevoir les observations décrites dans la thèse.

SOMMAIRE

Annexe C: "Line formation in the wind of AB Aur", C. Catala, P.B. Kunasz, F. Praderie, *Astron. Astrophys.* **134**,402 (1984)

Annexe D: "Line formation in the winds of Herbig Ae/Be stars. The Hα line", C.. Catala, P.B. Kunasz, *Astron. Astrophys.* **174**,158 (1987)

Annexe E: "The presence of Si^{3+} and C^{3+} in the wind of AB Aur", C. Catala, A. Talavera, *Astron. Astrophys.* **140**, 421 (1984)

Annexe F: "The wind and chromosphere of the Herbig Ae star AB Aur, as seen by IUE", C. Catala, Proc. 4^{th} European IUE Conf., Rome, ESA SP218, p.227 (1984)

Annexe G: "Line formation in the winds of Herbig Ae/Be stars. The C IV resonance lines", C. Catala, *Astron. Astrophys.*, soumis (1987)

Chapitre III: Activité

1 - Généralités

2 - Modulation rotationnelle dans AB Aur. Un modèle qualitatif

3 - Recherche de modulation rotationnelle dans d'autres ABHs

3-1 HD250550

3-2 BD+46°3471

3-3 HD163296

4 - Conclusion

Annexe H:"Short-term spectral variability in AB Aur: clues for activity in Herbig Ae stars. I. The UV lines of Mg II and Fe II", F. Praderie, T. Simon, C. Catala, A.M. Boesgaard, *Astrophys. J.* **303**,311 (1986)

Annexe I: "Short-term spectral variability in AB Aur: clues for activity in Herbig Ae stars. II. The Ca II K line", C. Catala, P. Felenbok, J. Czarny, A. Talavera, A.M. Boesgaard, *Astrophys. J.* **308**,791 (1986)

Annexe J: "Rotational modulation of the wind of the PMS star AB Aur: new observations in C IV and Mg II", C. Catala, F. Praderie, P. Felenbok, *Astron. Astrophys.* **182**,115 (1987)

CHAPITRE I

INTRODUCTION

1 - Les étoiles Ae/Be de Herbig:

Herbig (1960) fut le premier à penser qu'il était possible d'observer des étoiles de masse intermédiaire (typiquement entre 2 et 5 masses solaires) dans une phase pré-séquence principale. Ces étoiles seraient donc les contreparties plus massives des étoiles T Tauri, dont l'existence était bien connue à l'époque. Une estimation rapide du temps de contraction et de la durée de vie sur la séquence principale à ces masses-là lui apprit qu'un nombre non négligeable de ces objets devaient être observables. Il entreprit donc de sélectionner des candidats grâce à quatre critères qui peuvent servir aujourd'hui de définition observationnelle pour cette classe d'étoiles, appelées depuis lors "étoiles Ae/Be de Herbig". Ces critères sont les suivants:

i) Les candidats doivent être de type spectral A ou B: ce critère permet d'être certain de ne sélectionner que des objets de masse intermédiaire.

ii) Ils doivent avoir des raies en émission dans leur spectre: ce critère, introduit par analogie avec ce qu'on connaissait à l'époque des étoiles T Tauri, était considéré comme un signe de jeunesse.

iii) Ils doivent être enfouis dans ou à proximité d'une région de forte extinction: il s'agit là d'un autre critère de jeunesse, car une étoile jeune n'a pas eu le temps de s'éloigner de son nuage progéniteur.

iv) Ils doivent illuminer une nébuleuse par réflexion: ce dernier critère permet d'éliminer les objets qui ne se trouvent à proximité d'un nuage sombre que par un effet de projection.

Dans toute la suite cette thèse, nous adopterons cette définition observationnelle pour les étoiles Ae/Be de Herbig, nom que nous abrègerons en ABHs.

Grâce à ces quatre critères, et après un travail qui, selon ses propres dires, ne constituait pas une recherche systématique, Herbig publia une liste de 26 ABHs.

Cette liste fut récemment étendue à 57 objets par Finkenzeller et Mundt (1984), suivant les mêmes critères de sélection. Ce chiffre est assez éloigné du nombre supposé d'ABHs ayant $m_V \leq 13$, qui est plutôt de l'ordre du millier (Herbig, 1960). Cette différence

est due d'une part à ce que la plupart de ces étoiles se trouvent sans doute dans des régions très obscurcies, d'autre part à ce qu'on ne les a jamais recherchées de façon systématique (à l'aide d'un prisme objectif, par exemple).

A ces 57 ABHs, viennent s'ajouter un certain nombre d'étoiles dans des amas ouverts, répondant à certains des critères de sélection mentionnés plus haut (Thé et al., 1985a,b). L'appartenance de ces étoiles à la classe des ABHs n'est pas encore complètement établie, mais leur étude présente un intérêt majeur: on possède en effet une estimation de leur âge indépendamment des modèles théoriques d'évolution pré-séquence principale. Nous ne reviendrons pas sur ces objets dans la suite de cette thèse, mais il faut garder à l'esprit qu'ils représentent un terrain prometteur pour l'avenir de l'étude observationnelle des ABHs.

Les critères de sélection n'étant pas suffisants pour prouver la nature pré-séquence principale des ABHs, un certain nombre d'études ont été menées pour apporter d'autres arguments en faveur de cette interprétation (voir par exemple Mendoza, 1966; Strom et al., 1972; Cohen et Kuhi, 1979; Finkenzeller et Jankovics, 1984). Ces travaux sont passés en revue dans l'Annexe A, papier invité au colloque de l'UAI sur les "nuages moléculaire proches", tenu à Toulouse en Septembre 1984. On y découvrira que, bien qu'il n'y ait toujours pas de preuve directe du caractère pré-séquence principale des ABHs, cette hypothèse est étayée par un grand nombre d'arguments. Signalons toutefois une idée très récente selon laquelle les étoiles jeunes de type A présenteraient d'importantes pertes de masse au début de leur phase de combustion de l'hydrogène, ce qui les ferait évoluer vers le bas sur la séquence principale (Willson et al., 1987; Guzik et Willson, 1987). Les ABHs seraient alors des étoiles de la séquence principale dans cette phase de perte de masse. Cette spéculation semble être en contradiction avec un des arguments cités dans l'Annexe A. Strom et al. (1972) ont en effet montré que les gravités de surface de ces étoiles, déduites des ailes des raies de Balmer, les placent nettement au dessus de la séquence principale. Par conséquent, en dépit de cette nouvelle spéculation, nous considèrerons par la suite les ABHs comme représentant réellement la phase pré-séquence principale des étoiles de masse intermédiaire.

L'Annexe A présente également les propriétés supplémentaires des ABHs, comme par exemple la présence d'un excès d'émission infrarouge (Cohen, 1973, 1975, 1980), et fait le bilan de nos connaissances sur ces étoiles sur le plan observationnel. Notons cependant que ce papier a été écrit en Août 1984, et que notre savoir a évolué

depuis, en grande partie grâce aux travaux menés à Meudon, et présentés dans ce mémoire. En particulier, l'observation et l'interprétation de la modulation rotationnelle des raies de résonance de Mg II dans AB Aur ont fait l'objet d'une étude beaucoup plus avancée, qui constitue d'ailleurs une part importante de la présente thèse (voir Chapitre III). Le lecteur est donc invité à n'accorder qu'un intérêt limité au dernier paragraphe de l'Annexe A.

2 - Importance de leur étude:

La figure I-1 montre la position des ABHs dans le diagramme HR. Outre l'emplacement des principales classes d'étoiles, on y a représenté quelques trajets évolutifs vers la séquence principale, calculés par Gilliland (1986). Celui-ci n'ayant considéré que les étoiles de moins de $3M_{\odot}$ dans ses calculs, les trajets évolutifs correspondants aux objets plus massifs ne sont pas portés sur la figure I-1. Les températures effectives et luminosités des ABHs ont été tirées de Finkenzeller et Mundt (1984) et Finkenzeller (1985). Seules les ABHs pour lesquelles on connait bien ces deux paramètres sont présentes sur la figure I-1.

Fig I–1 – Diagramme HR

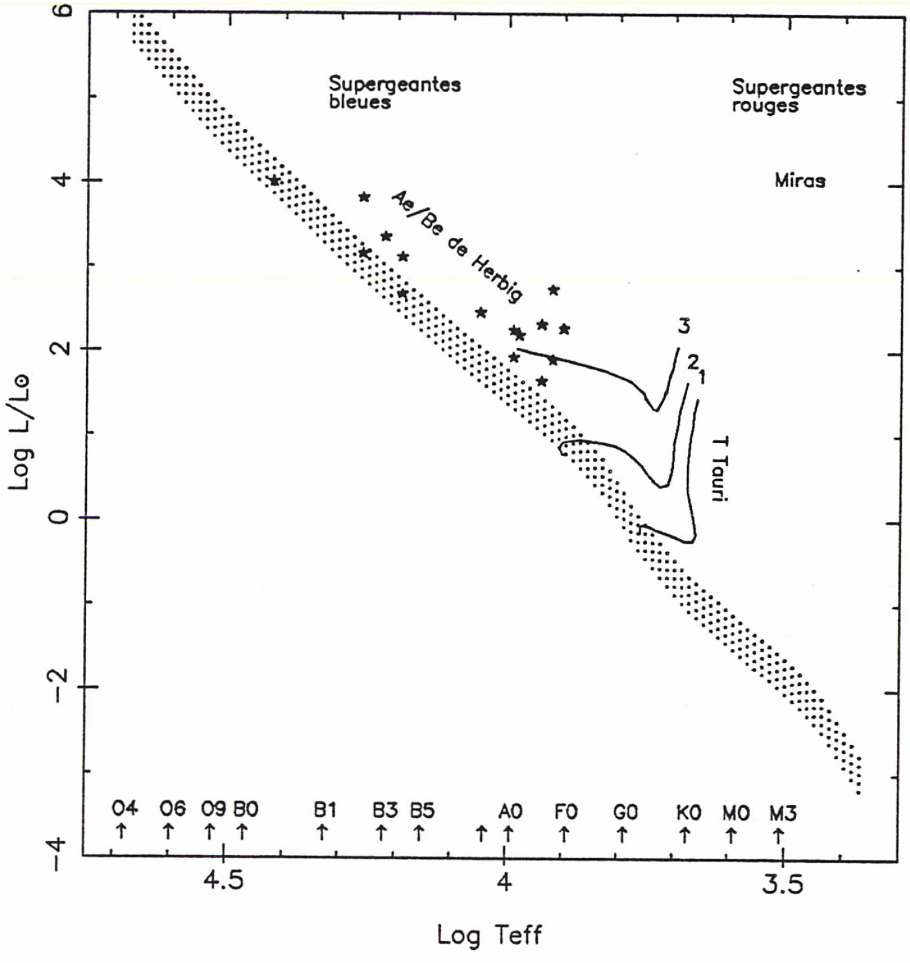

On trouve des objets pré-séquence principale de toutes masses, depuis les étoiles jeunes très massives observées en infrarouge (Jiang et al., 1984), jusqu'aux étoiles T Tauri, de masses inférieures ou égales à $1M_{\odot}$. Si l'on admet que les ABHs sont bien des objets pré-séquence principale, et si l'on fait confiance aux trajets évolutifs théoriques, il est clair que ces étoiles représentent également une tranche importante d'âges et de masses dans l'évolution stellaire. L'étude de l'évolution vers la séquence principale passe obligatoirement par une phase de comparaison des modèles théoriques d'évolution et des objets réellement observés. Les ABHs sont alors le seul "laboratoire" qui nous permette de tester les modèles pour les masses entre 2 et 5 $M_{\odot}$. Par conséquent, on ne saurait étudier un phénomène physique, quelqu'il soit, sans l'étudier en particulier pour les ABHs. Les problèmes qui vont nous occuper tout au long de cette thèse, à savoir les vents et chromosphères des ABHs, ainsi que leur activité, sont en fait des problèmes très généraux en astrophysique stellaire moderne. L'étude de ces phénomènes pour les ABHs s'inscrit donc dans le cadre d'un effort commun d'une fraction importante de la communauté astrophysique aux prises avec les mêmes problèmes à travers tout le diagramme HR.

Malgré leur importance dans cet effort général, les ABHs n'ont été que peu étudiées jusqu'ici, peut-être parce qu'on a préféré s'intéresser en premier lieu aux étoiles T Tauri, plus nombreuses et peut-être plus spectaculaires. Les travaux présentés dans cette thèse représentent un des premiers pas vers une étude systématique et quantitative de cette classe.

3 - Vents et chromosphères:

3-1Vents:

Les vents stellaires sont un phénomène très répandu, présent pour un grand nombre de classes d'étoiles. Des pertes de masse importantes, jusqu'à 9 ordres de grandeur plus élevées que celle de notre soleil, ont été observées pour les étoiles O et B, les supergéantes A, les géantes et les supergéantes K et M, et les étoiles pré-séquence principale (T Tauri et ABHs). Plusieurs catégories de modèles tentent d'expliquer ce phénomène pour ces différentes classes d'étoiles.

La pression thermique due à la présence d'une couronne est suffisante pour expliquer l'existence du vent solaire (Parker, 1958) et des travaux importants ont été effectués pour inclure les effets du champ magnétique et de la rotation du soleil (Weber et

Davis, 1967; Sakuraï, 1985). Les efforts se portent également sur la modélisation des structures 3D dues aux interactions entre jets lents et jets rapides dans le vent solaire (Siscoe, 1976; Pizzo, 1982; Burlaga, 1983, 1984; Hundhausen, 1985). Bien évidemment, notre compréhension des vents des autres étoiles est bien moindre. La pression thermique n'est a priori pas suffisante pour donner lieu aux énormes pertes de masse observées.

On distingue en gros trois autres types de modèles pour expliquer les vents stellaires à travers le diagramme HR. Le premier fait appel à la pression de rayonnement comme principale force agissant contre la gravité, que ce soit la pression de rayonnement sur les raies pour les étoiles O et B (Castor et al., 1975; Abbott, 1982), ou la pression de rayonnement sur les grains pour les géantes et supergéantes K et M (Kwok, 1975). Des variantes de ce modèle, incluant les effets du champ magnétique et de la rotation, ont été proposées pour les étoiles chaudes (Friend et MacGregor, 1984).

Dans le deuxième type de modèles, la présence d'ondes de Alfvèn donne naissance à un gradient de pression supplémentaire. Ce type de modèle a été envisagé pour expliquer les vents des géantes et supergéantes K et M (Hartmann et MacGregor, 1980; Holzer et MacGregor, 1985), ainsi que ceux des étoiles T Tauri (Hartmann et al., 1982).

Le troisième type de modèle, enfin, n'a été appliqué jusqu'à présent qu'aux étoiles Miras. On y suppose que le vent est poussé par les chocs engendrés par les pulsations radiales générées en dessous de la photosphère (Wood, 1979; Holzer et MacGregor, 1985).

Aucune tentative n'a été effectuée jusqu'à présent pour appliquer ces modèles aux ABHs. Un vent poussé par pression de rayonnement sur les grains ne peut pas être envisagé, du fait que la température de ces étoiles empêche la présence de grains jusqu'à des distances de 100 rayons stellaires (R_*) environ (Catala, 1983a). Le modèle de vent poussé par la pression de rayonnement sur les raies n'est probablement pas applicable tel quel pour les étoiles les plus froides de cette classe, Abbott (1982) donnant A0 comme type spectral limite pour l'efficacité de ce mécanisme. Cependant les effets additionnels de la rotation et du champ magnétique, s'il existe, ainsi que la prise en compte de la diffusion multiple des photons, pourraient être suffisants pour que ce modèle soit applicable à toutes les ABHs possédant des vents stellaires. Enfin, aucun argument immédiat ne permet d'écarter a priori les modèles de vent poussé par ondes de Alfvèn, ou entretenus par des chocs.

Nous n'allons pas résoudre le problème de l'origine des vents des ABHs dans

cette thèse. Notre approche du problème a été jusqu'à présent une approche semi-empirique, inspirée de celle qui a été suivie pour l'étude de la chromosphère et de la zone de transition du soleil. C'est-à-dire que nous nous sommes efforcés dans un premier temps de déterminer la structure des vents de ces étoiles (loi de vitesse, loi de température, taux de perte de masse...) grâce à l'interprétation des observations. Il s'agit là d'un premier pas vers la compréhension des vents des ABHs, où l'on ne cherche pas à ce que le modèle soit entièrement cohérent avec les équations de la MHD, mais simplement avec toutes les observations dont nous disposons. Cependant, comme nous le verrons, notre modèle est tout-de-même bâti en accord avec l'équation de conservation de la masse. C'est pourquoi nous parlerons de modèle semi-empirique. Ce modèle, une fois bâti, constitue un outil puissant pour contraindre les modèles théoriques.

3-2 Chromosphères:

Avant de nous lancer dans la description et l'étude des chromosphères des ABHs, il est indispensable de définir ce que nous entendons par ce mot. La définition d'origine ne se rapporte qu'à la chromosphère solaire, "région d'une étendue d'environ 10^4 km au dessus du limbe, visible dans des raies en émission d'atomes neutres ou une fois ionisés" (voir par exemple Linsky, 1980).

Linsky (1980) donne d'une chromosphère stellaire une définition plus générale, mais toujours inspirée de la chromosphère solaire: "région où le chauffage non radiatif domine le bilan énergétique et où le gradient de température dT/dz est positif et faible devant l'échelle de hauteur de pression". Cette définition s'applique très bien aux étoiles de type solaire et à toutes les étoiles où les couches externes sont structurées en photosphère, chromosphère, zone de transition, couronne. Le critère de faible gradient de température permet alors de distinguer la chromosphère de la zone de transition. Il serait imprudent d'adopter une telle définition pour les chromosphères des ABHs, qui n'ont aucune raison a priori d'avoir une structure des couches externes identique à celle du soleil. Nous n'avons d'ailleurs aucune évidence de l'existence de zones de transition ou de couronnes au sens solaire dans les ABHs (voir Annexe A). Comme nous allons le voir, l'atmosphère des ABHs comporte une région où la température remonte jusqu'à une valeur supérieure à la température effective T_{eff}, puis redescend. Le critère $dT/dz > 0$ présenterait donc un inconvénient majeur pour la classification d'une telle région de l'atmosphère, et nous serions amenés à introduire un nouveau mot dans la nomenclature déjà compliquée de la

physique stellaire.

La définition plus simple proposée par Praderie (1973, 1977, 1981) conviendrait mieux à notre cas: " région où est dissipée de l'énergie non radiative". Il y a cependant deux difficultés qui nous empêchent d'utiliser cette définition telle quelle. La première d'entre elles est très générale. Linsky (1980) fait remarquer qu'une fraction non négligeable de la dissipation d'énergie non radiative peut avoir lieu dans des couches atmosphériques profondes où le gradient de température est négatif, et que nous appelons intuitivement photosphères. La deuxième difficulté est liée à notre pauvre connaissance actuelle des atmosphères étendues et en expansion autour des étoiles pré-séquence principale. Il n'existe pas pour ces atmosphères de modèle en équilibre radiatif, en conséquence il nous est difficile de décider s'il y a ou non chauffage non radiatif, même après avoir déterminé avec précision la température de la région qui nous intéresse. En effet, en l'absence de modèle en équilibre radiatif, nous ne connaissons pas la remontée de température radiative à laquelle il faut s'attendre, par un effet semblable à celui décrit par Cayrel (1963, 1964) pour les atmosphères statiques.

Nous allons donc adapter ces définitions à nos besoins propres et à nos moyens d'investigation, et proposer la définition suivante: une chromosphère sera pour nous une région de l'atmosphère stellaire située au dessus de la photosphère, où la température est supérieure à la température effective de l'étoile et inférieure aux températures typiques des couronnes (~10^6 K). Cette définition ne fait pas intervenir l'étendue d'une telle région, ni le gradient de température, et est immédiatement applicable dès qu'on a estimé la température électronique. Elle nous conviendra donc parfaitement. Le lecteur doit cependant garder à l'esprit que les chromosphères que nous allons détecter en suivant cette définition peuvent différer largement de la chromosphère solaire par leur température et par leur étendue.

De même que les vents stellaires, les chromosphères sont présentes dans de nombreuses classes d'étoiles. On en trouve des indicateurs dans les naines et les géantes à partir du type spectral A9-F0 et dans les supergéantes à droite de la bande d'instabilité des Céphéides (Böhm-Vitense et Dettmann, 1980). Les étoiles T Tauri présentent également des chromosphères (Herbig, 1970; Dumont et al., 1973; Ulrich et Knapp, 1979; Calvet et al., 1984; Finkenzeller et Basri, 1987). Comme nous allons le montrer, les ABHs aussi en possèdent. Les supergéantes de type O et B montrent un phénomène dit de "superionisation", qui consiste en la présence d'espèces très ionisées comme N V et O IV. Il est probable que cette superionisation est due au rayonnement X produit par une mince

couronne à 10^6 K à la base des vents de ces étoiles (Cassinelli et Olson, 1979; Cassinelli, 1984), mais un autre modèle proposé par Lamers et Rogerson (1978) et Lamers et Snow (1978), faisant intervenir une région à 10^5 K, n'a pas été complètement rejeté. Cette région à 10^5 K correspondrait à la définition que nous avons choisie pour une chromosphère. Les étoiles Be classiques présentent également le phénomène de superionisation (Doazan, 1982) qui a été interprété jusqu'à présent comme indiquant des températures de 10^5 K dans les atmosphères de ces étoiles. Notons pour finir qu'on n'a pour l'instant aucune évidence de la présence de chromosphères ni de zones de transition dans les étoiles A de la séquence principale (Freire et al., 1978; Praderie et Crivellari, 1982).

Les modèles théoriques de chromosphères font tous appel à la dissipation d'ondes hydrodynamiques ou MHD. Une des grandes difficultés rencontrées lors de la construction de ces modèles est le calcul des pertes d'énergie radiatives. Là encore, rien de quantitatif n'a été fait pour les ABHs. Le premier pas doit donc être aussi une analyse semi-empirique des observations qui nous permettra de préciser la température et la densité des chromosphères des ABHs, et également d'estimer quelques contributions aux pertes radiatives. Ce modèle semi-empirique permettra dans l'avenir de tester et de contraindre les modèles théoriques de chromosphères.

4 - Activité:

La définition initiale de l'activité a aussi été donnée pour le soleil. On appelle activité solaire la manifestation d'une structuration horizontale au niveau de la photosphère, chromosphère et couronne, associée au champ magnétique, et présentant des variations temporelles. L'activité solaire se manifeste entre autres par des signatures spectrales bien caractéristiques, comme un renforcement de l'émission dans certaines raies (par exemple les raies H et K de Ca II), ou l'émission de rayonnement X.

Par analogie, on appelle également "activité" la présence des mêmes signatures spectrales dans des étoiles de type solaire, ainsi que dans des étoiles de type plus tardif. De nombreuses études suggèrent de façon indirecte que l'activité ainsi détectée est bien reliée au champ magnétique. Ces études consistent en général à mettre en évidence des corrélations entre certains indices d'activité et des quantités susceptibles d'être reliées à la présence du champ magnétique. C'est ainsi que Mangeney et Praderie (1984) ont montré la corrélation entre la luminosité X et le nombre de Rossby (rapport des forces d'inertie aux

forces de Coriolis) pour un échantillon d'étoiles allant du type O3 au type M5. Noyes et al. (1984) ont également mis en évidence une corrélation entre l'activité dans les raies H et K de Ca II et un nombre similaire au nombre de Rossby pour des étoiles tardives. Le même genre de corrélation a été récemment étudié pour les étoiles T Tauri par Simon et al. (1985), Bouvier et al. (1986) et Bouvier (1987).

Pour la plupart de ces étoiles, on peut donc interpréter avec une certaine confiance les signatures spectrales mentionnées plus haut comme indicatrices d'activité au sens solaire du terme. Ce n'est malheureusement pas le cas pour les ABHs. En effet, en l'absence de toute analyse quantitative et statistiquement représentative, rien ne nous permet de relier l'émission dans les raies H et K de Ca II par exemple avec un quelconque indicateur de champ magnétique. Une émission dans ces raies, si elle existe, peut très bien être due à un effet d'extension de leur région de formation et n'avoir aucun lien avec une structure en régions hétérogènes à la surface de l'étoile. Il serait donc dangereux d'utiliser d'emblée la présence des signatures spectrales de l'activité solaire comme indicateur d'activité dans les ABHs. L'analogie avec le soleil ne doit pas être poussée jusqu'à ce point.

Dans certaines étoiles tardives de la séquence principale, une structure non radiale (plages ou taches) a pu être mise en évidence par des observations avec résolution temporelle (Vaughan et al., 1981; Boesgaard et Simon, 1984). Cette technique consiste à repérer des variations temporelles de flux dans des continus ou dans des profils de raies, interprétées par l'alternance sur la ligne de visée de régions calmes et de régions actives dont la distribution n'est pas symétrique en longitude. La même technique a permis de détecter des structures analogues dans des étoiles de type RSCVn (Gondoin, 1986; Rodono et al., 1987) et des taches dans des étoiles T Tauri (Bouvier, 1987). Nous allons voir dans cette thèse que nous avons utilisé avec succès une technique semblable pour plusieurs ABHs. Grâce à l'applicabilité de cette méthode dite "de la modulation rotationnelle", nous pouvons adopter la définition suivante de l'activité dans les ABHs. On dira qu'une ABH est active lorsqu'on aura mis en évidence une structure non radiale de son atmosphère. Cette définition a l'avantage de ne pas utiliser d'interprétation hasardeuse de signatures spectrales. Son inconvénient est bien entendu la difficulté que présentent les observations avec résolution temporelle.

Dans toute la suite de ce travail, nous ferons une distinction entre le phénomène "chromosphère" et le phénomène "activité". Pour le soleil et les étoiles de type tardif, on

assimile souvent ces deux concepts. Cette assimilation est assez bien justifiée par les observations, qui jusqu'à présent montrent qu'aucune de ces étoiles ne présente l'un des deux phénomènes sans présenter également l'autre. Dans notre étude des ABHs, d'un type spectral moins tardif, nous nous devons d'être prudents, et de ne pas faire a priori cette assimilation. La chromosphère d'une ABH ne présente pas nécessairement de structure non radiale (par exemple si elle est chauffée par un mécanisme ne faisant pas intervenir le champ magnétique), et l'activité pourrait exister en l'absence de chauffage non radiatif dans ces étoiles (par exemple si le chauffage relié au champ magnétique ne domine pas le bilan énergétique).

De même que pour l'étude des vents et des chromosphères, l'analyse des phénomènes d'activité pour les ABHs est essentielle si nous voulons comprendre leur origine à travers tout le diagramme HR. Nous soupçonnons déjà que l'activité est d'origine magnétique pour la plupart des étoiles (dont le soleil). Il reste encore à déterminer si elle a vraiment une origine commune pour toutes les étoiles où elle se manifeste, et son étude pour les ABHs est un point de passage obligé si nous voulons atteindre ce but.

5 - Plan d'ensemble de la thèse:

La présente thèse se compose de 10 articles rédigés en anglais et d'un "guide" rédigé en français. Chacun des articles en anglais décrit un point précis, tandis que le guide en français permet de mieux discerner le lien entre ces divers points.

Environ 6 années de travail ont été nécessaires pour accumuler le matériel présenté dans ce mémoire. Nous avons utilisé les plus gros moyens à la disposition des astronomes français, tant sur le plan observationnel (une quinzaine de missions dans des observatoires français, dont le CFH, et étrangers, y compris le satellite IUE) que sur le plan du calcul (nous avons utilisé par exemple 16 heures de CPU sur le Cray-1 du CCVR et 10 heures sur le Cray-1 et le Cray-XMP du NCAR, à Boulder, Colorado).

Le chapitre II présente l'étude semi-empirique des vents et des chromosphères des ABHs. Par l'interprétation quantitative des différentes raies spectrales observées, on y construit en plusieurs étapes un modèle à symétrie sphérique qui décrit l'atmosphère étendue de ces étoiles. Au chapitre III, on aborde le problème de l'activité des ABHs. Les

observations de la modulation rotationnelle de certaines raies dans plusieurs de ces étoiles y sont décrites, et un modèle qualitatif hors symétrie sphérique est présenté. Le chapitre IV indique dans quelle direction nos efforts sont en train de se porter pour comprendre plus quantitativement les manifestations de l'activité des ABHs. Le chapitre V enfin contient les conclusions de ce travail.

THE ENVELOPES OF THE HERBIG Ae/Be STARS

C. Catala

Observatoire de Paris-Meudon
92195 Meudon Principal Cedex, France.

ABSTRACT

First identified by Herbig (1960), the Herbig Ae/Be stars are usually considered as pre-main sequence objects of intermediate mass, and are found at the edges of regions of heavy obscuration.

The study of the interaction of these stars with their surrounding clouds is subordinated to a good knowledge of the structure of their envelopes. The present paper is devoted to a brief review of the observational data available for these stars, and of the constraints on the structure of their envelopes that can be derived from these data.

I - INTRODUCTION

More than two decades ago, Herbig (1960) proposed to identify a list of 26 objects, which he called "Be and Ae type stars associated with nebulosity", with stars of intermediate mass still in their pre-main sequence (PMS) stage of evolution. This list of 26 Herbig Ae/Be stars had been compiled using the following selection criteria :

(1) The spectral type is A or earlier, in order to eliminate low mass stars or objects too far from the main sequence.

(2) They exhibit emission lines in their spectra : the presence of emission lines was thought to be a characteristic of young objects, by analogy with T Tauri stars.

(3) They lie in an obscured region, because if they are newly born stars, they have not had enough time to escape from their parental clouds.

(4) They illuminate a bright reflection nebula in their immediate vicinity, in order to eliminate those stars that would be projected on molecular clouds.

As Herbig himself mentioned, this list was likely to be incomplete, since it was not the result of a systematic survey. It was then of great interest to try to extend the list of such stars. Recently, a large amount of work has been done in this direction by Finkenzeller and Mundt (1984), who have extended Herbig's original list to 57 candidates.

If Herbig's identification for this group of stars is right, i.e. if they are really PMS stars, their study is of uttermost importance, since they represent a very important range of mass and age in the PMS evolution.

The aim of the present paper is to give a very brief review of the observational material available for these stars and to describe recent progress in the interpretation of some of these observations. In section 2, the problem of the PMS nature of these objects is addressed. A summary of the observational data on these stars is given in section 3. Section 4 gives an example of what can be derived quantitatively from the analysis of high resolution line profiles about the physical structure of the envelopes of these stars. General conclusions are presented in section 5.

2 - PRE-MAIN SEQUENCE NATURE :

The first question that must be addressed about these stars concerns their PMS nature : are they really PMS ? Herbig's criteria are not sufficient to answer this question. Since Herbig's work in 1960, several studies have tried to solve this main problem.

A very important argument in favor of the youth of these stars has been the discovery of a great infrared (IR) excess in most of them (Mendoza, 1966, 1967 ; Geisel, 1970 ; Gillett and Stein, 1971 ; Cohen, 1973, 1975). However, the presence of an IR excess does not constitute direct evidence of the PMS nature of a star, since certain types of stars showing IR excesses are not necessarily young ,like "classical" Be stars, for example, for which the IR excess can be explained by free-free emission alone. In the case of Herbig Ae/Be stars, however, the IR excess has been generally attributed to the presence of hot dust grains in the vicinity of the stars, which argues for the youth of these stars.

A further important argument in favor of the PMS nature of the Herbig Ae/Be stars came from a precise location of these stars in the HR diagram. Strom et al. (1972) have derived the effective temperatures and the surface gravities of 14 members of Herbig's original list, and have concluded that they lie above the main sequence. Later, Cohen and Kuhi (1979) reached the same conclusion by more accurately determining the bolometric luminosities of these stars. Again, this is not a direct proof of the PMS nature of these stars, since objects lying above the main sequence may well be post-main sequence stars.

More recently, Finkenzeller and Jankovics (1984) have compared the radial velocities of 27 Herbig Ae/Be stars from the catalog of Finkenzeller and Mundt (1984) with the radial velocities of the associated molecular clouds. The stellar radial velocities were derived from photospheric lines and the radial velocities of the

molecular clouds from observations of the CO, H_2CO, OH and NH_3 molecules (see references in Finkenzeller and Jankovics, 1984). This comparison shows that there is no systematic motion of the stars relative to the molecular clouds. This constitutes a powerful argument for the Herbig Ae/Be stars being physically associated with these clouds, but does not necessarily implies that they are really PMS objects.

In summary, although we have no direct evidence that the Herbig Ae/Be stars are young objects still on their PMS stage of evolution, numerous arguments are in favor of such an interpretation.

3 THE OBSERVATION OF THE HERBIG Ae/Be STARS

3-1 Generalities : Figure 1 is a schematic representation of what kind of information can be gained on the different parts of the star's extended atmosphere and its environment by the observations in the different wavelength ranges. In Fig. 1, the stellar atmosphere and its environment have been divided in three parts :

- the gaseous extended envelope, located in the immediate vicinity of the star. Most of the information on this gaseous envelope comes from the line profiles observed in the visible - ultraviolet (VIS-UV) range. A significant fraction of the Herbig Ae/Be stars show evidence for the presence of winds and chromospheres in their gaseous envelopes, as can be derived from the P Cygni profiles and the chromospheric indicators observed in their VIS-UV spectra. X-ray observations can provide information about the presence of corona in these gaseous envelopes, but X-ray emission has been detected only in 3 cases so far (see section 3-4). One could also expect to "see" the cooler parts of the gaseous envelopes thanks to their radio continuum emission, but the latter has never been detected so far in the Herbig Ae/Be stars (see section 3-2).

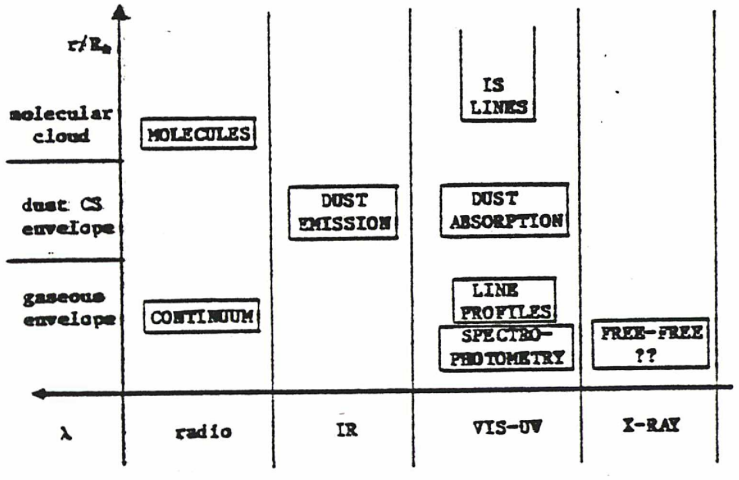

Figure 1: Schematic representation of the possibilities of investigation of the stellar atmosphere and its environment. R_* stands for the stellar photospheric radius

- the dust circumstellar (CS) envelope, containing hot dust grains and located

further out from the star. This dust CS envelope can be studied by the observation of dust emission in the IR (section 3.3) and of dust absorption in the VIS-UV range (section 3.5).

- the molecular cloud, in which the star and its CS envelope are embedded. It can be studied by the observation of molecular emission lines in the radio range (section 3.2), and of IS absorption lines, formed within the cloud, in the VIS-UV range (section 3.5).

The following parts of the present section are devoted to a survey of the observational data available for the Herbig Ae/Be stars, in the different wavelength ranges.

3-2 Radio observations : the largest number of observations of the Herbig Ae/Be stars at radio frequencies concern the ^{12}CO and ^{13}CO molecules in the millimetric wavelengths.

Loren et al. (1973) have observed the ^{12}CO (J=1→0) and ^{13}CO (J=1→0) transitions in the direction of 23 Herbig Ae/Be stars, and detected them in all the cases. One of their important results is that in most cases, the maximum of intensity coincides with the position of the star, both in ^{12}CO and ^{13}CO, which constitutes a further proof that these stars are physically associated with the molecular clouds. The fact that the ^{12}CO emission peaks in the direction of the stars in spite of the thickness of the ^{12}CO line is somewhat puzzling. Loren et al. (1973) proposed two possible explanations : the stars lie at the very edge of the molecular clouds, so that the ^{12}CO lines are optically thin, or the clouds are not homogeneous, but clumpy, so that the effective optical thickness of the ^{12}CO line remains small.

Cantó et al. (1984) have surveyed 11 Herbig Ae/Be stars in the ^{12}CO and ^{13}CO lines, trying to detect the presence of high velocity molecular flows. Their results were positive only in two cases. Moreover, the two stars associated with molecular flows have spectral types around B0, i.e. they lie at the hotter boundary of the Herbig Ae/Be class and cannot be considered as typical. The conclusion of Cantó et al. (1984) is that molecular flows are not a characteristic phenomenon for the Herbig Ae/Be stars. The absence of molecular flows associated with these stars raises the question of the physical processes that control molecular flows. Is the absence of molecular flows due to the particular structure of the surrounding material (absence of disk-shaped material for collimating the flows, for example) ? Or is it due to the weakness of the stellar winds of the Herbig Ae/Be stars (insufficient mass loss rates) ? Clearly, if we want to take further steps in the analysis of molecular flows, independent determinations of the mass loss rates of the Herbig Ae/Be stars are required. These independent determinations could come for example from the quantitative interpretation of the line profiles in the VIS-UV range (see section 4).

Several other molecules have been detected in the direction of the Herbig Ae/Be

stars : Loren (1977, 1979, 1981) reports the detection of H_2CO, HCN, HCO^+ and CS molecules in the vicinity of several Herbig Ae/Be stars. OH emission has been observed in a few cases, but it is probably not of circumstellar origin (Gahm et al., 1980). No H_2O maser emission has been detected so far (Dickinson, 1976).

Finally, continuous emission at different frequencies has been searched for in several Herbig Ae/Be stars, but the results were negative (Sistla and Hong, 1975 ; Altenhoff et al., 1976; Woodsworth and Hughes, 1977). There remains to be understood what is the basic difference between these stars and radio continuum emitting stars, like P Cygni, that causes this non-detection: difference in mass loss rate, temperature or emitting volume.

3-3 IR Observations : All the Herbig Ae/Be stars show strong IR excesses. In particular, their IR excesses are more intense than those of "classical" Be stars, which constitutes an easy way to distinguish the two classes.

The origin of the excess in the near IR range ($2 \rightarrow 4$ μ) is to some extent controversial. Most of the authors attribute it to thermal emission by CS dust (see e.g. Allen, 1973; Cohen, 1973, 1975). In this case, the temperature of the emitting grains should be in the range 1200 - 1500 K. The next step of the analysis consists of finding which grains are likely to be heated to such temperatures by the stellar radiation and to be responsible for the observed IR fluxes. Fitting the data with Plank functions is obviously not sufficient, since usually grains have non-grey absorption coefficients in the IR. On the other hand, several authors have considered the possibility that the near IR excess of some Herbig Ae/Be stars could be due to free-free emission from the H_2^- molecule (Milkey and Dyck, 1973 ; Lorenzetti et al., 1983). In this model, the emission originates from the cooler parts of the gaseous envelope and the electrons are provided by the ionization of metals to their first ionization stage.

Several stars show the 10 μ feature, either in emission (in 2 cases) or in absorption (in 2 cases), attributed to silicate grains (Cohen, 1980). In these particular cases, the presence of hot dust in the immediate vicinity of the star is doubtless.

Very few observations at longer wavelengths are available for the Herbig Ae/Be stars. Harvey et al. (1979) have carried out photometric observations at 40 and 60 μ for 4 Herbig Ae/Be stars. At these wavelengths, these stars still show excesses, which can reasonably be attributed to dust emission. Many other interesting results can be expected from IRAS observations at these wavelengths, but most of these observations are not yet available. However, Wesselius et al. (1984) have already reported IRAS observations of IR excesses in 2 Herbig Ae/Be stars.

Clearly, a big step would be taken if we could determine the nature, the size and the density of the grains in the CS envelopes of the Herbig Ae/Be stars. Such a

determination is possible in some particular cases by combining the analysis of the IR observations and of the observations in other wavelength ranges, and has been recently carried out for AB Aur, one of the brightest Herbig Ae/Be stars (Catala, 1983). This kind of approach may provide the beginning of the answer to the difficult problem of the origin of these grains : are they nucleated in the winds of the stars, are they the remnants of the proto-stellar clouds, or is there a permanent infall of dusty material from the surrounding molecular clouds ? Moreover, a good knowledge of the nature, size and density of the CS grains would allow us to address the problem of their dynamics, in particular their dynamical interactions with the stellar winds and with the surrounding molecular clouds.

3-4 X-Ray observations : X-ray observations are essential to understand the physics of the gaseous envelopes of these stars, since X-ray emission can in most cases be attributed to free-free emission from a corona, which can play a major role in the dynamics of the winds, for example. These observations are also very important for understanding the dynamics of the surrounding molecular clouds, since X-ray emission from the stars embedded in the clouds can control the ionization rate of the clouds, and since this ionization rate controls the coupling between the matter and the ambiant magnetic field.

Only 3 stars out of 11 observed have been detected in the X-ray range by the Einstein satellite (Feigelson and de Campli, 1981 ; Pravdo and Marshall, 1981 ; Sanders et al., 1982); therefore, the presence of X-ray emission does not seem to be typical of the Herbig Ae/Be stars. This can be interpreted in two different ways :

i) there are no coronae in the atmospheres of the Herbig Ae/Be stars, or their coronae are geometrically very thin, or their temperature does not reach 10^6 K.

ii) coronae are present in the Herbig Ae/Be stars, but their X-ray emission is reabsorbed by the cooler parts of their gas envelopes, located outwards of the coronae. This interpretation has been presented for T Tauri stars by Walter and Kuhi (1981).

3-5 VIS-UV observations

3-5-1 VIS-UV continuum : The VIS-UV continua of most of the Herbig Ae/Be stars show an anomalous extinction, i.e. an extinction different from that of the "average" IS medium (see e.g. Sitko et al., 1981). This anomalous extinction can probably be attributed to absorption and scattering by the CS dust grains. Sitko (1981) and Thé et al. (1981) have compared for several Herbig Ae/Be stars the energy missing in the VIS-UV range to the energy contained in the IR excess. They have found that these two quantities compare very well in most cases, which is what is expected if the extinction in the VIS-UV and the excess in the IR are both due to a CS dust shell of spherical shape. In some cases, as already mentioned (section 3.3), the analysis of the VIS-UV extinction curve, combined with the analysis of the IR observations, can lead to a determination of the nature, the size and the column

density of the CS grains (Catala, 1983).

Garrison (1978) has shown that the Paschen continuum and the Balmer jump of the Herbig Ae/Be stars are well represented by models of classical photospheres surrounded by optically thin expanding envelopes. These models are built on the assumption of optical thinness for the envelopes in the Balmer continuum, which is not supported, and must be considered as preliminary. But the results suggest that, although they are still surrounded by envelopes and embedded in dark clouds, the Herbig Ae/Be stars possess photospheres that look very much like those of main sequence stars.

3-5-2 VIS-UV high resolution spectroscopy: Many IS lines (CaII K, NaI D, KI, MgII, ...) have been observed in the spectra of the Herbig Ae/Be stars. In all cases, the "local standard of rest" velocities of the IS lines are the same as those of the surrounding molecular clouds (Felenbok et al., 1983 ; Finkenzeller and Jankovics, 1984), which supports the claim that these lines are formed within the clouds associated with the stars. Their equivalent widths can therefore be used for a determination of the column densities from the front edges of these clouds to the stars, and of the IS correction that must be applied to the stellar spectra (Felenbok et al., 1983).

Most of the information that we can get on the structure of the gaseous envelopes comes from high-resolution observations of stellar lines, i.e. lines formed within the gaseous envelopes. In that field, the most important work is the one of Finkenzeller and Mundt (1984) who have obtained the profiles of the Hα line, of the HeI 5876 Å line and of the NaI D lines for 57 candidate Herbig Ae/Be stars. One of their main results is that the Herbig Ae/Be stars can be divided into 3 subclasses, depending on their Hα profile : the "double-peak" profile subclass, representing 50 % of the whole class, the "single-peak" profile subclass (25 %) and the " P Cygni" profile subclass (20 %). Figure 2a displays an example of each profile type and figure 2b shows the distribution of the profile types as a function of spectral type. It is reasonable to think that these clear differences in the Hα profiles are due to differences of geometry (spherical or axial, for example) and/or structure (velocity, density, temperature runs) in the gaseous envelopes of these stars. But the interesting question one would like to answer is whether these differences in geometry and/or structure correspond to differences in evolution stage. If the answer to this question was positive, we would be able to classify the Herbig Ae/Be stars as a function of their ages, and we would have a whole sequence of PMS stars at different stages of evolution. Clearly, the first step toward this goal is to understand the geometry and the structure of the envelopes in each subclass. The following section shows an example of a quantitative approach that can be used to derive from the line profiles the physical structure of the regions in which the lines are formed.

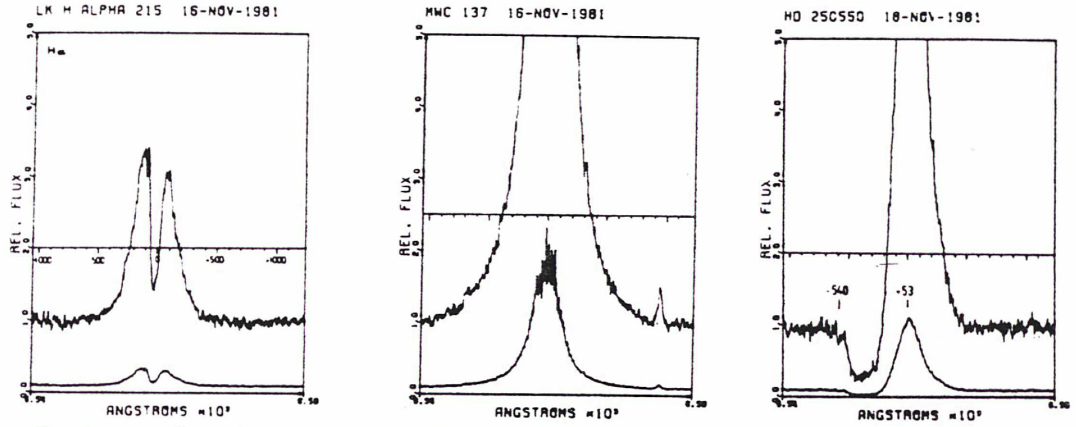

Figure 2a. (above) Examples of Hα profiles

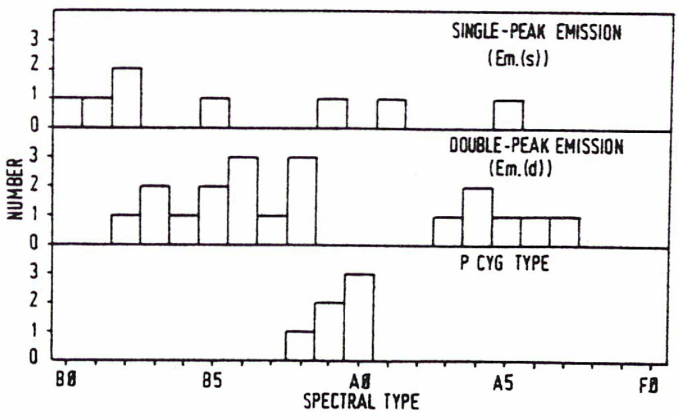

Figure 2b. (left) Distribution of the Hα profile types

(from Finkenzeller and Mundt, 1984)

4 - STUDY OF THE " P CYGNI " SUBCLASS

4-1 Spectral similarities : The first assumption to check is that the Hα profiles are really characteristic of a type of geometry and/or structure. One way of performing this check is to observe as many lines as possible for each subclass and to see if the Herbig Ae/Be stars showing similar Hα profiles also exhibit the same kind of similarities in the other lines. This work has recently been started for the stars of the " P Cygni " subclass, and the results will be published very soon (Felenbok et al., 1985). Figure 3a shows for example the MgII resonance lines for 3 stars of this subclass, and figure 3b, the CaII K line for the same stars. One notes that the profiles have the same shape in the 3 stars. This similarity is also obvious in other lines and for other stars of the " P Cygni " subclass (see Felenbok et al., 1985). The conclusion of this observational study is that the Hα P Cygni profile is indeed characteristic of a given type of geometry and/or structure. This also means that, to study in more detail the "P Cygni " subclass, it is sufficient to study one of its members and to consider it as representative of the subclass. AB Aur, which is the brightest Herbig Ae star in the Northern hemisphere, has been chosen for this more detailed analysis.

To derive quantitative information about the structure of the envelope of AB Aur

from its line profiles, a semi-empirical approach has been followed. A brief summary of this semi-empirical approach is given below.

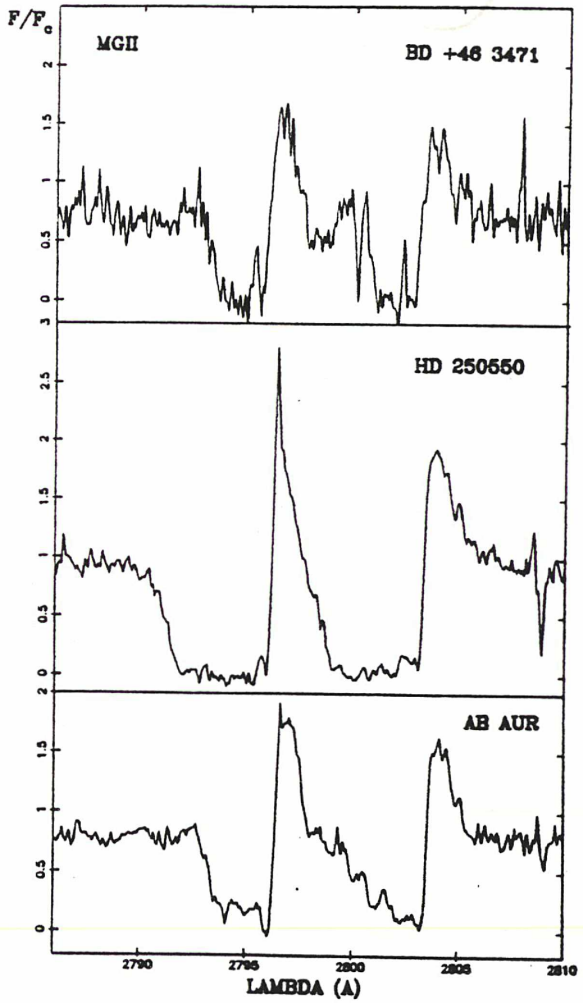

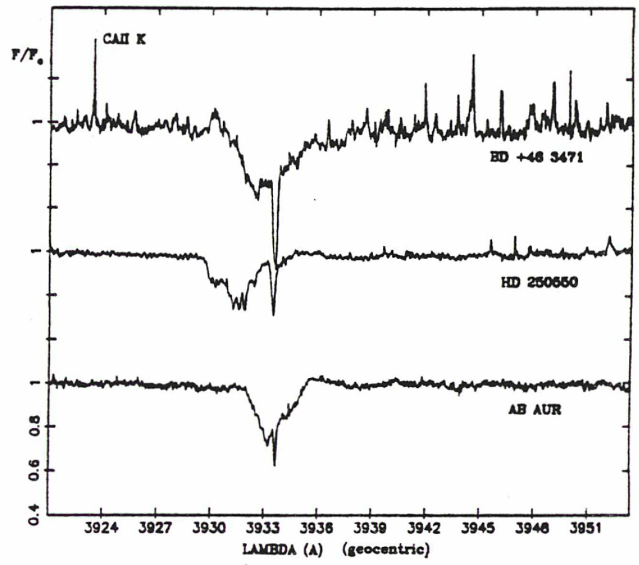

Figure 3a. (left)
The MgII resonance lines of 3 stars of the "P Cygni" subclass, observed with IUE

Figure 3b. (upper right)
The CaII K line for the same stars, observed at the CFH Telescope
(to be published in Felenbok et al., 1985)

4-2 General characteristics of the models : The general type of model that has been considered consists of a spherically-symmetric, expanding envelope surrounding a classical photosphere represented by a model of Kurucz (1979) for $T_{eff} = 10^4$ K and log g = 4. The assumption of spherical symmetry has been made for the sake of simplicity. The presence of an expanding envelope is shown by the P Cygni profiles of Hα (Felenbok et al., 1983) and of the MgII resonance lines (Praderie et al., 1982). The presence of a classical photosphere at the bottom of the wind is suggested by the observation of the Paschen continuum, of the Balmer jump (Garrison, 1978), and of the wings of Hδ (Praderie et al., 1982), which are all well represented by the Kurucz model mentioned above.

The observed maximum blue-shift in the absorption component of the MgII resonance lines on the spectrum presented by Praderie et al. (1982) is V_s=380 km s^{-1}, while neutral sodium D lines show P Cygni profiles with absorption components blue-shifted by 130 km s^{-1} (Felenbok et al., 1983). Since the NaI D lines are necessarily formed at greater distances from the stellar core than the MgII resonance lines, these observations indicate that the wind of AB Aur is decelerated after it has reached its maximum velocity. This maximum velocity is probably reached in the region of formation of the MgII resonance lines.

4.3 Interpretation of the Mg II resonance lines : The next step of this semi-empirical modelling has been a quantitative interpretation of the MgII resonance lines, in order to constrain the dynamical and thermal structure of the envelope (velocity and temperature runs). This work is presented in Catala et al. (1984). A quantitative interpretation of a line profile consists of fitting the observed profile with synthetic profiles computed from models consistent with all the constraints that have been derived from other observations. The problem is that the solution of the fitting is not unique. Several different models can lead to the same computed profile. In other words, it is impossible to calculate unambiguously the model corresponding to the reality by this kind of approach. On the other hand, it is possible to find a whole set of "wrong" models, which means that we are able to derive constraints on the structure of the line formation region. The constraints that have been placed on the structure of the wind of AB Aur by the interpretation of the MgII resonance lines can be summarized as follows :

- a deep, extended and expanding chromosphere is necessary to explain the profile of the MgII lines. The optical depth at 2800 Å of the temperature minimum is 10^{-2} - 10^{-3}. The width of the chromosphere must be higher than one stellar radius. This chromosphere is qualitatively consistent with the observation of the CaII K line (Praderie et al., 1982), of the HeI 5876 Å line and of the CaII IR triplet (Felenbok et al., 1983).

- the mass loss rate of AB Aur must lie between 4.10^{-11} and 7.10^{-9} $M_\odot\ yr^{-1}$.

4-4 Interpretation of the CIV resonance lines : The MgII resonance lines are formed in a very extended region (~ 50 stellar radii), so their interpretation has given only a global vision of the structure of the wind of AB Aur.

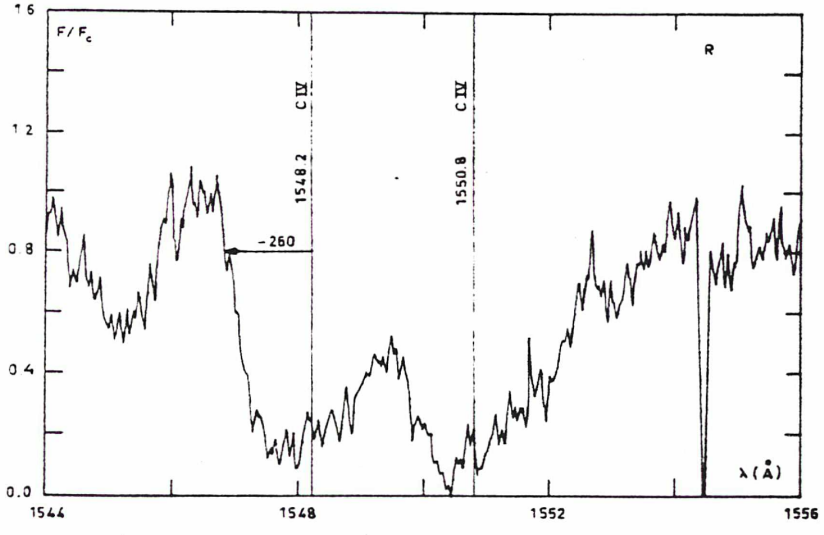

Figure 4. The CIV resonance lines of AB Aur, observed with IUE. The velocity measured on the spectrum is expressed in $km.s^{-1}$. The "R" indicates the position of a "reseau mark". (from Catala and Talavera, 1984)

The next step of this quantitative analysis had to be the interpretation of lines formed in a more localized area, in order to derive tighter constraints on this area. Figure 4 shows the CIV resonance lines observed in the spectrum of AB Aur. These

lines are likely to be formed in the chromosphere (Catala and Talavera, 1984), so we expect to get precise information about the chromosphere by quantitatively interpreting these lines. This work is presently under progress, but preliminary results have already been presented (Catala, 1984). The constraints that have been derived on the structure of the chromosphere are the following :

- the maximum temperature reached in the chromosphere is lower than 19,000 K.
- the width of the chromosphere is lower than 1.5 stellar radii.
- the velocity gradient at the base of the wind must be low (sonic point at more than 1.1 stellar radius from the star's center)
- the velocity near the outer boundary of the chromosphere (i.e. at 2.5 stellar radii from the star's center) must be of the order of 150 $km.s^{-1}$.

Additional modelling is required for a better understanding of the structure of the envelope of AB Aur, and hence of the general structure of the envelopes of the "P Cygni" subclass. In particular, the computation of the hydrogen lines and continua will probably lead to tighter constraints on this structure. Such computations are presently under progress, and will be presented in the near future (Catala and Kunasz, 1985).

4.5 Departures from spherical symmetry : Praderie et al. (1983,1985) have observed with IUE the MgII resonance lines of AB Aur continuously during 40 hours, which corresponds to the presumed rotational period of the star. One of their results is shown in Figure 5, where the maximum blue-shift of the absorption component of the MgII lines (V_s) is plotted as a function of time. The plot clearly suggests a rotational modulation of the MgII resonance lines. The interpretation proposed by Praderie et al. (1983,1985) is the alternation on the line of sight of slow and fast streams, the slow streams coming out from regions of the star where the magnetic loops are closed and the fast ones from regions of open magnetic loops. This model is inspired by observations of the solar wind. We could call it a "solar wind type" model. In the case of AB Aur, since the amplitude of variation of V_s(MgII) is about 100 $km.s^{-1}$, the velocity difference between the fast and the slow streams must be greater than 100 $km.s^{-1}$.

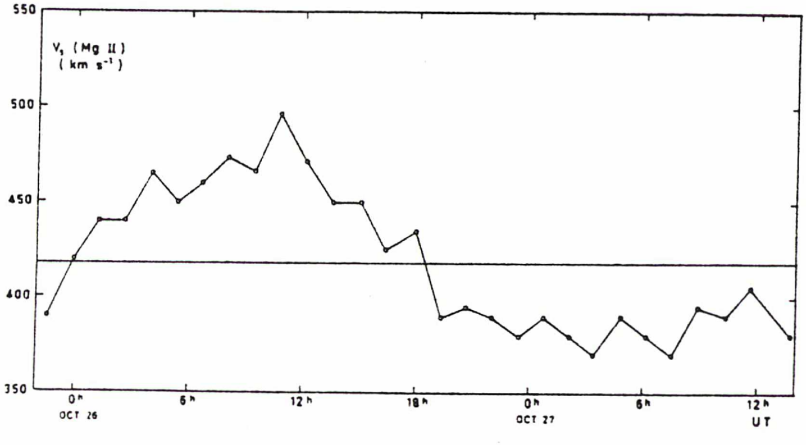

Figure 5. Short term variations of the maximum blue-shift of the MgII k line, V_s(MgII) (from Praderie et al., 1985, by permission).

If this interpretation of the short term spectroscopic variability of AB Aur is

right, the assumption of spherical symmetry is obviously no longer valid. One should then ask whether it is useful to continue the computations in spherically symmetric models. My opinion is that this type of calculations is still very useful, since they represent so far our only way of properly understanding the physics of the line formation. Once this physics is well known, it is easy to qualitatively understand the line formation problem in more difficult geometries. Moreover, the computations in spherical symmetry can provide to some extent information on the "average" structure of these envelopes, but in any case, we must be aware that our spherically symmetric models are not that close to the reality, and we must not go too far in the interpretation of the results.

The work on the "P Cygni" subclass that has been briefly summarized here should now be extended to the two other subclasses. First, observational programs should be carried out in order to look for spectroscopic similarities for these subclasses. Second, a theoretical effort should be made to understand the basic structure and geometry of the envelopes of the two other subclasses.

5 - CONCLUSION

From the present review, it is clear that many fundamental questions about the Herbig Ae/Be stars still remain unanswered.

The first set of questions concern the hydrodynamical problems :

- we have almost no idea at present of the mechanism(s) that produce(s) the winds of these stars and that heat(s) their chromospheres.

- it would be of great interest to understand better the interaction between expansion and rotation in these winds. This interaction can have important observational consequences, as we have seen in section 4.5.

- finally, we should address the problem of the interactions between the different components of the stellar environment (gaseous envelope, CS material, surrounding molecular clouds), these interactions including dynamical interaction, ionization, excitation and heating.

The second set of questions are related to evolutionary problems :

- the main problem in this area is probably to understand how these objects become main sequence stars. The Herbig Ae stars, for example, will become main sequence A stars, and will no longer show any wind nor chromosphere. This means that, in addition to finding mechanisms for driving the winds and heating the chromospheres of the Herbig Ae stars, we must also find a way of switching them off as the stars reach the main sequence.

- finally, there is the hope that a more detailed study of the Herbig Ae/Be stars can provide powerful tests for the computed evolutionary tracks. In particular, a comparison between their properties and those of T Tauri stars would provide a good

knowledge of the PMS evolution as a function of mass and age.

6 - REFERENCES

Allen, D.A.: 1973, Monthly Notices Roy. Astron. Soc. 161,145

Altenhoff, W.J., Braes, L.L.E., Olnon, F.M., Wendker, H.J.: 1976, Astron. Astrophys. 46,11

Cantó, J., Rodriguez, L.F., Calvet, N., Levreault, R.M.: 1984, Astrophys. J. 282,631

Catala, C.: 1983, Astron. Astrophys. 125,313

Catala, C., Kunasz, P.B., Praderie, F.: 1984, Astron. Astrophys. 134,402

Catala, C.: 1984, Proc. 4th European IUE Conf., Rome, May 1984, ESA SP218, p.227

Catala, C., Talavera, A.: 1984, Astron. Astrophys. 140,421

Catala, C., Kunasz, P.B.: 1985, in preparation

Cohen, M.: 1973, Monthly Notices Roy. Astron. Soc. 161,105

Cohen, M.: 1975, Monthly Notices Roy. Astron. Soc. 173,279

Cohen, M., Kuhi, L.V.: 1979, Astrophys. J. Suppl. 41,743

Cohen, M.: 1980, Monthly Notices Roy. Astron. Soc. 191,499

Dickinson, D.F.: 1976, Astrophys. J. Suppl. 30,259

Feigelson, E.D., de Campli, W.M.: 1981, Astrophys. J. 243,L89

Felenbok, P., Praderie, F., Talavera, A.: 1983, Astron. Astrophys. 128,74

Felenbok, P., Czarny, J., Catala, C., Praderie, F.: 1985, in preparation

Finkenzeller, U., Mundt, R.: 1984, Astron. Astrophys. Suppl. 55,109

Finkenzeller, U., Jankovics, I.: 1984, Astron. Astrophys. Suppl. 57,285

Gahm, G.F., Lindroos, K.P., Sherwood, W.A., Winnberg, A.: 1980, Astron. Astrophys. 83,263

Garrison, L.M.: 1978, Astrophys. J. 224,535

Geisel, S.L.: 1970, Astrophys. J. 161,L105

Gillett, F.C., Stein, W.A.: 1971, Astrophys. J. 164,77

Harvey, P.M., Thronson Jr, H.A., Gatley, I.: 1979, Astrophys. J. 231,115

Herbig, G.H.: 1960, Astrophys. J. Suppl. 4,337

Kurucz, R.L.: 1979, Astrophys. J. Suppl. 40,1

Loren, R.B., Van den Bout, P.A., Davis, J.H.: 1973, Astrophys. J. 185,L67

Loren, R.B.: 1977, Astrophys. J. 218,716

Loren, R.B.: 1979, Astrophys. J. 227,832

Loren, R.B.: 1981, Astron. J. 86,69

Lorenzetti,D., Saraceno, P., Strafella, F.: 1983, Astrophys. J. 264,554

Mendoza, E.E.: 1966, Astrophys. J. 143,1010

Mendoza, E.E.: 1967, Astron. J. 72,816

Milkey, R.W., Dyck, H.M.: 1973, Astrophys. J. 181,833

Praderie, F., Talavera, A., Felenbok, P., Czarny, J., Boesgaard, A.M.: 1982, Astrophys. J. 254,658

Praderie, F., Simon, T., Boesgaard, A.M., Felenbok, P., Catala, C., Czarny, J., Talavera, A., Le Contel, J.M., Morel P., Sareyan, J.P., Valtier, J.C.: 1983, 2nd France-Japan Seminar, Paris, eds. J. C. Pecker and Y. Uchida, p.132

Praderie, F., Simon, T., Boesgaard, A.M.: 1985, in preparation

Pravdo, S.H., Marshall, F.E.: 1982, Astrophys. J. 248,591

Sanders, W. T., Cassinelli, J.P., Anderson, C.M.: 1982, Bull. American Astron. Soc. 14,629

Sistla, G., Hong, S.S.: 1975, Astron. Astrophys. 44,477

Sitko, M.L., Savage, B.D., Meade, M.R.: 1981, Astrophys. J. 246,161

Sitko, M.L.: 1981, Astrophys. J. 247,1024

Strom, S.E., Strom, K.M., Yost, J., Carrasco, L., Grasdalen, G.L.: 1972, Astrophys. J. 173,353

Thé, P.S., Tjin A Djie, H.R.E., Bakker, R., Bastiaansen, P.A., Burger, M., Cassatella, A., Fredga, K., Galin, G., Liseau, R., Smyth, M.J., Viotti, R., Wamsteker, W., Zenge, W.: 1981, Astron. Astrophys. Suppl. 44,451

Walter, F.M., Kuhi, L.V.: 1981, Astrophys. J. 250,254

Wesselius, P.R., Beintema, D.A., Olnon, F.M.: 1984, Astrophys. J. 278,L37

CHAPITRE II

VENTS ET CHROMOSPHERES: ETUDE SEMI-EMPIRIQUE

1 - Généralités:

Nous présentons dans ce chapitre les étapes successives de la construction d'un modèle semi-empirique pour les atmosphères des ABHs. Ce modèle est à symétrie sphérique, sans rotation, et stationnaire. Retirer ces hypothèses est au-delà de nos possibilités actuelles: la prise en compte de la rotation ou d'éventuelles asymétries introduirait au moins une dimension supplémentaire; la résolution de l'équation de transfert à 2 ou 3 dimensions, en présence d'un champ de vitesse, n'est pas totalement inenvisageable à l'heure actuelle (Kunasz et Auer, 1987), mais nécessite encore certains développements. L'introduction d'une dépendence temporelle compliquerait énormément le problème, et le rendrait inaccessible avec les moyens de calcul disponibles.

Cependant, nous sommes forcés de constater que ces trois hypothèses sont contredites par certaines observations. Tout d'abord, il est notoire que les ABHs ont des vitesses de rotation photosphériques non négligeables (Davis et al., 1983; Finkenzeller, 1985), et on peut penser que leurs atmosphères étendues tournent également. D'autre part, la variabilité de certaines raies suggère des écarts à la symétrie sphérique et à la stationnarité (voir Annexes H et I). Notre modèle semi-empirique doit donc être considéré comme un modèle "moyen", ne nous renseignant que sur la structure globale des atmosphères des ABHs. L'inadéquation de notre modèle à la réalité va nous obliger à prendre certaines précautions.

En particulier, la plus grande prudence s'impose lors de l'interprétation des composantes en absorption de certaines raies. En effet, ces composantes se forment dans les régions de l'atmosphère se projetant sur le disque stellaire du point de vue de l'observateur, et n'englobant par conséquent qu'un petit volume. Ces composantes en absorption sont donc très sensibles au passage d'inhomogénéités sur la ligne de visée. L'analyse détaillée d'une observation unique d'une raie en absorption ne nous renseignera guère sur la structure globale de l'atmosphère d'une ABH.

La plupart des composantes en émission des ABHs, au contraire, se forment

dans des régions très étendues de l'atmosphère. Il est donc probable que ces composantes en émission contiennent l'information sur la structure moyenne de l'atmosphère. Cependant, les résultats quantitatifs que nous allons obtenir par l'interprétation des composantes en émission sont fondés sur l'hypothèse suivante: un modèle à symétrie sphérique ayant les propriétés moyennes d'un milieu sans symétrie sphérique conduit à des composantes en émission identiques à celles produites par ce milieu ("moyenne" ici signifie moyenne longitudinale et latitudinale). Les futurs calculs de transfert de rayonnement dans des géométries à 2 ou 3 dimensions permettront de tester cette hypothèse. Dans l'immédiat, nous ne pouvons que l'adopter en nous fiant à notre intuition.

Par suite de ces limitations, nous estimons que le modèle semi-empirique à symétrie sphérique, sans rotation, et stationnaire, que nous décrivons dans ce chapitre, a été mené à sa limite. Tenter de l'affiner dans le cadre de ces hypothèses constituerait sûrement une surinterprétation des résultats.

2 - AB Aurigae: un prototype:

Finkenzeller et Mundt (1984) ont montré qu'on pouvait grouper les ABHs en trois sous-classes, suivant le profil de leur raie Hα:

- Hα en émission "double pic" (représentant 50% de la totalité des ABHs).
- Hα en émission "simple pic" (25%)
- Hα avec un profil P Cygni (20%)

Les 5% restant présentent des profils plus complexes pour la raie Hα.

Par la suite, nous appellerons ces trois sous-classes "double pic", "simple pic" et "P Cygni", respectivement. Les étoiles de la sous-classe "P Cygni" sont les seules pour lesquelles nous avons une évidence directe de la présence d'un vent stellaire (par le profil P Cygni de la raie Hα). Les profils en émission "double pic" et "simple pic" sont également compatibles avec la présence d'un vent, mais leur interprétation est plus ambigüe.

Bien que minoritaires, les étoiles de la sous-classe "P Cygni" sont mieux adaptées à une analyse détaillée, et leur étude constitue donc un bon point de départ pour notre travail. En particulier, il est important de déterminer si les étoiles de cette sous-classe ont des atmosphères semblables. Cette comparaison permet en effet de savoir si on est en présence d'un groupe d'étoiles ayant des propriétés physiques identiques. Dans le cas contraire, il serait arbitraire de les grouper dans une même sous-classe.

L'Annexe B présente une étude observationnelle poussée d'un échantillon

d'ABHs appartenant à la sous-classe "P Cygni". Il y est démontré que plusieurs raies, outre Hα, présentent des similitudes frappantes dans le spectre de ces étoiles. Ces raies (Mg II h et k, Ca II K, Ca II triplet infrarouge, raies D de Na I) se formant dans des régions différentes de l'atmosphère d'une ABH, on en conclut que la structure des vents de ces étoiles est similaire, depuis la photosphère, où se forme en partie la raie K de Ca II, jusqu'à des distances de 50 à 100 R_*, où se forment les raies D de Na I.

Nous pouvons donc considérer une de ces étoiles comme représentant de la sous-classe "P Cygni", et l'étudier en détail. Les résultats de cette étude seront alors applicables en partie à l'ensemble de la sous-classe. AB Aurigae (A0Ve, m_v=7.2) est l'étoile la plus brillante de la sous-classe "P Cygni". C'est aussi l'ABH la plus brillante de l'hémisphère Nord. Nous disposons pour cette étoile d'un grand nombre d'observations, et ses paramètres fondamentaux sont assez bien connus (Table II-1). Nous allons donc nous concentrer sur l'étude semi-empirique de cette étoile, la considérant comme prototype de la sous-classe "P Cygni".

Table II-1

AB Aur - Paramètres stellaires

	m_v	S.T.	log $L/L_\odot$	$M/M_\odot$	d(pc)	v_R (km.s^{-1})	vsini (km.s^{-1})
valeur	7.1	A0 Ve	2	2.8	160	+21	75 (1) 140 (2)
réf.	CDS	6	2, 4	1	2	5	(1) 3 (2) 6

1 - Cohen (1973)
2 - Cohen et Kuhi (1979)
3 - Davis et al. (1983)
4 - Finkenzeller et Mundt (1984)
5 - Finkenzeller et Jankovics (1984)
6 - Finkenzeller (1985)

Des résultats postérieurs à la publication de l'Annexe B suggèrent que certaines ABHs (par exemple HD163296, BD+46°3471) varient suffisamment dans le temps pour passer d'une sous-classe à une autre, sur des échelles de temps de l'ordre de quelques mois. Ces observations montrent qu'il nous faut être extrêmement prudents dans notre classification des ABHs. La similitude des atmosphères des étoiles de la sous-classe "P Cygni" n'est pas remise en question, mais une spéculation avancée dans l'Annexe B semble aujourd'hui contredite: si une même étoile change de sous-classe au cours de ses variations, cette classification ne peut pas être reliée au stade d'évolution des ABHs, comme l'idée en avait été émise dans l'Annexe B. Cette variabilité long terme (voir aussi Praderie et al., 1984) n'est pas comprise pour l'instant, et un travail sérieux d'observation reste encore à mener à bien pour en dégager précisément les caractéristiques.

3 - Premières contraintes:

La suite de ce chapitre II est donc consacrée à la construction d'un modèle semi-empirique pour l'atmosphère d'AB Aur. Un certain nombre d'observations nous permettent de placer des contraintes préliminaires sur ce modèle, avant même toute analyse quantitative. Ces contraintes ayant déjà été discutées dans la thèse de troisième cycle de l'auteur (Catala, 1983b), nous n'en donnons ici qu'un bref aperçu, nécessaire cependant pour des raisons d'unité de la présentation de ce mémoire.

Tout d'abord, les observations de la discontinuité de Balmer, du continu de Paschen dérougi et des ailes de la raie Hδ montrent que la photosphère d'AB Aur est semblable à celle d'une étoile A0 sur la séquence principale. Ceci est une indication qu'AB Aur en est probablement à la phase ultime de son évolution pré-séquence principale. Notre modèle doit donc comporter une photosphère classique en équilibre hydrostatique et en équilibre radiatif, que nous représentons par un modèle de Kurucz (1979) correspondant aux paramètres stellaires d'AB Aur ($T_{eff}=10^4$ K, log g=4).

D'autre part, l'existence de profils P Cygni (Hα, Mg II h et k; voir Annexe B) indique la présence d'une atmosphère étendue et en expansion. Notre modèle doit donc comporter un vent stellaire, et s'étendre jusqu'à des distances importantes.

Enfin, certaines observations indiquent la possibilité d'existence d'une chromosphère (Praderie et al., 1982; Felenbok et al., 1983), sans toutefois la prouver.

Nous devons donc envisager d'avoir à introduire une chromosphère dans notre modèle.

4 - Interprétation quantitative des raies de résonance de Mg II:

Ce travail constitue la thèse de troisième cycle de l'auteur (Catala, 1983b). Les résultats ont également été publiés sous une forme différente dans "Astronomy and Astrophysics". Cet article est présenté dans l'Annexe C. C'est un souci d'unité qui nous a poussés à introduire cet article dans le présent mémoire. Nous ne donnons ci-dessous qu'un résumé succint de cette étude. Certains points ayant été précisés depuis lors sont néanmoins traités plus en détail.

La structure atomique de Mg II se prête assez bien à cette première étape de l'étude quantitative de la formation des raies dans l'atmosphère d'AB Aur. On peut en effet considérer l'ion Mg II comme un système à 2 niveaux ($3s^2S$ et $3p^2P°$), les autres niveaux étant beaucoup plus énergétiques. Cette approximation facilite énormément la résolution des équations couplées du transfert radiatif et de l'équilibre statistique. En effet, le couplage entre ces deux équations se traduit alors directement dans l'expression de la fonction source dans la raie (on considère que la fonction source est la même pour les deux raies du doublet de résonance):

$$S_L = (1-\varepsilon) \int \phi_\nu J_\nu \, d\nu + \varepsilon B_\nu \qquad \text{(II–1)}$$

où ϕ_ν est le profil intrinsèque de la raie, B_ν la fonction de Planck à la température électronique locale, J_ν l'intensité moyenne du rayonnement, et ε le paramètre de thermalisation:

$$\varepsilon = \frac{C_{21}}{A_{21}+C_{21}} \qquad \text{(II-2)}$$

A_{21} et C_{21} étant les taux de désexcitation radiatif et collisionnel, respectivement.

La présence d'un champ de vitesse complique la résolution de l'équation de transfert, par l'introduction d'un effet Doppler important qui rend anisotropes les propriétés de la matière (opacité, émissivité) dans le référentiel du laboratoire. Dans l'Annexe C, et tout au long de cette thèse, nous avons choisi de traiter l'équation de transfert dans le

référentiel du fluide, dans lequel opacité et émissivité sont isotropes. La méthode de résolution de l'équation de transfert dans le référentiel du fluide est décrite dans Mihalas et al. (1975, 1976a,b,c).

L'obstacle principal auquel on se heurte lors de l'interprétation d'un profil de raie est la non-unicité du modèle conduisant à un accord entre profils observé et calculé. Quelle que soit la raie interprétée, il est toujours possible d'exhiber plusieurs modèles complètement différents conduisant au même profil calculé. Par exemple, si on reprend les résultats de l'Annexe C, on s'aperçoit qu'on peut obtenir le même profil pour la raie k de Mg II avec un modèle à fort taux de perte de masse ($\dot{M}$) et haute température de rayonnement (T_r) qu'avec un modèle à faible $\dot{M}$ et faible T_r. Si cette sorte d'analyse ne permet pas de bâtir d'un seul coup un modèle réaliste, elle permet par contre de comprendre les processus physiques contrôlant la formation des raies étudiées et d'en déduire des contraintes plus ou moins précises sur la structure de la région de formation de ces raies. En répétant ce travail pour toutes les raies observées, on peut alors espérer aboutir à des contraintes assez sévères pour décrire la structure de l'atmosphère avec des détails suffisants pour contraindre fortement les modèles hydrodynamiques ou MHD à venir.

Les contraintes sur la structure de l'atmosphère d'AB Aur déduites de l'interprétation des raies de résonance de Mg II sont résumées ci-dessous. Le lecteur est renvoyé à l'Annexe C pour plus de détails.

Le résultat fondamental de cette étude est la mise en évidence d'une chromosphère à la base du vent d'AB Aur. Ce résultat est déduit de l'intensité de la composante en émission dans le profil P Cygni de la raie k de Mg II, et n'est donc pas affecté par le problème des écarts à la symétrie sphérique décrit au paragraphe II-1. La chromosphère envisagée a une extension supérieure à 1 R_*, et est donc très différente de la chromosphère solaire qui ne s'étend que sur 10^{-2} $R_\odot$ environ. Notons cependant que cette chromosphère répond à la définition que nous avons proposée au chapitre I, puisque sa température (15000 - 20000 K, contrainte affinée au paragraphe II-6) est supérieure à la température effective de l'étoile. Il est intéressant de remarquer que des chromosphères étendues ont aussi été détectées dans les géantes et les supergéantes rouges (Stencel et al., 1981; Carpenter et al., 1985), qui présentent également des vents stellaires. Par contre, les chromosphères des étoiles de la séquence principale, qui ne possèdent pas de vent détectable spectroscopiquement, sont peu étendues. Notre travail semble donc confirmer la possibilité d'un lien entre les vents stellaires et l'extension des chromosphères.

L'Annexe C donne également des contraintes sur $\dot{M}$. Cependant, ces contraintes

sont obtenues par l'analyse de la composante en absorption du profil P Cygni de la raie k de Mg II, et sont donc sujettes au problème des écarts à la symétrie sphérique (l'Annexe C a été publiée avant que ces écarts à la symétrie sphérique soient pleinement reconnus). D'autre part, l'estimation de la température de rayonnement T_r pour la transition MgII-MgIII joue un rôle fondamental dans le calcul de la fraction $MgII/Mg_{total}$ et donc pour l'obtention des contraintes sur $\dot{M}$. Or, T_r est obtenu sous l'hypothèse que le rayonnement ionisant pour cette transition est thermalisé dans la chromosphère. Un calcul complet a montré plus tard que ce n'était pas toujours le cas (voir Annexe D). Par conséquent, les contraintes sur $\dot{M}$ déduites dans l'Annexe C sont suspectes, et nous préférons attendre des résultats ultérieurs pour contraindre plus précisément $\dot{M}$ (voir paragraphe II-5 et Annexe D).

Enfin, le décalage vers le rouge de la composante en émission nous oblige à introduire une vitesse Doppler aléatoire (v_D) supersonique. Cette vitesse Doppler aléatoire se compose de la vitesse d'agitation thermique v_{th}, et de tous les mouvements à petite échelle, comme par exemple la turbulence. Il n'est pas très clair pour l'instant si la valeur importante trouvée pour v_D (45 km s^{-1}) indique la présence de turbulence supersonique, ou simplement des inhomogénéités de vitesse à petite échelle, impossibles à prendre en compte dans notre modèle à symétrie sphérique. Le paramètre v_D est cependant le seul dont nous disposons pour regrouper tant bien que mal ces phénomènes de turbulence et d'inhomogénéité.

5 - Interprétation quantitative de Hα et d'autres raies et continus de l'hydrogène:

Le problème de la formation des raies de l'hydrogène est d'une complexité supérieure à celui de la formation des raies de Mg II. En effet, il n'est pas question de considérer l'hydrogène comme un atome à deux niveaux. Nous devons donc résoudre le système couplé des équations d'équilibre statistique et de l'équation de transfert. La méthode de "l'atome équivalent à deux niveaux" (nous utiliserons par la suite l'abréviation anglaise ETLA) permet de résoudre ce problème dans le référentiel du fluide. Cette méthode est décrite en détail dans Mihalas et Kunasz (1978). Elle consiste à isoler chaque transition du reste de la structure atomique et à la traiter comme un problème à deux niveaux, en considérant les taux faisant intervenir les autres niveaux comme fixés. Ce calcul est alors plongé dans un processus général d'itération.

L'Annexe D traite de l'interprétation quantitative des raies et continus de l'hydrogène. La méthode ETLA dans le référentiel du fluide y est utilisée. L'hydrogène est considéré comme un système à 6 niveaux + 1 continu, et toutes les transitions entre ces niveaux (raies et continus) sont traitées de façon explicite. Ce calcul ne souffre donc pas des défauts signalés plus haut pour l'approximation "atome à 2 niveaux", en particulier concernant l'estimation de la température de rayonnement.

L'Annexe D montre que la structure globale du modèle déduit de l'interprétation des raies de Mg II est cohérente avec la raie Hα et les continus de l'hydrogène. Les raies Hβ et Hγ, bien que calculées, ne peuvent pas être comparées directement aux observations, car elles sont dominées par l'élargissement Stark au type spectral A0, et celui-ci n'a pas été pris en compte dans les calculs. Les raies de Paschen et de Brackett ont également été calculées et leurs profils sont globalement semblables aux profils observés.

La contrainte la plus importante déduite de ces calculs concerne le taux de perte de masse. On trouve $1.0\ 10^{-8} < \dot{M} < 1.8\ 10^{-8}\ M_\odot$/an. Ce résultat, obtenu à partir de la composante en émission du profil P Cygni de Hα et du continu de Balmer, n'est pas affecté par les écarts à la symétrie sphérique.

On montre également que la température dans la région post-chromosphérique doit être inférieure à 10000 K, et que la région du minimum de température à la base de la chromosphère est à environ 7100 K.

6 - Interprétation quantitative des raies de résonance de C IV:

Des contraintes beaucoup plus précises sur la structure de la chromosphère ont été obtenues par l'interprétation des raies de résonance de C IV. La première partie de l'Annexe E montre ces raies telles qu'observées par le satellite IUE en Janvier 1983. D'autre part, une série de 5 spectres a été obtenue en Janvier 1986 (voir Annexe J). Il est très remarquable que ces raies soient présentes dans le spectre d'une étoile A0. En général, elles sont absentes aux types spectraux plus tardifs que B5. Bien que très variables, les raies de résonance de C IV d'AB Aur présentent toujours les mêmes caractéristiques: elles sont purement en absorption, et intenses.

La simple présence de ces raies indique des températures supérieures à la température effective de l'étoile, et constitue donc un argument de poids pour l'existence d'une chromosphère dans l'atmosphère d'AB Aur. Le modèle le plus commun suppose que ces raies se forment dans une région chaude à environ 10^5 K (voir par exemple Doazan,

1982; Lamers et Snow, 1978). Un équilibre coronal, c'est-à-dire entre les ionisations collisionnelles et les recombinaisons radiatives, contrôle alors la transition C III - C IV. Cependant, un tel modèle se heurte à des difficultés si on veut l'appliquer au cas d'AB Aur. En effet, il conduit généralement à des raies en émission pour C IV. Pour le voir, considérons l'ion C IV comme un système à deux niveaux. La fonction source dans les raies de résonance peut alors être évaluée par l'équation II-1. On peut exprimer C_{21} en fonction de la force de choc Ω:

$$C_{21} = 8.65\ 10^{-6}\ \Omega\ n_e\ T_e^{-1/2}\ g_2 \qquad \text{(unités c.g.s.)} \qquad \text{(II-3)}$$

où n_e est la densité électronique, T_e la température électronique, et g_2 le poids statistique du niveau supérieur de la transition. Ω peut être calculé à partir des sections efficaces de collision publiées par Taylor et al. (1977). On obtient $\Omega \approx 8$ pour $T=10^5$ K.

Si l'on considère que la région chaude à 10^5 K se trouve à la base du vent, où $n_e \approx 10^{12}$ cm^{-3} (voir Annexe D), on trouve $C_{21} \approx 1.3\ 10^6$ s^{-1}. Wiese et al. (1969) donnent $A_{21}=2.65\ 10^{-8}$ s^{-1} pour cette transition. On obtient donc $\varepsilon \approx 5\ 10^{-3}$ dans ces conditions.

Une raie apparait en absorption si la fonction source dans la raie au point où $\tau_L=1$ est inférieure à la fonction source dans le continu au point où $\tau_c=1$, τ_L et τ_c étant les profondeurs optiques dans la raie et dans le continu, respectivement. Or, d'après l'équation II-1:

$S_L(\tau_L=1) > \varepsilon\ B_\nu(10^5 K)$, si l'on admet que la région de formation des raies de C IV est optiquement épaisse dans ces raies, et

$S_c(\tau_c=1) \approx B_\nu(10^4 K)$

On en tire $S_L(\tau_L=1)/S_c(\tau_c=1) > 30$, ce qui montre qu'on obtiendrait les raies de résonance de C IV fortement en émission avec un tel modèle.

Si l'on considère que la région chaude à 10^5 K se trouve plus loin dans le vent, on obtient par contre un profil P Cygni très marqué (voir Annexe F), avec une forte composante en émission qui n'est pas observée.

L'Annexe E propose une alternative à ce modèle, qui plus est en accord avec les contraintes déduites précédemment sur la structure de l'atmosphère d'AB Aur. Il s'agit de supposer que le rayonnement ionisant pour la transition C III - C IV (seuil à 259.9 Å, c'est-à-dire $\nu = 1.157\ 10^{16}$ s^{-1}) est thermalisé dans la région de formation des raies. Dans ces conditions, l'équilibre d'ionisation C III - C IV est entièrement radiatif, et le rapport n(CIII)/n(CIV) est décrit par l'équation de Saha. On peut alors montrer que, dans les

conditions de température et de densité invoquées pour la chromosphère d'AB Aur (T_e=15000-18000 K, n_e=10^{11}-10^{12} cm^{-3}), on obtient du C IV en quantité suffisante pour envisager la présence de ses raies de résonance.

La suite de l'analyse consiste donc à calculer ces raies à l'aide de ce modèle. Des résultats préliminaires sont présentés dans l'Annexe F. Dans ces calculs, l'ion C IV est considéré comme un système à deux niveaux, ce qui constitue une excellente approximation. Les résultats sont obtenus dans l'hypothèse présentée au paragraphe précédent, c'est-à-dire qu'on a utilisé l'équation de Saha pour décrire l'équilibre d'ionisation C III - C IV. Comme prévu, on obtient bien les raies de résonance de C IV en absorption avec une chromosphère à température modérée (T_e=18000 K).

Certaines contraintes préliminaires sur la structure de la chromosphère sont obtenues dans l'Annexe F. Ces contraintes seront reprises et affinées dans l'Annexe G. Il convient néanmoins d'insister sur l'une d'entre elles. Pour expliquer la largeur des raies de résonance de C IV, on a dû envisager une valeur de v_D (vitesse Doppler aléatoire) supérieure à celle obtenue dans l'Annexe C. Comme il est suggéré dans l'Annexe F, et comme nous l'avons vu précédemment (paragraphe II-4), il n'est pas du tout évident que v_D mesure seulement la vitesse turbulente dans la région de formation des raies. La vitesse Doppler aléatoire v_D doit aussi inclure tous les mouvements à petite échelle ne pouvant pas être pris en compte par le modèle ("petite échelle" pouvant aller jusqu'à 1R_* environ). En particulier, on peut très bien imaginer la coexistence à la base du vent de mouvements descendants et d'un mouvement global d'expansion. D'autre part, la structure en jets rapides et jets lents, proposée dans les Annexes H et I, doit contribuer elle aussi à augmenter v_D. Cependant, il est clair qu'une telle complexité de mouvements ne peut pas être représentée de façon réaliste par le seul paramètre v_D. C'est pourquoi, comme nous l'avons déjà signalé, il est préférable de ne pas tenter de déduire des contraintes précises sur la structure de l'atmosphère à partir de raies en absorption. Le résultat v_D=100 km s^{-1} obtenu dans l'Annexe F ne doit donc être considéré que comme une indication de l'importance des mouvements à petite échelle dans ce problème.

Bien entendu, ces résultats s'appuyant sur l'hypothèse de base de thermalisation du rayonnement ionisant, ils ne sont pas entièrement satisfaisants. Grâce à la méthode ETLA (voir paragraphe II-5), il est cependant possible de mener un calcul complet du système C III - C IV - C V, faisant intervenir toutes les transitions (raies et continus) entrant en jeu, et tenant compte de sources d'opacité réalistes. On peut par conséquent calculer le profil des raies de résonance de C IV sans faire l'hypothèse de thermalisation du

rayonnement ionisant. Le rayonnement ionisant C III en C IV est calculé de façon cohérente avec les populations des différents niveaux d'énergie du système C III - C IV - C V, ainsi qu'avec les populations des sources extérieures d'opacité (H, He, C, N, O, Si, etc...). Ces calculs sont présentés dans l'Annexe G. Ils montrent qu'on obtient bien un profil en absorption pour les raies de résonance de C IV. Ils permettent également de vérifier directement que l'hypothèse de thermalisation du rayonnement ionisant est justifiée. La source principale d'opacité aux fréquences entrant en jeu est l'ionisation de He I à partir de son niveau fondamental.

Les raies de résonance de C IV d'AB Aur ont été observées à maintes reprises (2 spectres d'archives IUE, voir Annexe E; 1 spectre présenté dans l'Annexe E; 5 spectres présentés dans l'Annexe J). Sur tous ces spectres obtenus à des moments différents, leur profil est toujours purement en absorption, avec une intensité résiduelle $F_{abs}/F_c \approx 0.2$. L'Annexe G fait usage de ces deux caractéristiques, qui ne semblent pas être affectées par les inhomogénéités dans le vent, pour déduire des contraintes supplémentaires sur la structure physique de la chromosphère. On trouve 16000 K < T_{max} < 18000 K et $\Delta_2 < 2.5 R_*$, où T_{max} est la température maximum atteinte dans la chromosphère et Δ_2 est l'étendue de cette dernière. Ces résultats sont en accord avec le fait qu'on n'ait pas détecté de couronne avec le satellite Einstein (Feigelson et De Campli, 1981), et avec l'absence des raies de résonance de N V (Catala et Praderie, en préparation).

7 - Récapitulation des contraintes sur la structure physique de l'atmosphère d'AB Aur:

Nous résumons ci-dessous les contraintes déduites des travaux décrits plus haut, et dont les modèles hydrodynamiques à venir devront tenir compte:

a) *Loi de température:* au dessus de la photosphère, la température décroit jusqu'à 7100 K (Annexe D), puis augmente pour atteindre 16000-18000 K (Annexe G). Au delà de la chromosphère, la température descend au dessous de 10000 K (Annexe D). L'étendue de la chromosphère est supérieure à $1R_*$ (Annexe C) et inférieure à $2.5R_*$ (Annexe G). La figure ci-dessous présente les contraintes obtenues pour la loi de température. La courbe en trait plein correspond au modèle n°1 de l'Annexe D. Les deux courbes en trait discontinu peuvent être considérées comme des situations extrêmes pour la loi de température. Les régions hachurées représentent les domaines acceptables pour la température maximum et pour la température dans la région post-chromosphérique.

Loi de temperature

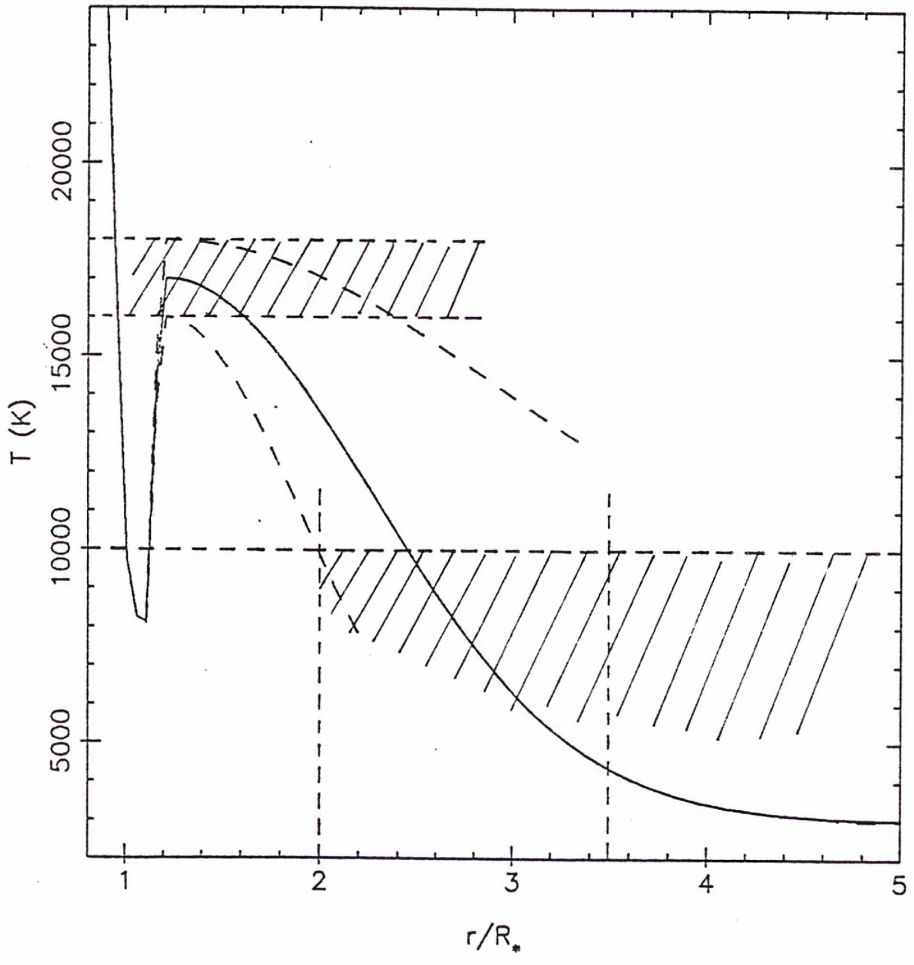

b) *Loi de vitesse:* la vitesse atteinte au sommet de la chromosphère est d'au moins 150 km s^{-1} (Annexe F), et probablement variable. La vitesse maximale du flot est variable, et comprise entre 250 et 500 km s^{-1}. Dans les régions les plus éloignées du vent, la vitesse redécroit au moins jusqu'à 150 km s^{-1} (Annexe C et Felenbok et al., 1983).

c) *Taux de perte de masse:* $\dot{M}$ est compris entre 1.0 10^{-8} et 1.8 10^{-8} $M_\odot$ /an (Annexe D).

Bien entendu, ceci ne représente que la structure "moyenne" du vent d'AB Aur. Ne perdons pas de vue que ce vent n'est pas à symétrie sphérique, mais se compose d'une alternance entre jets lents et jets rapides.

8 - Apport de quantité de mouvement et pertes radiatives:

Notre modèle semi-empirique conduit naturellement à une estimation de l'apport de quantité de mouvement dans le vent d'AB Aur, ainsi que des pertes radiatives correspondant aux transitions que nous avons calculées.

L'écoulement d'un flot autour d'une étoile est décrit par les équations de l'hydrodynamique:

$$\frac{\partial \rho}{\partial t} + \nabla.(\rho \underset{\sim}{v}) = 0 \qquad \text{(conservation de la masse)} \qquad \text{(II-4)}$$

$$\rho \frac{\partial \underset{\sim}{v}}{\partial t} + \rho(\underset{\sim}{v}.\nabla)\underset{\sim}{v} = -\nabla P - \rho \frac{GM_*}{r^2} \underset{\sim}{e_r} + \underset{\sim}{D} \qquad \text{(conservation de la quantité de mouvement)} \qquad \text{(II-5)}$$

$$\frac{\partial}{\partial t}\left(\frac{1}{2}\rho v^2 + \frac{P}{\gamma-1} - \rho\frac{GM_*}{r}\right) + \nabla.\left[\underset{\sim}{v}\left(\frac{1}{2}\rho v^2 + \frac{\gamma}{\gamma-1}P - \rho\frac{GM_*}{r}\right)\right] = Q \qquad \text{(conservation de l'énergie)} \qquad \text{(II-6)}$$

où tous les symboles utilisés sont décrits à la fin de ce mémoire et où $\underset{\sim}{D}$ et Q représentent les apports de quantité de mouvement et d'énergie, respectivement. Le terme Q dans l'équation II-6 peut être considéré comme le bilan des pertes radiatives (E^-) et de l'apport d'énergie non radiative (E^+):

$$Q = E^+ - E^-$$

Nous n'avons pas tenu compte explicitement du champ magnétique dans les équations II-4 à II-6, mais on peut considérer que ses effets sont contenus dans $\underset{\sim}{D}$ et Q.

Si on suppose que le flot est à symétrie axiale (expansion + rotation par exemple) et si on n'exprime que la composante radiale de l'équation II-5, on obtient, en coordonnées sphériques:

$$\frac{\partial \rho}{\partial t} + \frac{1}{r^2}\frac{\partial}{\partial r}(\rho w r^2) = 0 \qquad \text{(II-7)}$$

$$\rho\frac{\partial w}{\partial t} + \rho w\frac{\partial w}{\partial r} - \rho\frac{v_\varphi^2}{r} = -\frac{\partial P}{\partial r} - \rho\frac{GM_*}{r^2} + D \qquad \text{(II-8)}$$

$$\frac{\partial}{\partial t}\left(\frac{1}{2}\rho v^2 + \frac{P}{\gamma-1} - \rho\frac{GM_*}{r}\right) + \frac{1}{r^2}\frac{\partial}{\partial r}\left[\rho w r^2\left(\frac{1}{2}v^2 + \frac{\gamma}{\gamma-1}P - \frac{GM_*}{r}\right)\right] = Q \qquad \text{(II-9)}$$

Si on fait l'hypothèse supplémentaire que le flot est stationnaire, les dérivées temporelles disparaissent des équations II-7 à II-9, et on aboutit à

$$\rho w r^2 = C^{te} = \dot{M} / 4\pi \qquad \text{(II-10)}$$

$$w\frac{\partial w}{\partial r} - \frac{v_\varphi^2}{r} + \frac{1}{\rho}\frac{\partial P}{\partial r} + \frac{GM_*}{r^2} = D / \rho \qquad \text{(II-11)}$$

$$\dot{M}\frac{\partial}{\partial r}\left(\frac{1}{2}v^2 + \frac{\gamma}{\gamma-1}\frac{P}{\rho} - \frac{GM_*}{r}\right) = 4\pi r^2 Q \qquad \text{(II-12)}$$

La construction d'un modèle théorique de vent stellaire consiste à résoudre l'un de ces systèmes d'équations, suivant le degré de complexité envisagé, à partir d'hypothèses sur les contributions principales à D et Q. Une des justifications principales de notre modèle semi-empirique est qu'il peut nous fournir une première estimation de D et de certaines contributions à E^-, donc à Q.

8-1 Apport de quantité de mouvement:

Notre modèle semi-empirique permet d'estimer tous les termes du membre de gauche de l'équation (II-11), et donc d'évaluer la distribution radiale de l'apport de quantité

de mouvement nécessaire pour entretenir le vent d'AB Aur, sous l'hypothèse que ce dernier est à symétrie axiale et stationnaire. Les calculs présentés ci-dessous ont été obtenus avec le modèle n°1 de l'Annexe D. Ce modèle ne représentant pas nécessairement la réalité (rappelons que l'analyse semi-empirique permet de placer des contraintes sur la structure physique de l'atmosphère, pas d'exhiber un modèle parfait), les résultats qui suivent sont donnés à titre indicatif, mais il s'agit-là de la meilleure approche possible actuellement.

La figure II-1 montre la distribution de l'accélération D/ρ calculée de la façon indiquée plus haut, avec deux hypothèses extrêmes sur la composante azimuthale de la vitesse, $v_\varphi = 0$ et $v_\varphi = cte = v_{rot}$, où v_{rot} est la vitesse de rotation de l'étoile à la photosphère, estimée à 100 km s^{-1}, grâce à la modulation rotationnelle du vent décrite au chapitre III.

Fig II–1 Acceleration

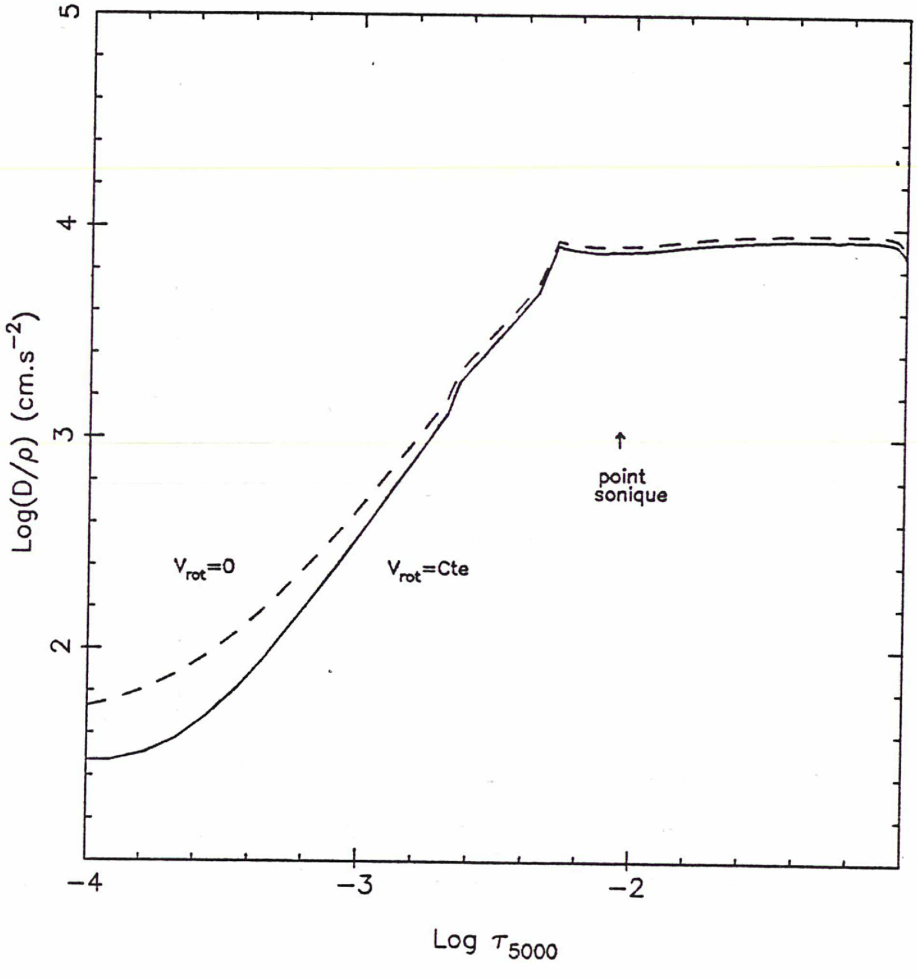

Plusieurs conclusions peuvent être tirées de cette figure:

- on remarque tout d'abord que la force centrifuge ne joue pratiquement aucun rôle à la base du vent, les deux solutions correspondant aux deux hypothèses extrêmes sur v_φ étant pratiquement identiques. Or, on sait que le taux de perte de masse est contrôlé par l'apport de quantité de mouvement dans la région subsonique (Holzer et MacGregor, 1985). Donc $\dot{M}$ ne sera pas modifié par l'introduction d'une force centrifuge réaliste, quel que soit le mécanisme envisagé pour la production du vent d'AB Aur.

- la force centrifuge n'est cependant pas forcément négligeable dans la partie supersonique du flot, comme en témoigne l'écart entre les deux courbes de la figure II-1. Etant donné que l'apport de quantité de mouvement dans les régions supersoniques contrôle la vitesse terminale du flot (Holzer et MacGregor, 1985), il n'est pas exclu que la force centrifuge joue un rôle important à ce niveau.

- l'accélération D/ρ est maximale vers la base du vent, et vaut environ $8\ 10^3$ cm s^{-2}, valeur proche de l'accélération gravitationnelle à la photosphère ($1.1\ 10^4$ cm s^{-2}). Il est donc clair que notre modèle semi-empirique est en contradiction avec un vent purement thermique, pour lequel on aurait $D/\rho \approx 0$. Cette contradiction est bien sûr due à l'absence de couronne dans le modèle semi-empirique. Une mince couronne pourrait éventuellement apporter la quantité de mouvement nécessaire à la base du vent, mais devrait être de faible étendue pour ne pas contredire les observations (raies de résonance de Mg II, de C IV, Hα,...). Or, la figure II-1 montre que la quantité D/ρ est importante sur une région étendue. On aurait donc toujours besoin d'un apport supplémentaire de quantité de mouvement dans les régions post-coronales. On en conclut que la pression thermique dans une mince couronne, si une telle couronne existe, ne constitue pas le seul mécanisme de production du vent d'AB Aur.

- enfin, on note que l'accélération D/ρ décroit vers l'extérieur. Ceci peut nous permettre de tirer des conséquences quant à l'adéquation du mécanisme de production de vent par pression de rayonnement. En effet, tous les modèles construits jusqu'à présent pour ce type de mécanisme (Castor et al., 1975; Weber, 1981; Leroy et Lafon, 1982; Migozzi, 1984; Pauldrach et al., 1986) conduisent à une accélération radiative qui croit vers l'extérieur. On peut facilement comprendre pourquoi dans le cadre de la théorie simplifiée de Castor et al. (1975). L'accélération radiative due à une raie spectrale forte est en effet obtenue par l'expression:

$$D_L / \rho = \frac{\pi F_\nu}{c} \frac{\Delta\nu_D}{\rho v_D} \frac{dw}{dr} \qquad \text{dans l'approximation de Sobolev} \qquad \text{(II-13)}$$

où F_ν est le flux de rayonnement dans le continu adjacent à la raie, c la vitesse de la lumière et $\Delta\nu_D$ la largeur Doppler de la raie. Si on suppose que $F_\nu \propto r^{-2}$ (milieu optiquement mince pour le rayonnement continu), on en déduit:

$$D_L/\rho \propto d(v^2)/dr$$

quantité qui a plutôt tendance à augmenter vers l'extérieur dans notre modèle, à l'endroit où D/ρ commence à décroitre. Pour une raie spectrale faible, par contre, la théorie de Castor et al. (1975) prévoit:

$$D_L / \rho = \frac{\pi F_\nu}{c} \Delta\nu_D \sigma_L \qquad \text{(II-14)}$$

où σ_L est la section efficace d'absorption (en $cm^2\ g^{-1}$) dans la raie. Avec la même hypothèse que précédemment sur F_ν , on obtient:

$$D_L/\rho \propto f r^{-2}$$

où f est la fraction (en nombre) de l'absorbant considéré. Il est donc plus aisé d'envisager une décroissance de D_L/ρ dans ce deuxième cas, en invoquant par exemple une fraction d'ionisation constante. Dans tous les modèles théoriques bâtis jusqu'à présent, les raies fortes jouent un rôle important dans la région d'accélération du flot, conduisant donc à une croissance de la force radiative vers l'extérieur.

D'autre part, la limite théorique du taux de perte de masse obtenu par ce mécanisme est:

$$\dot{M}_{max} = L / (v_\infty c)$$

où L est la luminosité de l'étoile, et v_∞ la vitesse terminale du flot (voir Cassinelli, 1979). Pour AB Aur, on en tire $\dot{M}_{max} < 3\ 10^{-9}\ M_\odot$/an, valeur inférieure au taux de perte de masse déterminé plus haut. Cependant, cette relation n'est valable que dans l'hypothèse où chaque photon n'est diffusé qu'une fois. On peut alors espérer augmenter cette limite supérieure en considérant les effets de la diffusion multiple des photons (Abbott et Lucy, 1985).

En résumé, bien que n'ayant pas d'argument définitif pour écarter cette théorie,

nous prévoyons qu'il sera très difficile de l'appliquer au vent d'AB Aur: les effets de diffusion multiple doivent nécessairement être pris en compte, et les raies spectrales faibles doivent avoir une contribution prépondérante à l'apport de quantité de mouvement.

8-2 Pertes radiatives:

L'évaluation des pertes radiatives est toujours un problème délicat. Une première méthode consiste à mesurer le flux dans certaines raies et continus, et à en déduire la perte d'énergie par rayonnement intégrée sur toute la région de formation des raies et continus considérés. Cette méthode n'est valable qu'en géométrie plane, et ne pourrait pas être utilisée dans notre cas. Pour s'en convaincre, il suffit de supposer que l'atmosphère étendue d'une ABH est en équilibre radiatif. Les pertes radiatives sont donc nulles. Or, de nombreuses composantes en émission apparaissent dans son spectre, du fait de l'extension de l'atmosphère. Une telle méthode conduirait donc à des pertes radiatives importantes.

Une autre méthode, plus complexe, mais bien plus sûre, utilise un modèle semi-empirique et la résolution directe de l'équation de transfert pour calculer les pertes radiatives. Dans ce cas, on peut estimer en tout point de l'atmosphère la perte d'énergie par rayonnement dans les transitions calculées. Cette méthode, utilisable quelle que soit la géométrie du problème, est donc supérieure à la méthode précédente, qui ne fournit que l'intégrale des pertes radiatives. Etant donnée sa complexité (nécessité de bâtir un modèle semi-empirique au préalable), elle n'a été employée que dans de rares cas, comme le soleil (Vernazza et al., 1981). Notre modèle semi-empirique nous permet de l'utiliser à notre tour.

La quantité d'énergie perdue par rayonnement à chaque altitude r peut s'écrire:

$$E^{-}(r) = 4\pi \int_0^{\infty} \chi_\nu \, (S_\nu - J_\nu) \, d\nu \quad (\text{en ergs.cm}^{-3}.\text{s}^{-1}) \qquad \text{(II-15)}$$

où χ_ν est le coefficient d'absorption (en cm^{-1}), J_ν l'intensité moyenne du rayonnement et S_ν la fonction source. Les pertes radiatives doivent être évaluées dans le référentiel du fluide, car l'équation d'énergie est une équation Lagrangienne (voir Mihalas et Mihalas, 1984, p.432). De plus, le référentiel du fluide est le seul dans lequel les propriétés de la

matière sont isotropes (opacité, émissivité), et calculer les pertes radiatives dans un autre référentiel n'aurait pas de sens.

E^- est une quantité difficile à évaluer, car elle est composée d'un grand nombre de contributions (raies, continus), où tous les effets hors ETL doivent être pris en compte. Nous ne présentons ci-dessous que quelques-unes de ces contributions, à savoir les raies et continus de l'hydrogène, ainsi que les raies de résonance de C III, C IV et Mg II.

Pour une raie, l'équation II-15 conduit à:

$$E^-(\text{raie}) = 4\pi \chi_L \Delta\nu_D (S_L - \bar{J}) \qquad \text{(II-16)}$$

où $\bar{J} = \int \phi_\nu J_\nu \, d\nu$ et $\chi_L = (\int \phi_\nu \chi_\nu \, d\nu) / \Delta\nu_D$

Pour un continu:

$$E^-(\text{continu}) = 4\pi \int_{\nu_0}^{\infty} \chi_\nu (S_\nu - J_\nu) \, d\nu \qquad \text{(II-17)}$$

où ν_0 est le seuil du continu en question.

Les figures II-2, II-3, II-4, II-5 montrent les pertes radiatives correspondant aux continus de l'hydrogène, aux raies de l'hydrogène (10 raies), et aux raies de résonance de C III, C IV et Mg II, respectivement, obtenues avec le modèle n°1 de l'Annexe D. Avec la convention de signe utilisée, une perte d'énergie est considérée comme positive. On constate que la contribution principale aux pertes radiatives est le continu de Balmer. Celui-ci contribue au chauffage à la base de la chromosphère, mais devient un radiateur très efficace dans la région du maximum de température. Les continus de Paschen et Brackett sont également de bons radiateurs sur toute l'étendue de la chromosphère. Notons que le continu de Lyman, trop opaque, contribue très peu aux pertes radiatives dans la chromosphère. Vers le haut de la chromosphère et dans la région post-chromosphérique, les pertes radiatives sont très petites, à cause de la faible densité de ces régions. Les pertes radiatives dues aux raies de l'hydrogène sont beaucoup moins importantes. On notera toutefois que Hα est un radiateur efficace à la base de la chromosphère. Il est intéressant de constater sur la figure II-4 que les raies de résonance de C IV contribuent si peu aux pertes radiatives. Ceci est dû à la faible population de cet ion.

Fig II–2 Pertes Radiatives Continus de H

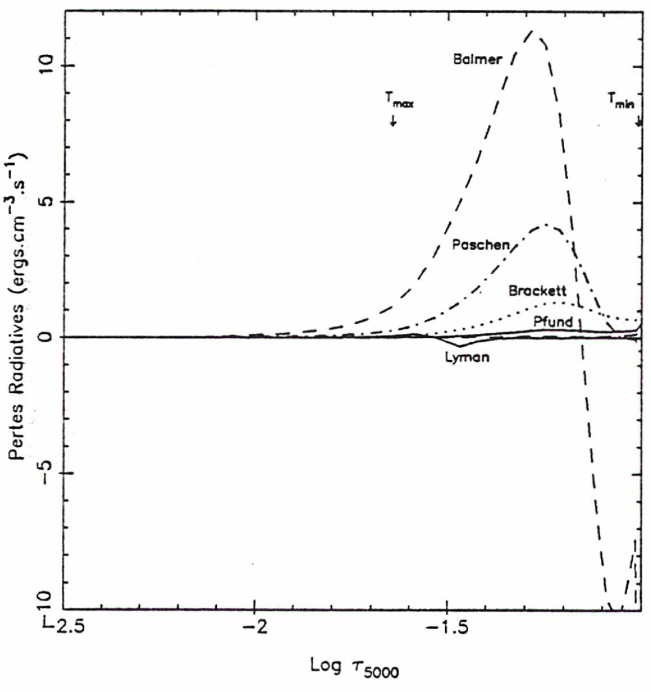

Fig II–3 Pertes Radiatives Raies de H

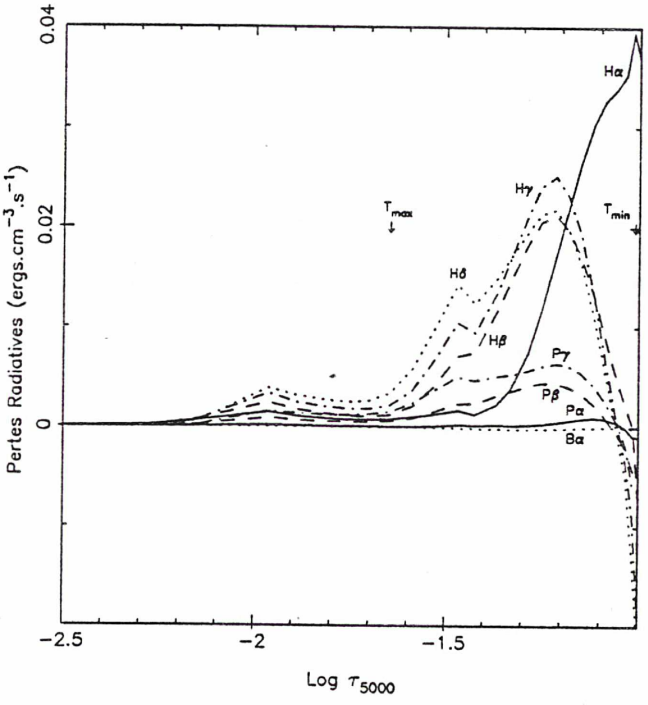

Fig II–4 Pertes Radiatives Raies de CIII–CIV

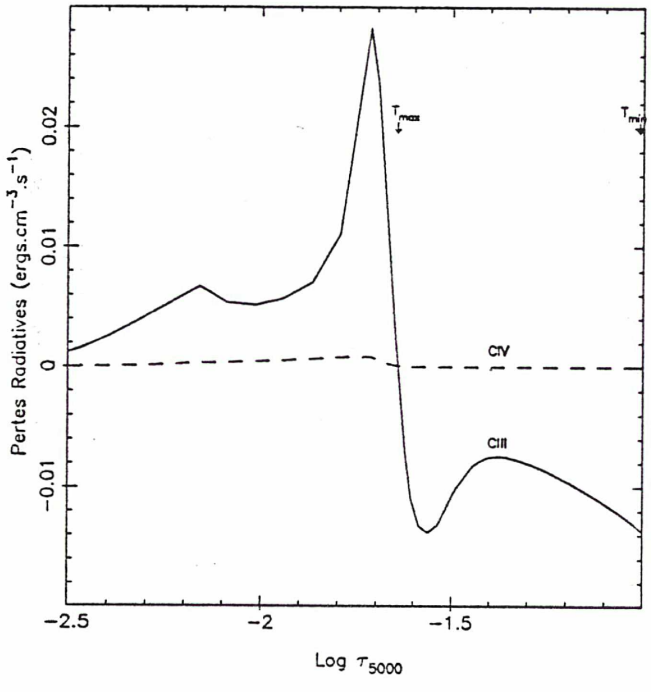

Fig II–5 Pertes Radiatives Raies de MgII

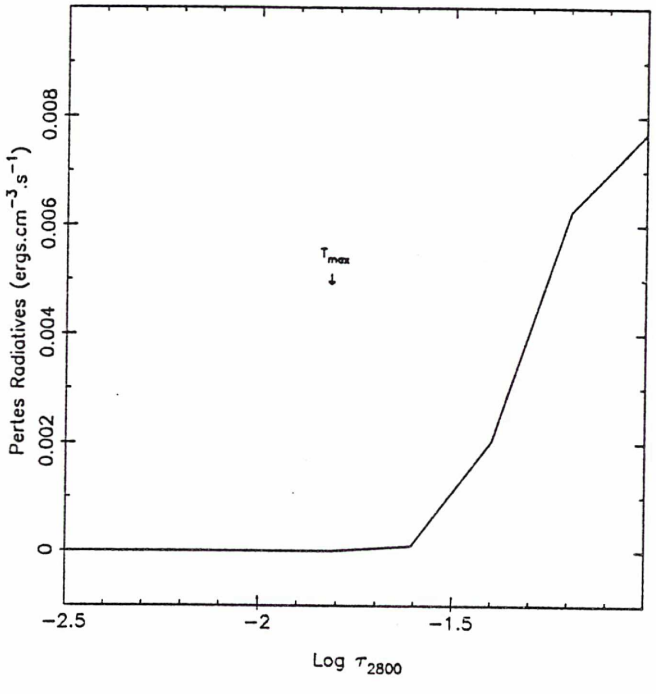

Il est important de calculer également la quantité totale d'énergie perdue par rayonnement dans la chromosphère pour chacune de ces transitions. Cette quantité s'exprime comme:

$$E^-_{tot} = \int_{chrom.} 4\pi r^2 \; E^-(r) \, dr$$

La table II-2 présente E^-_{tot} pour chaque transition, ainsi que le flux de densité d'énergie correspondant:

$$F^-_{tot} = E^-_{tot} / (4\pi R_*^2)$$

Les conventions de signe de la table II-2 sont les mêmes que celles des figures II-2 à II-5. Pour chaque transition, on a intégré les pertes radiatives à partir du minimum de température, jusqu'à la limite supérieure de la chromosphère. Cependant, pour les transitions fournissant un gain net d'énergie pour la matière à la base de la chromosphère (continu de Balmer par exemple), l'intégration a été démarrée seulement au point où les pertes radiatives deviennent positives

On aboutit à une perte totale d'énergie d'environ 2 10^{34} ergs s^{-1} dans la chromosphère pour les transitions considérées, ce qui représente environ 10% de la luminosité bolométrique d'AB Aur (tirée de Cohen et Kuhi, 1979). Cette valeur est considérable. A titre de comparaison cependant, notons que certaines étoiles T Tauri présentent des pertes radiatives (mesurées par la méthode "observationnelle" décrite au tout début de ce paragraphe) correspondant à quelques % de leur luminosité totale (Bouvier, 1987; Calvet et Albarran, 1984).

D'autre part, on peut montrer, grâce aux contraintes décrites dans ce chapitre, que l'intégrale sur toute la chromosphère du membre de gauche de l'équation II-12 reste inférieure à 4 10^{33} ergs s^{-1}. L'énergie nécessaire pour entretenir le vent est donc faible devant l'énergie à fournir pour contrecarrer les pertes radiatives.

Dans notre cas, seules quelques contributions aux pertes radiatives ont été calculées. Il est possible que les transitions non calculées (par exemple la raie K de Ca II) puissent conduire à un gain d'énergie aussi bien qu'à un surcroit de perte d'énergie. Intuitivement, on imagine cependant que le continu de Balmer restera toujours dominant, auquel cas les ordres de grandeur donnés plus haut seront toujours valables.

Table II-2

Transition	Pertes radiatives E^-_{tot} (ergs.s^{-1})	F^-_{tot} (ergs.cm^{-2}.s^{-1})
CIII ^{1}S-^{1}P°	9.7 (+31)	2.5 (+8)
CIV ^{2}S-^{2}P°	4.2 (+30)	1.1 (+7)
MgII ^{2}S-^{2}P°	1.1 (+31)	3.0 (+7)
Hα	1.1 (+32)	2.9 (+8)
Hβ	5.2 (+31)	1.4 (+8)
Hγ	5.5 (+31)	1.4 (+8)
Hδ	6.3 (+31)	1.6 (+8)
Pα	1.7 (+31)	4.4 (+7)
Pβ	2.1 (+31)	5.4 (+7)
Pγ	2.8 (+31)	7.3 (+7)
Bα	2.6 (+30)	6.8 (+6)
Bβ	5.0 (+30)	1.3 (+7)
Pfα	6.5 (+29)	1.7 (+6)
Lyman C	1.5 (+32)	3.9 (+8)
Balmer C	1.5 (+34)	3.9 (+10)
Paschen C	4.7 (+33)	1.2 (+10)
Brackett C	1.4 (+33)	3.6 (+9)
Pfund C	3.2 (+32)	8.3 (+8)
Humphrey C	6.7 (+31)	1.7 (+8)
TOTAL	2.2 (+34)	5.7 (+10)

9 - Conclusion:

L'analyse semi-empirique décrite dans ce chapitre nous a donné une vision d'ensemble de l'atmosphère d'AB Aur, et par là-même de celle des ABHs de la sous-classe "P Cygni". C'est ainsi que nous avons mis en évidence l'existence d'une chromosphère étendue de température modérée (≈ 17000 K), et que nous avons fortement contraint les paramètres des vents de ces étoiles.

Nous estimons avoir mené l'analyse semi-empirique des atmosphères des ABHs de la sous-classe "P Cygni" aussi loin qu'il était possible. Comme nous l'avons déjà signalé, tenter d'affiner le modèle représenterait une sur-utilisation de l'hypothèse de symétrie sphérique. Abandonner cette hypothèse n'est pas non plus une bonne idée dans

l'immédiat, car cela nous conduirait à bâtir des modèles complexes avec un très grand nombre de paramètres, qui ne seraient pas faciles à contraindre. Il est donc temps d'utiliser le modèle simple décrit dans ce chapitre pour tenter de comprendre les processus physiques responsables de la production du vent et du chauffage de la chromosphère. La construction d'un modèle hydrodynamique de l'atmosphère d'AB Aur constitue donc un volet de la suite à envisager pour cette étude.

Il reste bien sûr un certain nombre de questions sur la structure des atmosphères de ces étoiles. En particulier, le changement de structure responsable de la variabilité long terme détectée pour certaines de ces étoiles n'est pas clair à l'heure actuelle. Un effort sur le plan observationnel sera nécessaire dans les années à venir pour tenter de mieux cerner ce problème.

Le modèle semi-empirique que nous avons bâti s'étend jusqu'à environ 100 R_*. Les observations dans l'infrarouge montrent la présence de grains au-delà de cette distance (Catala, 1983a). L'interaction dynamique entre le vent et cette enveloppe de grains est encore à explorer. En particulier, elle pourrait jouer un rôle important dans la décélération du vent qui a été mise en évidence par des observations des raies D de Na I (Felenbok et al., 1983).

Enfin, certaines observations à venir pourraient modifier notre vision de l'atmosphère des ABHs. En particulier, si des observations X révélaient l'existence de couronnes minces (compatibles avec les observations dans le visible et l'UV), notre modèle semi-empirique devrait être révisé. Celui-ci est cohérent avec toutes les observations dont nous disposons à ce jour, mais il est possible que de futures observations nous apportent des surprises.

Astron. Astrophys. 154, 103–114 (1986)

ASTRONOMY AND ASTROPHYSICS

Spectral similarities in the visible and UV spectrum of Herbig Ae/Be stars

C. Catala[2,★,★★], J. Czarny[1,★,★★], P. Felenbok[1,★], and F. Praderie[2,★★★]

[1] Unité de recherche associée au CNRS 812, Observatoire de Paris, Section de Meudon, F-92195 Meudon Principal Cedex, France
[2] Unité de recherche associée au CNRS 264, Observatoire de Paris, Section de Meudon, F-92195 Meudon Principal Cedex, France

Received April 4, accepted July 2, 1985

Summary. The pre-main sequence Herbig Ae/Be stars can be divided into three subclasses, according to their Hα profile: the "double-peak" subclass, the "single-peak" subclass, and the "P Cygni" subclass. We address the question of whether the envelopes of the stars belonging to a same subclass are similar. Therefore, we have carried out high resolution spectroscopic observations of four members of the "P Cygni" subclass. In addition to Hα, we have found that Mg II resonance lines, the Ca II K line, the Ca II infrared triplet lines, and the Na I D lines have similar shapes in the spectra of these stars. Since these lines are formed in distinct regions in the envelopes of the stars, close to the photosphere for the Ca II lines, much farther out for the Na I D lines, and very extended region for Hα and the Mg II resonance lines, these similarities show that the envelopes of the stars of the "P Cygni" subclass have basically the same structure. We still have to figure out whether this structure is characteristic of a stage of evolution.

Key words: pre-main sequence stars – stellar winds – stellar chromospheres

1. Introduction

More than two decades ago, Herbig (1960) suspected the existence of stars of intermediate masses ($2-7\,M_{\odot}$), still in a pre-main sequence (PMS) stage of their evolution. He compiled a list of 26 candidates for this class, according to criteria pleading for their youth. A few years later, strong infrared (IR) excesses were discovered for several of these Herbig Ae/Be stars (Mendoza, 1966, 1967; Geisel, 1970; Gillett and Stein, 1971; Cohen, 1973a). A location in the HR diagram of 14 of them (Strom et al., 1972), then of a greater number (Cohen, 1973b; Cohen and Kuhi, 1979), placed them above the zero-age main sequence, a further argument in favor of their PMS nature.

The original list of 26 candidates given by Herbig has recently been extended to 57 objects by Finkenzeller and Mundt (1984). These authors have obtained high resolution profiles for the Hα lines of these presumed Herbig Ae/Be stars and have divided them in three subclasses:

(i) those showing a double-peak emission Hα line (50%),
(ii) those showing a single-peak emission Hα line (25%),
(iii) those showing a P Cygni profile at Hα (20%).

Only for the last subclass do we have a direct evidence of the presence of a stellar wind, although the Hα profiles for the other two subclasses can also be interpreted in terms of stellar winds. The differences in the Hα line profiles could be due to differences in the geometry of the extended atmospheres of these stars, or in their density, velocity or temperature structure. These different geometries or structures could in turn be the sign of different evolution stages.

If we want to give more credit to these speculations, two types of questions must now be addressed:

(i) is the Hα line profile really characteristic of a type of geometry or structure? In other words, do the Herbig Ae/Be stars showing similar Hα profiles exhibit the same kind of similarities in other lines?

(ii) if yes, what can be derived from the line profiles about the structure of the envelopes in which they are formed?

Detailed studies of one of the brightest Herbig Ae/Be stars, AB Aur, have been carried out in the recent past. Praderie et al. (1982) and Felenbok et al. (1983) have obtained high resolution profiles for a number of lines for this star, thus providing a fairly complete spectral coverage. This spectral coverage turned out to be essential in providing quantitative information about the structure of AB Aur's envelope (Felenbok et al., 1983; Catala et al., 1984).

AB Aur belongs to the subclass of Herbig Ae/Be stars showing P Cygni profiles at Hα. The further step to be taken in this study is then to see if the global picture that has been derived for the structure of AB Aur's envelope can apply to the other stars of its subclass. In other words, we need to know if the other Herbig Ae/Be stars of the same subclass exhibit the same spectral features as AB Aur. For this purpose, we have carried out a series of high resolution spectroscopic observations for three other stars of this subclass, obtaining for two of them a spectral

Send offprint requests to: P. Felenbok

★ Visiting Astronomer, Canada-France-Hawaii Telescope operated by the National Research Council of Canada, the Centre National de la Recherche Scientifique of France, and the University of Hawaii.

★★ Visiting Astronomer, Observatoire de Haute-Provence, operated by the Centre National de la Recherche Scientifique of France.

★★★ Guest Observer on the International Ultraviolet Explorer (IUE) at the Villafranca Tracking Station of the European Space Agency

coverage as complete as it is for AB Aur. The instruments we used are the International Ultraviolet Explorer (IUE) for the ultraviolet (UV) range, the Canada-France-Hawaii (CFH) 3.60 m telescope and the 1.52 m telescope of the Observatoire de Haute-Provence (OHP) for the visible range.

Section 2 is devoted to a brief description of the observations and the data reduction. In Sect. 3, the line profiles are presented and compared. We have also tried to make explicit the information that can be derived from the similarities or the differences between the lines. General conclusions are given in Sect. 4.

2. Observations and data reduction

2.1. Ground-based observations

All the observations in the visible and near IR wavelength range were made with the coudé equipment resp. of the CFH 3.60 m telescope at Mauna Kea and of the OHP 1.52 m telescope. The log of these observations is given in Table 1, as well as the resolution (FWHM) of the spectra.

At the CFH 3.60 m telescope, the detector was a cooled RL 1872*F*/30 Reticon with $15\mu \times 750\mu$ pixels. Due to the good performances of the Reticon ($450e^-$ of read-out noise) and to the high elevation of the Mauna Kea site (4200 m), the long exposures (≥ 1 h) are contaminated by cosmic rays giving narrow spikes randomly distributed on the spectra. Moreover, the spectrum of HD 150193 in the region of the Ca II IR triplet (see Fig. 4) has been contaminated by a small remanance of the Th/Ne calibration lamp. This contamination has been removed during data reduction. All reduction technics have been fully described previously (Felenbok et al., 1983).

At the OHP 1.52 m telescope, the detector was an electronographic Lallemand camera. The echelle spectrograph of the coudé equipment was used in its monoorder configuration. Due to the smaller size of the telescope, the lower sensitivity of the detector at Hα, and the poorer weather conditions, the Hα spectra obtained at OHP are noisier than those obtained at CFH (also water vapor lines contaminate the Hα lines obtained at OHP, see Fig. 2b and 2c). However, these drawbacks do not affect the conclusions reached below. The OHP spectrograms were scanned with a PDS microdensitometer at the Institut d'Optique (Orsay, France), and the data reduction procedure was the same as the one used for the CFH Reticon spectra.

2.2. IUE observations

The observations in the UV range have been obtained in the high resolution (0.2 Å), large aperture, long wavelength mode of IUE. The log of the observations is given in Table 1. The fluxes in the spectral region of the Mg II lines were derived from the 3rd file of the GO tape. Except for the Jan. 82 spectrum of HD 250550, no further correction has been introduced for background removal, since the standard extraction procedure does not introduce important errors in the region of the Mg II resonance lines. The ripple-correction was applied using the formulae and coefficients given by Ake (1982) for the LWR images and by Cassatella (1984) for the LWP images. In the case of the Jan. 82 spectrum of HD 250550, a few pixels were saturated at the top of the emission component of the Mg II k line. In order to recover the flux at the top of the emission, we have reextracted the spectrum with the FASMII software developed at Paris-Meudon Observatory (Borsenberger, internal report). This software starts from the photometrically corrected IUE image and fits each cross-section (perpendicular to the dispersion) with a set of gaussians representing the different orders and a polynomial representing the background. For the three stars, the continuum has been placed interactively in two line-free spectral regions (2758 and 2844 Å). The wavelength scale has been set with reference to the interstellar Mg I λ 2852.13 Å, which appears on the three spectra. The Mg II lines of AB Aur and HD 250550 have already been

Table 1. Log of observations

Stars		HD 250550	AB Aur	BD + 46°3471	HD 150193
Lines	Resolution ($km.s^{-1}$)	Date; Exposure Time (mn); S/N[a] at continuum			
Mg II	21	Jan. 82; 395; 19 (LWR 12395) Jan. 84; 236; 13 (LWP 2663)	Jan. 81; 30; 21 (LWR 9790)	Jan. 83; 860; 12 (LWP 1768)	
Hα	10 (CFHT) 25 (OHP)	Sep. 83; 68; 90 Jan. 84; 270; 20	Sep. 83; 19; 120 Jan. 83; 200; 50	Sep. 83; 120; 90 –	Jul. 84; 60; 60 –
Ca II K	10	Oct. 83; 110; 180	Oct. 82; 60; 90	Sep. 83; 160; 50	–
Ca II IR[b]	9	Sep. 83; $\frac{110}{60}$; 65	Sep. 83; $\frac{31}{33}$; 200	Sep. 83; $\frac{110}{145}$; 140	Jul. 84; $\frac{110}{80}$; 180
He I + Na D	10		Jan. 81[c]; 60; 85	Sep. 83; 90; 60	Jul. 84; 96; 130

[a] S/N defined as the ratio of mean value over RMS in a 50 pixel range.

[b] The Ca II IR spectrum needs two exposures to cover the three Ca II lines. The upper one is centered at 8540 Å and the lower one at 8630 Å.

[c] Spectrum taken for us by G. Cayrel

published (Talavera et al., 1982), as well as a first spectrum of BD + 46°3471, of very bad quality. The spectrum of the latter star that we present here has been obtained with a "deep" exposure of 860 min thus increasing considerably the signal/noise ratio.

2.3. Measurement procedure

For each line presented in this paper, we have measured, when it was possible, the equivalent widths of the different components, their positions and their full widths at half maximum. The mean accuracy of the measurements is ± 5 mÅ for the equivalent widths and ± 1 km.s^{-1} for the positions and the full widths at half-maximum.

The equivalent width of each component has been defined as the area between the spectrum, the $F/F_c = 1$ base and vertical lines containing the boundaries of the component, as is schematically shown on the right side of Fig. 2*d*.

The velocity of each component, measured at its center, is given in the LSR frame, for practical reasons. In order to obtain the velocities in the heliocentric frame, one must add 13.8 km.s^{-1} for HD 250550, 9.2 for AB Aur, -13.8 for BD + 46°3471 and -11.1 for HD 150193.

For the Mg II resonance lines, we have measured the maximum blueward displacement of the absorption component (v_s), by extrapolating the blue wing of the line up to the $F/F_c = 1$ base, as shown on the top panel of Fig. 1a. Note that all the velocities corresponding to the Mg II lines are not given in the LSR frame, but in a wavelength frame defined with respect to the interstellar Mg I 2852.13 Å line. Thanks to the work of Felenbok et al. (1983) and Finkenzeller and Jankovics (1984), who have shown that these stars move with the same radial velocity as their local interstellar medium, we can consider that the frame defined by this line is the star center reference frame.

2.4. The star sample

The stars have been selected from the Herbig Ae/Be star catalog of Finkenzeller and Mundt (1984) on the basis of a P Cygni profile at Hα and a V magnitude lower than 11, in order to obtain good quality spectra with integration times not exceeding 2 hours in the visible. Because of the general faintness of Herbig Ae/Be stars, only four stars visible from CFH could be selected. Some physical parameters of these four stars are given in Table 2. Note that their spectral types span the range *A*0–*A*4.

3. The lines profiles

3.1. Mg II resonance lines

The Mg II h and k lines for the three stars we have observed are shown in Fig. 1a. All the measures corresponding to these lines are given in Table 3. The profiles are globally identical for the three stars, namely type IV P Cygni profiles, according to Beals' classification (Beals, 1951). In particular, the relative strength of the absorption component with respect to the emission component is more or less the same for the three stars. Another important similarity is the redward displacement of the emission component, which is not very different for the three stars. Catala et al. (1984) have quantitatively interpreted the Mg II resonance

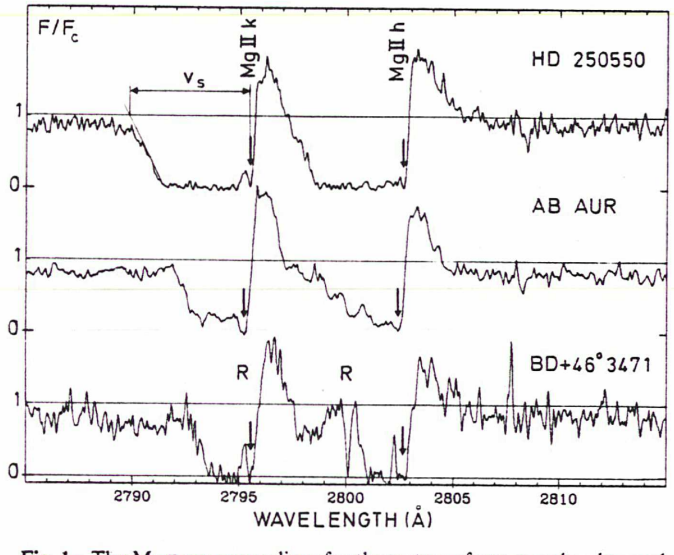

Fig. 1a. The Mg II resonance lines for three stars of our sample, observed by IUE. The wavelength scale is set with respect to the interstellar Mg I 2852.13 Å line. On the spectrum of BD + 46°3471, the "*R*"s indicate the position of reseau marks. The vertical arrows indicate the narrow components described in Table 3 and discussed in the text. On the spectrum of HD 250550, we have indicated how v_s has been measured. The differences in v_s from star to star are clearly seen. Note that the absorption components are saturated in HD 250550 and BD + 46°3471 and not in AB Aur. The spectrum of AB Aur is from Praderie et al. (1982)

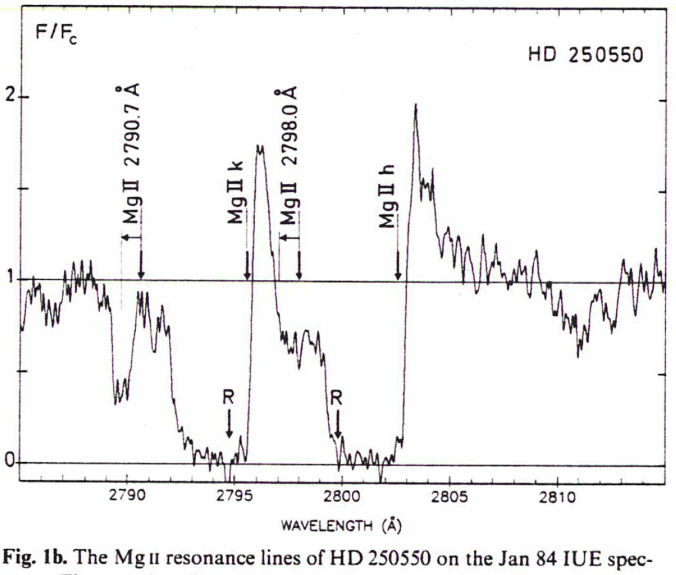

Fig. 1b. The Mg II resonance lines of HD 250550 on the Jan 84 IUE spectrum. The wavelength scale is set with respect to the interstellar Mg I 2852.13 Å line. The two vertical arrows indicate the rest wavelength of the Mg II subordinate lines $\lambda\lambda$ 2790.7 and 2798.0 Å. Note the blue shift of the λ 2790.7 Å line. The variability of the absorption component of the resonance lines is clearly seen

Table 2. Physical parameters of the observed stars. The bracketted numbers indicate the references from which the parameters have been taken

Star	m_v	S.T.	$\log L/L_\odot$	$M/M_\odot$	d (pc)	V_R (km.s^{-1}) heliocentric	vsini (km.s^{-1})
HD 250550	9.1 (8)	A0e (6)	2.2 (4)	2.9 (1)	700 (1)	+31 (5)	110 (6)
AB Aur	7.1 (8)	A0Ve (6)	1.9 (4)	2.8 (1)	160 (2)	+21 (5)	75 (3) 140 (6)
BD + 46°3471	10.1 (8)	A4e (6)	2.1 (4)	2.6 (1)	960 (7)		150 (6)
HD 150193	9.2 (8)	A4e (6)					100 (6)

References: (1) Cohen (1973). (2) Cohen and Kuhi (1979). (3) Davis et al. (1983). (4) Finkenzeller and Mundt (1984). (5) Finkenzeller and Jankovics (1984). (6) Finkenzeller (1985). (7) Roger and Irwin (1982). (8) Catalog of Stellar Identification, issued by CDS, Strasbourg

Table 3. Mg II k line λ 2795.5 Å

Star	Component	F/F_c		FWHM (km.s^{-1})		W_λ (Å)		Position/IS Mg I (km.s^{-1})		
		Em.	Abs.	Em.	Abs.	Em.	Abs.	Em.	Abs.	v_s
HD 250550	Main	1.7	0.0	113	541	0.65	4.9	79		−607
	Narrow		0.0		22				−6	
AB Aur	Main	1.9	0.2	115	308	1.0	2.6	69		−403
	Narrow		0.0		51				−39	
BD + 46°3471	Main	1.8	0.0	99	293	0.7	2.6	113		−320
	Narrow		0.0		48				−2	

lines of AB Aur, and have shown that this displacement measures the broadening of the Mg II lines intrinsic profile, which would then be the same for the stars of our sample. This broadening had been found to be 45 km.s^{-1} for AB Aur.

They have also shown that the region of formation of the Mg II resonance lines in AB Aur extends from the photosphere up to about 50 stellar radii. Because of the large size of this region of formation, we can only expect an "integrated" information about the structure of the envelopes from the Mg II h and k lines. The similarity of the three profiles of Fig. 1a means that the basic conclusions reached by the quantitative analysis of AB Aur's Mg II resonance lines (Catala et al., 1984) can also be applied to the other two stars. Thus, following this analysis, we can infer from the observations the presence of a deep extended chromosphere at the base of the wind of these stars. More precise information about the structure of these chromospheres (temperature, size), as well as about the mass loss rates, can be obtained from a detailed quantitative interpretation of the Mg II resonance lines and of the other observed lines, following the same steps as for AB Aur, but this work is beyond the scope of the present paper.

Several differences can be noted in the Mg II resonance lines of Fig. 1a, though.

A first difference concerns the measured maximum blue-shift of the absorption component (v_s), displayed in Table 3. These values of v_s correspond to the maximum velocities reached in the winds of these stars. The comparison of these values shows us that the velocities of these winds somewhat differ from star to star.

The Mg II resonance lines are saturated (i.e. the absorption component reaches zero intensity) in HD 250550 and BD + 46°3471, and are not saturated in the spectrum of AB Aur shown here. However, other IUE spectra of AB Aur, obtained for the study of its variability, show that its Mg II resonance lines are saturated most of the time (see Praderie et al., 1984). All our observations of AB Aur have shown that its Mg II h and k lines, as well as its Fe II lines, are highly variable on different time scales. The same kind of variability can be expected for the other stars, but the study of this variability would require a large number of observing hours, and the present paper does not intend to report on preliminary results. However, we must keep in mind the existence of this variability when comparing the stars with each other or different lines of a single star, observed at different epochs.

As has been shown by Lucy (1982), the saturation of the absorption component of the Mg II resonance lines, and in particular the one observed in HD 250550, is very difficult to explain in terms of a spherically symmetric wind, with a monotonically increasing velocity law, because of the unavoidable forward scattering of the photons, which tends to fill in the absorption component. However, such a saturation can be obtained if there are

several resonance regions for each observed frequency on the line of sight. Large scale inhomogeneities in the line formation region could produce this effect. The scale for these inhomogeneities must be larger than the characteristic scale for the line transfer, which is of the order of one stellar radius. In terms of this interpretation, HD 250550 would have the most inhomogeneous wind among the three stars. Different mechanisms can be invoked to explain this kind of inhomogeneities: they can be generated by the presence of shocks, as proposed by Lucy (1982) for the winds of hot stars, or by the "solar-wind type" model proposed by Catala (1984) and by Praderie et al. (1985) for the wind of AB Aur, involving a structure of slow and fast streams corotating with the star and thus accounting for the periodic aspects of the variability found in AB Aur.

Our observations then suggest that these inhomogeneous flows are a common characteristic of the "P Cygni" subclass of the Herbig Ae/Be stars, as well as the presence of a deep and extended chromosphere at the base of their winds.

On the spectrum of HD 250550, the Mg II k line emission component is less intense than the one of the h line, which is puzzling since the k line has the highest oscillator strength. However, this behavior can be explained by a blend of the k line emission component with the h line absorption component and the λ 2798 Å subordinate line of Mg II. On another IUE spectrum of HD 250550, taken by us in Jan. 84, the λ 2791 Å subordinate line of Mg II is clearly visible, and shifted by 0.9 Å to the blue (see Fig. 1b). The same shift can be expected for the λ 2798 Å line, which would then contaminate the k line emission component. This important blueward shift (95 km.s^{-1}) implies that the Mg II subordinate lines are not photospheric. A blueward shift of 140 km.s^{-1} is present for the Fe II lines on this spectrum. Note that on the Jan 84 spectrum of HD 250550, the k line emission component is still less intense than the h line emission, and that there is no saturated pixel. A comparison of the two spectra of HD 250550 shows that the Mg II resonance lines are highly variable in this star, mainly in the value of the maximum velocity (v_s) reached by the wind.

Finally, we notice that the narrow components in the Mg II h and k lines (depicted by arrows in Fig. 1a) have a very low velocity in HD 250550 and BD + 46°3471, and can be considered as interstellar, while the ones of AB Aur have a velocity of -39 km.s^{-1} relative to the frame defined by the Mg I resonance line. However, for the time being, we are unable to decide whether this Mg I line rather than the Mg II lines is of interstellar origin.

3.2. *Hα line*

The Hα lines of the 4 stars of our sample are shown in Fig. 2. Characteristic quantities measured on the spectra are displayed in Table 4. The Hα profiles of the "P Cygni" subclass stars are of course globally similar, by definition of the subclass. The comparison of the Hα lines of AB Aur and HD 250550 taken at different dates confirms the variability of these stars. The variability of the Hα lines is further asserted by a comparison of the spectra shown in the present paper with those of Finkenzeller and Mundt (1984), Felenbok et al. (1983) and Garrison and Anderson (1977). The detailed study of this variability is delayed to a subsequent paper. Here again, we must be aware of this variability when

Table 4. Hα λ 6562.8 Å

Star	Date	Component	F/F_c		FWHM (km.s^{-1})		W_λ(Å)		Position/LSR (km.s^{-1})	
			Em.	Abs.	Em.	Abs.	Em.	Abs.	Em.	Abs.
HD 250550	Sep. 83	1		0.63		101		0.81		−407
		2		0.55		101		1.05		−240
		3		0.88		14		0.06		−102
		4	9.41		219		42.10		68	
HD 250550	Jan. 84	1	1.48		91		1.24		−303	
		2		0.75		140		0.74		−172
		3	7.46		185		29.90		103	
AB Aur	Jan. 83	1		0.88		21		0.07		−248
		2	1.61		39		0.77		−176	
		3	8.75		182		33		49	
AB Aur	Sep. 83	1		0.66		34		0.77		−359
		2		0.57		46		0.80		−257
		3	7.32		203		32.2		42	
BD + 46°3471	Sep. 83	1	1.03		28		0.02		−314	
		2		0.68		92		0.56		−225
		3	3.62		227		12.90		61	
HD 150193	Jul. 84	1	1.24		38		0.24		−138	
		2		0.69		44		0.29		−75
		3	3.39		135		7.58		50	

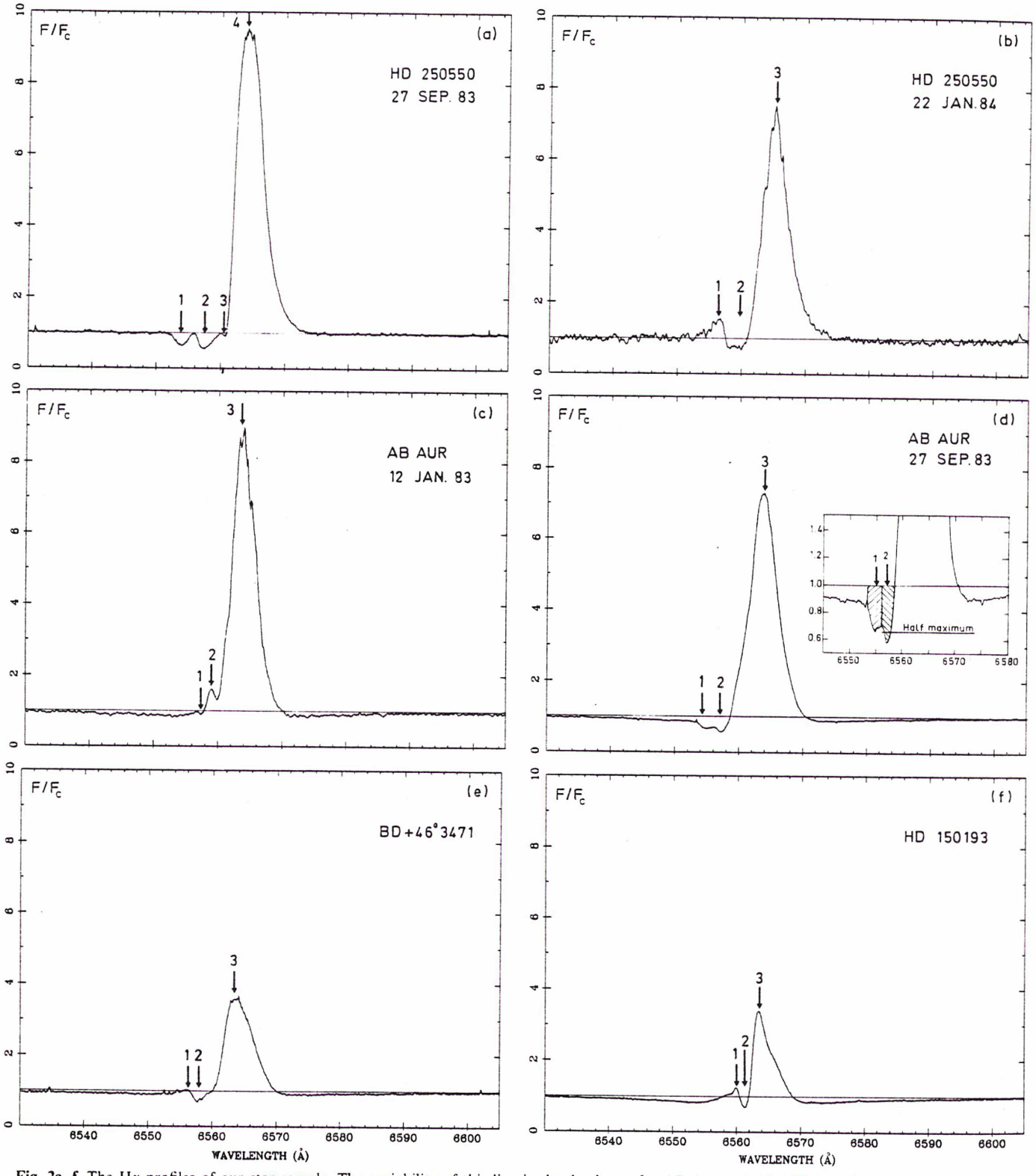

Fig. 2a–f. The Hα profiles of our star sample. The variability of this line is clearly shown for AB Aur and HD 250550. The arrows are pointing components described in Table 4. The measurement procedure is indicated in **d** insert. The wavelength scale is set with respect to LSR

comparing the stars with each other. In particular, since one can imagine a shift from one profile type to another for a given star, the classification of the Herbig Ae/Be stars into three subclasses from their Hα profiles could be considered as hazardous. However, taking into account all the Hα profiles we observed (most of them yet unpublished), and those available in the literature, we did not notice any subclass shift, except for HD 163296, which is not embedded in an obscured region, and cannot therefore be considered as a "full" Herbig star (Thé et al., 1985).

The region of formation of the Hα line in this type of stars is likely to be very extended. Preliminary results of a detailed computation of this line in the wind of AB Aur show that it extends from the photosphere up to 30 stellar radii (Catala and Kunasz, 1985). As for the Mg II lines, the similarity of the Hα profiles is then the sign of an "integrated" resemblance of the envelopes of these stars.

Figure 2 shows that all the observed stars exhibit at times a small emission component on the blue edge of their Hα line, typical of type III P Cygni profiles, according to Beals' classification (Beals, 1951). Several interpretations of this type of profile can be found in the literature, or imagined.

(i) Wagenblast et al. (1983) suggest that it could be formed in a geometrically thin shell around the star, provided several conditions on the velocity law, the source function and the absorption coefficient are fulfilled. This explanation seems unlikely in the case of AB Aur, HD 250550 and BD + 46°3471, although the presence of such a shell in these stars would be consistent with the observation of narrow absorption components in the Ca II K line (see Fig. 3) and in the Na I D lines (see Fig. 5). The main contribution to the Hα lines of these three stars indeed comes from the region which is also responsible for the Mg II resonance lines, as the computations have shown. It would be impossible for a geometrically thin shell to produce the broad and almost saturated absorption components of the Mg II lines seen in Fig. 1. Moreover, the shells suggested by the observation of the Na I D lines and/or the Ca II K line of the 4 stars would have velocities which do not match the velocities of the absorption components of the Hα line (see Tables 4, 5 and 7). The differences are so important that they cannot be due to a variability of the shell velocities (except may be for HD 150193). This shows that the Hα lines are not formed in these hypothetical thin shells, at least for three stars out of the four of our sample.

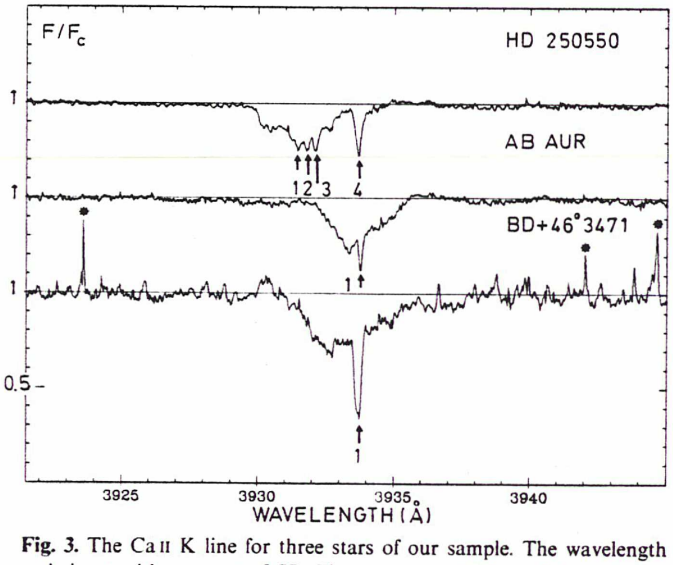

Fig. 3. The Ca II K line for three stars of our sample. The wavelength scale is set with respect to LSR. The spectrum of BD + 46°3471 is contaminated by cosmic rays (*), due to the long exposure. The narrow components described in Table 5 and discussed in the text are indicated by arrows

(ii) Another interpretation is given by Mihalas and Conti (1980). They suggest that type III P Cygni profiles are formed in envelopes combining rotation and expansion. In their interpretation, the inner parts of the envelope (radial distance smaller than Alfvèn radius) are corotating with the star, while expansion dominates in the outer regions. In this case, the blue emission peak on the P Cygni profile has a higher velocity than the projected rotational velocity (vsini) of the photosphere. Values of the projected rotational velocities for the Herbig Ae/Be stars have recently been obtained by Finkenzeller (1985). From his results and from Table 4, we can conclude that this interpretation may be valid for AB Aur (vsini = 140 ± 30 km.s^{-1}), HD 250550 (vsini = 110 ± 40 km.s^{-1}), BD + 46°3471 (vsini = 150 ± 30 km.s^{-1}) and HD 150193 (vsini = 100^{+20}_{-30} km.s^{-1}). It should be noted here that previous determinations of the rotational velocity of AB Aur had given different results: vsini ≤ 90 km.s^{-1} (Praderie et al., 1982) and vsini = 75 km.s^{-1} (Davis et al., 1984). These values do not affect the validity of the interpretation given above.

(iii) This type of profile can also be obtained in an envelope where a cool decelerated wind surrounds a hot expanding chromosphere. A "normal" P Cygni profile is then "dug" into the broad emission line produced by the chromosphere. A remote decelerated region is present in AB Aur (Felenbok et al., 1983), but its existence is not proved for the other stars of our sample, so the latter interpretation could be invalid. Moreover, it cannot simply explain the successive appearance and disappearance of the blue emission peak, since in this model the velocity in the chromosphere is always higher than the velocity in the outer regions.

(iv) The same kind of profile can also be produced if a hot region, in which turbulent motions, or organized motions (e.g. loops) of high velocity are present, is surrounded by a cooler accelerated region. The condition to be fulfilled is that the maximum expanding velocity in the line formation region must remain smaller than the mass motion velocity in the hot region. In this interpretation, the successive appearance and disappearance of the blue emission peak can be explained by a variation of the velocity law in the cool region where the wind velocity would be successively higher and smaller than the mass motion velocity in the hot region. This kind of velocity variation in the outer region can have the same effect on the Hα profile in the framework of interpretation (ii).

We notice a difference in the intensities of the emission components of the Hα line of the stars of our sample. This is probably due to differences in the mass loss rates for the different stars. In the computations of Hα in the wind of AB Aur, this line turned out to be extremely sensitive to the mass loss rate $\dot{M}$, but the results showed that the intensity of the emission is not necessarily a monotonic function of $\dot{M}$, if the temperature gradient is large in the line formation region (Catala and Kunasz, 1985). This means that the star having the most intense Hα line is not necessarily the one having the highest mass loss rate. However, out data suggest a correlation between the intensities of the emission component of the Mg II resonance lines and the Hα line.

But we know that the Hα line and the Mg II resonance lines are variable in these stars. We must then not give too much weight to this correlation, since all these lines have not been observed simultaneously. For the same reason, we must avoid to draw any conclusion about the velocity law by simply comparing the maximum blueward displacements of the absorption components of the Hα line and of the Mg II resonance lines.

A striking feature in Fig. 2 is the absence of photospheric wings in the Hα line of HD 250550, on both spectra (Sept. 83 and Jan. 84). Photospheric wings are also absent on the spectrum published by Finkenzeller and Mundt (1984), taken in Nov. 81. We also note that the Hα wings in BD + 46°3471 are very weak. The absence of photospheric wings in the Hα line of HD 250550 is puzzling since they are present in the other Balmer lines (see Finkenzeller and Jankovics, 1984). A possible explanation would be that the wings of Hα and the continuum at 6562 Å are formed in an almost isothermal region above the photosphere (at a temperature minimum for example), while the other Balmer line wings and their adjacent continua are formed deeper into the photosphere. HD 250550 could then have the same temperature structure than the other observed stars, but a higher density in the wind (higher mass loss rate) would move the region of formation of the Hα wings and of the continuum at 6562 Å away from the photosphere. However, a crude calculation showed that the ratio of the depths of formation (in a τ_{5000} scale) of the wings of Hβ and of Hα at 10 Å from the line center and the ratio of the depths of formation of their adjacent continua (4861 and 6562 Å) are only respectively about 1.7 and 2.5. The data for Stark broadening of Hα and Hβ were taken from Vidal et al. (1973). These values show that the two regions of formation are not very far away from each other, therefore this interpretation would imply a very specific temperature run in these regions and a very specific value for the mass loss rate. Anyway, this argument is not sufficient to discard this explanation.

Finally, we notice that HD 250550 is also the star showing at times the most complex structure in its Hα lines. This complex structure is probably the sign of important inhomogeneities in the envelope of this star, which is also qualitatively consistent with the Mg II resonance lines being completely saturated on a wide range of wavelengths (Sect. 3-1).

3.3. Ca II lines

The Ca II K lines for the three observed stars are shown in Fig. 3 and the lines of the Ca II IR triplet for the four stars of our sample can be seen in Fig. 4. The measurements corresponding to these lines are given in Tables 5 and 6. The general outlook is the same for the three stars. The Ca II K line is in absorption and asymmetric and exhibits a narrow component at very low velocity, on which we will come back in Sect. 3-6, while the Ca II IR triplet is in emission. Note here that the P14 line (λ 8598 Å) appearing on the same spectra as the Ca II IR triplet gives an idea of the intensities of the P13, P15 and P16 lines which are blended with the Ca II IR triplet lines. These intensities are in any case too low to be responsible for the emission lines of Fig. 4, which can then be attributed without any doubt to the Ca II IR triplet. Here again, we note a trend for the intensities of the

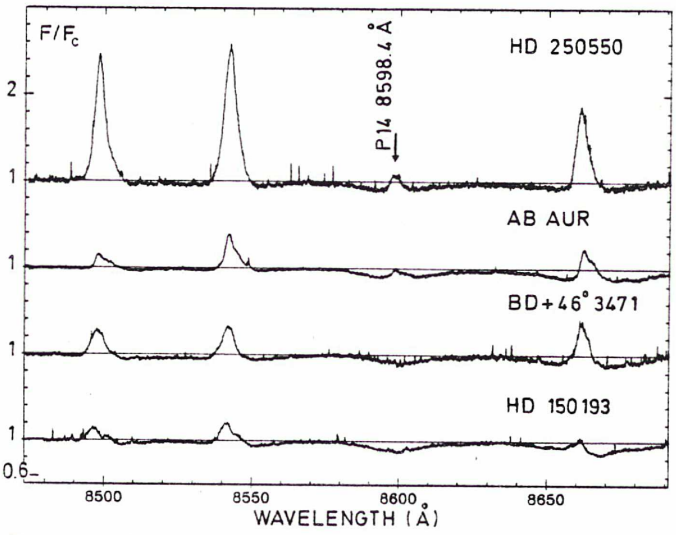

Fig. 4. This figure shows the Reticon tracings in the Ca II IR spectral range. The Ca II IR lines look alike for the four stars of our sample, but the P14 line (arrow) shows an emission component in HD 250550 and AB Aur and does not in BD + 46°3471 and HD 150193. The wavelength scale is set with respect to LSR

Table 5. Ca II K – λ 3933.6 Å

Star	Component	F/F_c	FWHM (km s^{-1})	W_λ(Å)	Position/LSR (km s^{-1})
		Abs.	Abs.	Abs.	Abs.
HD 250550	1	0.75	14	0.009	−168
	2	0.75	12.5	0.012	−143
	3	0.75	12	0.022	−119
	4	0.73	17	0.064	1.2
AB Aur	main	0.71	140	0.482	−6.0
	1	0.62	10	0.036	6.2
BD + 46°3471	main	0.69	218	0.909	−32
	1	0.36	19	0.151	2.9

Table 6. Ca II IR lines

	λ 8498.0				λ 8542.1				λ 8662.1			
	F/F_c	FWHM ($km.s^{-1}$)	W_λ (Å)	Position ($km.s^{-1}$)	F/F_c	FWHM ($km.s^{-1}$)	W_λ (Å)	Position ($km.s^{-1}$)	F/F_c	FWHM ($km.s^{-1}$)	W_λ (Å)	Position ($km.s^{-1}$)
HD 250550	2.5	137	6.9	6	2.6	237	8.2	13	1.9	139	3.8	11
AB Aur	1.2	114	0.6	25	1.4	204	1.7	21	1.2	100	0.8	24
BD + 46°3471	1.3	164	1.4	−11	1.3	211	1.5	−6	1.4	130	1.5	−6
HD 150193	1.1	135	0.7	−56	1.2	227	0.9	−25	1.1	37	0.1	−32

Ca II IR triplet to correlate with the intensities of the emission component of the Hα line and of the Mg II lines, although the Ca II IR lines of BD + 46°3471 seem to be too intense with respect to those of AB Aur. A similar correlation is also suggested for the Pl4 line, which does not exhibit a central emission in BD + 46°3471 and HD 150193, while it does in HD 250550 and AB Aur.

The Ca II lines are formed at the base of the wind, in a more localized area than the Mg II resonance lines or the Hα line. Calcium indeed is about 10 times less abundant than magnesium, and Ca II is more easily ionized to Ca III than Mg II to Mg III in the typical conditions of the studied stars. In the models of the envelope of AB Aur built by Catala et al. (1984), the ratio Mg II/Ca II is ~200 in the chromospheric region (T_e = 15000 K, $n_e = 10^{11}\,cm^{-3}$), and ~1000 in the photosphere (T_e = 10000 K, $n_e = 10^{14}\,cm^{-3}$) and in the outer regions (T_e = 5000K, $n_e = 10^{7}\,cm^{-3}$). The Ca II lines are then likely to be formed in denser regions than the Mg II resonance lines, namely at the base of the wind and the chromosphere. The similarity of the profiles of the Ca II K line for 3 stars (Fig. 3) and of the Ca II IR triplet for 4 stars (Fig. 4) suggests the similarity of the structure of the stellar envelopes in these fairly deep regions.

Here again, HD 250550 is peculiar, to some extent. The very complex structure of its Ca II K line, as well as the fact that the line is globally shifted to the blue, might be interpreted as the sign of important inhomogeneities at the base of its wind (i.e. successive dense and diffuse regions on the line of sight). The wind of HD 250550 is then probably inhomogeneous from the photosphere up to the outer parts of the region of formation of Hα and of the Mg II resonance lines. The base of the wind of the other observed stars could be inhomogeneous, too, on a smaller spatial scale, as witnesses the variability of the Ca II K line of AB Aur (Praderie et al., 1982, 1983; Catala et al., 1985).

Finally, the fact that the Ca II K line is in absorption, while the Ca II IR triplet is in emission can be easily explained by the presence of a chromosphere (see Felenbok et al., 1983).

3.4. He I 5876 Å line

The presence of a chromosphere at the base of the winds of the "P Cygni" subclass is also confirmed by the observation of the He I 5876 Å line in three stars (Fig. 5 and Table 7). One notes from Fig. 5 that its shape varies significantly from star to star: very weak and very broad emission in HD 150193, stronger emission displaced to the blue and an absorption component in AB Aur and BD + 46°3471 (see Felenbok et al., 1983, for a detailed

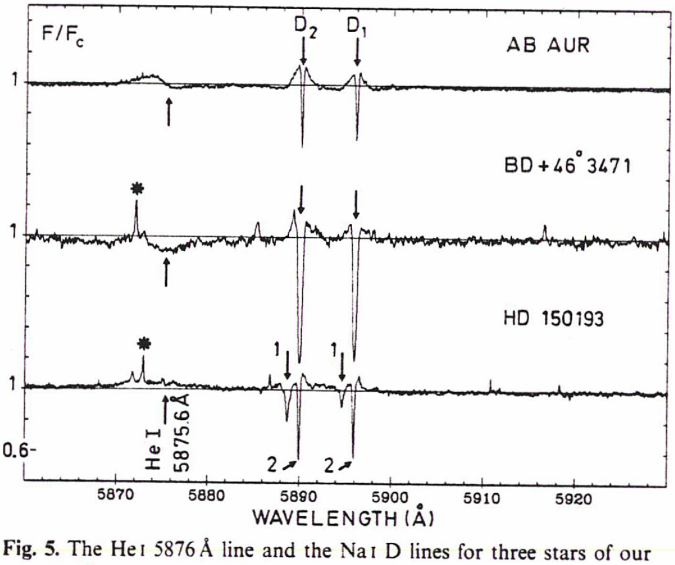

Fig. 5. The He I 5876 Å line and the Na I D lines for three stars of our sample. The wavelength scale is set with respect to LSR. The narrow components described in Table 8 and discussed in the text are indicated by arrows. The He I line is contaminated by spikes (*) in the two lower spectra

description of this line in AB Aur). On the spectra published by Finkenzeller and Mundt (1984), the He I 5876 Å line of HD 250550 appears in absorption and the one of BD + 46°3471 does not show a blue emission component, as the spectrum we publish here. The spectra of AB Aur and HD 150193 obtained by Finkenzeller and Mundt (1984) are of lower resolution and cannot be simply compared with our results. The He I 5876 Å line, either in emission or in absorption, is certainly a chromospheric indicator in Herbig stars, since the levels involved in this line are of high excitation. The differences between the He I lines of the stars of our sample could argue against the similarity of the chromospheres of these stars, in which the line is formed. However, the atomic structure of the He I is very complex and the lower level involved in the 5876 Å line ($2p^3P^0$) can be populated or depopulated by numerous mechanisms. The He I 5876 Å line is then expected to be extremely sensitive to very small differences in the chromospheres of these stars. For this reason, we cannot consider that the differences noted in the He I profiles of the different stars are really the sign of important differences in the structure of their chromospheres.

Table 7. Helium λ 5875.6 line

Star	F/F_c		FWHM (km.s^{-1})		W_λ (Å)		Position/LSR (km.s^{-1})	
	Em.	Abs.	Em.	Abs.	Em.	Abs.	Em.	Abs.
AB Aur	1.05	0.97	188	130	0.13	0.075	−119	40
BD + 46°3471	1.03	0.90	69	228	–	0.47	−152	17
HD 150193	1.06		367		0.41		−92	

3.5. Na I D lines

In the three observed stars, the Na I D doublet (Fig. 5 and Table 8) shows a wide emission which is probably of stellar origin, and narrow absorption components, on which we will come back in Sect. 3-6. The Na I D lines of BD + 46°3471 are qualitatively similar to the ones observed by Finkenzeller and Mundt (1984).

The stellar Na I D lines are likely to be formed in a very remote region, simply because neutral sodium cannot survive close to stars with an effective temperature of the order of 10,000 K. It can be easily estimated that it is impossible to find Na I in sufficient quantity at less than ~ 50 stellar radii from the photosphere in this type of stars. At these distances, the Na I D lines are probably formed by recombination (Felenbok et al., 1983). The global similarity of the stellar components of the Na I D lines indicates a globally similar structure for these remote regions in the different stars.

The stellar emission components of the Na I D lines clearly exhibited by our observations have intensities which seem to correlate with the intensities of the emission component of the Hα line and of the Mg II resonance lines. This trend is confirmed on other stars of the subclass observed by Finkenzeller and Mundt (1984), in particular HD 250550. We could see here an indication that these remote regions still have a dynamical link with the inner parts of the winds or in other words that the winds feed these remote regions.

Felenbok et al. (1983) mentioned the presence of a decelerated region in the wind of AB Aur, shown by the low value (130 km.s^{-1}) of the blueward displacement of the Na I D line absorption components. Since no stellar absorption is clearly visible for the other stars, a similar conclusion cannot be reached with these objects.

3.6. The narrow components

Narrow components at very low velocities are present in the Ca II K line of the three observed stars (Fig. 3), and in the Na I D lines of the 3 observed stars (Fig. 5). In HD 150193, we also note the presence of such a narrow component at a higher velocity (60 km.s^{-1}). It is important to stress that for the stars observed both in the Ca II K line and in the Na I D lines (AB Aur and BD + 46°3471), the two components have the same velocity, which suggests that they are formed in the same region. All these narrow components are symmetric.

We can divide these components in two categories: those with a width close to the instrumental width, and those with a width larger than the instrumental width. The first category can be found in AB Aur (Ca II K line and Na I D lines). These components can be considered as interstellar. The LSR velocity of these components (6 km.s^{-1}) match the one derived by Cantó et al. (1984) for the surrounding molecular cloud, from CO

Table 8. Sodium lines

Star	Component	F/F_c		FWHM (km.s^{-1})		W_λ (Å)		Position/LSR (km.s^{-1})	
		Em.	Abs.	Em.	Abs.	Em.	Abs.	Em.	Abs.
AB Aur									
λ 5889.9		1.13	0.59	85	11.4	0.25	0.120	−1	6.6
λ 5895.9		1.09	0.64	67	11.4	0.16	0.111	3	6.6
BD + 46°3471									
λ 5889.9		1.14	0.18	114	26	–	0.466	17	2.1
λ 5895.9		1.09	0.20	110	23	–	0.412	20	2.1
HD 150193									
λ 5889.9	1		0.80		28.5		0.125		−62.4
	2		0.55		11.5		0.119		2.7
λ 5895.9	1		0.90		23		0.055		−61.1
	2		0.57		11.5		0.115		2.5

observations. It can then be concluded that they are formed within this cloud or at its border. The second category of narrow components can be found in HD 250550 (Ca II K line) and BD + 46°3471 (Ca II K line and Na I D lines). The half-width ($\frac{1}{2}$ FWHM) of these components is around 10 km.s^{-1} (see Tables 5 and 8), which is higher than the typical random velocity for the dense clouds surrounding the Herbig Ae/Be stars (~ 3 km.s^{-1}, see Cantó et al., 1984). This implies that these components are formed in a medium where important turbulent motions (of the order of 10 km.s^{-1}) are present. The region of formation of these components is then likely to be located relatively closer to the stars (several hundreds of stellar radii), where the stellar winds are still able to maintain these turbulent velocities. Since in BD + 46°3471 and HD 250550, these components have very low LSR velocities (see Tables 5 and 8), similar to the one of the surrounding molecular cloud in the case of HD 250550 (see Cantó et al., 1984), the possible presence of interstellar components in their spectra is undetectable. Moreover, we note the presence of both categories of components in the Na I D lines of HD 150193, thanks to an important blue-shift of the widest component. We also notice that these widest components have equivalent widths whose ratio is very close to their oscillator strength ratio, which means that they are not saturated. We can then easily estimate the neutral sodium column density producing these components. We find $N(\mathrm{Na\,I}) = 5.5 \pm 0.5\ 10^{11}\ \mathrm{cm}^{-2}$.

Finally, it should be noted that the present low velocity components probably are of different origin than the components observed in the UV lines of hot stars (Lamers et al., 1982; Heinrichs, 1984), which are blue-shifted to high velocities, and then probably formed within the winds of these stars.

Thus, except for AB Aur, which does not seem to be typical in this respect, our spectra show the presence of cool regions of very low velocities, rather close to the stars as compared to the molecular clouds, where important turbulent motions take place. These turbulent motions are probably powered by the stellar winds.

4. Conclusion

The basic result of this study is that four Herbig Ae/Be stars of the "P Cygni" subclass show remarkable similarities in the Mg II h and k lines, the Ca II K line, the Ca II IR triplet lines, and the Na I D lines. Since the region of formation of these different lines are distinct and since their junction spans the whole envelope of these stars, from the photosphere up to very remote regions (> 50 stellar radii), we can conclude that these envelopes are similar for the stars of our study. From this observational result, we can draw two conclusions.

First, we can consider the brightest star of the "P Cygni" subclass, AB Aur, as representative of the part of its subclass that we have studied. This means that the conclusions reached from the quantitative analysis of the different lines observed in AB Aur (Catala et al., 1984; Catala, 1984; Catala and Kunasz, 1985) also apply for the other stars of our study. These results include the presence of a deep expanding chromosphere at the base of the wind, and the existence of high velocity random motions in the wind.

Second, it is tempting to imagine that these stars could represent the same stage of evolution on their PMS tracks, their envelopes being so similar. However, the present study is only the first step of a more general one, which should include the same kind of observations for all known Herbig Ae/Be stars. Such a general study would tell us whether the same similarities are present in other subclasses. If this turns out to be true, a detailed analysis of the lines of one representant of each subclass could be carried out, in order to derive the basic differences in the structures of the envelopes of the three subclasses.

A better understanding of the evolutionary status of the Herbig Ae/Be stars is clearly needed. Then, a comparison of their properties with those of T Tauri stars would provide a good knowledge of the PMS evolution as a function of mass and age. Moreover, a good understanding of the evolution of these stars during their PMS phase would clarify the question of how they will become main sequence stars, without any remaining signature of winds and chromospheres at this spectral type.

Acknowledgements: We wish to thank A. Talavera for his help in several of the IUE observations. We are also very grateful to J. Borsenberger for his support in the reduction of the IUE spectra of HD 250550. We thank U. Finkenzeller for a careful reading of the manuscript.

References

Ake, T.B.: 1982, IUE NASA Newsletter, No. 19, p. 37
Beals, C.S.: 1951, *Publ. Dominion Astrophys. Obs.* **9**, 1
Cassatella, A.: 1984, private communication
Catala, C., Kunasz, P.B., Praderie, F.: 1984, *Astron. Astrophys.* **134**, 402
Catala, C.: 1984, Proc. 4th European IUE Conf., Rome, ESA SP218, p. 227
Catala, C., Felenbok, P., Czarny, J., Talavera, A., Boesgaard, A.M.: 1985, *Astrophys. J.* (submitted)
Catala, C., Kunasz, P.B.: 1986 (in preparation)
Cantó, J., Rodriguez, L.F., Calvet, N., Levreault, R.M.: 1984, *Astrophys. J.* **282**, 631
Cohen, M.: 1973a, *Monthly Notices Roy. Astron. Soc.* **161**, 85
Cohen, M.: 1973b, *Monthly Notices Roy. Astron. Soc.* **164**, 395
Cohen, M., Kuhi, L.V.: 1979, *Astrophys. J. Suppl.* **41**, 743
Davis, R., Strom, K.M., Strom, S.E.: 1983, *Astron. J.* **88**, 1644
Elias, J.H.: 1978, *Astrophys. J.* **224**, 857 & 453
Felenbok, P., Praderie, F., Talavera, A.: 1983, *Astron. Astrophys.* **128**, 74
Finkenzeller, U., Mundt, R.: 1984, *Astron. Astrophys. Suppl.* **55**, 109
Finkenzeller, U., Jankovics, I.: 1984, *Astron. Astrophys. Suppl.* **57**, 285
Finkenzeller, U.: 1985, preprint
Garrison, L.M., Anderson, C.M.: 1977, *Astrophys. J.* **218**, 438
Geisel, S.L.: 1970, *Astrophys. J.* **161**, L105
Gillett, F.C., Stein, W.A.: 1971, *Astrophys. J.* **164**, 77
Heinrichs, H.: 1984, Proc. 4th European IUE Conf., Rome, ESA SP218, p. 43
Herbig, G.H.: 1960, *Astrophys. J. Suppl.* **4**, 337
Lamers, H.J.G.L.M., Gathier, R., Snow, T.P., Jr: 1982, *Astrophys. J.* **258**, 186
Lucy, L.B.: 1982, *Astrophys. J.* **255**, 278
Mendoza, E.E.: 1966, *Astrophys. J.* **143**, 1010
Mendoza, E.E.: 1967, *Astron. J.* **72**, 816

Mihalas, D., Conti, P.S.: 1980, *Astrophys. J.* **235**, 515

Praderie, F., Talavera, A., Felenbok, P., Czarny, J., Boesgaard, A.M.: 1982, *Astrophys. J.* **254**, 658

Praderie, F., Simon, T., Boesgaard, A.M., Felenbok, P., Catala, C., Czarny, J., Talavera, A., Le Contel, J.M., Morel, P., Sareyan, J.P., Valtier, J.C.: 1983, 2nd France-Japan Seminar, Paris, ed. J.C. Pecker and Y. Uchida, p. 132

Praderie, F., Catala, C., Czarny, J., Felenbok, P.: 1984, Workshop on "Space Research Prospects in Stellar Activity and Variability", Obs. de Paris-Meudon, eds. F. Praderie and A. Mangeney, p. 265

Praderie, F., Simon, T., Catala, C., Boesgaard, A.M.: 1986, *Astrophys. J.*, (in press)

Roger, R.S., Irwin, J.A.: 1982, *Astrophys. J.* **256**, 127

Strom, S.E., Strom, K.M., Yost, J., Carrasco, L., Grasdalen, G.L.: 1972, *Astrophys. J.* **173**, 353

Talavera, A., Catala, C., Crivellari, L., Czarny, J., Felenbok, P., Praderie, F.: 1982, Proc. 3rd European IUE Conf., Madrid, ESA SP176, p. 99

Thé, P.S., Felenbok, P., Cuypers, H., Tjin A Djie, H.R.E.: 1985, *Astron. Astrophys.* **149**, 429

Vidal, C.R., Cooper, J., Smith, E.W.: 1973, *Astrophys. J. Suppl.* **25**, 37

Wagenblast, R., Bertout, C., Bastian, U.: 1983, *Astron. Astrophys.* **120**, 6

Astron. Astrophys. 134, 402–413 (1984)

ASTRONOMY AND ASTROPHYSICS

Line formation in the wind of AB Aur

C. Catala[1,*], P. B. Kunasz[2], and F. Praderie[1,*]

[1] Observatoire de Paris-Meudon, DESPA, F-92195 Meudon Principal Cedex, France
[2] 315, Skylark Way, Boulder, CO 80303, USA

Received November 12, 1983; accepted January 18, 1984

Summary. The Herbig Ae variable AB Aur shows a line spectrum characteristic of a stellar wind. We present here the results of a detailed quantitative interpretation of the Mg II resonance lines of AB Aur. Extensive semi empirical modelling of an expanding, spherically symmetric atmosphere was carried out, in which the different parameters were heavily constrained by the numerous spectroscopic and spectrophotometric observations at our disposal, in particular IUE observations of the Si IV and C IV resonance doublets. The Mg^+ ion was treated as a NLTE two-level atom.

The results showed the presence of a deep and extended chromosphere in the wind of AB Aur. A detailed analysis of the sensitivity of the results to the physical structure of the wind provided estimates of the maximum temperature reached in the chromosphere ($T_{max} \sim 15{,}000$–$20{,}000$ K), as well as the position and the extension of the latter.

Constraints on the velocity gradient at the bottom of the wind have been determined, but the profiles of the Mg II resonance lines are not sensitive enough to the details of the velocity law $v(r)$ in intermediate and outer regions of the wind to provide estimates of $v(r)$ in these regions.

The mass loss rate has been found to lie between $4\,10^{-11}$ and $7\,10^{-9}\,M_\odot\,yr^{-1}$.

A pure thermal Doppler broadening is not sufficient to explain the profile of the Mg II resonance lines, and an additional broadening mechanism must be envisaged.

Key words: pre-main-sequence stars – stellar winds – stellar chromospheres – line formation

I. Introduction

The irregular variable AB Aur (spectral type A0 ep) belongs to the class of Herbig Ae stars. Since the pioneering work of Herbig (1960), this class of stars has been observed and studied, and it is now fairly widely believed that they are in a pre-main sequence (PMS) stage of their evolution (Strom et al., 1972, 1975) and can be considered as higher mass counterparts of T Tauri stars. Other characteristic properties have been determined for these stars, such as infrared (IR) excess (Cohen, 1973, 1975, 1980; Sitko, 1981) and irregular variability (Herbig, 1960); Strom et al., 1975).

Send offprint requests to: C. Catala
* Laboratoire Associé au CNRS 264

More recently, high resolution spectroscopic observations of the brightest Herbig Ae stars have provided new information about the outer layers of these stars. It has been shown that they exhibit spectral features indicating a stellar wind and chromospheric activity (Praderie et al., 1982; Talavera et al., 1982; Finkenzeller and Mundt, 1983). In the spectrum of AB Aur, these features are variable, which suggests variability in both the wind and the physical properties of the chromosphere (Praderie et al., 1982; Catala et al., 1984).

Nothing is known about the mechanisms of wind production and of chromospheric heating in such stars. Different mechanisms have been proposed in the past ten years to explain stellar winds in several parts of the HR diagram (see Cassinelli, 1979). Radiatively driven winds are believed to be present in hot and luminous stars, such as O and B stars (see e.g. Castor et al., 1975). It has been shown by Abbott (1982) that this mechanism is efficient for spectral types earlier than A0. On the other hand, the winds of solar-type stars are believed to be due to the Parker mechanism (Parker, 1958), for which the presence of a corona is necessary. Herbig Ae stars do not fulfil these different conditions: except one, they do not yet show any sign of the presence of a corona (although a geometrically thin corona would not be inconsistent with observations), and are not luminous enough to enter the category of stars for which the validity of radiatively driven wind theory is well established.

Moreover, a realistic model should explain both wind production and chromospheric heating. To the best of our knowledge, no theoretical model of chromospheric heating by deposition of non-radiative energy exists for PMS stars, although some effort has been recently made to schematically explain winds and activity of T Tauri stars by dissipation of Alfvén waves (Hartmann et al., 1983). It has not yet been proven that such a mechanism could work in the winds of Herbig Ae stars.

As the basic mechanisms of wind production or chromospheric heating in Herbig Ae stars are still elusive, the very first step towards the comprehension of physical processes at work in such stars should be a precise determination of the structure of their atmospheres, i.e. the determination of velocity and temperature runs in their winds, as well as their mass loss rates.

This kind of determination is possible by a semi-empirical modelling of those stars for which we have a sufficient quantity of high resolution spectroscopic observations. New techniques for solving the non-LTE transfer equation in moving media (Mihalas et al., 1975, 1976a–c; Mihalas and Kunasz, 1978) make it possible to quantitatively interpret lines formed in stellar winds.

The aim of the present work is to study the physical structure of the wind of AB Aur, the brightest Herbig Ae star in the northern

hemisphere, by an interpretation of the lines observed in its spectrum. From UV, visual and IR observations, it can be seen that most of the other Herbig Ae stars exhibit the same spectral features as AB Aur (Talavera et al., 1982; Finkenzeller and Mundt, 1984), so that this star can be considered as representative of its class. This work must be considered as a first step in a systematic treatment of the winds and chromospheres of Herbig Ae stars, which will provide constraints to be placed on the mechanisms of wind production and chromospheric heating for these stars.

In this paper, we present our results on spectral line synthesis of the Mg II resonance lines in AB Aur. This interpretation is based on a set of models of the expanding outer layers that are built consistently with all the other observations of the star.

In Sect. II, the models used for the interpretation of the Mg II resonance lines are presented. The basic assumptions and calculations are discussed and the various constraints placed by observations upon the free parameters are described. In Sect. III, the best method for solving the non-LTE transfer equation in the present case is described. Section IV contains the results of our analysis. The influences of the parameters on the model are examined, and conclusions as to the physical structure of the wind and chromosphere of AB Aur are given. A summary and general conclusions are presented in Sect. V.

II. The model

A semi-empirical approach has already been followed to study the line formation problem in the wind of the A2Ia star α Cygni (Kunasz and Praderie, 1981, hereinafter KP). Since the method used here for the construction of the models is basically the same as the one described in KP, the reader is referred to their paper and references therein. In the following paper, we will put emphasis on those points that differ from KP.

a) Observational constraints on the model

Observations of P Cygni profiles, such as in Mg II resonance lines (Praderie et al., 1982), or Hα (Felenbok et al., 1983) indicate that the atmosphere of AB Aur is extended and expanding. Since no speckle interferometric observation has been carried out up to now for this star, the atmospheric extension is unknown. In practice, in all of our models, we have made sure that the region contributing to the formation of the Mg II resonance lines has been entirely considered by running a similar model with an increased extension and checking that it had no effect on the computed line profile. The extension to be considered depends on the mass loss rate and the radiation temperature for Mg^+ ionization (see Sect. IVb), but is typically of about 50 stellar radii for the set of models we have considered. This great extension for the line formation region implies that among the one dimensional geometries spherical geometry is the best choice.

Spectrophotometric and spectroscopic observations in the visible show that the Paschen continuum, the Balmer jump and the wings of Hδ are well represented by a model of a classical photosphere in hydrostatic and radiative equilibrium, with $T_{\rm eff} = 10{,}000$ K and $\log g = 4$ (Garrison, 1978; Praderie et al., 1982). This suggests strongly that a classical photosphere must be present at the bottom of the wind. Therefore, below the layer corresponding to $\tau_c = 2/3$, τ_c being the continuum optical depth at the wavelength of Mg II resonance lines (2800 Å), all our models are set identical to a model of Kurucz (1979) for $T_{\rm eff} = 10{,}000$ K and $\log g = 4$. This condition makes our models easily intercomparable, since the photospheric layers are always the same, whatever the physical conditions in the wind.

The Ca II K line shows at times an emission in its core (Praderie et al., 1982) and the He I 5876 Å is seen in emission (Felenbok et al., 1983). These two features constitute evidence for the presence of a chromosphere. This evidence is reinforced by the observation of Paschen lines and of the Ca II IR triplet in emission (Felenbok et al., 1983). Moreover, high resolution spectra obtained with IUE in the short wavelength range ($1150\,\text{Å} \leqq \lambda \leqq 2000\,\text{Å}$) (archive images as well as one spectrum obtained by us in January 1983) show unambiguously the presence of the Si IV and C IV resonance doublets ($\lambda\lambda$1394, 1402 Å and $\lambda\lambda$1548, 1550 Å). The four lines are in absorption, with no P Cygni emission component, they are strong but not saturated. These observations will be presented in a further publication. The presence of Si^{3+} and C^{3+} in the wind of AB Aur is another indication for the existence of hot regions in the atmosphere of this star. We will see below (Sect. IIc) in more detail how this can be accounted in our models.

b) The velocity law

As mentioned above, the purpose of this work is a quantitative interpretation of Mg II resonance lines in AB Aur. For this first step towards the quantitative study of the wind of this star, the choice of Mg II resonance lines is ideal because these lines are formed over large regions, so they will provide global information about the structure of the wind. On the contrary, lines formed in more localized regions, such as Ca II, Si IV, and C IV resonance lines will help to refine the global vision derived from Mg II analysis, and hence their interpretation must be considered as the second step of the study of the wind of AB Aur. Here, we have chosen to interpret the Mg II k line (λ 2796 Å), in order to minimize the effect of the unlikely, but possible blend with the Mg II subordinate lines ($\lambda\lambda$ 2798, 2790 Å). The profile of the k line, which can be seen in Praderie et al. (1982), is of P Cygni type IV, according to Beals' classification (Beals, 1951). Such a profile can be qualitatively explained either by an accelerating or a decelerating wind. Kuan and Kuhi (1975) choose the second possibility for AB Aur, arguing that a decelerating wind is the only way to obtain both a deep absorption component and a narrow emission component for Hβ P Cygni profile, through occultation effects. Actually, a similar line profile can be obtained with an accelerating wind, if the density sufficiently decreases outwards, as can be deduced from the present study. Moreover, since the wind initiates from approximately static layers (see Sect. IIa), a purely decelerating wind would imply a strong discontinuity in velocity and density runs at the base of the atmosphere. It is more realistic to consider a wind which accelerates gently near the photosphere, then more steeply to its maximum velocity further in the atmosphere.

In the spectrum presented by Praderie et al. (1982), taken in January 1981, the observed maximum blue shift in the absorption component of Mg II resonance lines is $V_s = 380\,\text{km s}^{-1}$, and is the highest blue shift for all the lines observed in the spectrum of AB Aur. Neutral sodium D lines exhibit P Cygni profiles with an absorption component blue-shifted by $130\,\text{km s}^{-1}$ (Felenbok et al., 1983). This low value suggests that the acceleration region of the wind is followed by a deceleration zone. There are very few arguments to decide at which distance the wind begins to decelerate. Here, we have assumed that the wind is accelerating out at least until 50 stellar radii, which is not inconsistent with the observation of Na I D lines, since neutral sodium can survive only at greater distances from the stellar core, and which is also consistent with Mg II k line profile, as we will see below. In our

models, the velocity is then monotonically increasing over the whole Mg II line formation region. However, the possibility that the decelerating region is located closer to the star (Finkenzeller and Mundt, 1983) is not excluded by our analysis. Since the intrinsic line profile is not perfectly narrow, we also note that the measured value V_s is higher than the terminal velocity V_∞, defined as the velocity reached in the outermost parts of the line formation region.

The equation of continuity

$$\dot{M}=4\pi r^2\varrho(r)v(r) \tag{1}$$

couples the density $\varrho(r)$ and the velocity $v(r)$ through a scaling factor, the mass loss rate $\dot{M}$. The continuum optical depth at the photospheric radius, R_{ph}, is:

$$\tau_*=\frac{\dot{M}}{4\pi}\int_{R_{ph}}^{\infty}\frac{\sigma_c(r)dr}{r^2v(r)}, \tag{2}$$

where $\sigma_c(r)$ is the continuum absorption cross section per unit mass (in $cm^2\,g^{-1}$) at distance r, including electron scattering. The mass loss rate can then be computed consistently with the velocity law and the continuum absorption cross section, provided we have fixed the value of τ_*:

$$\dot{M}=\frac{4\pi\tau_*}{\int_{R_{ph}}^{\infty}\frac{\sigma_c(r)dr}{r^2v(r)}}. \tag{3}$$

In this equation, the main contribution to the integral comes from the bottom of the wind, and hence the mass loss rate is fixed by the conditions at the base of the wind. In practice, any velocity law leading to a reasonable fit of the Mg II k line profile provides a consistent value of the mass loss rate as an output of the analysis. It is possible in this way to derive estimates for the mass loss rate (see Sect. IVc). If now we impose a connection with a given model at the photospheric radius and at a continuum optical depth of 2/3, we must set $\tau_*=2/3$, and the velocity law must verify the relation:

$$\frac{\tau_*}{\int_{R_{ph}}^{\infty}\frac{\sigma_c(r)dr}{r^2v(r)}}=R_{ph}^2\varrho_{ph}v(R_{ph}). \tag{4}$$

Here ϱ_{ph} is the density of the classical photospheric model at $\tau_c=2/3$.

In KP's analysis of the wind of α Cygni, σ_c was assumed constant over the atmosphere, which is a good approximation for a supergiant. In the present work, σ_c can no longer be assumed constant, since in a dwarf like AB Aur, the hydrogen density is much higher near the photosphere than in a supergiant and hence the electron scattering contribution to the continuum opacity is no longer dominant all over the wind. σ_c must then be evaluated at each depth, and since it depends in a complicated way on the mass loss rate, an iterative procedure is necessary for the construction of the model. This procedure is described in Sect. IIe.

c) The ionization balance

If dielectronic recombination and autoionization are neglected, the equation of ionization equilibrium equates radiative plus collisional ionizations to radiative plus collisional recombinations. Radiative processes involve the radiation field, hence the ionization equilibrium and the transfer equation are coupled. However it is possible to describe qualitatively the ionization state of a species by adequate approximations on the ionizing radiation.

At the bottom of the wind, the ionizing radiation corresponding to a given ion is thermalized. It can then be shown that, for a star of spectral type A0 and for all the ions of interest for our analysis, radiative processes dominate the ionization balance. Since the mean intensity of the ionizing radiation is given by the Planck function at the local electron temperature, the ionization equilibrium is described by the well-known Saha equation.

Let us call the layer where the ionizing radiation begins to depart from the local Planck function the "dethermalizing layer". We can then define a "dethermalizing layer" for each ion considered. Typically, the dethermalization occurs at $\tau_{\nu_0}\sim 2$, ν_0 being the photoionization threshold of the ion. Note that for most of the ions of interest for our analysis (Mg^+, Si^{2+}, Si^{3+}, C^{2+}, C^{3+}, ...), this threshold is in the far UV, beyond the Lyman discontinuity, and hence the dethermalizing layer corresponding to these ions is located far from the stellar core (typically at $\tau_{\nu_L}\sim 10^{-5}$, ν_L being the frequency of Mg II resonance lines, which corresponds to 12 to 15 stellar radii). Above the dethermalizing layer, the medium can be considered as optically thin to the ionizing radiation and we can write:

$$J_{\nu_0}\sim W(r)B_{\nu_0}(T_r), \tag{5}$$

where

$$W(r)=\tfrac{1}{2}[1-\sqrt{1-(R_1/r)^2}]. \tag{6}$$

R_1 being the radial distance to the dethermalizing layer and T_r is the so-called radiation temperature, defined as the electron temperature of the dethermalizing layer. In these outer regions, if the electron temperature is everywhere lower than the radiation temperature, radiative processes still dominate the ionization equilibrium and the latter is described by the Strömgren formula:

$$\frac{N^{++}n_e}{N^+}=\left(\frac{2\pi m_e kT_r}{h^2}\right)^{3/2}\frac{2g^{++}}{g^+}xW(r)(T_e/T_r)^{1/2}\exp(-h\nu_0/kT_r), \tag{7}$$

where all the quantities have their usual meaning, and x accounts for the fraction of recombinations populating the ground state. This number has been taken as $\frac{1}{2}$. Note that the dilution factor W is $\frac{1}{2}$ at the dethermalizing layer, which leads to a discontinuity between Saha's and Strömgren's formulae. This discontinuity comes from the fact that, in this schematic representation, we jump from an optically thick region to an optically thin one, without accounting for the radiative transfer of the ionizing radiation. A connection zone is therefore necessary between the two regions (see below). However, if somewhere outwards of the dethermalizing layer the electron temperature rises above the radiation temperature, the ionization is dominated by collisional processes, and the ionization balance becomes a coronal equilibrium, i.e. a balance between collisional ionizations and radiative recombinations.

Two models can then be proposed to account for the presence of Si^{3+} and C^{3+} in the wind of AB Aur:

The "remote chromosphere" model, in which a temperature rise occurs beyond the dethermalizing layers for Si^{2+} and C^{2+}. In this case, the existence of a coronal equilibrium requires temperatures of about 10^5 K to account for the presence of C^{3+}. It is a model with coronal ionization equilibrium that has been envisaged, explicitly or implicitly, in all the works trying to explain the presence of superionized material in stellar atmospheres (see for example Lamers and Snow, 1978; Doazan, 1982). As will be stressed below, for the formation of Mg II resonance lines, the temperature law is crucial mainly near the photosphere: practically, as far as the formation of Mg II resonance lines is

Table 1. Atomic data for Mg II k line transition (λ 2795.53 Å)

Quantity	f_{12}	$A_{21}(s^{-1})$	g_1	g_2	Ω_{21}	$\Gamma_{rad}(s^{-1})$	$\Gamma_e(s^{-1})$
Value	0.64	$2.72\,10^8$	2	4	5.92	$2.67\,10^8$	$3.26\,10^8$
Reference	Wiese et al. (1969)				Sahal-Bréchot (1977)	Wiese et al. (1969)	Sahal-Bréchot (1977)

Notes to Table 1: f_{12}: oscillator strength of the transition. A_{21}: probability of spontaneous emission. g_1, g_2: statistical weights of levels 1 and 2. Ω_{21}: collisional strength of the transition. Γ_{rad}: radiative damping coefficient. Γ_e: electronic damping coefficient

concerned, this model reduces to its monotonically decreasing temperature part.

The "deep chromosphere" model, in which a temperature rise occurs below the dethermalizing layers for Si^{2+} and C^{2+}, typically located at $\tau_{2800} \sim 10^{-5}$. In this model, temperatures of about 15,000–20,000 K are sufficient to explain the presence of Si^{3+} and C^{3+}, for the electron densities of our models (typically 10^{10} cm^{-3} in this region). Note that this kind of model could also explain the superionization observed in some Be stars or in some O and B stars. In our case, the temperature rises up to 15,000–20,000 K above the photosphere, then decreases again to reach a specified surface value.

For both types of models, the magnesium ionization equilibrium has been treated for number ratios of successive ions by writing Saha's equation below the dethermalizing layers and Strömgren's equation above them. A connection zone has been introduced between the two regions, by writing a linear combination of Saha and Strömgren formulae to insure a smooth transition from one region to the other. For the case of neutral Mg, whose photoionization threshold is not beyond the Lyman discontinuity ($\lambda_\infty = 1620$ Å), we have introduced a treatment of the coronal equilibrium when $T_e > T_r$. In any case, the population of neutral Mg is completely negligible over all the wind. The treatment of the coronal equilibrium has been also used for the other ions for running a test case with a remote temperature rise (see Sect. IVa).

The ionization of hydrogen can be treated in the same way, i.e. one can write:

$$\frac{n_e n_p}{N(\mathrm{H\,I})} = S(T_e), \tag{8}$$

where n_e is the electron density, n_p the proton density, N(H I) the number density of neutral hydrogen and $S(T_e)$ is given by Saha's formula below the dethermalization layers, by Strömgren's formula above, by a linear combination of the two formulae in the connection zone and by a formula corresponding to a coronal equilibrium when necessary. If now we assume $n_e = n_p$ and that helium is present, but not metals, we find:

$$\frac{1}{S(T_e)} n_e^2 + n_e - \frac{\varrho}{1.4\, m_H} = 0, \tag{9}$$

where $\varrho(r)$ is the mass density in the wind and m_H the mass of the hydrogen atom. The solution of (9) gives $n_e(r)$.

d) The opacity

Once the ratio of the Mg^+ density to the total magnesium density has been computed, the line opacity $\chi_L(r)$ is derived in the same way as in KP. We used the solar abundance for magnesium (Mg/H $= 3.47\,10^{-5}$). All the atomic data concerning the transition are given in Table 1.

As already mentioned, the analysis of the wind of a dwarf star requires an evaluation of the continuum opacity $\chi_c(r)$ at each depth. χ_c has been computed by using data and formulae from Kurucz (1970). The ionization equilibrium has been treated as described above and the populations of excited levels of hydrogen have been computed assuming LTE. The different sources of opacity that have been considered are the following:

H I bound-free opacity
H II free-free opacity
H^- bound-free opacity
H^- free-free opacity
H I Rayleigh scattering
electron Thomson scattering.

It has been found that Thomson scattering dominates the continuum opacity in the outer regions of the wind (down to $\tau_c \sim 10^{-2}$), while near the photosphere ($\tau_c \geqq 10^{-2}$), the continuum opacity is controlled by H I bound-free opacity. The continuum absorption cross section σ_c varies by more than a factor 100 over the wind, which shows that the assumption of a depth invariant σ_c made by KP for α Cygni is not valid for a dwarf star.

e) The construction of the model

After the basic parameters defining the star, namely T_{eff} and R_{ph}, have been given, the velocity law $v(r)$ is specified as a piecewise linear function of r/R_{ph} and the temperature law $T(r)$ is given analytically as described below (see Sect. IV). In the photosphere, T is defined by the Kurucz' model and v is computed consistently with the density of the latter.

The first step is a rough estimate of the mass loss rate assuming that the continuum absorption cross section is constant and has its photospheric value $\sigma_{c_{ph}}$:

$$\dot{M}^{(1)} = \frac{4\pi\tau_*}{\sigma_{c_{ph}} \int_{R_{ph}}^{\infty} \frac{dr}{r^2 v(r)}}. \tag{10}$$

A fine optical depth mesh is then generated. The lower boundary is chosen deep enough to ensure thermalization by background sources and sinks, namely $\tau_c = 15$. After the corresponding radial mesh has been determined, we calculate $\varrho(r)$, $n_e(r)$, $\chi_c(r)$, $\sigma_c(r)$ at each depth, using prespecified values for the radiation temperatures. The mass loss rate is then reevaluated by writing Eq. (3) with the new values of $\sigma_c(r)$. The positions of the dethermalizing layers are specified by their optical depths in the Mg II line frequency scale. These optical depths have been previously determined by running typical models and computing

the continuum opacity at the photoionization threshold frequencies. Radiation temperatures for the different ions can thus be redefined at each iteration. We then check that relation (4) is verified. If not, the photospheric velocity is recomputed by:

$$v^{(2)}(R_{\rm ph}) = \frac{\dot{M}^{(2)}/4\pi}{R_{\rm ph}^2 \varrho_{\rm ph}}. \qquad (11)$$

Turning back to the initial depth mesh, the new corresponding radial mesh is defined, by using the computed values of $\sigma_c(r)$ and of the radiation temperatures.

This procedure is then iterated to convergence. In practice, at most five iterations are needed for all cases of interest. When convergence is reached, the computed mass loss rate is consistent with both the velocity law and the requirement that a given classical photosphere is present at the bottom of the wind.

f) The Doppler velocity

As in KP, the total Doppler random velocity v_D is specified directly as a free parameter. From the analysis of KP, we guess that it will be necessary to envisage high values for v_D to explain the wide saturation of the absorption component of the Mg II lines. We also know from KP that v_D may vary across the wind, so we must keep the possibility of a variable intrinsic line profile. In practice, this raises a numerical problem of sampling of the intrinsic profile, and the amplitude of the variation of v_D could not be set larger than a factor 3 for our computer.

III. Solution of the transfer equation

Once the model atmosphere has been constructed, the interaction of the radiation field with the matter constituting the atmosphere can be studied. This interaction is described by the well-known transfer equation. When the radiation crosses a moving medium, as is the case in a stellar wind, Doppler shift effects introduce a coupling between the frequencies and the directions of propagation of photons. This problem can be easily solved in two different cases:

When the velocity field is low everywhere in the wind, the transfer equation can be solved directly in the observer's frame. The width of the intrinsic profile in this frame is $2\nu_L v/c$, so this method becomes intolerably costly for our computer as soon as the flow velocity v reaches a few Doppler velocities (see Kunasz and Hummer, 1974). In our case, we know that there are regions in the wind where the velocity reaches 300 km s^{-1}, that is to say about 120 thermal Mg^+ Doppler widths, hence the cost of such a method is prohibitive.

When $v(r)/v_D(r) \gg 1$ in the line formation zone, the regions of the atmosphere interacting with the radiation at a given frequency are geometrically localized. The use of Sobolev's method (e.g. Castor, 1970; Castor and Lamers, 1979) greatly simplifies the transfer problem in that case. In the wind of AB Aur however, the photospheric regions are almost static (see Sect. II), hence this method cannot apply over the total extent of the wind.

The coupling between the frequencies and the directions of propagation of photons can be suppressed by working in the comoving frame. An economic method of solution of the NLTE transfer equation in the comoving frame has been fully described in a series of papers (Mihalas et al., 1975, 1976a–c, Mihalas and Kunasz, 1978). It can treat the case of any velocity field, weak or strong, provided the latter is monotonic. Since the wind of AB Aur can be reasonably assumed monotonic in the whole Mg II

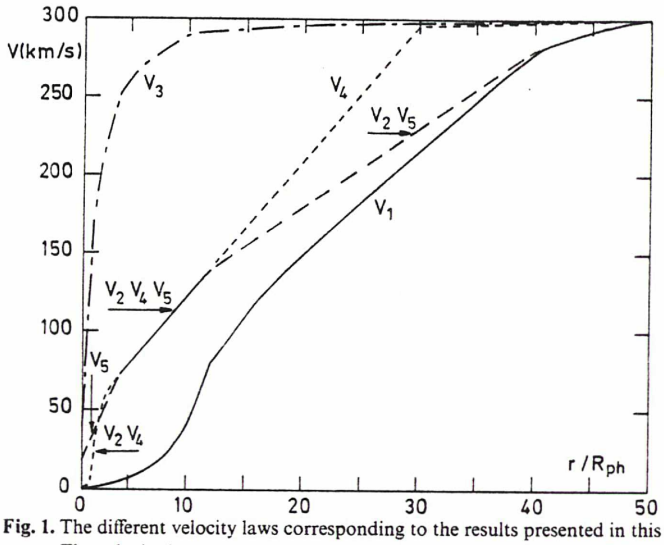

Fig. 1. The different velocity laws corresponding to the results presented in this paper. The velocity law v_3 is one of those used by Castor and Lamers (1979) to build their atlas of P Cygni profiles ($\beta = 1$)

line formation (see Sect. IIb), the comoving frame method is well adapted to its case. It is this method we have used here, in the same way as described in KP. Our treatment is similar to their method in the following ways:

The comoving frame calculation leads to the determination of the line source function S_L and the continuum source function S_c, consistently with the radiation field. Subsequently calculations in the observer's frame lead to the emergent flux at each frequency of a specified frequency mesh. This flux can then be directly compared to observations.

The importance of partial redistribution has been assumed to be small. A recent study of partial redistribution effects on the line transfer in expanding atmosphere tends to show that these effects are small when the velocity field is strong ($\geqq 6 v_D$) (Drake and Linsky, 1983), because in this case the major cause of photon escape is the Doppler shift due to expansion. For the sake of simplicity and because our velocity field is strong enough in most of the wind, we have assumed complete redistribution.

The intrinsic line profile is a Voigt profile. A fiducial damping parameter $a_{\rm fid}$ corresponding to a Doppler random velocity equal to the thermal velocity $v_{\rm th}$ has been determined by using the atomic data given in Table 1. We find that $a_{\rm fid} = 5\,10^{-3}$ near the photosphere. The value of $a_{\rm fid}$ has been taken constant over the wind. This approximation is justified, since in most of the regions of the wind, $a_{\rm fid}$ is dominated by radiative damping, which does not vary with n_e. The real damping parameter "a" is computed as $a_{\rm fid} v_{\rm th}/v_D$. The effects of the damping parameter on the line source function S_L and on the emerging profile have been investigated by giving to $a_{\rm fid}$ the values 0, 10^{-6}, $5\,10^{-3}$, 10^{-2}. The results show that the importance of "a" in the calculation of S_L can be great in models without a deep chromosphere, but is usually small in models with a deep chromosphere. However, even in models with a deep chromosphere, changing the value of "a" can lead to important variations in the emission component of the emerging profile. These tests show that the shape of the intrinsic line profile is of great importance in such a problem.

As in KP, Mg^+ is considered as a two-level atom. Its second and third excited levels indeed lie well above the first one. Moreover, the subordinate lines reaching these levels ($\lambda\lambda$ 2790, 2798 Å, and $\lambda\lambda$ 2928, 2936 Å) do not appear on IUE spectra. It is

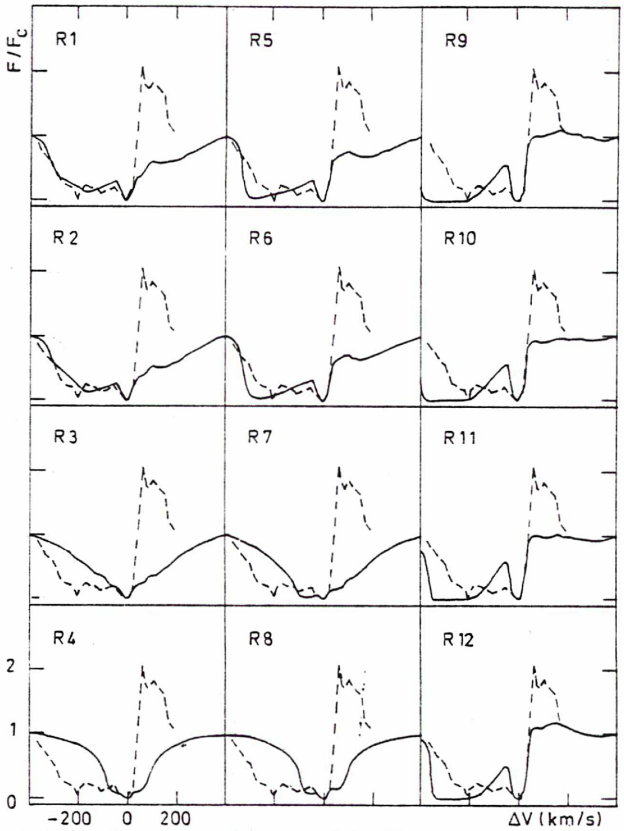

Fig. 2. Results corresponding to models with a monotonically decreasing temperature law. The models are described in Table 2. Each emerging profile (full line) is compared to the observed profile (dashed line), taken from Praderie et al. (1982). On the computed profiles, the interstellar component has been empirically reproduced by assuming that the interstellar optical thickness was a Gaussian function of the frequency, chosen to obtain the best fit on 5 central points of the flux profile

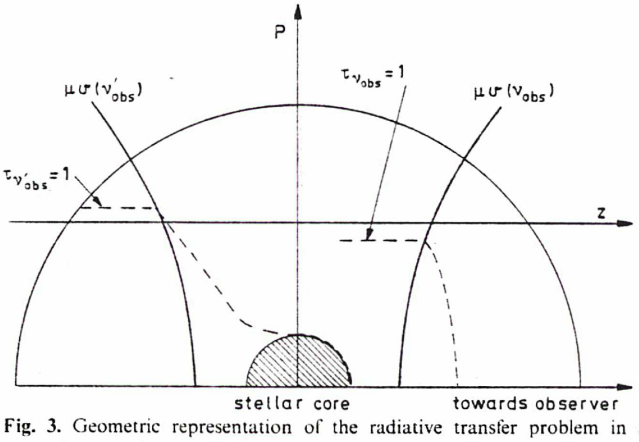

Fig. 3. Geometric representation of the radiative transfer problem in an expanding spherical atmosphere. The form of the iso-velocity curves $\mu v(v_{obs})$ and $\mu v(v'_{obs})$ and of the curves $\tau_{v_{obs}}=1$ and $\tau_{v'_{obs}}=1$ are qualitative. v_{obs} and v'_{obs} represent two frequencies in the observer's frame symmetric with respect to the line center

then likely that these two levels are not populated enough to perturb the population of the ground level and of the first excited level, and hence the two-level atom assumption is well justified. The destruction probability ε has been computed by using the values of A_{21} and Ω_{21} given in Table 1. The importance of ε has also been tested by running test cases with $\varepsilon=0$. The influence of ε on S_L is found small ($\leqq 20\%$) except near the base of the wind ($\sim 40\%$), but it is sufficient to induce important changes in the emission component of the emerging profile ($\geqq 50\%$). This shows that a purely scattering wind would be a poor approximation for the problem considered here. The results concerning the importance of the damping parameter and the destruction probability are discussed in details in Catala (1983b).

The entire calculation, i.e. the construction of the model and the solution of the transfer equation, was run on the CNES Cyber 170/750 computer. Given the capacity of this machine, it has been possible to solve the transfer equation in the comoving frame on meshes of 90 depth points and 21 frequency points, which we believe to be sufficient for our problem.

IV. The expanding chromosphere of AB Aur: Discussion

a) Results with decreasing $T(r)$

As will be demonstrated below (this section), the main effect of the temperature law on the Mg II resonance line formation occurs near the photosphere. Hence, a model with a monotonically decreasing temperature law is equivalent to a remote chromosphere model, as far as Mg II line formation is concerned. This will be discussed in more detail in the following. We have chosen to represent analytically the temperature law by a function of the type:

$$T(r)=T_{\rm eff}\exp\left\{\ln\left(\frac{T_0}{T_{\rm eff}}\right)\frac{\dfrac{1}{(r-R_c)^{\alpha}}-\dfrac{1}{(R_{\rm ph}-R_c)^{\alpha}}}{\dfrac{1}{(R_{\rm max}-R_c)^{\alpha}}-\dfrac{1}{(R_{\rm ph}-R_c)^{\alpha}}}\right\}, \tag{12}$$

where T_0 is the temperature reached at $r=R_{\rm max}$, α is a positive parameter describing the rapidity of decrease of $T(r)$ and R_c is computed in such a way as to insure the continuity of dT/dr at the photosphere:

$$R_c=R_{\rm ph}-\alpha T_{\rm eff}\frac{\ln(T_0/T_{\rm eff})}{T'_{\rm ph}}, \tag{13}$$

where

$$T'_{\rm ph}=\frac{dT}{dr}(r=R_{\rm ph}). \tag{14}$$

The economy of the comoving frame method for solving the transfer equation in moving media (about 60 s of CPU per model) allows us to let the different parameters vary in a systematic way, in order to understand their influences on the emergent profile. About 80 models with decreasing $T(r)$ were run. The results for 12 of them are presented in Fig. 2. The velocity laws for these models can be seen in Fig. 1. They are typically of all the velocity laws considered in this analysis. The other quantities defining the 12 models are given in Table 2.

The important result to be noted is that none of our 80 models could reproduce as intense an emission component as observed. This absence of an intense emission component can be easily understood if one remembers that the flux at a given frequency in the observer's frame, v_{obs}, is obtained by summing the specific intensity $I(v_{obs}, z_{max}, p)$ over all the impact parameters p. A geometric representation of the problem is given in Fig. 3. Since the source function globally decreases outward, the Eddington-Barbier relation gives a rough estimate of the intensity at the outer boundary of each ray:

$$I(v_{\rm obs}, z_{\rm max}, p)\approx S_v(\tau_{v_{\rm obs}}=1). \tag{15}$$

Table 2. Models with a monotonically decreasing temperature law

Model no.	Parameters			$\dot{M}(M_\odot\,\mathrm{yr}^{-1})$	Position of the sonic point (stellar radii)
	Velocity law	α	T_0(K)		
$R1$	v_1	1	5000	$7.8\,10^{-11}$	6.58
$R2$	v_1	0.01	5000	$7.6\,10^{-11}$	6.58
$R3$	v_1	1	7000	$5.4\,10^{-11}$	6.58
$R4$	v_1	0.01	7000	$4.3\,10^{-11}$	6.58
$R5$	v_2	1	5000	$3.9\,10^{-10}$	1.83
$R6$	v_2	0.01	5000	$3.8\,10^{-10}$	1.83
$R7$	v_2	1	7000	$2.7\,10^{-10}$	1.83
$R8$	v_2	0.01	7000	$2.2\,10^{-10}$	1.83
$R9$	v_3	1	5000	$1.2\,10^{-7}$	1.03
$R10$	v_3	0.01	5000	$1.0\,10^{-7}$	1.03
$R11$	v_3	1	7000	$7.1\,10^{-8}$	1.03
$R12$	v_3	0.01	7000	$5.4\,10^{-8}$	1.03

For all the models, $R_{ph}=1.75\,10^{11}$ cm, $T_{eff}=10{,}000$ K, $v_D=30\,\mathrm{km\,s^{-1}}$, $R_{max}=50\,R_{ph}$

One must be careful, in moving media, to evaluate the source function at $\tau_{\nu_{obs}}$ where $\tau_{\nu_{obs}}$ is the optical depth at frequency ν_{obs} along the ray, and ν is given by:

$$\nu=\nu_{obs}-\nu_L\mu v/c\,, \tag{16}$$

where μv is the projection of the fluid velocity vector along the photon flight path.

Hence, the main contribution to the radiation at frequency ν_{obs} does not come from the iso-velocity surface $\mu v=c(\nu_{obs}-\nu_L)/\nu_L$, as is the case in the Sobolev approximation, but from the surface where $\tau_{\nu_{obs}}=1$.

Let us first consider the rays that hit the stellar core. For the "red" photons (depicted by ν'_{obs} in Fig. 3) travelling on these rays, the whole expanding envelope is completely transparent, since such photons do not encounter any region for which they are in resonance with the local line frequency. Thus, for these "red" photons, the medium is equivalent to a classical static photosphere and hence, the intensity profile on the rays hitting the core exhibits on its red side a wide photospheric wing, as the one observed in normal stars. The width of this red wing depends on the value of the damping parameter "a" and on the Doppler random velocity $v_D(R_{ph})$. On these rays, the blue part of the intensity profile is in absorption.

On the rays that do not hit the core, the intensity profile appears more and more in emission as one gets further and further from the core, since the background radiation against which the line is formed decreases and then vanishes. On the rays close enough to the core, the emission component in the intensity profile is redward displaced, because the points $\tau_{\nu_{obs}}=1$ are usually located before the resonance points with respect to the observer, and hence in regions of higher source function for the red frequencies (ν'_{obs}) than for the blue ones (ν_{obs}). The red displacement therefore depends on the width of the intrinsic profile. On remote rays, the medium becomes optically thin and the intensity profile is symmetric.

In Fig. 4, the intensity profile corresponding to model $R5$ is plotted for a set of chosen rays. This plot illustrates the qualitative remarks made above.

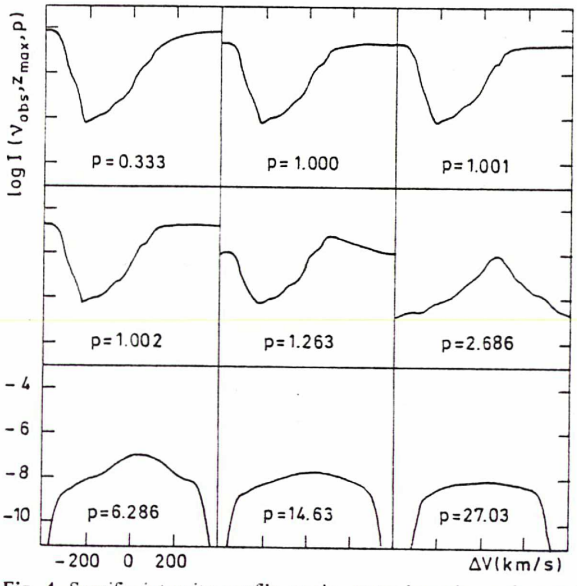

Fig. 4. Specific intensity profile at the outer boundary of several rays for model $R5$. The rays are labeled by their impact parameter p expressed in stellar radii. The interstellar component has not been taken into account here

It is now very easy to understand that an intense red emission component can be present in the resulting flux profile only if the red emission in the intensity profile on the rays that do not hit the core is sufficient to fill in the red absorption in the intensity profile on the rays that hit the core. This is not the case in models with a decreasing temperature law near the photosphere, because of the wide red photospheric wing formed in the static layers at the bottom of the wind. As can be seen from Fig. 2, some of the profiles obtained with decreasing temperature laws are similar to those observed in A type supergiants (KP; Kunasz et al., 1983), which suggests that Mg II line formation in A supergiants behaves in the same way as described above, quantitatively supporting an idea already presented by Lamers et al. (1978).

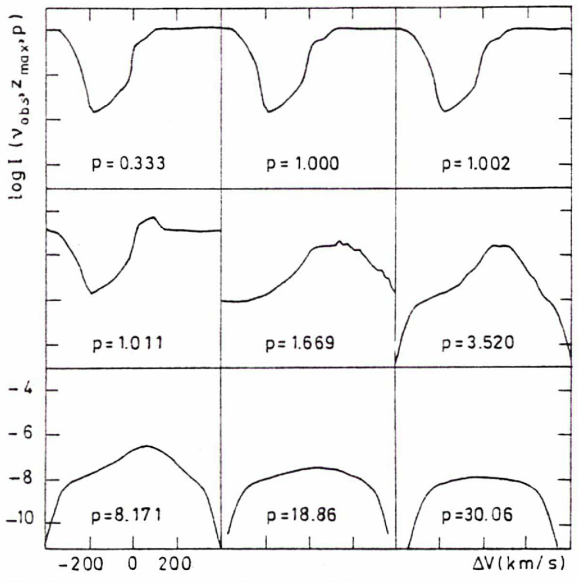

Fig. 5. Same as Fig. 4, but for the model *D* 1

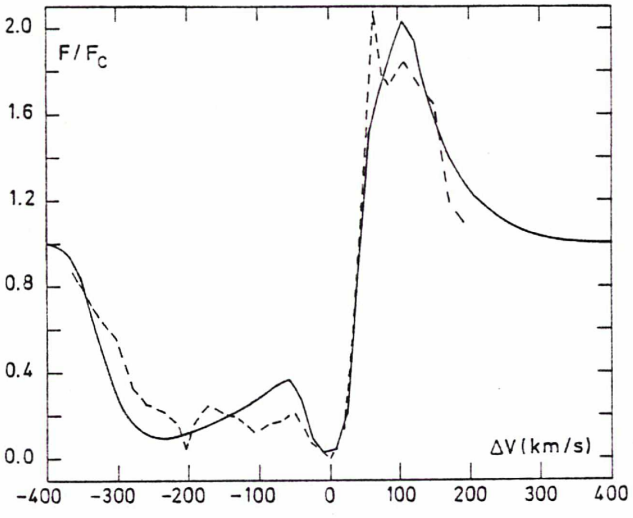

Fig. 6. Emerging flux profile corresponding to model *D* 1

Several solutions could be envisaged to increase the emission component in the resulting flux profile:

1) The use of velocity laws leading to less dramatic decreases in the density run (e.g., nearly constant $v(r)$ up to large distances from the stellar core). But because of the necessary presence of a classical photosphere at the base of the wind (see Sect. IIb), such velocity laws lead to very low mass loss rates and the whole line disappears almost entirely, because the line becomes thin in the wind.

2) The diminution of the Doppler random velocity v_D, which leads to a narrowing of the red photospheric absorption wing in the intensity profile on the rays hitting the core. But the smaller v_D, the less important the red asymmetry of the intensity profile on the rays that do not hit the core. As a result, when v_D decreases, the emission component is enhanced, but blueward displaced with respect to the observed position. Moreover, one needs to give high values to v_D in order to obtain a wide saturation of the blue component as observed. It seems impossible to reproduce the observed profile in this way.

3) The use of variable Doppler random velocity. If v_D increases with r, its low value at the bottom of the wind leads to a narrow red photospheric wing, while its high value in more remote regions ensures that the emission component is located at the right place in frequency. However, even with a variation of v_D of a factor 3, which is the maximum amplitude allowed by the computer we used, it has not been possible to find an emission component as intense as the observed one. However, since the results seemed to go in the correct direction, but not far enough, further calculations on a more powerful computer with a more variable v_D would be of great interest. However, a physical mechanism leading to a greatly variable Doppler velocity is still to be found.

The presence of a remote chromosphere does not change drastically the results presented for the Mg II resonance lines, since the formation of an intense emission component is prevented by the conditions in the region located just above the photosphere. A test case has been run, in which a steep temperature rise up to 10^5 K, 16 stellar radii wide, was placed at 30 stellar radii and the results were not fundamentally different from a similar case with a decreasing temperature law (model *R* 5). As mentioned above, our models with decreasing temperature laws are equivalent to remote chromosphere models, as far as Mg II line formation is concerned.

In conclusion, models with a decreasing temperature law near the bottom of the wind do not permit a fit to the entire profile of the Mg II *k* line. It is then very unlikely that the temperature is monotonically decreasing above the photosphere, even if, for some reason, a remote temperature rise would be present (to account for the presence of C IV and Si IV resonance lines).

b) Results with a "deep chromosphere"

The analytical form chosen to represent the temperature law in deep chromosphere models is the following:

$$T(r) = T_0 + (T_{max} - T_0) \exp\left\{ -4\ln 2 \frac{(r - R_{ch})^2}{\Delta_1^2} \right\} \quad \text{if} \quad R_{ph} \leqq r \leqq R_{ch} \tag{16}$$

$$= T_0 + (T_{max} - T_0) \exp\left\{ -4\ln 2 \frac{(r - R_{ch})^2}{\Delta_2^2} \right\} \quad \text{if} \quad r > R_{ch} \tag{17}$$

where

$$R_{ch} = R_{ph} + (\Delta_1/2)\sqrt{\ln 2}\sqrt{\ln\{(T_{max} - T_0)/(T_{eff} - T_0)\}}\,. \tag{18}$$

T_{max} is the maximum temperature reached in the chromosphere, Δ_1 and Δ_2 are parameters that allow a control of both the position (Δ_1) and the extension (Δ_2) of the chromospheric regions. Note that with this form of $T(r)$, the temperature drops down to T_0 very steeply after the chromospheric region. Our models are then almost isothermal in the outermost regions of the wind. However, the dethermalizing layers for the ions of interest in this analysis (Mg^+, C^{2+}, Si^{2+}) are located at great distances from the photosphere (see Sect. IIc), and it can be reasonably assumed that they lie further than the chromospheric region (see Sect. IVc). The main influence of the temperature law in these outer regions is to fix the values of the radiation temperatures T_r for the different ions considered, and then a model with a constant temperature above the chromosphere is equivalent to a model with any form of temperature law leading to the same radiation temperatures. Though physically unrealistic, the assumption of nearly constant temperature in the outermost regions of the wind ensures that $T_r \approx T_0$, which gives an easy way to control T_r through T_0.

The presence of a deep chromosphere has two effects on the radiative transfer in the wind:

Table 3. Models with a deep chromosphere

Model no.	Parameters				$\dot{M}(M_\odot\ \mathrm{yr}^{-1})$	Position of the sonic point (stellar radii)
	Velocity law	Δ_1 (stellar radii)	Δ_2	T_{max}(K)		
$D1$	v_2	0.08	4	15,000	$1.9\,10^{-10}$	1.83
$D2$	v_2	0.04	4	15,000	$1.9\,10^{-10}$	1.83
$D3$	v_2	0.08	6	15,000	$1.9\,10^{-10}$	1.83
$D4$	v_2	0.08	4	20,000	$1.9\,10^{-10}$	1.83
$D5$	v_4	0.08	4	15,000	$1.9\,10^{-10}$	1.83
$D6$	v_1	0.08	4	15,000	$3.8\,10^{-11}$	6.58
$D7$	v_2	0.08	4	15,000	$1.9\,10^{-10}$	1.83

For all the models, $R_{ph}=1.75\,10^{11}$ cm, $T_{eff}=10{,}000$ K, $R_{max}=50\,R_{ph}$, $T_0=5000$ K, $v_D=45\,\mathrm{km\,s^{-1}}$ (except for $D7$: $v_D=60\,\mathrm{km\,s^{-1}}$)

1) In the deepest chromospheric layers, the source function is coupled with the electron temperature and hence, the chromospheric rise leads to a rise in S_L. This creates a small emission component near the line center in the intensity profile on the rays hitting the core and enhances the red emission component in the intensity profile on the rays that do not hit the core, but that hit the base of the chromosphere.

2) In the hottest parts of the chromosphere, Mg^+ is severely depleted. Hence, the opacity is much lower than in the "remote chromosphere" models. As a consequence, the width of the red photospheric wing in the intensity profile on the rays hitting the core is narrower than in the "remote chromosphere" models.

These two effects can be seen in Fig. 5, where the intensity profile corresponding to model $D1$ on different rays has been plotted.

Thus, in models with a deep chromosphere, to fill in the red absorption wing is very easy because the latter is very narrow, and it is possible to obtain an intense emission component. Figure 6 shows the emerging flux profile for the model giving the best fit (model $D1$). All the information concerning this model can be found in Table 3.

In summary, the chromosphere acts on the emission component through a coupling of the source function with the temperature, and through the Mg^+ ion fraction governed by the temperature, the depth and the extension of the chromospheric region.

From this result and from the results of Sect. IVa, we conclude that the presence of a deep chromosphere is necessary to account for the shape of Mg II k line (we remind the reader that "deep" here means below the dethermalization layer for Mg II, which typically lies at $\tau_{2800}\sim 10^{-5}$).

In Fig. 7 are plotted the emerging profiles corresponding to the models described in Table 3, compared with the result of model $D1$, taken as reference. This comparison shows the influence of each parameter on the resulting profile.

Δ_1 and Δ_2 control the position and width of the chromosphere, and T_{max} its maximum temperature. When the chromosphere becomes deeper and deeper (as Δ_1 decreases), or hotter and hotter (as T_{max} increases), the emission component becomes more and more intense. This is due to the fact that the deeper or the hotter the chromosphere, the lower the Mg^+ column density and the narrower the red absorption wing on the central rays. Another effect of decreasing Δ_1 or increasing T_{max} is to enhance the emission component on the rays hitting the core or the bottom of the chromosphere. The influence of the extension of the chromosphere is more complex. Let us call the region contributing to the emission component "the emitting zone". This emitting zone extends to less than 10 stellar radii in all cases of interest because of the decrease of density in the wind. For small values of $\Delta_2(\leqq 2\,R_{ph})$, the chromosphere intersects only a small part of the emitting zone, and hence has little influence on it. When Δ_2 is small, an increase of the chromospheric extension leads to a diminution of the Mg^+ column density, and hence to an enhancement of the emission component for the reason mentioned just above. For higher values of Δ_2, the chromosphere intersects most of the emitting zone: when the chromospheric extension increases, the region where the Mg^+ is depleted gets bigger and bigger, and hence the emitting area becomes smaller and smaller. Then, the emission component decreases as Δ_2 increases.

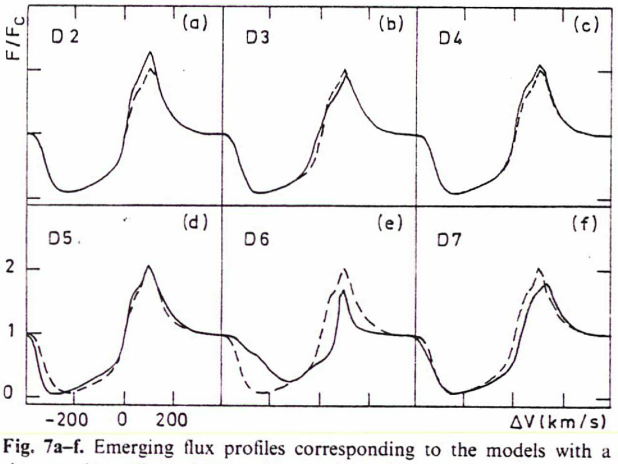

Fig. 7a–f. Emerging flux profiles corresponding to the models with a deep chromosphere. The models are described in Table 3. Each emerging profile *(full line)* is compared with the profile corresponding to model $D1$ *(dashed line)*. These comparisons illustrate the influence of the different parameters of the models. The interstellar component has been omitted here

As mentioned above, the parameter T_0 acts on the resulting profile only through the determination of the radiation temperatures T_r, because of the relative position of the chromosphere and the dethermalizing layers and the form chosen for the temperature law. It has little influence on the source function but a preponderent one on the absorption component of the emerging profile. When T_r increases indeed, Mg^+ becomes

more and more depleted in the outermost regions and the saturation near the violet edge of the line decreases, as can be seen in Fig. 2 for the case of decreasing temperature laws. The parameter T_r has also a great influence on the extension to be considered for the Mg II line formation region: the higher T_r the smaller the region of interest for the radiative transfer in Mg II resonance lines. The effect of T_0 (alias T_r) is exactly the same for models with a deep chromosphere.

The influence of the temperature law on the emerging profile can then be summarized as follows:

The blue absorption component is sensitive mainly to the value of the radiation temperature T_r, which is specified through the parameter T_0 in our models.

The red emission component is sensitive mainly to the temperature law in the chromospheric region.

In our models, the form of the velocity law in the outermost regions of the wind influences only the blue absorption component of the line. The outermost regions of the wind act on the emerging profile only through the central rays. It is then obvious that the deeper the point corresponding to a given value of the velocity, the darker the line at the frequency corresponding to this velocity.

At the bottom of the wind, the major parametric role played by the velocity law is to fix the value of the mass loss rate [Eq. (3)]. Experience and Eq. 3 show that the higher the velocity gradient at the bottom of the wind, the higher the mass loss rate. The global density in the wind being proportional to $\dot{M}$, the lower $\dot{M}$, the less enhanced the different parts of the line profile (Fig. 7e).

The Doppler random velocity governs the width of the intrinsic profile (expressed in velocity units). It then influences the location of the point $\tau_{\nu_{obs}} = 1$ with respect to the resonance point for a given frequency ν_{obs} and a given ray. Hence, when v_D increases, the point $\tau_{\nu_{obs}} = 1$ gets closer to the observer, that is to say in a region of lower source function for the blue observed frequencies and of higher source function for the red ones. Then, when v_D increases, the emission component is shifted to the red and the absorption component gets more saturated. Moreover, the absorption component is widened to the blue (see Sect. IIb).

c) Conclusions on the physical structure

We have shown in this paper that a deep chromosphere at the bottom of the wind of AB Aur explains the formation of the Mg II k line profile. The existence of such a chromosphere is consistent with the observations of the Ca II K line (Praderie et al., 1982), of He I λ 5875 Å and the Ca II IR triplet (Felenbok et al., 1983) and of the resonance lines of Si IV and C IV (see Sect. II). Nevertheless, this consistency must be quantitatively checked. A detailed analysis of the formation of the Ca II K line and Si IV and C IV resonance lines is under progress.

As already stressed, the temperature law in the chromospheric region influences only the emission component of the emerging profile. Since this emission component is highly sensitive to other parameters, in particular to the mass loss rate through the form of $v(r)$ at the bottom of the wind, it is impossible to derive precise information on the depth and the temperature of the chromosphere through the interpretation only of Mg II resonance lines. All we can do is to give estimates of the temperature structure in the chromosphere.

A lower limit for the maximum temperature can be inferred by the observation of C^{3+} in the wind of AB Aur. At temperatures lower than 15.000 K, there is not enough C^{3+} to give rise to deep absorption lines as the ones observed. Here again, a quantitative interpretation of the C IV resonance lines will provide a more precise answer to this question.

We can also estimate an upper limit to the depth reached by the chromosphere: observations indeed show that there is no emission in the Balmer continuum for AB Aur (see Garrison, 1978; Catala, 1983a). Too deep a chromosphere would produce an emission in that continuum. The maximum optical depth considered in our computations for the chromosphere is $\tau_{2800} \sim 10^{-2}$, which corresponds to $\Delta_1 \sim 0.04\, R_{ph}$. A better determination of this limit requires an accurate calculation of the Balmer continuum, and is deffered to a subsequent paper. On the other hand, the experience showed that the temperature rise had to occur rather close to the photosphere, in order to account for the Mg II k line profile. Typically, in the models leading to a Mg II k line profile globally similar to the one observed, the temperature minimum is located at $\tau_{2800} \sim 10^{-2} - 10^{-3}$, which shows that the chromosphere in AB Aur is deeper than the solar chromosphere, but not as deep as the chromospheres of the models built for T Tauri stars (Calvet et al., 1984).

An upper limit to the extension of the chromosphere can also be determined from the present study. When the chromosphere extends too far, the resulting emission component in the emerging profile becomes too wide. We found that the extension of the chromosphere could not be greater than 8 or 9 stellar radii. It has also been impossible to reproduce the Mg II k line profile with a geometrically thin chromosphere, as the one observed in the Sun. The very minimum extension to be considered for the chromosphere of AB Aur is of about one stellar radius, which is by orders of magnitude greater than the solar case.

Since the temperature law in the chromospheric region influences only the emission component on the emerging profile, the absorption component provides a better way of determination of the mass loss rate. Its saturation increases with $\dot{M}$ (Fig. 7e). However, the radiation temperature for Mg^+ (governed by T_0) has the opposite effect on the saturation of the absorption component. Hence, it is necessary to set limits on T_r in order to obtain limits on the mass loss rate. An upper limit is in fact sufficient, because when $T_r(Mg^+) \geqq 5000$ K, almost all the magnesium material is under the form Mg^+, so that 5000 K can be considered as a lower limit for $T_r(Mg^+)$ in our computations. As mentioned above, the chromosphere cannot extend to distances greater than 8 or 9 stellar radii. We have seen that the dethermalizing layer, whose electron temperature gives the radiation temperature, is located further from the stellar core, at more than 10 stellar radii (see Sect. IIc). It is then reasonable to think that the dethermalizing layer lies in a region in radiative equilibrium. If it was a classical grey radiative equilibrium, the temperature would be of the order of 3000 K at such distances. For safety, we have decided to double this value and to take 6000 K as upper limit for T_r. With this range of T_r, we can determine the following limits for $\dot{M}$:

$$4\,10^{-11} \leqq \dot{M} \leqq 7\,10^{-9}\, M_\odot\, \mathrm{yr}^{-1}. \qquad (19)$$

This result is consistent with that of Garrison (1978), who finds $10^{-8}\, M_\odot\, \mathrm{yr}^{-1}$ as an upper limit for $\dot{M}$, from the absence of an excess emission in the Balmer continuum. Talavera et al. (1982) found $\dot{M} \sim 10^{-11}\, M_\odot\, \mathrm{yr}^{-1}$, using a non saturated line of Fe II and estimates of the velocity law derived at the very beginning of the present study. Such a method is highly sensitive to the form of the velocity law near the photosphere. It will be interesting to use this method again, with a better estimate of $v(r)$, and our way of treating ionization equilibria. Such a work is presently under progress. Kuan and Kuhi (1975) found $\dot{M} = 3\,10^{-7}\, M_\odot\, \mathrm{yr}^{-1}$, by a fit of the observed maximum intensity in the emission component of Hβ with that of a model with a decelerating wind, using the Sobolev approximation. We have already argued against the

assumption of a decelerating wind in Sect. IIb. The experience also showed that a steep acceleration at the bottom of the wind, like the one necessary to connect static layers to a decelerating wind, leads to a mass loss rate far too high to be consistent with Mg II resonance lines profile. Moreover, the use of the Sobolev approximation is inadequate for a computation of the maximum intensity of the emission component, since the latter lies in the line center where the Sobolev approximation is known to be unvalid (Hamann, 1981). Anyway, this example shows that the results on the values of mass loss rate depend greatly on the basic assumptions and so these assumptions must be tested further by observations.

Since the mass loss rate is closely related to the velocity gradient at the bottom of the wind, inequality (19) can be interpreted as an estimate of this gradient. We then find that the velocity gradient lies between that of the law v_1 (corresponding to $\dot{M}=4\,10^{-11}\,M_\odot\,\mathrm{yr}^{-1}$) and that of the law v_5 (corresponding to $\dot{M}=7\,10^{-9}\,M_\odot\,\mathrm{yr}^{-1}$). This condition eliminates for example the velocity laws of Castor and Lamers (1979) for $\beta=1/2$ and $\beta=1$, which have too strong a gradient at the bottom of the wind. Finally, inequality (19) can also be interpreted as an estimate of the position of the sonic point, which must lie between that of the law v_5 ($1.03\,R_{ph}$) and that of the law v_1 ($6.58\,R_{ph}$).

It is not possible by the interpretation only of the Mg II resonance lines to set precise constraints on the velocity law in the outer and the intermediate regions of the wind. Too many other parameters indeed, particularly the form of the temperature law in the chromosphere, act at the same time on the emerging profile. Nevertheless, by a quantitative study of lines formed in more localized regions (such as Si IV, C IV, Ca II resonance lines), it will be possible to get more precise information about the temperature law in the chromosphere, and this information will be useful to derive tighter constraints on the whole velocity law, by using the results of the present study.

Finally, the position of the emission component being sensitive to the Doppler random velocity v_D, and to this parameter only, it is easy to determine v_D by a comparison of the observed and the computed positions. We find $v_D \sim 45\,\mathrm{km\,s}^{-1}$. This value is supersonic. It corresponds to the flow velocity at 2.5 stellar radii in model $D1$. The Doppler random velocity v_D is then completely dominated by its non-thermal component, since the thermal component v_{th} is of about $3\,\mathrm{km\,s}^{-1}$. This high value of v_D is comparable to that found by KP for the wind of α Cygni, $30\,\mathrm{km\,s}^{-1}$. But it is the first time that a supersonic Doppler velocity is brought to light in the wind of a dwarf star. The broadening of the intrinsic profile corresponding to this value of v_D may not be due to microturbulence, as is often believed, but to an unknown broadening mechanism.

In summary, it is clear that AB Aur possesses a chromosphere, which is deeper than the solar one, but not as deep as is usually believed for the chromospheres of T Tauri stars. However, the chromosphere of AB Aur does not look like the solar or the T Tauri stars chromospheres: its extension indeed is greater by orders of magnitude than in the solar or the T Tauri stars cases. Could such a layer be heated by radiative effects in an extended atmosphere? Extended temperature rises have been reproduced for static extended atmospheres in radiative equilibrium of very massive stars (Kunasz et al., 1975), and picket-fence models for expanding atmospheres in radiative equilibrium show in some cases important increases in temperature in remote layers (Mihalas et al., 1976a). However, there is no evidence that such effects could be efficient in Herbig Ae stars and the presence of such heated layers needed in AB Aur probably implies a non-radiative heating source. If so, this suggests that this star possesses a convection zone. This would mean that the final phase of PMS evolution for objects of that mass ($2.5\,M_\odot$) is not entirely radiative.

The wind of AB Aur is by far denser than the solar wind, but not as dense as the winds of T Tauri stars, whose mass loss rates are typically of $10^{-7}\,M_\odot\,\mathrm{yr}^{-1}$ (Kuhi, 1964). Such an analysis should be carried out for the other Herbig Ae stars, in order to estimate their mass loss rates. This would tell us if the low density of the wind brought to light in the case of AB Aur is a common property of this class and if the mass loss rates are related to the closeness to the main sequence for stars on a PMS stage of their evolution.

V. Conclusion

This work is one of the very first steps towards the quantitative description of the extended atmospheres of Herbig Ae/Be stars. Our purpose was to investigate the structure of the atmosphere of one of these stars, AB Aur, in order to provide a way of testing the different models that will be proposed in theoretical approaches of the problem of their chromospheric activity and wind production.

The results of the present study can be summarized as follows:

The stellar core is surrounded by an expanding deep chromosphere, which is necessary to account for the intense emission component observed in the Mg II k line profile. This chromosphere is deeper than the solar one, but less deep than the chromospheres of the models proposed for T Tauri stars. The fundamental difference between the case of AB Aur and the solar and the T Tauri stars cases lies in the extension of the chromosphere, which is here greater by orders of magnitude than had ever been envisaged.

The mass loss rate must lie between $4\,10^{-11}\,M_\odot\,\mathrm{yr}^{-1}$ and $7\,10^{-9}\,M_\odot\,\mathrm{yr}^{-1}$, which is far greater than for the solar wind, but quite lower than the mass loss rates derived for T Tauri stars. AB Aur may then appear as intermediate between main sequence stars and stars in the early phases of PMS evolution. The simultaneous knowledge of the mass loss rate and of the terminal velocity of a wind constitutes a powerful test of any stellar wind theory. This estimate of $\dot{M}$ will then be very useful in the future.

It has been possible to set constraints on the velocity law at the bottom of the wind. This can also be very useful, since it is likely that the base of the wind plays a major role in the wind production.

We have also estimated the Doppler random velocity, which has been found to be $45\,\mathrm{km\,s}^{-1}$. This supersonic value shows that thermal effects are not the dominant broadening mechanism.

The continuation of this work lies in a quantitative study of lines which are formed in regions more localized than Mg II resonance lines. Si IV and C IV resonance lines, for example, are formed in the chromospheric region, and Ca II resonance lines are formed in the photosphere and the chromosphere. The interpretation of these lines, which is under progress, will help us to refine the global insight that could be put on AB Aur's envelope by the interpretation of Mg II k line. A quantitative interpretation of hydrogen lines would also constitute a powerful test for our models. The detailed calculation of the Balmer lines Hα, Hβ, and Hγ is under progress.

The model proposed here to account for line formation in the wind of AB Aur is spherically symmetric. However, several recent observations of this star tend to show that it is spectroscopically variable on different time scales, the lowest one being as small as two hours (Praderie et al., 1982, 1983; Felenbok et al., 1984; Catala et al., 1984). This variability may be related to the presence of inhomogeneities in the wind, which evolve on several time scales,

because of the rotation or because of macroscopic random motions in the wind. This kind of behavior strongly suggests important departures from the spherical symmetry that has been assumed here. Our results must then be regarded as giving a preliminary representation of the atmosphere of this star, and they will provide the basic framework for the subsequent more realistic models.

Acknowledgements. We are very grateful to J. Borsenberger for helping us with all the computational problems.

References

Abbott, D.C.: 1982, *Astrophys. J.* **259**, 282
Beals, C.S.: 1951, *Publ. Dominion Astrophys. Obs.* **9**, 1
Calvet, N., Basri, G., Kuhi, L.V.: 1984, *Astrophys. J.* **277**, 725
Cassinelli, J.P.: 1979, *Ann. Rev. Astron. Astrophys.* **17**, 275
Castor, J.I.: 1970, *Monthly Notices Roy. Astron. Soc.* **149**, 111
Castor, J.I., Abbott, D.C., Klein, R.I.: 1975, *Astrophys. J.* **195**, 157
Castor, J.I., Lamers, H.J.G.L.M.: 1979, *Astrophys. J. Suppl.* **39**, 481
Catala, C.: 1983a, *Astron. Astrophys.* **125**, 313
Catala, C.: 1983b, Thése de troisième cycle, Université Paris 7
Catala, C., Felenbok, P., Talavera, A., Praderie, F., Czarny, J.: 1984 (in preparation)
Cohen, M.: 1973, *Monthly Notices Roy. Astron. Soc.* **161**, 105
Cohen, M.: 1975, *Monthly Notices Roy. Astron. Soc.* **173**, 279
Cohen, M.: 1980, *Monthly Notices Roy. Astron. Soc.* **191**, 499
Doazan, V.: 1982, in *B stars with and without emission lines*, NASA SP 456, p. 377
Drake, S.A., Linsky, J.L.: 1983, *Astrophys. J.* **273**, 299
Felenbok, P., Praderie, F., Talavera, A.: 1983, *Astron. Astrophys.* **128**, 74
Felenbok, P., Catala, C., Czarny, J., Talavera, A.: 1984 (in preparation)
Finkenzeller, U., Mundt, R.: 1984, *Astron. Astrophys. Suppl.* **55**, 109
Garrison, L.M.: 1978, *Astrophys. J.* **224**, 535
Hamann, W.R.: 1981, *Astron. Astrophys.* **93**, 353
Hartmann, L., Edwards, S., Avrett, E.: 1982, *Astrophys. J.* **261**, 279
Herbig, G.H.: 1960, *Astrophys. J. Suppl.* **4**, 337
Kuan, P., Kuhi, L.V.: 1975, *Astrophys. J.* **199**, 148
Kuhi, L.V.: 1964, *Astrophys. J.* **140**, 1409
Kunasz, P.B., Hummer, D.G.: 1974, *Monthly Notices Roy. Astron. Soc.* **166**, 57
Kunasz, P.B., Hummer, D.G., Mihalas, D.: 1975, *Astrophys. J.* **202**, 92
Kunasz, P.B., Praderie, F.: 1981 (KP), *Astrophys. J.* **247**, 949
Kunasz, P.B., Morrison, N.D., Spressart, B.: 1983, *Astrophys. J.* **266**, 739
Kurucz, R.L.: 1970, ATLAS SAO Special Report, 309
Kurucz, R.L.: 1979, *Astrophys. J. Suppl.* **40**, 1
Lamers, H.J.G.L.M., Snow, T.P.: 1978, *Astrophys. J.* **219**, 504
Lamers, H.J.G.L.M., Stalio, R., Kondo, Y.: 1978, *Astrophys. J.* **223**, 207
Mihalas, D., Kunasz, P.B., Hummer, D.G.: 1975, *Astrophys. J.* **202**, 465
Mihalas, D., Kunasz, P.B., Hummer, D.G.: 1976a, *Astrophys. J.* **203**, 647
Mihalas, D., Kunasz, P.B., Hummer, D.G.: 1976b, *Astrophys. J.* **206**, 515
Mihalas, D., Kunasz, P.B., Hummer, D.G.: 1976c, *Astrophys. J.* **210**, 419
Mihalas, D., Kunasz, P.B.: 1978, *Astrophys. J.* **219**, 635
Parker, E.N.: 1958, *Astrophys. J.* **128**, 664
Praderie, F., Talavera, A., Felenbok, P., Czarny, J., Boesgaard, A.M.: 1982, *Astrophys. J.* **254**, 658
Praderie, F., Simon, T., Boesgaard, A.M., Felenbok, P., Catala, C., Czarny, J., Talavera, A., Le Contel, J.M., Morel, P., Sareyan, J.P., Valtier, J.C.: 1983, 2nd France-Japan Seminar, Paris, eds. J.C. Pecker, Y. Uchida (in press)
Sahal-Bréchot, S.: 1977 (private communication of numerical codes)
Sitko, M.L.: 1981, *Astrophys. J.* **247**, 1024
Strom, S.E., Strom, K.M., Yost, J., Carrasco, L., Grasdalen, G.L.: 1972, *Astrophys. J.* **173**, 353
Strom, S.E., Strom, K.M., Grasdalen, G.L.: 1975, *Ann. Rev. Astron. Astrophys.* **13**, 187
Talavera, A., Catala, C., Crivellari, L., Czarny, J., Felenbok, P., Praderie, F.: 1982, *Proc. 3rd European IUE Conf.*, ESA SP 176, p. 99
Wiese, W.L., Smith, M.W., Miles, B.M.: 1969, Atomic Transition Probabilities, Vol. II, NSRDS – NBS 22

Astron. Astrophys. 174, 158–172 (1987)

ASTRONOMY AND ASTROPHYSICS

Line formation in the winds of Herbig Ae/Be stars. The Hα line

C. Catala[1]* and P.B. Kunasz[2]

[1] High Altitude Observatory, National Center for Atmospheric Research,** PO Box 3000, Boulder CO 80307, USA
[2] 315 Skylark Way, Boulder CO 80303, USA

Received July 21, accepted September 24, 1986

Summary. We present the results of a detailed quantitative interpretation of Hα and other hydrogen lines of AB Aur, considered as representative of part of the pre-main sequence Herbig Ae/Be stars.

We have used the equivalent-two-level-atom approach to solve the radiative transfer problem and the equations of statistical equilibrium in the context of the multi-level hydrogen atom. The radiative transfer equation is solved in the comoving frame of the flow.

Our calculations show that the model which had been derived previously from the interpretation of the Mg II and the C IV resonance lines, and which involves a wind including an extended chromosphere, is also successful in reproducing the observed emission component of Hα. Additional constraints are derived for the temperature minimum below the chromosphere and for the temperature outward of the chromosphere. The mass-loss rate is the parameter which is the most constrained by this analysis, and we find $1\,10^{-8} \leq \dot{M} \leq 1.8\,10^{-8}\,M_{\odot}\,\mathrm{yr}^{-1}$, making use of the present analysis and previous line interpretation.

Also, this analysis allows us to study the dependency of the Hα profile upon the different parameters of the model, and some interesting features are described and analyzed, in particular a non-monotonic variation of the Hα emission component with the mass-loss rate.

Finally, as a by-product of the Hα calculations, the profiles of Hβ, Hγ, Pα, Pβ, and Bα have been computed, as well as the emergent continuum flux.

Key words: pre-main-sequence stars – stellar winds – stellar chromospheres – line formation

1. Introduction

More than two decades ago, Herbig (1960) produced a list of 26 candidate pre-main sequence Ae/Be stars. His original conjecture that these stars are pre-main sequence objects, higher-mass counterparts of the T Tauri stars, has now been confirmed (Strom et al., 1972; Cohen and Kuhi, 1979). Recently, Finkenzeller and Mundt (1984) have extended this list to 57 candidates and have shown that these stars can be divided in three subclasses, according to their Hα profile (double-peak emission profile, single-peak emission profile or P Cygni profile). The challenge that now lies before us is to characterize the physical processes at work in these three subclasses and to recognize the main differences between them.

Clearly, the first step toward this goal is a semi-empirical modelling of these stars, in order to determine the structure of their outer layers. A systematic effort has been made in this direction in the past few years for the stars of the "P Cygni" subclass. It has been shown that these stars exhibit striking similarities in several other lines, from which a significant degree of structural similarity has been concluded (Catala et al., 1986a). This allows us to consider the brightest member of this subclass, AB Aur (A0Ve, $m_V = 7.2$), as representative of the whole subclass.

Previous work on AB Aur, based on the assumption of a non-rotating, steady-state, spherically symmetric wind, led to tentative structured models. The quantitative interpretation of its Mg II resonance lines implied the existence of an extended chromosphere, and some constraints for the velocity and temperature runs in its wind (Catala et al., 1984, hereafter CKP). Tighter constraints were placed on the chromosphere by the observation and interpretation of the C IV resonance lines (Catala, 1984; Catala and Talavera, 1984).

In spite of these efforts, our knowledge of the structure of AB Aur's envelope is far from being satisfactory. Assuming that the basic modelling assumptions are valid, the problem encountered when interpreting a line profile is the nonuniqueness of the model. The only way to circumvent this problem is to require that the model predicts several lines. A very powerful test of the existing model for AB Aur, as well as a way of constraining more its parameters, is the interpretation of the hydrogen lines. The Hα line has been observed many times in AB Aur (Garrison and Anderson, 1977; Felenbok et al., 1983; Finkenzeller and Mundt, 1984; Catala et al., 1986a; Guerin et al., 1987) and is the most suitable candidate for our purpose: its very well marked P Cygni profile indicates that it is formed in the star's wind. The higher Balmer lines exhibit a dominant photospheric absorption profile (Finkenzeller and Jankovics, 1984) and therefore constitute a poor test for our wind and chromosphere model. In the infrared, observations exist for the Pβ and Pγ lines (Maillard and Chalabaev, 1986) and for the Bγ line (Harvey, 1984; Maillard and Chalabaev, 1986). All of these infrared lines appear in emission. In the ultra-

Send offprint requests to: C. Catala

* On leave of absence from Observatoire de Paris, Section de Meudon

** The National Center for Atmospheric Research is sponsored by the National Science Foundation

violet, no observation is available for the Lyman lines. Hα, being the line observed with the highest resolution and the highest signal-to-noise ratio, is therefore the one on which we shall concentrate our effort in the present paper. Our goal is to carry out a quantitative interpretation of the Hα line in AB Aur, on the basis of a spherically symmetric model atmosphere, including a wind, and an extended chromosphere whose existence has been demonstrated by previous work (CKP; Catala and Talavera, 1984).

Section 2 points to the problem of the time variability of Hα, which forces us to question interpretations of any single profile in terms of a spherically symmetric and steady-state model. Section 3 reviews the constraints previously determined for the model of AB Aur's wind and chromosphere. Section 4 describes the equivalent-two-level-atom approach in the comoving frame, which has been used in this work for solving the radiative transfer problem, and Sect. 5 presents the results and consequences of the present analysis. Finally, a summary and general conclusions are given in Sect. 6.

2. Hα observations. Variability

The various observations of the Hα profile in AB Aur, carried out at different dates, have clearly shown that this line is variable in this star. The best example of this variability can be found in Catala et al. (1986a), who showed that the profile can vary from a type II P Cygni profile (Beals, 1951), i.e. a blueshifted absorption component, an intense redshifted emission component, and photospheric wings, to a type III P Cygni profile, i.e. a similar profile, but with an additional emission component on the blue side of the absorption feature.

The detailed study of the time variability of the Mg II resonance lines and the Ca II K line showed that these lines are modulated by the rotation of the star and of its envelope. A model involving the alternation on the line of sight of fast and slow streams was proposed to explain this rotational modulation (Praderie et al., 1986; Catala et al., 1986b). Although such a detailed study has not yet been carried out for Hα variability, it is likely that the observed variations of this line are due to the same phenomenon. It might then seem questionable to attempt a detailed modelling of the formation of Hα in spherically symmetric geometry, since the alternation of fast and slow streams in the wind as the star rotates implies important departures from spherical symmetry.

However, keeping in mind that a spherically symmetric model may be a poor representation of the reality, there are still several things that can be done. The first point is to recognize that, in a P Cygni profile, the absorption component is formed in the region of the envelope that is projected on the stellar disk, and which therefore encompasses only a very small volume. The absorption component is therefore expected to be very sensitive to local variations in density, temperature and velocity on the line-of-sight to the observer, as the star and its envelope rotate. We cannot therefore expect to derive any valuable information on the average structure of the envelope from the interpretation of the absorption component. By contrast, the emission component of a P Cygni profile, which is formed throughout the expanding envelope, is more likely to represent average physical properties, and we can expect to derive average information about the line formation region from its analysis. This point is supported by the observation of the time variability of the absorption and emission components of Hα. Guerin et al. (1987) report that the emission component varies only by 17%, while the absorption component varies by 65%, on a 24-hour time scale. However, any quantitative result that can be derived from the interpretation of the Hα emission component is based on the assumption that a homogeneous medium with the average properties of an inhomogeneous medium could produce an emergent emission profile similar to that produced by the inhomogeneous medium. Work in progress on two- and three- dimensional non-LTE line transfer (Kunasz and Auer, 1986) may allow our assumption to be tested. If it turns out to be wrong, many conclusions drawn in this paper on the physical structure of AB Aur's envelope will have to be dropped. In the work reported here, it is assumed that we cannot derive anything from the absorption component, other than the maximum velocity reached in the line-formation region, and that the emission component can provide average information about the physical structure of the envelope, under the basic assumption given above.

Yet another reason for carrying out these computations in spherical symmetry is that they will tell us about the physics of line formation for Hα in the context of a wind with an embedded chromosphere. We can derive valuable information such as the region of formation of the Hα line, the dominant processes of population and depopulation of the different levels of hydrogen, etc ... With this knowledge it could be possible to qualitatively extrapolate the results to more complicated cases, involving two- or three-dimensional geometries.

3. The model

In this section, we review the previous constraints that have been derived for the structure of AB Aur's envelope, and indicate how we have constructed the models used for the computations of the hydrogen lines. All of these constraints have been placed at a time when the departures from spherical symmetry had not yet been fully recognized in that star, and some of the previous conclusions have to be moderated. In particular, such notions as velocity law or mass-loss rate lose part of their general meaning when one goes from a one-dimensional spherically symmetric, steady-state representation to a geometrically more complex and time-dependent model. Since we try to represent the complex structure of AB Aur's envelope by a simple one-dimensional model, all of the parameters used in our model must be understood as average properties of the flow.

3.1. Photospheric layers

Garrison (1978) has shown that the Balmer jump and the Paschen continuum of AB Aur are very well represented by an LTE Kurucz (1979) model of photosphere in hydrostatic and radiative equilibrium, with $T_{\rm eff} = 10{,}000$ K and $\log g = 4$. Moreover, Praderie et al. (1982) have shown that this same model reproduces the observed wings of Hδ. Finally, Sitko (1981) and Catala (1983) have checked that the discrepancy which is found between this Kurucz model and the observations of the Balmer continuum can be accounted for by extinction by the circumstellar dust grains also detected in the infrared. All of these observations strongly suggest that a classical photosphere with $T_{\rm eff} = 10{,}000$ K and $\log g = 4$ must be present at the base of the wind.

3.2. Velocity law

Several authors have proposed in the past that the wind of AB Aur is decelerated (Kuan and Kuhi, 1975; Finkenzeller, 1983; Finkenzeller and Mundt, 1984) on the following basis: they argue that the so-called "blue asymmetry" for P Cygni profiles (the maximum blueward displacement in the absorption component of a P Cygni profile being larger than the maximum redward displacement in the emission component) can be explained only by the strong occultation effect obtained when the highest velocity regions are close to the stellar photosphere, as is the case for a decelerating wind, when the deceleration occurs very close to the star's surface. We show here, in very simple terms, that this idea is wrong, and that the "blue asymmetry" can be expected in the absence of any occultation, due to effects of scattering alone. Suppose an expanding spherically symmetric envelope is illuminated by a point source at its center (no occultation). Let us assume that the velocity is monotonically increasing with the distance from the center. Let us also assume an optically thick, pure scattering medium for a spectral line. Clearly, a P Cygni profile will be formed. Now consider a small frequency bin near the blue edge of the line. The region of the envelope interacting with the source radiation in this frequency bin is a thin layer delimited by two surfaces of constant velocity projected on the line-of-sight, corresponding to the width of the frequency bin. The photons removed from this bin are those which reach this layer, and are scattered in any direction except the observer's direction. Consider now the frequency bin of the same width symmetric to the previous one with respect to the line center. Again, the volume interacting with the source radiation in this red frequency bin is delimited by the surfaces of constant projected velocity, which are symmetric to the previous ones with respect to the center of symmetry of the envelope. The "red" interaction region then has the same volume as the "blue" one. But the photons added to the red frequency bin are those which reach this volume, and are scattered in the observer's direction. The number of photons added in the red frequency bin is therefore much smaller than the number of photons removed from the blue frequency bin. Although the radiation added in the red frequency bin is not zero, it is extremely weak and unlikely to be detected above a continuum orders of magnitude more intense. As a consequence, the observed maximum blueward displacement of the absorption component in an observed P Cygni profile is larger than the observed maximum redward displacement of the emission component, even in the absence of any occultation effect. We conclude from this simple example that the "blue asymmetry" observed in several lines with P Cygni profiles in AB Aur's spectrum does not necessarily indicate a strong occultation effect, and does not therefore constitute a proof that the wind of AB Aur is decelerated. As an example, the Hα profiles we obtain in the present analysis show a "blue-asymmetry", whereas the occultation effects are negligible in our models (see Figs. 2, 4, 5, 6).

Also, previous analysis of the Mg II resonance lines and of the C IV resonance lines show that their profiles are consistent with a monotonically increasing velocity law in the wind (CKP, Catala, 1984). Moreover, the simultaneous observation of the Ca II K line, showing a maximum blueward displacement of 310 km s^{-1}, and of the Mg II resonance lines with a maximum blueward displacement of 450 km s^{-1}, on October 26, 1982 (Catala et al., 1986b) constitutes further evidence that the wind of AB Aur is accelerated outwards in the formation region of these lines. The blue edge of the Ca II K line is indeed likely to be formed closer to the photosphere than the blue edge of the Mg II lines (Catala et al., 1986a).

The outermost layers of the wind are, however, another matter. Observation of a P Cygni profile for the Na I D lines, with an absorption component blueward displaced by 130 km s^{-1} (Felenbok et al., 1983) shows that the wind must decelerate at a distance from the photosphere where the temperature has decreased (CKP). But CKP showed that this observation was not inconsistent with an accelerating wind in all of the region of formation for the Mg II lines, because the regions of formation of the Mg II lines and of the Na I D lines are distinct, and the same assumption will be made here concerning the region of formation of the Hα line. Nonetheless, we stress here that no further observational evidence rules out the possibility that the aforementioned deceleration could occur somewhere in the Hα or the Mg II formation region.

The interpretation of the Mg II and C IV resonance lines has brought some constraints on the velocity law, especially at the base of the wind and in the chromosphere (CKP, Catala, 1984): the velocity gradient must be low above the photosphere to explain the deep absorption in the C IV lines near the line center, the velocity at the outer boundary of the chromosphere must be as high as 150 km s^{-1} to explain the blueward broadening of the same lines, and the maximum velocity in the flow must be around 300 km s^{-1} to explain the Mg II line profile. We note however that, except the first one, these constraints must not be considered as very tight, because of the aforementioned variability of the observed features on which they are based.

3.3. Temperature law

The temperature law has already been tightly constrained by the previous analysis by CKP, Catala and Talavera (1984) and Catala (1984). These studies have shown that AB Aur possesses an extended chromosphere with a maximum temperature between 15,000 K and 19,000 K. The temperature rise must be sharp above the photosphere and the extension of the chromosphere must be between 1 and 1.5 stellar radii.

No constraint exists so far for the temperature minimum in the photosphere, nor do we know much about the temperature in the region surrounding the chromosphere. These quantities will then remain free parameters in the present work.

3.4. Mass-loss rate

In CKP, constraints for the mass-loss rate $\dot{M}$ were derived from the analysis of the Mg II resonance lines. However, the model was very sensitive to the assumed radiation temperature for the ionization of Mg II. The upper limit found for $\dot{M}$ was therefore dependent on the estimated upper limit for this radiation temperature. CKP derived this upper limit with the assumption that the ionizing radiation for Mg II was thermalized throughout the chromospheric region. Now, from the results of the calculations presented in this paper, we realize that this assumption is verified only for high values of $\dot{M}$, which would be inconsistent with the shape of the Mg II lines and the Hα line. It is found here that the ionizing radiation for Mg II thermalizes only below the chromosphere and therefore the upper limit for its radiation temperature has been underestimated in CKP. As a consequence, the upper limit for $\dot{M}$, $7\,10^{-9}\,M_{\odot}\,\mathrm{yr}^{-1}$, has also been underestimated.

Other estimates of $\dot{M}$ in AB Aur can be found in the literature. Kuan and Kuhi (1975) found $\dot{M} = 3\,10^{-7}\,M_\odot\,\mathrm{yr}^{-1}$, using the assumption of a decelerated wind, against which we have already argued. On the other hand, Garrison (1978) found an upper limit of $10^{-8}\,M_\odot\,\mathrm{yr}^{-1}$ from the absence of Balmer continuum excess, using a simple optically thin Balmer emission model. The clear discrepancy between these two results points to the difficulty of obtaining reliable results from fitting a single feature, and justifies the multi-feature analysis which has been the guideline for CKP, Catala and Talavera (1984), Catala (1984), and the present paper.

3.5. *Doppler random velocity*

A supersonic Doppler random velocity v_D has been necessary to explain the Mg II and C IV line profiles in CKP and Catala (1984). A constant value of $v_D = 45\,\mathrm{km\,s}^{-1}$ has been assumed for the interpretation of the Mg II resonance lines, and a larger value ($100\,\mathrm{km\,s}^{-1}$) has been envisaged in the preliminary results of the C IV line analysis (Catala, 1984). It is not clear whether these high values show the existence of high velocity turbulent motions on small scales, or if they simply witness our inability to represent correctly the complexity of the 3-D macroscopic velocity field. Near the base of the wind for example, rotation, which has not been included in any of the previous analysis, could play an important role in widening the C IV resonance lines. Besides, downdrafts could coexist within the chromosphere with an average outward-directed flow, and also contribute to the broadening of these lines. If present, all of these phenomena, which cannot be included in the computation, make it necessary to introduce a large Doppler broadening for the calculations in spherically symmetric and monotonically accelerated flows.

3.6. *Construction of the models*

All of the models used in the present analysis were constructed as described in CKP. All of them include hydrostatic layers at the base of the wind, where the density and the temperature runs were taken from a Kurucz model for $T_{\mathrm{eff}} = 10{,}000\,\mathrm{K}$ and $\log g = 4$. For each model, the mass loss rate $\dot{M}$ was computed consistently with the given velocity law, in order that the continuum optical depth at 2800 Å be 2/3 at the photospheric radius (see CKP for details). The models built in this way are thus comparable to those built in CKP for the analysis of the Mg II resonance lines. Because of this requirement, $\dot{M}$ is controlled by the form of the velocity law at the base of the wind: the higher the velocity gradient in these regions, the higher $\dot{M}$. In all of our models, the velocity law is given as a piecewise linear function of r, the distance from the star's center. The density is derived from the velocity law and the mass loss rate through the continuity equation. Since nothing is known about the driving mechanism for the winds of Herbig Ae/Be stars, no attempt has been made to build models in consistency with the momentum and energy conservation equations. Our models are therefore semi-empirical. The temperature law remains given by the Kurucz model above the photospheric radius, until it reaches a given temperature minimum. Beyond this point begins the chromosphere, where the temperature law has the same form as in CKP, namely:

$$T(r) = \begin{cases} T_0 + (T_{\max} - T_0)\exp\left\{-4\ln 2\,\dfrac{(r-R_{\mathrm{ch}})^2}{\Delta_1^2}\right\} & \text{if } R_{\mathrm{ph}} \le r \le R_{\mathrm{ch}} \\ T_0 + (T_{\max} - T_0)\exp\left\{-4\ln 2\,\dfrac{(r-R_{\mathrm{ch}})^2}{\Delta_2^2}\right\} & \text{if } r > R_{\mathrm{ch}} \end{cases}$$

where

$$R_{\mathrm{ch}} = R_{\mathrm{ph}} + (\Delta_1/2\sqrt{\ln 2})\sqrt{\ln\{(T_{\max} - T_0)/(T_{\mathrm{eff}} - T_0)\}}$$

and

$$\Delta_1 \ll \Delta_2\,.$$

With this particular form for the temperature law, it is easy to control the maximum temperature ($T_{\max}$), the position of this maximum above the photosphere (Δ_1) and the chromospheric extension (Δ_2). This choice also implies the presence of an isothermal region surrounding the chromosphere where the temperature is T_0. Finally, as in CKP, an important Doppler random velocity was introduced in the models. The free parameters for our models are then the following: minimum temperature above the photosphere ($T_{\min}$), maximum temperature, position and extension of the chromosphere (resp. $T_{\max}$, Δ_1 and Δ_2), temperature in the outer region (T_0), mass loss rate $\dot{M}$ (controlled in practice by the velocity gradient at the base of the wind), velocity law ($V(r)$) and Doppler random velocity (v_D).

4. Numerical solution technique

Our task is to solve the simultaneous equations of radiative transfer and statistical equilibrium for the level populations of H and H^+, then to compute the emergent flux profiles in the direction of the observer. These two steps are performed by entirely different methods, and we shall start by describing the first.

4.1. *Solution of the multi-level-atom problem*

The method of solution of the non-LTE multi-level-atom problem is dictated by the assumptions concerning the expanding atmosphere. For small flows, i.e. less than a few line widths, techniques for static atmospheres can be modified to handle the limited macroscopic Doppler shifts without departing from the fixed inertial frame of the star. For this, either the equivalent-two-level-atom (ETLA) method, or the method of complete linearization (Auer and Mihalas, 1969; Auer, 1973) would suffice. For stellar winds with amplitudes of more than a few line widths, the transfer equation is best solved in the comoving frame of the flow, assuming that the flow rises monotonically from the photosphere. In the case of AB Aur, the maximum velocity lies in the range 300 to $400\,\mathrm{km\,s}^{-1}$, and the flow is assumed here to be monotonic within the line-formation zone of the hydrogen subordinate lines. The lines are assumed to be broadened primarily by Doppler random motions, with speeds up to $45\,\mathrm{km\,s}^{-1}$. Hence, the amplitude of the wind will be about 7 line widths, dictating the choice of the comoving frame solution. The comoving frame solution is not yet available in the context of the complete linearization technique, but has been used extensively within the ETLA method, as developed for stellar winds by Mihalas and Kunasz (1978). The ETLA is an iterative method. A typical iteration cycle

consists of a radiative transfer step in which each line and continuum transition is isolated from its atomic multi-level context and solved as independent non-LTE two-level problem, and a "statistical equilibrium" step in which the level populations are determined by solving the set of simultaneous rate equations. The rate equations are determined by the radiative rates found from the solution of the transfer equations, and the transfer equations are determined by the populations found from the solution of the rate equations. In the method of Mihalas and Kunasz (1978), the isolated non-LTE line-transfer problems are solved in the assumed spherical symmetry of the wind by the comoving frame method of Mihalas et al. (1976). The continuum scattering transitions are treated similarly, but without the inclusion of the macroscopic Doppler shift. The atomic model for hydrogen includes 6 bound levels and 1 ionized level. Complete redistribution has been assumed in this work, and we have taken a Doppler profile for the intrinsic shape of the lines. Background sources and sinks of radiation are included from a detailed list of the relevant trace species, and their bound-free cross-sections and thresholds. The background species, including He, He^+, C, N, O, Ne, Si, and their ions, are assumed to be in LTE, with normal abundances. Table 1 and appendix give the relevant atomic data for H, He, and He^+.

The most difficult aspects of the problem at hand are 1) the existence of enormously thick resonance lines in hydrogen, and 2) the presence of a chromosphere embedded in the wind. The first problem, which is encountered in most hydrogen-modelling works, was solved by putting the resonance lines in detailed balance, which allowed us to analytically cancel their radiative rates in the statistical equilibrium equations. This was justified in the context of AB Aur by laboriously and expensively performing several calculations with full treatment of the resonance lines, which can be 8 orders of magnitude thicker than the higher subordinate lines. The results for the populations relevant to the Balmer lines were nearly the same as for the computations with the Lyman lines in detailed balance. The full treatment requires as many as 20 ETLA iterations and requires about 20 minutes of CPU on a Cray-1A computer, for which the code is optimized.

Table 1. Hydrogen oscillator strengths

Lower Level \ Upper Level	1	2	3	4	5	6
1		0.4162	0.0791	0.02899	0.01394	0.007799
2			0.6407	0.1193	0.0467	0.02209
3				0.8421	0.1506	0.05584
4					1.038	0.1793
5						1.231
6						

Also, a powerful acceleration method developed by Ng (1974) has been used to improve the rate of convergence. This method consists of a global extrapolation from four iterates in which the extrapolation factors are computed in order to minimize the difference between the vector solution (whose components are the radiation field values at each depth point) and the extrapolated value. Without the use of this acceleration method, the ETLA scheme often failed to converge when resonance lines were included.

Even in the context of detailed balance in the resonance lines, the standard ETLA cycle is very difficult to converge, due to the effect of the steep-sided chromosphere on the Lyman continuum. This problem was overcome by iterating on the Lyman continuum, by itself, until the ionization balance stabilized. This occurs after some 60 to 90 iterations. Then the entire set of transitions, including the Lyman continuum, were iterated to convergence, typically reached after 6 iterations. The calculation with the Lyman lines in detailed balance takes about 4 minutes on a Cray-1A computer.

The ETLA-comoving frame method has been a useful workhorse for a number of stellar wind applications, including those of Kunasz and Van Blerkom (1978), Kunasz (1980), and Kunasz and Morrison (1982). Despite its lack of mathematical simultaneity, and the attendant danger of non-convergence for tightly interlocked lines, it has almost always converged well in stellar winds, in which strong lines are partially desaturated by the differential velocity. In our case, the ETLA scheme never failed to converge with the Lyman lines in detailed balance, and a convergence to less than a percent was always reached after 6 to 8 iterations.

4.2. The new observer's frame method

The second step is the calculation of emergent flux profiles for direct comparison with observations. Input for this step consists of emissivities and opacities based on the converged populations of H and H^+, and the assumed background species. The computation of emergent line profiles and continuum bands is carried out on a set of parallel rays lying on a plane passing through the center of the star, as illustrated in Fig. 1. These rays consist of a set which are one-on-one with the radial shells on which the opacities are known, and an additional set which terminate on the lower boundary of the radial mesh. As shown, the impact parameters of the outer set are just the radial mesh values, so that each radial shell generates a ray. On each ray, a mesh is induced by the crossing points of the shells outward of the ray's impact parameter. In the comoving frame of the wind, this mesh is used without refinement to solve the transfer equation. However, in the observer's frame, line resonances can be highly localized, and the mesh must be rezoned accordingly.

We assume that the line profile function Φ is a gaussian with half-width determined by v_D, the mean Doppler random velocity. If v_c is the frequency measured in the comoving frame, transformation to the observer's frame is given by

$$v = v_c + v_0 \frac{\hat{n} \cdot V}{c}$$

where v_0 is the line-center frequency, and $\hat{n}$ is the direction to the observer. The observer's frame profile is a notoriously sensitive function of distance along a line-of-sight. There are always certain mesh intervals in which the gradient of $\hat{n} \cdot V$ is large, due to a

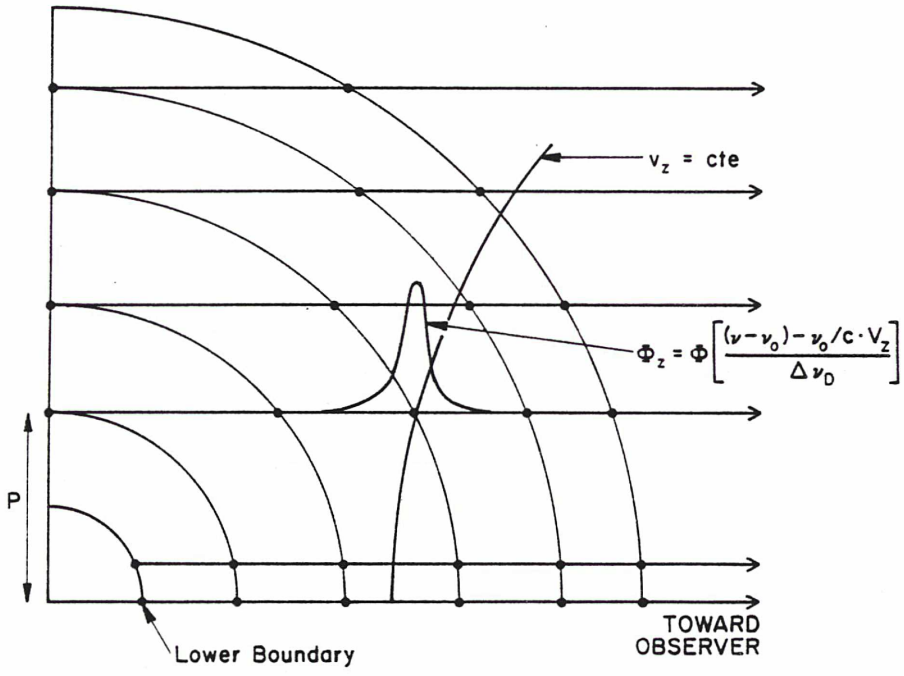

Fig. 1. Line transfer in the observer's frame. A surface of constant velocity projected on the line-of-sight is shown (v_z = cte). It corresponds to an observed frequency ν. ν_0 is the frequency at line center in the rest frame and $\Delta\nu_D$ is the frequency Doppler width of the line. The velocity field tends to localize the opacity for any given observed frequency. The coarse mesh used in the comoving frame is obviously not sufficient here

large kinematic gradient or rapid change in the projection factor. Due to the steepness of the profile function, such zones must be subdivided so as to allow an accurate computation. For each of the rays in the outer set, there is a rapid change in the projection factor in the vicinity of the impact parameter, unless the adjacent radial step is exceedingly small. It turns out that for a velocity amplitude of even a single line width, refinement will probably be necessary somewhere, if accuracy in the observer's frame step is to be consistent with that in sources and sinks from the ETLA step. In the works cited above, the problem was solved by first determining for each ray, each mesh interval, and each frequency point, the change in the value of the profile argument, and its proximity to line resonance. If the change was greater than, say, half a line-width, and the argument was in the neighborhood of the line resonance, the interval would be subdivided accordingly, and the mesh computation would advance to the next interval. After the initial coarse mesh on the ray had been so refined, the radiative transfer two-point boundary-value problem along the ray would be solved, for the observer's frame frequency in question, for the two-way-average intensity. The process would then be repeated, with new rezoning, for each frequency in the large observer's frequency set. An advantage of this scheme is that it minimizes the number of space points on which the transfer equation must be solved, because, for fast flows, line resonance occurs only on small fractions of a given ray, for a given frequency. A disadvantage is that a substantial amount of logic must be executed in the mesh-construction procedure, which dominates the calculation. For vectorized computations, a new method, described below, which is generally more accurate, is also faster.

In the new observer's frame solution, each ray is refined uniquely for the entire frequency set. Zoning is based only on the change in the profile argument, saving a great deal of construction time, and producing a smoother mesh, used for all frequencies. Vectorization of the computation over the frequency set usually saves more computation time than is lost to the global refinement on the rays. As an example of timing, our computations, involving 59 frequencies, 90 depth points in the original coarse mesh, and up to 400 depth points on the refined rays, require only 0.6 seconds of CPU for each line on a Cray-1A.

5. Results

5.1. Sensitivity to the parameters

A complete parameter analysis of a problem with this complexity would require a tremendous amount of computing time. For this reason, the results presented here do not constitute a systematic survey of the totality of the parameter space. However, we believe that they are sufficient to allow us to understand the basic physics of the line formation for Hα in this type of atmosphere. About 80 models were run, and we present 15 of them here, to illustrate the influence of the different parameters. The description of these 15 models is given in Table 2. The corresponding piecewise-linear velocity laws are indicated in Table 3. Let us now discuss in details the influence of each parameter on the Hα computed profile.

5.1.1. Velocity law

The response of the Hα profile to the velocity law is illustrated in Fig. 2. All of the velocity laws used in our calculations obey the previously determined constraints (see Sect. 4), i.e. the velocity gradient is low at the base, the velocity increases to 150 km s^{-1} at the outer boundary of the chromosphere, and then accelerate to reach a terminal value of 300 km s^{-1}. The only difference among the models corresponding to Fig. 2 is the way the flow is accelerated between the outer boundary of the chromosphere and the outer boundary of the envelope, which constitutes the only degree of freedom left by these constraints. As one goes from model Nr. 1 to model Nr. 3, the velocity gradient near the lower boundary of the cool region surrounding the chromosphere increases, and the terminal velocity is reached closer to the photosphere.

Table 2. Presentation of the models. Δ_1 and Δ_2 are in stellar radii, $\dot{M}$ in $M_\odot\,yr^{-1}$ and v_D in $km\,s^{-1}$

Model No.	Velocity Law	Chromosphere			T_{min}	T_0	$\dot{M}$	v_D
		Δ_1	Δ_2	T_{max}				
1	V_1	0.08	1.5	17000	7100	3000	1.1×10^{-8}	45
2	V_2	0.08	1.5	17000	7100	3000	1.1×10^{-8}	45
3	V_3	0.08	1.5	17000	7100	3000	1.1×10^{-8}	45
4	V_4	0.08	1.5	18000	10000	6000	1.9×10^{-9}	45
5	V_5	0.08	1.5	18000	10000	6000	1.5×10^{-8}	45
6	V_6	0.08	1.5	18000	10000	6000	2.2×10^{-8}	45
7	V_7	0.08	1.5	18000	10000	6000	3.7×10^{-8}	45
8	V_8	0.08	1.5	18000	10000	6000	7.3×10^{-8}	45
9	V_9	0.08	1.5	18000	10000	6000	2.8×10^{-7}	45
10	V_{10}	0.08	1.5	18000	10000	6000	4.3×10^{-7}	45
11	V_1	0.08	1.5	17000	7100	5000	1.1×10^{-8}	45
12	V_1	0.08	1.5	17000	7100	8000	1.1×10^{-8}	45
13	V_{11}	0.08	1.5	18000	10000	6000	7×10^{-9}	20
14	V_{11}	0.08	1.5	18000	10000	6000	7×10^{-9}	45
15	V_{11}	0.08	1.5	18000	10000	6000	7×10^{-9}	60

As can be seen in Fig. 2, the intensity of the Hα emission component decreases from model Nr. 1 to model Nr. 3, while the absorption component moves toward the blue. The interpretation of this behavior is straightforward: as the velocity gradient increases near the chromosphere, the Sobolev optical thickness for the frequencies corresponding to this spatial region decreases. This explains why the emission component decreases in intensity. On the other hand, the column density of material moving at $-300\,km\,s^{-1}$ increases as the point where the flow reaches its terminal velocity gets closer to the photosphere. Therefore, the contribution of this velocity to the profile becomes more and more important and the whole absorption component appears bluer and bluer.

5.1.2. Mass-loss rate

The mass-loss rate $\dot{M}$ acts on the model as a scaling factor for the density, through the continuity equation. Intuitively, we would expect the intensity in the emission component to increase with $\dot{M}$. However, the computations have shown a more complex behavior. Figure 3a displays the results obtained with 4 models differing only by their mass-loss rate. As can be seen on this figure, the intensity of the emission component is not a monotonic function of $\dot{M}$. Figure 3b shows this behavior for a more complete set of models (models 4-10): the maximum intensity of Hα increases until $\dot{M}$ reaches $3.7\,10^{-8}\,M_\odot\,yr^{-1}$, drops as $\dot{M}$ continues to increase, then increases again when $\dot{M}$ goes above $7.3\,10^{-8}\,M_\odot\,yr^{-1}$. The total variation of this intensity when $\dot{M}$ increases from $1.5\,10^{-8}$ to $4.3\,10^{-7}\,M_\odot\,yr^{-1}$ is 300%. On the other hand, the absorption component does not change very much. Its variation for the same range of $\dot{M}$ is only 10%. The absorption strength increases when $\dot{M}$ goes from $2\,10^{-9}$ to $1.5\,10^{-8}\,M_\odot\,yr^{-1}$, then decreases with increasing $\dot{M}$.

Let us first discuss in detail the behavior of the emission component. The intensity in the Hα emission component is of course very sensitive to the population of the $n = 3$ level. We have found in our computations that, in the line formation region (outwards of the chromosphere), direct recombinations and cascades on the $n = 3$ level play an important role in the population of this level. The Hα emission component is therefore very sensitive to the population of the ionized state. Now the computations have shown that this population is almost completely controlled by photoionizations from the ground level. This photoionization process is in turn controlled entirely by the radiation field in the Lyman continuum. The intensity in the Lyman continuum is therefore a key factor for the population of the $n = 3$ level,

Table 3. Velocity laws (in km s^{-1})

r/R_*	V_1	V_2	V_3	V_4	V_5	V_6	V_7	V_8	V_9	V_{10}	V_{11}
1	0.001	0.001	0.001	0.001	0.001	0.001	0.001	0.001	0.001	0.001	0.001
1.003										60	
1.005									50		
1.01	0.69	0.69	0.69	0.5	4	6	10	20			2
1.05				1.5	30	40	70	80	80	80	20
1.1	8	8	8								
1.2	50	50	50								
1.3	100	100	100	100	100	100	100	100	100	100	
1.5	114	114	114								
2				150	150	150	150	150	150	150	
2.5	150	150	150								
4											70
6			290								
12											140
20		290		220	220	220	220	220	220	220	180
40				280	280	280	280	280	280	280	280
50	290			300	300	300	300	300	300	300	300
70	300	300	300	300	300	300	300	300	300	300	300

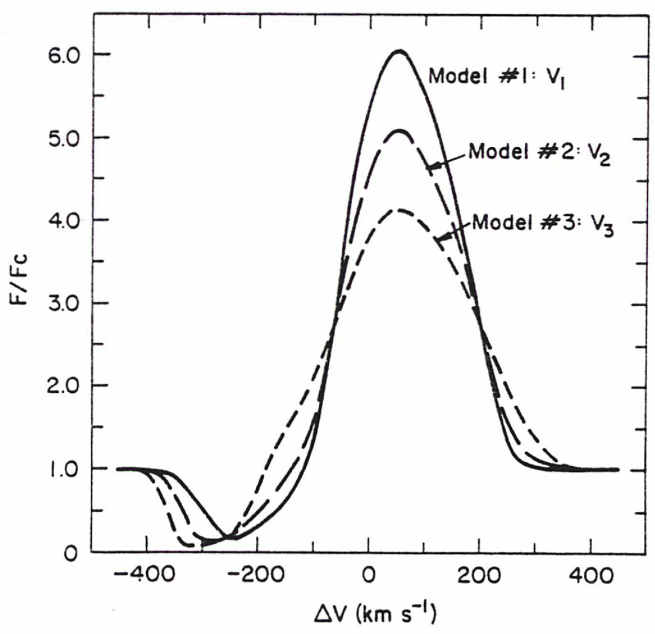

Fig. 2. Influence of the velocity law outward of the chromosphere on the Hα profile. The velocity law V_1 has a low velocity gradient after the chromosphere, V_2 an intermediate velocity gradient, and V_3 a strong velocity gradient. See text for details

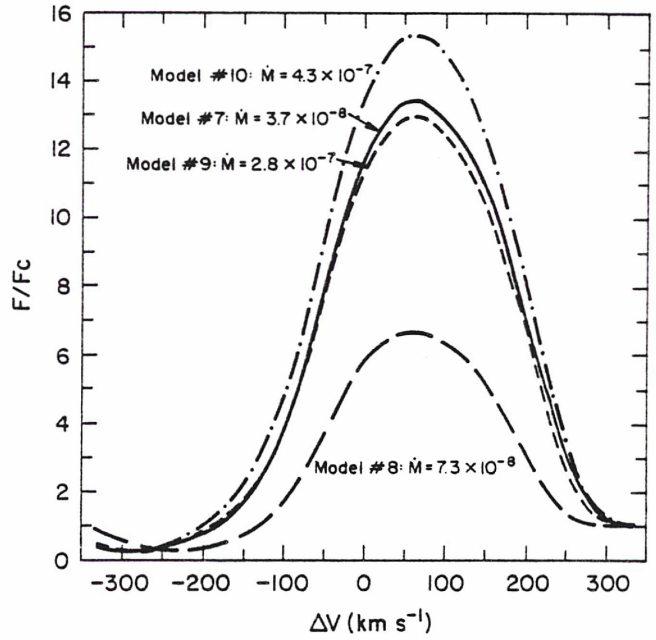

Fig. 3a. Influence of the mass loss rate on the Hα profile. Note that the intensity of the emission component is not a monotonic function of $\dot{M}$. See text for details

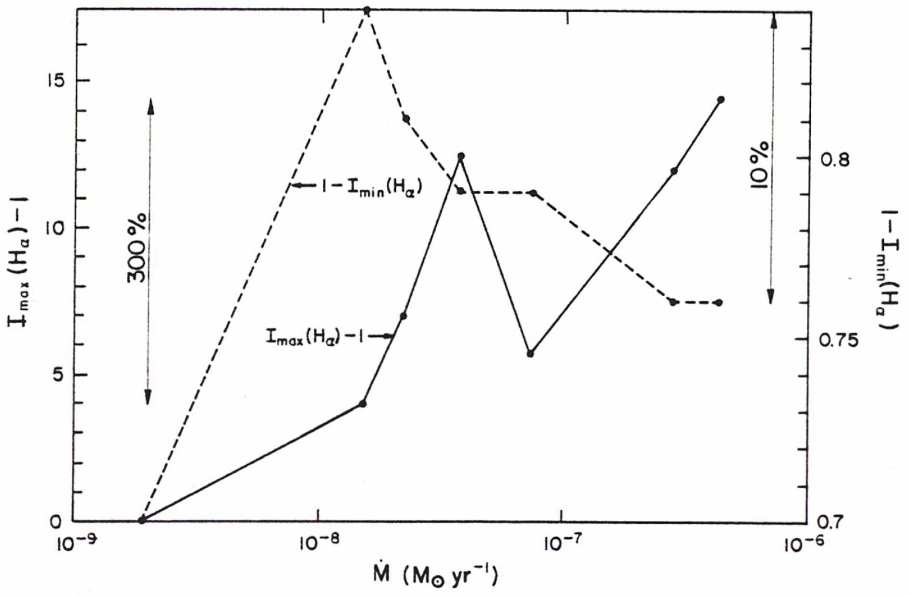

Fig. 3b. Variation of the intensity in the emission component and the absorption component of Hα with $\dot{M}$. Note that the absorption component varies only by 10% for two orders of magnitude of variation for $\dot{M}$

through photoionizations from the ground level and direct recombinations or cascades. The problem is now to understand how the Lyman continuum in the line formation region varies with the mass loss rate. When $\dot{M}$ is small, the Lyman continuum is optically thin throughout the line formation region and the chromosphere, and thermalizes only below the chromosphere, in the temperature minimum region. Since, in our models, the temperature minimum is lower than 10,000 K, the radiation temperature for the Lyman continuum is also lower than 10,000 K in this case. As $\dot{M}$ increases, the point where the Lyman continuum thermalizes moves outwards, and eventually reaches the inner part of the chromosphere. The radiation temperature for the Lyman continuum is then higher than 10,000 K. For these values of $\dot{M}$, since both the density and the Lyman continuum radiation temperature increase with $\dot{M}$, the intensity of the Hα emission component also increases with $\dot{M}$. As long as the thermalization depth for the Lyman continuum remains on the inner side of the chromosphere, an increase in $\dot{M}$ leads to an increase of the Hα emission component. But if $\dot{M}$ becomes high enough that the thermalization depth for the Lyman continuum is located on the outer side of the chromosphere, the situation is reversed, and the Lyman continuum radiation temperature decreases with increasing $\dot{M}$. Because of the important temperature gradient in the region just beyond the temperature maximum, and because of the exponential dependence of the Lyman continuum intensity on the radiation temperature (Wien limit), this effect can exceed the effect of the increase in density, leading to a weakening of the Hα emission component as $\dot{M}$ increases. If we still let $\dot{M}$ increase from this point, the thermalization depth eventually reaches the region of low temperature gradient surrounding the chromosphere, and the effect of the increasing density prevails again. For these high values of the mass-loss rate, an increase in $\dot{M}$ results in an increase of the Hα emission component. In our models, the critical range of $\dot{M}$ for which the thermalization depth for the Lyman continuum is located on the outer side of the chromosphere is between $3.7\,10^{-8}$ and $7.3\,10^{-8}\,M_\odot\,\mathrm{yr}^{-1}$. This result shows that the formation of Hα can be very complex in a medium with strong temperature gradients, and that the intensity of Hα emission is not necessarily a good tracer of the mass-loss rate.

The behavior of the Hα absorption component is easier to understand. As long as the emission component is very weak (low $\dot{M}$), the partial filling in of the absorption component is not important, and the strength of the absorption component increases with $\dot{M}$. When $\dot{M}$ is high enough though, this filling in becomes important, and the strength of the absorption component decreases as $\dot{M}$ increases. Finally, we note that the maximum depth of the absorption in the specific intensity on the central ray does not change very much with $\dot{M}$, for $\dot{M} > 3.7\,10^{-8}\,M_\odot$ yr^{-1}. This shows that the Hα absorption component is saturated in these models. For example, the Sobolev optical thickness corresponding to $-220\,\mathrm{km\,s}^{-1}$ in model Nr. 9 is about 13. This relatively high value for the Sobolev optical thickness explains why the absorption component changes so little with $\dot{M}$.

5.1.3. Parameters of the chromosphere

The parameters describing the chromosphere are the maximum temperature (T_{max}), the position of this temperature maximum above the photosphere (Δ_1) and the extension of the chromosphere (Δ_2). As mentioned before, these parameters have already been constrained by previous work (CKP; Catala, 1984). Our calculations have shown that the Hα profile is insensitive to these parameters, when they remain in the limits imposed by the previous constraints. The straightforward explanation for that is the complete depletion of neutral hydrogen in the chromosphere, implying that this region is optically thin for all of the hydrogen lines and continua. Its influence on the line formation is therefore only indirect, for example through a decrease of the size of the Hα emitting region accompanying an increase of the extension of the chromosphere. This kind of effect is only minor.

5.1.4. External temperature

The electron temperature in the line formation region is another matter. Figure 4 shows the influence of this parameter on the Hα profile. All of the models presented in Fig. 4 are identical except

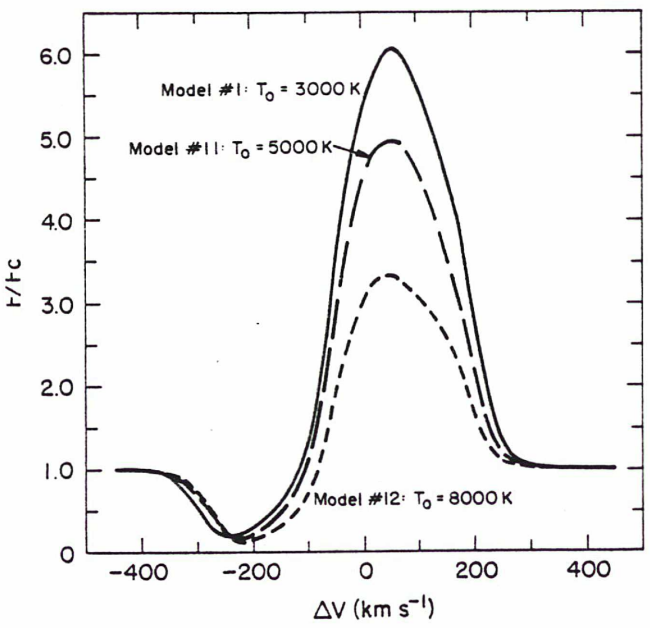

Fig. 4. Influence of the temperature in the outer regions on the Hα profile. See text for details

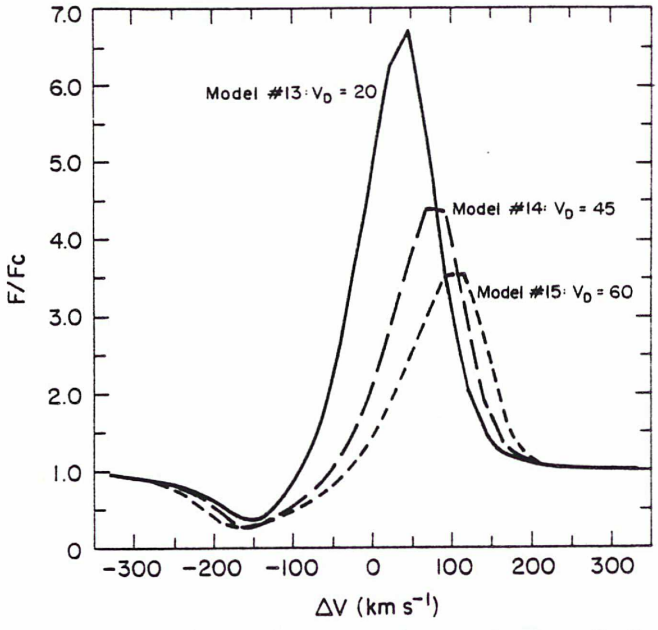

Fig. 5. Influence of the Doppler random velocity on the Hα profile. See text for details

for the temperature outside of the chromosphere, which is taken constant with the distance from the photosphere. It can be readily seen that the Hα emission component increases when T_0 decreases, whereas the absorption remains more or less constant.

The bound-free transitions for all of the hydrogen levels are dominated by radiation in most of the line formation region. Consider a bound level i and the continuum state k. We then have:

$$R_{i\to k} = 4\pi \int_{\nu_0}^{\infty} \frac{\alpha_\nu}{h\nu} J_\nu \, d\nu \quad \text{(photoionization rate)} \tag{1}$$

$$R_{k\to i} = 4\pi \left(\frac{n_i}{n_k}\right)^* \int_{\nu_0}^{\infty} \frac{\alpha_\nu}{h\nu} \left(\frac{2h\nu^3}{c^2} + J_\nu\right) \exp\left(-\frac{h\nu}{kT_e}\right) d\nu$$

(radiative recombination rate) (2)

where α_ν is the photoionization cross-section, ν_0 the photoionization threshold and J_ν the mean intensity of the radiation field in the continuum corresponding to level i. J_ν does not change with T_0, because it is controlled by the conditions in the region where the ith continuum is formed, namely the photosphere, inner or outer chromosphere (depending on $\dot{M}$) for the Lyman continuum, and the photosphere for all of the other continua. Therefore, the photoionization rates do not change with T_0. On the other hand, it can be shown from Eq. (2) that:

$$R_{k\to i} \propto n_e T_0^{-1/2}$$

in the line formation region, where n_e is the local electron density. Since hydrogen is almost entirely ionized in these models, the electron density does not change with T_0. Therefore the recombination rates scale as $T_0^{-1/2}$, which explains why the Hα emission component decreases when T_0 increases.

5.1.5. Doppler random velocity

The influence of this parameter is illustrated by Fig. 5, where 3 results corresponding to 3 different values of v_D are presented. As v_D increases, the absorption component is broadened, whereas the emission component decreases and moves to the red. This behavior is quite similar to that of the Mg II resonance lines described in CKP, and the explanation is the same as the one given in that paper, to which the reader is referred for further details.

5.1.6. Advection in the wind

In our models, the results were obtained without the presence of advection terms in the statistical equilibrium equations. However, model Nr. 1, which was the most successful (see below), was re-run with advection introduced in the final ETLA iteration, as a consistency check. The resulting corrections were insignificant.

5.2. Comparison with the observations

We have chosen to compare our computed Hα profiles to a profile observed in Nov. 84, which will be published shortly (Guerin et al., 1987). This type of profile is indeed the most frequent in AB Aur. It is a P Cygni type II profile (Beals, 1951), where the absorption trough does not go deeper than half the continuum level, and the emission component reaches an intensity 6 times higher than the continuum. In this section, we present the model giving the best fit to the emission component of the Hα profile. The presentation of this best fit is by no means a claim that the corresponding model is the right one, and the reader is referred to Sect. 5.3 for the constraints these new calculations bring on the model.

Figure 6 shows the best fit we have obtained for the emission component. Although we have stated that the absorption component is not representative of the average structure of the envelope, it is interesting to note that none of our 80 models was able to reproduce an absorption trough as weak as the observed one without losing completely the fit to the emission component. The reason for this failure is easy to understand. The parameters

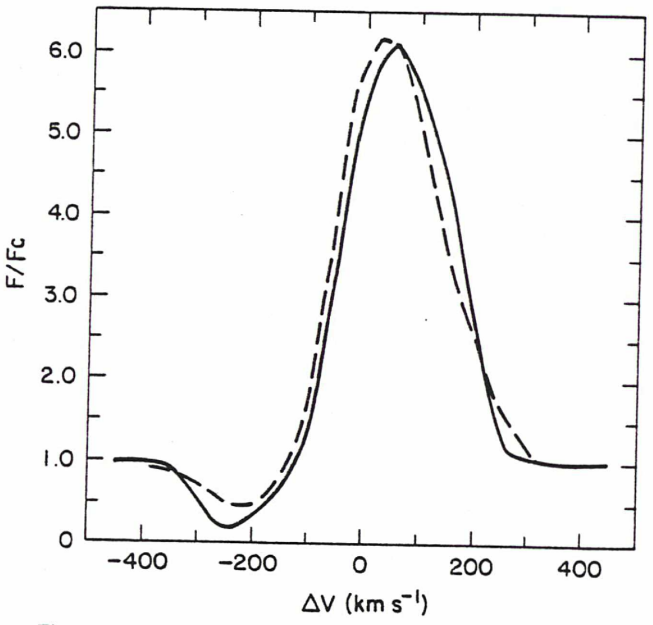

Fig. 6. Hα profile computed with model Nr. 1 (full line), compared to the profile observed in Nov. 84 by Guerin et al. (1987) (dashed line)

acting on the line profile are the velocity law, the mass loss rate $\dot{M}$, the external temperature T_0, and the Doppler random velocity v_D. Among them, the Doppler random velocity and the velocity law have been strongly constrained by previous analysis. The interpretation of the Mg II resonance line led to a value of $45\,km\,s^{-1}$ for v_D, and since the regions of formation of Hα and of the Mg II lines are not very different, this quantity cannot be changed significantly for the computations of Hα. As mentioned above, the only remaining degree of freedom for the velocity law is the velocity gradient in the region surrounding the chromosphere, which leaves us with a very reduced liberty of maneuver. The only other parameters having a significant influence on the Hα profile are $\dot{M}$ and T_0. Both of them act in the same way on the populations of levels 2 and 3, which means that if we decrease the absorption component by changing one of these 2 parameters, we decrease the emission component as well. Moreover, the Sobolev optical thickness at $-250\,km\,s^{-1}$ in our best model is about 2, which shows that the absorption component is close to saturation. Any change in the absorption component is therefore accompanied by a much bigger change in the emission component. This behavior is obvious in the 15 models presented here and in the 80 models that have been run. We conclude that it is impossible to obtain a better fit to the absorption component if we want to keep a good fit to the emission component. We note that the same problem has been encountered by Kunasz and Morrison (1982) in their attempt to model the wind of α Cygni.

The explanation for the weakness of the observed absorption component must therefore be searched among possible breakdowns of the basic assumptions of our computations. The first obvious possibility is of course the existence of fast and slow streams in AB Aur's envelope. The densities of the different streams have no reason to be identical, and it could be imagined that a low density region is located on the line of sight to the star, while the average density in the lateral parts of the envelope is higher. In this particular situation, a weak absorption component may coexist with a strong emission component. This idea can be tested observationally. The Hα profile would indeed show at times a strong absorption component corresponding to the moments when a high density region passes on the line-of-sight. An observation with a good phase coverage should answer this point.

Another possibility is the existence of a density gradient in the latitudinal direction, giving a disk shape to the envelope. If the disk is not seen edge-on, we expect to obtain both a weak absorption component and a strong emission component for Hα. However, this picture might be difficult to reconcile with the profile of the Mg II resonance lines, which show a very deep absorption component and a relatively moderate emission component.

A full 3-D calculation is needed to investigate the two possibilities mentioned above. Observer's frame transfer codes for moving multi-dimensional media are now being developed (Kunasz and Auer, 1986), and it can be foreseen that these calculations will soon be possible.

Finally, another of our basic assumptions is that of complete frequency redistribution. It is possible that partial redistribution effects are important for the hydrogen resonance lines in this type of atmosphere, in which case they could indirectly influence the populations of levels 2 and 3. A full calculation including partial redistribution is needed to explore this possibility. However, the introduction of partial redistribution in the comoving frame ETLA code goes beyond the scope of the present paper. It might prove an interesting direction of research for the future.

5.3. Details of the best model

Although we have not been able to reproduce the observed absorption component, the model giving the best fit to the emission component can be used as a reference, and we give below some details about this model.

5.3.1. Hα

The computed Hα profile obtained with this model is shown in Fig. 6. Figure 7 displays the specific intensity profiles on a chosen set of rays labelled by their impact parameters p. The absorption component is roughly centered at $-250\,km\,s^{-1}$, the velocity reached at 30 stellar radii from the photosphere. Moreover, on the rays that hit the core, the absorption component extends to the line center. We conclude that the region of formation of the absorption component is constituted by the photosphere and the region of the temperature minimum which contribute to the line center, and by the cool region surrounding the chromosphere, up to 30 stellar radii, which contributes to the blueward displaced absorption component. Hence, the whole envelope, up to 30 stellar radii, except the chromosphere, contributes to the formation of Hα. This upper limit of 30 stellar radii is of course dependent on the mass loss rate. In model Nr. 7, for example, in which $\dot{M} = 3.7\,10^{-8}\,M_\odot\,yr^{-1}$, this region extends up to 50 stellar radii. It can also been derived from Fig. 7 that the region of formation of the emission component is the same cool region surrounding the chromosphere.

5.3.2. Other hydrogen lines

Figure 8 shows the profiles of all of the other hydrogen lines for this model (except the Lyman lines, which are not computed). Among the Balmer lines shown in this figure, Hβ is the only one that can possibly be compared to the observations, because all

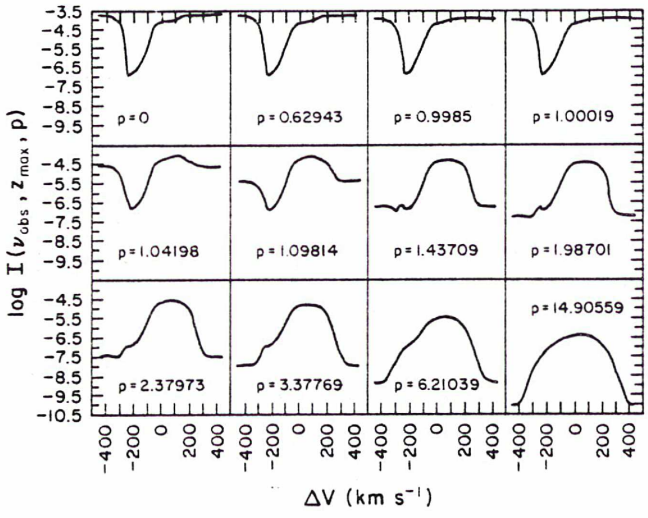

Fig. 7. Specific intensity profiles at the outer boundary of a chosen set of rays for model Nr. 1. The rays are labelled by their impact parameters p expressed in stellar radii

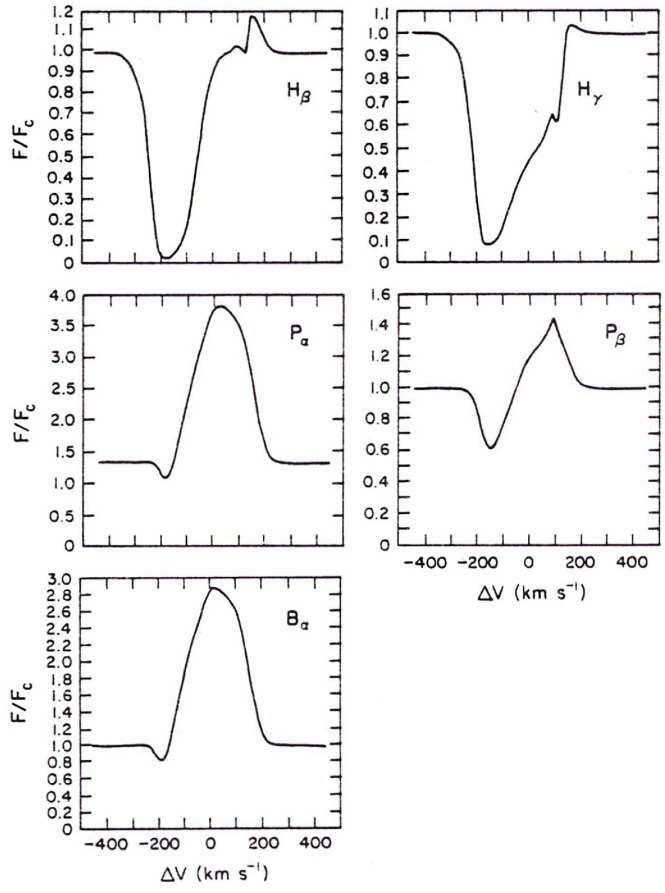

Fig. 8. Profiles of the hydrogen lines computed with model Nr. 1

of the others are completely dominated by the photospheric Stark profile which has not been included in the calculations. An observation of Hβ, obtained simultaneously with the Hα profile we have used in this work, is available (Guerin et al., 1987).

The comparison of the computed Hβ profile with the P Cygni part of the line in the observed Hβ profile (which also has very broad Stark wings) shows a good agreement in the emission component, but again the computed absorption component is clearly too deep. For the Paschen and Brackett lines, no simultaneous observation is available, and therefore no direct comparison will be made. However, we note that the computed profiles are of P Cygni type, while the observed profiles for Pβ and Pγ show no absorption component (Maillard and Chalabaev, 1986). This discrepancy might have the same origin as the discrepancy between the deep computed absorption component of Hα, and the weak observed absorption component.

5.3.3. Continuum

Figure 9 shows a comparison of the continuum flux predicted by this model and the Kurucz model for $T_{\rm eff} = 10{,}000$ K and $\log g = 4$. A very small computed excess shows up in the Balmer continuum. The corresponding Balmer jump excess is $\Delta D_{\rm B} = 0.12$. Garrison (1978) reports no excess emission in the Balmer continuum, to within 0.1 mag, therefore this model is not inconsistent with his observations. The minimum temperature of this model is 7100 K. We have checked that a minimum temperature of 8500 K is sufficient to produce an excess of 0.38 mag in the Balmer continuum. The value of 7100 K for the minimum temperature is then close to the upper limit above which an important excess is produced in the Balmer continuum. Also, we have found that mass loss rates higher than $1.8\,10^{-8}\,M_{\odot}\,{\rm yr}^{-1}$ lead to an important excess in the Balmer continuum ($\Delta D_{\rm B} \geq 0.25$). Figure 9 shows a very small excess in the Paschen continuum, also consistent with Garrison's observations. Finally, the infrared excess of the model beyond 2μ is far below the observed infrared excess (see e.g. Cohen, 1975). The wind and chromosphere of AB Aur therefore do not explain this infrared excess, which is probably due to dust emission.

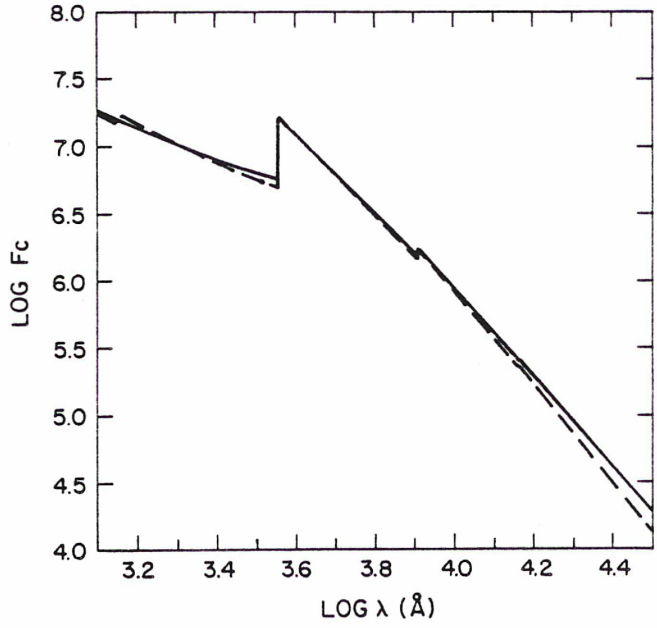

Fig. 9. Continuum flux computed with model Nr. 1 (full line), compared to Kurucz's model for $T_{\rm eff} = 10{,}000$ K and $\log g = 4$ (dashed line)

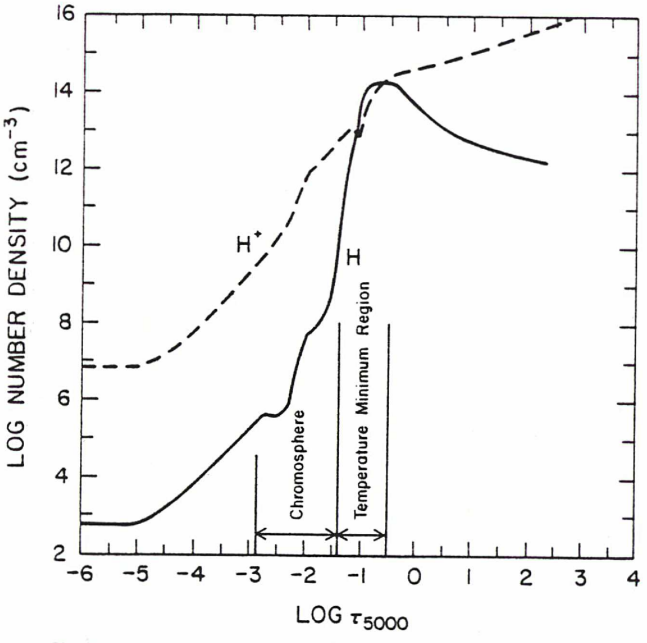

Fig. 10. Hydrogen ionization for model Nr. 1. Note that hydrogen is mostly ionized everywhere, except in the temperature minimum region. In our models, $n_e \approx n_{H^-}$ to within a few percent

5.3.4. Hydrogen ionization

Our calculations provide us with a very accurate description of hydrogen ionization, including non-LTE effects. Figure 10 shows the density of neutral and ionized hydrogen for model Nr. 1, giving the best fit to the Hα emission component. As seen from this figure, hydrogen is mostly ionized everywhere in the atmosphere, except in the region of the temperature minimum. Moreover, since in our models helium is predominantly neutral, $n_e \approx n_{H^+}$, to within a few percent.

We find that radiative processes dominate the ionization from and recombination to the ground level, even below the temperature minimum region. At $\tau_{5000} = 250$, the ratio of radiative to collisional ionization rates for level 1 is still about 30. At this depth, however, thermalization is achieved thanks to the other opacity sources. On the contrary, collisional ionizations from excited levels play a significant role in the chromosphere and the temperature minimum region, and become the dominant process at $\tau_{5000} > 3$. Collisional recombinations on excited levels are significant only in the temperature minimum region and below, becoming dominant at $\tau_{5000} > 3$.

5.4. Constraints on the physical structure

The time variability of Hα makes it difficult to derive precise constraints on the structure of AB Aur's envelope from its interpretation. Let us remind the reader that these constraints are based on the assumption that the emission component is representative of the average structure of the envelope. No use has been made of the absorption component, because the latter is too sensitive to the aforementioned departures from spherical symmetry. The results presented in this section must be considered as constraints on the average structure of AB Aur's envelope. In particular, such a quantity as the velocity is probably highly dependent on the longitude and there is no real point in trying to derive precise constraints for it from our average model. The basic picture which has been drawn for the velocity law from the interpretation of the Mg II and C IV lines still holds, but trying to refine it would be an overinterpretation of our spherically symmetric model.

Also, our model is too crude to refine the constraints we already have on the Doppler random velocity. This parameter has been found to be 45 km s^{-1} in the analysis of the Mg II resonance lines, and since the Hα emission component is formed in a region included in the Mg II lines formation region, we consider this value as given.

We have seen in Sect. 5.1.3 that the precise structure of the chromosphere has no influence on the Hα profile. Therefore, no further constraint can be derived for the chromosphere from the present analysis.

The only parameters which are left are the mass loss rate $\dot{M}$, the velocity law in the region surrounding the chromosphere, and the external temperature T_0. Since the dependence of the Hα emission component on T_0 is weak ($T_0^{-1/2}$), we have chosen to let this parameter vary within a reasonable range and derive limits on $\dot{M}$. As mentioned above, the velocity law used in our spherically symmetric model has no real meaning, so no attempt will be made to constrain it. We will also let it vary to derive limits on $\dot{M}$.

From Fig. 3, we deduce that 2 ranges of $\dot{M}$ can lead to good fit to the observed Hα emission component. The first range has an order of magnitude of $1\,10^{-8}\,M_\odot\,\mathrm{yr}^{-1}$, and the second one of $7\,10^{-8}\,M_\odot\,\mathrm{yr}^{-1}$. However, all of the models with $\dot{M} \sim 7\,10^{-8}\,M_\odot\,\mathrm{yr}^{-1}$ lead to a large unobserved excess in the Balmer continuum and must therefore be rejected. This leaves us with the first range of $\dot{M}$.

A reasonable lower limit for the external temperature is $T_0 > 3000$ K. It simply corresponds to the temperature of a spherical envelope in grey radiative equilibrium at 10 stellar radii, which is right in the middle of the region of formation of the Hα emission component. This lower limit for T_0 allows us to find a lower limit for $\dot{M}$. In order to find it, we used a velocity law which leads to the maximum intensity in the emission component, i.e. one with a low gradient near the outer boundary of the chromosphere (see Sect. 5.1.1). With T_0 fixed at its lower limit, we adjusted $\dot{M}$ until a good fit was obtained for the Hα emission component. We find $\dot{M} \geq 1\,10^{-8}\,M_\odot\,\mathrm{yr}^{-1}$. An upper limit for $\dot{M}$ cannot be found in the same way, since we have no obvious upper limit on T_0. However, we note that when $\dot{M} \geq 1.8\,10^{-8}\,M_\odot\,\mathrm{yr}^{-1}$, an important excess appears in the Balmer continuum, which is not observed. This value can then be considered as an upper limit for $\dot{M}$. Note that our constraints on $\dot{M}$ have been derived by making full use of previous line analysis. In particular, the velocity law in the Hα line formation region is tightly constrained by the analysis of the C IV resonance lines, which gives us an estimate of the wind velocity at the outer boundary of the chromosphere. Therefore, these results come from a multi-feature analysis, and not from the hydrogen line interpretation only. These constraints, $1\,10^{-8} \leq \dot{M} \leq 1.8\,10^{-8}\,M_\odot\,\mathrm{yr}^{-1}$, are much tighter than those which had been derived so far. The discrepancy between these values and those published in CKP has already been discussed in Sect. 3.4. Kuan and Kuhi (1975) found $\dot{M} \sim 3\,10^{-7}\,M_\odot\,\mathrm{yr}^{-1}$. Arguments against their method can be found in CKP and in Sect. 3.2 of the present paper.

Our constraints on $\dot{M}$ reflect only the average properties of the envelope at the moment of the observation. However, Guerin

et al. (1987) find that the maximum intensity in the Hα emission component never goes below $F/Fc = 5$. We have checked that a mass loss rate $\dot{M} = 9\,10^{-9}\,M_\odot\,\mathrm{yr}^{-1}$ leads to such an intensity, when we keep all of the other parameters as in model Nr. 1. Our lower limit of $1\,10^{-8}\,M_\odot\,\mathrm{yr}^{-1}$ for $\dot{M}$ is therefore close to the minimum value we can propose. Moreover, monitoring of the Balmer continuum at 3500 Å and 2800 Å showed no variation during the 1982 Oct. and 1984 Nov. observation campaigns (Praderie et al., 1986). However, a more complete monitoring of the Balmer continuum is still needed to conclude that the Balmer discontinuity does not vary on any time scale. Such an observational study would tell us if the absence of an excess emission in the Balmer continuum can be considered as a characteristic of the star, in which case we could keep the upper limit of $1.8\,10^{-8}\,M_\odot\,\mathrm{yr}^{-1}$. However, before further observations are carried out, we cannot rule out the possibility that the mass loss rate might be variable in time.

Finally, the upper limit on $\dot{M}$ allows us to derive an upper limit on T_0. In order to find it, we used a velocity law with a low gradient near the outer boundary of the chromosphere, leading to a maximum intensity in the Hα emission component. With $\dot{M}$ fixed at its upper limit, we adjusted T_0 until a good fit was obtained. We find $T_0 \leq 10{,}000$ K. However, this constraint only applies to the average structure, since the temperature in the outer region has no reason to be constant as it is in our simple model.

6. Conclusion

This work constitutes a new step in the effort of modelling of the envelopes of the Herbig Ae/Be stars, represented by AB Aur, which has been shown to be a good prototype of at least part of its class (Catala et al., 1986a). In previous works, the existence of a deep and extended chromosphere had been shown and some constraints had been derived for its structure and for the cooler region surrounding it (CKP; Catala and Talavera, 1984; Catala, 1984). However, the newly discovered time variability of the Mg II and Ca II resonance lines points to important departures from the spherical symmetry which has been assumed in all of the previous works, as well as in the present paper. The results of the present study are based on the assumption that the emission component of Hα is representative of the average structure of the envelope. Future 3-D calculations will hopefully allow us to test this basic assumption.

The goals of this paper were the following:

1) Check that the already existing model for AB Aur's envelope is able to reproduce the observed Hα profile.

2) Study the influence of the model parameters on the formation of Hα.

3) Derive additional constraints on the physical structure of AB Aur's envelope.

We have not been able to reproduce both the absorption and the emission component of the observed Hα profile. The reasons we suggest for this discrepancy include departures from spherical symmetry and effects of partial redistribution for the Lyman lines. However, the model was perfectly able to explain the intensity and shape of the emission component of Hα.

The analysis has yielded some interesting dependencies, in particular a non-monotonic variation of the Hα emission component with the mass-loss rate.

The basic constraint that has been derived on the structure of AB Aur's envelope from this study is on the mass-loss rate. We have found that $1\,10^{-8} \leq \dot{M} \leq 1.8\,10^{-8}\,M_\odot\,\mathrm{yr}^{-1}$. This constraint, added to all of the other constraints already placed by previous analysis, gives us a good idea of the average structure of AB Aur's wind. Further refinements of this spherically symmetric model would constitute an overinterpretation.

Time is ripe for a new step in this general study of the Herbig Ae/Be stars, namely to understand the physical processes responsible for wind production and chromospheric heating in these stars. AB Aur can still be used as a good prototype for this future study. Any theoretical model should be able to explain the different features which have been derived in the course of this semi-empirical modelling. Let us summarize them:

1) *Temperature law:* above the photosphere, the temperature drops down to ~7100 K, then increases again and reaches ~18,000 K in the chromosphere. Beyond the chromosphere, the temperature drops again. The extension of the chromosphere is between 1 and 1.5 stellar radii.

2) *Velocity law:* the velocity gradient is low at the very base of the chromosphere, then increases, so that the velocity reaches $\sim 150\,\mathrm{km\,s}^{-1}$ at the outer boundary of the chromosphere (this value is probably variable). After the chromosphere, the velocity goes on increasing until it reaches its maximum value of about $300\,\mathrm{km\,s}^{-1}$ (also likely to vary). Further away, the flow is decelerated down to at least $150\,\mathrm{km\,s}^{-1}$. The location of the deceleration region is unknown.

3) *Mass loss rate:* the mass loss rate is between $1\,10^{-8}$ and $1.8\,10^{-8}\,M_\odot\,\mathrm{yr}^{-1}$.

This picture represents only an average structure for AB Aur's wind. We must still keep in mind that the wind is not spherically symmetric, but probably constituted of fast and slow streams rotating with the star. More details about this stream structure can be found in Praderie et al. (1986) and Catala et al. (1986b).

Acknowledgements. We acknowledge fruitful discussions with J. Borsenberger, E. Simmoneau, and F. Praderie, and we thank B. Lites and F. Praderie for carefully reading the manuscript. We would also like to thank G. Olson, who helped us to implement the Ng acceleration method in our code. We are indebted to J. Guerin, P. Felenbok, and J. Czarny for allowing us to use their Hα observations in advance of publication. Our thanks also go to J.P. Maillard and A. Chalabaev for showing us their hydrogen infrared line observations prior to publication. Part of the computing time necessary for this work has been attributed by the "Conseil Scientifique du Centre de Calcul Vectoriel pour la Recherche", which is thanked for this allocation. This work, initiated at Meudon Observatory, was completed while C.C. was a one-year visitor at the High Altitude Observatory, which he wishes to thank for its kind invitation.

Appendix

Radiative and collisional cross-sections

The computations presented in this paper are based on a 6-level + continuum atomic model for hydrogen. The background opacity and emissivity sources include 4 additional levels for H, 10 levels for He, 20 levels for He^+, and a total of 24 levels for C, N, O, Ne, Si and their ions. We give below some details about how the radiative and collisional cross-sections have been

computed for the major contributors to the opacity, namely H, He, and He^+.

A1. Photoionizations

The photoionization cross-sections for hydrogen are given by:

$$\alpha_\nu(H,n) = \begin{cases} \dfrac{2.815\,10^{29}}{\nu^3 n^5}\, g(n,\nu) & \text{if } \nu > \dfrac{3.29\,10^{15}}{n^2} \\ 0 & \text{if } \nu < \dfrac{3.29\,10^{15}}{n^2} \end{cases}$$

where $g(n,\nu)$ is the Gaunt factor for level n, at frequency ν, taken from Mihalas (1967).

We have used the same formula for levels 3 through 10 of neutral helium. For level 1 (1^1S), we have used the following approximation formula, taken from Burgess and Seaton (1960):

$$\alpha_\nu(He,1) = \begin{cases} 7.3\,10^{-18}\exp(-2.311\,10^{-16}\,\nu + 1.373) & \text{if } \nu > 5.94862\,10^{15} \\ 0 & \text{if } \nu < 5.94862\,10^{15} \end{cases}$$

Level 2 is composed of the individual levels ^1S, ^1P, ^3S, ^3P, for which approximation formulae can be found in Gingerich (1964). We find:

$$\alpha_\nu(He,2) = \begin{cases} 1/16\left\{3\left(\dfrac{2.04\,10^{35}}{\nu^{3.5}} + \dfrac{3.02\,10^{35}}{\nu^{3.6}}\right) + \dfrac{4.46\,10^{11}}{\nu^{1.91}}\right. \\ + 9\left(\dfrac{3.72\,10^{26}}{\nu^{2.9}} + \dfrac{1.15\,10^{31}}{\nu^{3.3}}\right) + 3\exp[-278.3 \\ \left. + \log\nu(14.88 - \log\nu\,0.2311)]\right\} & \text{if } \nu > 8.225\,10^{14} \\ 0 & \text{if } \nu < 8.225\,10^{14} \end{cases}$$

The photoionization cross-sections for He^+ (hydrogenic ion, Z = 2) have the same form as those of H.

A2. Collisional ionization cross-sections for H

We have used the approximation formula:

$$C_{n\to k} = n_e\left(C_0 + C_1\log T_e + C_2(\log T_e)^2 + \frac{C_{-1}}{\log T_e} + \frac{C_{-2}}{(\log T_e)^2}\right)$$

This formula and the coefficients C_0, C_1, C_2, C_{-1}, C_{-2} have been taken from Mihalas (1967).

A3. Collisional excitation cross-sections for H

For all transitions, except Lyα, we have used the following formula, taken from Klein and Castor (1978):

$$C_{ij} = 5.465\,10^{-11}\,T_e^{1/2} n_e 4 f_{ij}\left(\frac{1}{i^2} - \frac{1}{j^2}\right)^{-2}\frac{\chi_{ij}}{kT_e} \times\left[E_1\left(\frac{\chi_{ij}}{kT_e}\right) + 0.148\,\frac{\chi_{ij}}{kT_e}\,E_5\left(\frac{\chi_{ij}}{kT_e}\right)\right]$$

where χ_{ij} is the transition energy, f_{ij} the oscillator strength, and E_1 and E_5 are exponential-integral functions.

For Lyα, we have used a different formula, also taken from Klein and Castor (1978):

$$C_{12} = 4T_e^{1/2} n_e \exp\left(-\frac{\chi_{12}}{kT_e}\right)\sum_{r=1}^{N} a_r T_r(\log T_e - 4)$$

where the T_r's are Chebyshev polynomials and the a_r's are tabulated by Crandall et al. (1974).

References

Auer, L.H., Mihalas, D.: 1969, *Astrophys. J.* **158**, 641
Auer, L.H.: 1973, *Astrophys. J.* **180**, 469
Beals, C.S.: 1951, *Publ. Dominion Astrophys. Obs.* **9**, 1
Burgess, A., Seaton, M.J.: 1960, *Monthly Notices Roy. Astron. Soc.* **121**, 471
Catala, C.: 1983, *Astron. Astrophys.* **125**, 313
Catala, C., Kunasz, P.B., Praderie, F.: 1984, *Astron. Astrophys.* **134**, 402 (CKP)
Catala, C.: 1984, Proc. 4th European IUE Conf., Rome, ESA SP 218, p. 227
Catala, C., Talavera, A.: 1984, *Astron. Astrophys.* **140**, 421
Catala, C., Czarny, J., Felenbok, P., Praderie, F.: 1986a, *Astron. Astrophys.* **154**, 103
Catala, C., Felenbok, P., Czarny, J., Talavera, A., Boesgaard, A.M.: 1986b, *Astrophys. J.* **308**, 791
Cohen, M.: 1975, *Monthly Notices Roy. Astron. Soc.* **173**, 279
Cohen, M., Kuhi, L.V.: 1979, *Astrophys. J. Suppl.* **41**, 743
Crandall, D.H., Dunn, G.H., Gallagher, A., Hummer, D.G., Kunasz, C.V., Leep, D., Taylor, P.O.: 1984, *Astrophys. J.* **191**, 789
Felenbok, P., Praderie, F., Talavera, A.: 1983, *Astron. Astrophys.* **128**, 74
Finkenzeller, U.: 1983, *Astron. Astrophys.* **124**, 157
Finkenzeller, U., Mundt, R.: 1984, *Astron. Astrophys. Suppl.* **55**, 109
Finkenzeller, U., Jankovics, I.: 1984, *Astron. Astrophys. Suppl.* **57**, 285
Garrison, L.M., Anderson, C.M.: 1977, *Astrophys. J.* **218**, 438
Garrison, L.M.: 1978, *Astrophys. J.* **224**, 535
Gingerich, O.: 1964, 1st Harvard-Smithsonian Conf. on Stellar Atmospheres, Harvard College Observatory
Guerin, J., Czarny, J., Felenbok, P.: 1987 (in preparation)
Harvey, P.M.: 1984, *Publ. Astron. Soc. Pacific* **96**, 297
Herbig, G.H.: 1960, *Astrophys. J. Suppl.* **4**, 337
Klein, R.I., Castor, J.I.: 1978, *Astrophys. J.* **220**, 902
Kuan, P., Kuhi, L.V.: 1975, *Astrophys. J.* **199**, 148
Kunasz, P.B., Van Blerkom, D.: 1978, *Astrophys. J.* **224**, 193
Kunasz, P.B.: 1980, *Astrophys. J.* **237**, 819
Kunasz, P.B., Morrison, N.D.: 1982, *Astrophys. J.* **263**, 226
Kunasz, P.B., Auer, L.H.: 1986, (preprint)
Kurucz, R.L.: 1979, *Astrophys. J. Suppl.* **40**, 1
Maillard, J.P., Chalabaev, A.: 1986 (in preparation)
Mihalas, D.: 1967, *Astrophys. J.* **149**, 169
Mihalas, D., Kunasz, P.B., Hummer, D.G.: 1976, *Astrophys. J.* **210**, 419
Mihalas, D., Kunasz, P.B.: 1978, *Astrophys. J.* **219**, 635
Ng, K.C.: 1974, *J. Chem. Phys.* **61**, 2680
Praderie, F., Talavera, A., Felenbok, P., Czarny, J., Boesgaard, A.M.: 1982, *Astrophys. J.* **254**, 658
Praderie, F., Simon, T., Catala, C., Boesgaard, A.M.: 1986, *Astrophys. J.* **303**, 311
Sitko, M.L.: 1981, *Astrophys. J.* **247**, 1024
Strom, S.E., Strom, K.M., Yost, J., Carrasco, L., Grasdalen, G.L.: 1972, *Astrophys. J.* **173**, 353

Astron. Astrophys. 140, 421–426 (1984)

ASTRONOMY AND ASTROPHYSICS

The presence of Si^{3+} and C^{3+} in the wind of AB Aur*

C. Catala[1,] and A. Talavera[2]**

[1] Observatoire de Paris-Meudon, DESPA F-92190 Meudon, France
[2] Astronomy Division ESTEC, Villafranca Tracking Station, P.O. Box Apartado 54065, Madrid, Spain

Received February 7, accepted July 11, 1984

Summary. The Herbig Ae variable AB Aur (spectral type A0) exhibits a line spectrum characteristic of a stellar wind. IUE observations of the Si IV and C IV resonance lines in AB Aur are reported here. These lines are strong and in absorption. Two models can explain the presence of Si^{3+} and C^{3+} in the wind of AB Aur: a "remote chromosphere" model, with a temperature rise up to 10^5 K, occurring beyond the point where the ionizing radiation begins to depart from the local Planck function, and a "deep chromosphere" model, with a temperature rise up to 15,000–18,000 K, located just above the stellar photosphere. Several additional observational arguments are in favor of the "deep chromosphere" model.

Key words: pre-main sequence stars – superionization – stellar chromospheres – stellar winds – UV spectra

1. Introduction

The irregular variable AB Aur (spectral type A0) belongs to the class of Herbig Ae stars, which are believed to be pre-main sequence (PMS) stars and can be considered as higher mass counterparts of T Tauri stars. A description of Herbig Ae stars can be found in Herbig (1960) and Strom et al. (1972, 1975).

Recent high resolution spectroscopic observations of AB Aur show that this star exhibits spectral features indicating a stellar wind and chromospheric activity (Praderie et al., 1982; Felenbok et al., 1983). A detailed quantitative study of the line formation in the wind of AB Aur (Catala, 1983; Catala et al., 1984) led to the conclusion that this star possesses a deep and extended chromosphere, where the temperature reaches at least 15,000 K. This analysis provided also constraints on the wind structure.

In the present paper, observations of Si IV and C IV resonance doublets in absorption in AB Aur are shown and discussed in the framework of the results of Catala (1983) and Catala et al. (1984). The observation of these lines is extremely seldom in A0 stars. Si IV resonance lines are usually no longer observed in absorption at spectral types later than B7 and C IV resonance lines at spectral types later than B5, either for dwarfs or for supergiants. To the best of our knowledge, the only A0 dwarf star for which C IV and Si IV resonance lines are observed in absorption, except AB Aur, is HD 119921 (Molaro et al., 1983). This star is not a PMS star and has a high $v \sin i$.

The presence of Si^{3+} and C^{3+} in the wind of an A0 star requires temperatures higher than the effective temperature of the star, $T_{\rm eff} = 10{,}000$ K, indicating the existence of hot regions above the photosphere, possibly heated by deposition of non-radiative energy. This phenomenon of superionization has already been observed in some O and early B stars (see Lamers and Snow, 1978, and references therein), and in some Be stars (Doazan, 1982). Several types of models have been proposed up to now to explain the superionization in hot stars. The first one is the so-called "warm wind model" (Lamers and Snow, 1978), in which very high temperatures are reached in the wind (10^5 K for C^{3+}). The second one is a model proposed by Castor (1979), in which the different species are ionized by optically thick radiation. A third type of model is the so-called corona + cool wind model (Olson and Castor, 1981), in which the superionization is explained by the presence of a thin corona at the base of the wind, producing enough X-ray radiation to ionize species like O^{5+} via the Auger mechanism. Lucy (1982) has also proposed that the Auger mechanism is responsible for the superionization in very hot stars, but that the X-ray radiation could be produced by a series of shocks in the stellar wind. Since no X-ray radiation has been detected for AB Aur by the Einstein satellite (Feigelson and de Campli, 1981), and since, as we will see below, the models involving X-ray radiation are not necessary to explain the presence of C^{3+} and Si^{3+} (although they could probably work out perfectly), we focus in this paper on the first two models, and investigate the implication of the presence of Si^{3+} and C^{3+} in the wind of AB Aur in the framework of both types of models. For this purpose, we will use a very simplified treatment of the ionization equilibrium. Section II describes the observations of Si IV and C IV resonance lines. In Sect. III, the treatment of the ionization equilibrium is explained, and both types of models are examined. Discussion and conclusion are given in Sect. IV.

2. Observations

Two spectra of AB Aur obtained by the IUE satellite in the high resolution mode (~ 0.2 Å) and in the short wavelength range (1150 Å $\leqq \lambda \leqq$ 2000 Å) are available in IUE archives. In addition, another IUE spectrum was taken by us in January 1983. The log of the three observations is given in Table 1.

Send offprint requests to: C. Catala

* Based on observations made by the International Ultraviolet Explorer (IUE) and collected at the Villafranca Satellite Tracking Station of the European Space Agency

** Laboratoire associé au CNRS 264

Table 1. Log of IUE observations of AB Aur in the high resolution mode, short wavelength range

Image number	Aperture	Exp. time (min)	Date of observation	Program
SWP 3682	*L*	220	23 Dec. 78	NH051
SWP 4907	*L*	300	9 Apr. 79	TTBCI
SWP 18987	*L*	367	11 Jan. 83	EA107

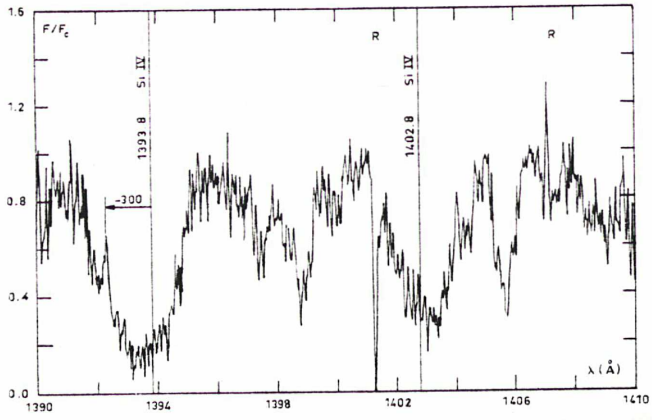

Fig. 1. The Si IV resonance lines observed on the IUE SWP 18987 image. The blueshift indicated on the figure has been measured at $F/F_c = 0.8$ and is expressed in km s^{-1}. The "*R*" indicate the positions of the reseau marks or of the "bright spots"

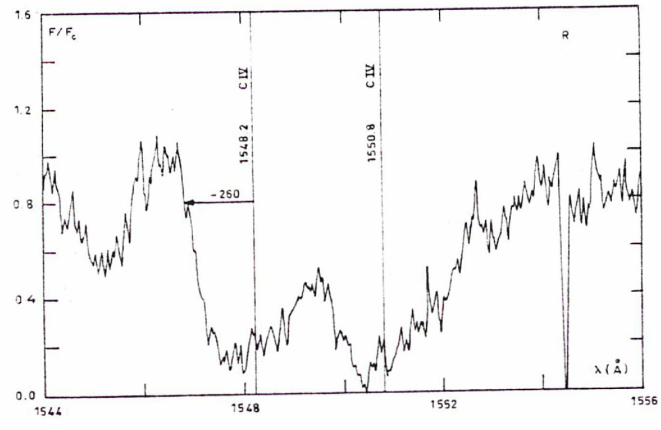

Fig. 2. Same as Fig. 1, but for the C IV resonance lines

Figures 1 and 2 show the regions of Si IV and C IV resonance doublets for the spectrum of January 1983. The fluxes have been normalized to the continuum placed "by eye" near the top of the noise fluctuations within a 20 Å range around the center of the lines. A wavelength shift has been corrected thanks to the detection of the interstellar line of C I at 1656.93 Å, initiating from the ground level. On the uncorrected spectrum, the IUE wavelength scale was shifted by 0.14 Å to the blue.

The identification of the two sets of lines seen in Figs. 1 and 2 with Si IV and C IV resonance lines requires some care. The two C IV lines, as well as the Si IV λ1394 Å line can be mistaken with blends of Fe III lines. We have strong evidence for the presence of Fe^{2+} in the wind of AB Aur thanks to the intense lines of this ion detected in the 1800–1900 Å range, although the IUE spectra of AB Aur are overexposed in that range. The Si IV λ1402 Å could be mistaken with a blend of Si II lines. Here again, the detection of the Si II resonance lines at λλ1527, 1533 Å demonstrates the presence of Si^+ in the atmosphere of AB Aur. However, a detailed analysis showed the absence of the other lines of Fe III initiating from the same level as the lines that could be mistaken with the C IV resonance lines (level $3d^5(a^6s)4p^7P^\circ$), such as for example the Fe III lines λλ1531.29, 1531.64, 1531.86 Å. It seems that we cannot avoid identifying the lines seen in Fig. 2 with the C IV resonance lines. Since the C^{3+} ion is present in the wind of AB Aur, it is likely that the Si^{3+} ion is present too and that the lines seen in Fig. 1 are the Si IV resonance lines.

It is important to notice that the four lines are purely in absorption, and in particular that they do not exhibit a P Cygni emission component. The Si IV and C IV resonance lines in AB Aur are not saturated, but very strong. They are far stronger than the Si IV and C IV resonance lines detected in the A0 star HD 119921 (Molaro et al., 1983), and even stronger than in main sequence B5 stars (see Underhill, 1980, 1982). They have general characteristics similar to the Si IV and C IV resonance lines observed in some classical Be stars (Doazan, 1982). As can be seen in Figs. 1 and 2, the four lines are very wide. The maximum blueward displacement with respect to the rest wavelengths (placed by offset with the observed interstellar C I line) is 1.4 Å for the Si IV resonance lines, corresponding to $\Delta V = -300\,\mathrm{km\,s^{-1}}$, and 1.3 Å for the C IV resonance lines, corresponding to $\Delta V = -260\,\mathrm{km\,s^{-1}}$. These high values suggest that the four lines are widened by the velocity field of the wind of AB Aur. The profiles of the same lines on the two IUE archive spectra are globally similar, but some differences can be noticed, in particular the values of the maximum blueward displacements. These differences are not surprising, since the star is known to be spectroscopically variable on several time scales (e.g. Praderie et al., 1982, 1983).

3. The ionization equilibrium

If autoionization and dielectronic recombinations are neglected, the ionization equilibrium between two ions of ionization state i and $i+1$, that we suppose to be assimilated to their ground state, writes:

$$n_i C_{i,i+1} + n_i R_{i,i+1} = n_{i+1}(n_i/n_{i+1})^* C_{i+1,i} + n_{i+1}(n_i/n_{i+1})^* R_{i+1,i}, \quad (1)$$

where n_i and n_{i+1} are the populations of the two ions, $C_{i,i+1}$ and $C_{i+1,i}$ respectively the collisional ionization and recombination rates, $R_{i,i+1}$ and $R_{i+1,i}$ respectively the radiative ionization and recombination rates, and where $(n_i/n_{i+1})^*$ represents the ratio of the populations at thermal equilibrium.

The different ionization and recombination rates can be computed from (see Mihalas, 1978, p. 134):

$$C_{i,i+1} = C_{i+1,i} = 1.55\,10^{13} n_e T_e^{-1/2} \bar{g}\alpha(\nu_0)\frac{kT_e}{h\nu_0}\exp(-h\nu_0/kT_e)\ (\mathrm{cgs}), \quad (2)$$

$$R_{i,i+1} = 4\pi \int_{\nu_0}^{\infty} \frac{\alpha(\nu)}{h\nu} J_\nu d\nu, \quad (3)$$

$$R_{i+1,i} = 4\pi \int_{\nu_0}^{\infty} \frac{\alpha(\nu)}{h\nu}\left(\frac{2h\nu^3}{c^2} + J_\nu\right)\exp(-h\nu/kT_e)\,d\nu, \quad (4)$$

where ν_0 is the photoionization threshold of the ion considered, $\alpha(\nu)$ the photoionization cross-section at frequency ν, n_e and T_e respectively the electron density and the electron temperature of the medium, J_ν the mean intensity of the local radiation field and $\bar{g}$ a correction factor between 0.1 and 0.3. Equation (1) is in principle coupled with the radiative transfer equation, because J_ν appears in the expression of the radiative rates. However, it is possible to describe the ionization equilibrium by appropriate approximations on J_ν.

When the opacity at the wavelengths of the ionizing radiation varies in a regular way throughout the wind, one can define for each ion considered a "dethermalizing layer", that is to say a layer where the ionizing radiation begins to depart from the local Planck function. Note that for the ions considered here, the photoionization thresholds are in the far UV. If the opacity at these wavelengths does not drop drastically as one gets deeper and deeper in the envelope, the wind can be divided in two regions, separated by the "dethermalizing layer", depending on whether the local medium is optically thin or thick to the ionizing radiation. Outwards of the dethermalizing layer, we make the approximation that the medium is optically thin to the ionizing radiation, i.e. we can write:

$$J_\nu \sim W(r)\, B_\nu(T_r), \tag{5}$$

where T_r is the so-called radiation temperature, defined as the electron temperature of the dethermalizing layer, and $W(r)$ is a geometric dilution factor, computed as:

$$W(r) = \tfrac{1}{2}\{1 - [1 - (R_1/r)^2]^{1/2}\}, \tag{6}$$

where R_1 is the radial distance to the dethermalizing layer.

Below the dethermalizing layer, J_ν is given by the local Planck function.

Thanks to these simplifications, it is now easy to evaluate the radiative rates $R_{i,i+1}$ and $R_{i+1,i}$. In the hydrogenoid approximation, we can write:

$$\alpha(\nu) = \alpha(\nu_0)\, \nu_0^3/\nu^3. \tag{8}$$

Moreover, the photoionization threshold frequencies for Si^{2+}, C^{2+}, Si^{3+}, C^{3+} are very high (see Table 2), so that even for the lowest one (Si^{2+}) the Planck function can be approximated by Wien's formula for temperatures up to 10^5 K.

Outwards of the dethermalizing layer, the radiative ionization rate writes:

$$R_{i,i+1} \sim \frac{8\pi}{c^2} W(r)\, \alpha(\nu_0)\, \nu_0^3\, E_1(h\nu_0/kT_r), \tag{9}$$

where $E_1(x)$ is the first order integroexponential function, while below the dethermalizing layer:

$$R_{i,i+1} \sim \frac{8\pi}{c^2} \alpha(\nu_0)\, \nu_0^3\, E_1(h\nu_0/kT_e). \tag{10}$$

For the calculation of the radiative recombination rate, we first notice that $J_\nu \ll 2h\nu^3/c^2$ in all cases relative to our analysis, so we can write:

$$R_{i+1,i} \sim 4\pi \int_{\nu_0}^{\infty} \frac{\alpha(\nu_0)}{h\nu} \frac{\nu_0^3}{\nu^3} \frac{2h\nu^3}{c^2} \exp(-h\nu/kT_e)\, d\nu$$

$$\sim \frac{8\pi}{c^2} \alpha(\nu_0)\, \nu_0^3\, E_1(h\nu_0/kT_e). \tag{11}$$

Table 2. Photoionization thresholds for the studied ions

Ion	λ_∞ (Å)	ν_0 (s^{-1})
Si^{2+}	370.6	$8.095\ 10^{15}$
C^{2+}	259.2	$1.157\ 10^{16}$
Si^{3+}	275.0	$1.091\ 10^{16}$
C^{3+}	192.5	$1.559\ 10^{16}$

We can now make use of the asymptotic behavior $E_1(x) \sim x^{-1} e^{-x}$ when $x \gg 1$ to write:

$$R_{i,i+1} \sim \frac{8\pi}{hc^2} W(r)\, \alpha(\nu_0)\, kT_r\, \nu_0^2 \exp(-h\nu_0/kT_r) \quad \text{if} \quad r \geqq R_1, \tag{12}$$

$$R_{i,i+1} \sim \frac{8\pi}{hc^2} \alpha(\nu_0)\, kT_e\, \nu_0^2 \exp(-h\nu_0/kT_e) \quad \text{if} \quad r < R_1, \tag{13}$$

$$R_{i+1,i} \sim \frac{8\pi}{hc^2} \alpha(\nu_0)\, kT_e\, \nu_0^2 \exp(-h\nu_0/kT_e). \tag{14}$$

If now we evaluate the ratios of radiative to collisional ionizations and recombinations, we find:

$$\frac{R_{i,i+1}}{C_{i,i+1}} \sim \frac{8\pi W(r)\nu_0^3}{1.55\ 10^{13}\, \bar{g}\, c^2} \frac{T_r}{n_e \sqrt{T_e}} \cdot \exp\left[-\frac{h\nu_0}{k}\left(\frac{1}{T_r} - \frac{1}{T_e}\right)\right] \quad \text{if } r \geqq R_1, \tag{15}$$

$$\frac{R_{i,i+1}}{C_{i,i+1}} \sim \frac{8\pi\nu_0^3}{1.55\ 10^{13}\, \bar{g}\, c^2} \frac{\sqrt{T_e}}{n_e} \quad \text{if} \quad r < R_1, \tag{16}$$

and

$$\frac{R_{i+1,i}}{C_{i+1,i}} \sim \frac{8\pi\nu_0^3}{1.55\ 10^{13}\, \bar{g}\, c^2} \frac{\sqrt{T_e}}{n_e}. \tag{17}$$

The analysis of expressions (16) and (17) shows immediately that radiative recombinations dominate in all the atmosphere of an A0 star, and that radiative ionizations dominate below the dethermalizing layer. Outwards of this layer, as seen from expression (15), radiative ionizations still dominate if $T_r > T_e$, but collisional ionizations can be dominant if T_e becomes higher than T_r. For example, with $T_e = 2T_r = 10{,}000$ K, $W(r) = 0.5$, $\nu_0 = 8.1\ 10^{15}\, s^{-1}$ (threshold of Si^{++}), $\bar{g} = 0.1$, $n_e = 10^6\, cm^{-3}$, we find $R_{i,i+1}/C_{i,i+1} \sim 3\ 10^{-6}$.

It is then possible to describe schematically the ionization balance in the different parts of the wind:

i) Below the dethermalizing layer

If the medium is everywhere optically thick to the ionizing radiation below the dethermalizing layer, the ionization balance is dominated by the radiative processes, and the ionizing radiation is thermalized. Equation (1) and expressions (13) and (14) give:

$$n_{i+1}/n_i = (n_{i+1}/n_i)^* \tag{18}$$

which tells us that the ionization equilibrium is described by the Saha equation.

ii) Outwards of the dethermalizing layer

If $T_e \leqq T_r$ in this region, the ionization balance is still dominated by the radiative processes, but the medium is here considered as optically thin to the ionizing radiation. Equation (1) and expressions (12) and (14) then give:

$$\frac{n_{i+1}}{n_i} = \left(\frac{n_{i+1}}{n_i}\right)^* W(r) \frac{T_r}{T_e} \exp(-h\nu_0/kT_r) \exp(+h\nu_0/kT_e) \qquad (19)$$

which is similar to the well-known Strömgren (1948) equation.

If now $T_e \geqq T_r$ somewhere in this region, the ionization balance becomes a coronal equilibrium, i.e. an equilibrium between collisional ionizations and radiative recombinations. In that case, we have:

$$\frac{n_{i+1}}{n_i} = 1.55\ 10^{13}\ \bar{g} \frac{c^2}{8\pi\nu_0^3} T_e^{-1/2} 2 \frac{g_{i+1}}{g_i} \left(\frac{2\pi mkT_e}{h^2}\right)^{3/2} \cdot \exp(-h\nu_0/kT_e), \qquad (20)$$

where all the quantities have their usual meaning and must be expressed in c.g.s. units.

Two different models can then be proposed to explain the presence of Si^{3+} and C^{3+} in the wind of AB Aur, irrespective of any mechanism to account for the temperature run.

i) The "remote chromosphere" model

The term "remote" here means that the temperature rise occurs outwards of the dethermalizing layers for Si^{2+} and C^{2+}. In this case, the ionization balance is a coronal equilibrium, as demonstrated above. The ionization ratios do not depend on the electron density (Eq. 20), and very high temperatures (10^5 K) must be envisaged to account for the presence of C^{3+}. Note that at these temperatures, the hydrogen and helium continua are optically thin, and that it is impossible to locate "a priori" the dethermalizing layers. The temperature rise can then occur at any distance from the stellar core. The ionizing radiation will thermalize only below the region of very high temperature. If the temperature rise occurs at the base of the wind, this model is equivalent to the "warm wind model" for O and B stars (Lamers and Snow, 1978). Since this model has been widely discussed by these authors, it is not necessary to explain it in detail here.

ii) The "deep chromosphere" model

The term "deep" means that the temperature rise occurs below the dethermalizing layer, in a region where the ionizing radiation is thermalized. This is possible only if the temperature in this region is low enough for the medium to be optically thick to the ionizing radiation. In such a situation, the ionization equilibrium is described by the Saha equation. The ionization ratios then depend on the electron density, and it is possible to obtain Si^{3+} and C^{3+} in reasonable quantities at temperatures of about 15,000–18,000 K, if n_e is sufficiently low. Table 3 gives the results for the ratios Si^{3+}/Si_{total} and C^{3+}/C_{total} for different temperatures in that range and at different electron densities. The analysis of Catala (1983) and Catala et al. (1984) shows that a deep chromosphere, at these temperatures and at electron densities of about 10^{10}–10^{11} cm^{-3}, is necessary to explain the shape of the Mg II resonance lines in AB Aur. It must then be checked that the hydrogen or helium continuum is still thermalized in such a medium. This check has been provided by the computation of the continuum at 455 Å in the models described in Catala (1983) and Catala et al. (1984), by using the Equivalent Two-Level Atom (ETLA) code developed by Mihalas and Kunasz (1978). This code provides a detailed computation of the hydrogen lines and continua, and the complete results will be presented in a further publication. The preliminary results show that the radiation at 455 Å (bluest wavelength of the mesh we used) is thermalized (i.e. $J_\nu = B_\nu$, to within 10%) in models with chromospheres where $T_{max} = 15{,}000$–$18{,}000$ K (T_{max} is the maximum temperature reached in the chromosphere; see Catala et al. (1984) for the form of the temperature law in these models) and the mass loss rate $\dot{M} = 7\ 10^{-9}\ M_\odot\ yr^{-1}$, corresponding to electron densities in the chromosphere in the range 10^{10}–10^{11} cm^{-3}. In these models, the radiation at 455 Å begins to dethermalize only at about 3 stellar radii from the stellar core. The situation at the photoionization thresholds for Si^{2+} and C^{2+} (370 and 260 Å) is likely to be similar to the one described here. We can then check in Table 3 that the model proposed by Catala (1983) and Catala et al. (1984) is consistent with the presence of Si^{3+} and C^{3+} in the wind of AB Aur.

Figure 3 gives a schematic representation of the temperature law in the two kinds of models. The regions of formation of the lines are indicated on the figure.

Table 3. Fractions of Si^{3+} and C^{3+} in percentage in deep chromosphere models, at different temperatures and different densities

Si^{3+}/Si_{tot} / C^{3+}/C_{tot}		T_e(K) 15,000	17,000	20,000
n_e(cm^{-3})	10^9	97 / 0.2	81 / 14	3.4 / 95
	10^{10}	91 / 0.02	98 / 1.4	26 / 71
	10^{11}	50 / 0.002	95 / 0.14	78 / 19

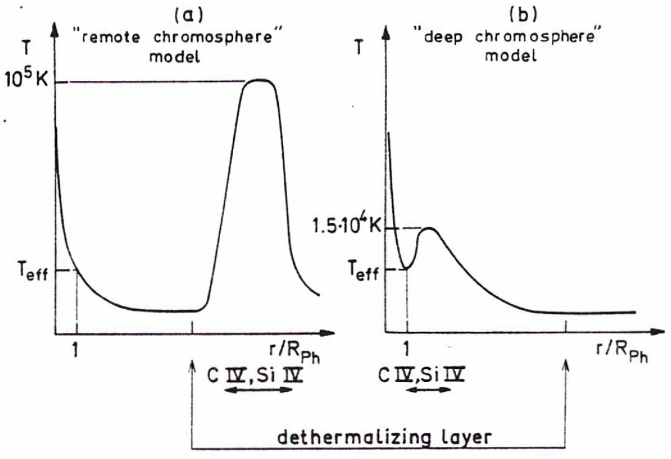

Fig. 3. Schematic representation of the two models discussed in the text. The effective temperature of the star is 10,000 K. R_{ph} stands for the photospheric radius of the star

4. Discussion and conclusion

At the present stage of this very simple analysis, we have seen that two types of models already proposed in the literature can account for the presence of Si^{3+} and C^{3+} in the wind of AB Aur. We have voluntarily omitted to include the corona + cool wind model (Olson and Castor, 1981) in our analysis, although it is probably consistent with the observations, too. The reason for this omission is that it is not needed to explain the observations and seems too sophisticated for our simple analysis.

The consistency of the two models mentioned in Sect. 3 with the observations must be quantitatively checked, in order to choose which of them, if any, is the most adapted to the particular case of AB Aur. This can be performed by computing the profiles of the lines that have been observed with a high spectral resolution. A detailed computation of the Mg II resonance lines has already been published (Catala et al., 1984) and detailed computations of the C IV resonance lines, of the Ca II resonance lines and of the hydrogen Balmer lines are now in progress. But before this complete analysis is carried out to its end, we can make use of the preliminary results that have already been obtained to critically examine the two models.

As already mentioned, in the "remote chromosphere" model, the temperature rise can occur at any distance in the wind. However, the computations of the C IV resonance lines (preliminary results presented in Catala, 1984) have shown that, when the hot region is located far away from the stellar core, these lines exhibit a strong P Cygni profile, which is not observed. This hot region must then be located at the base of the wind, and must not be too extended. The preliminary results presented in Catala (1984) show that the size of the line formation region must not exceed 1.5 stellar radii, otherwise a strong emission component appears on the red side of the line. In other words, our "remote chromosphere" model must be reduced to a truncated "warm wind model", surrounded by a cooler region. But the calculation of the C IV resonance lines with such a model leads to intense emission lines, when collisional deexcitation is not neglected. This means that the temperature rise in this model is located too deep in the wind, or that the temperature is too high. Although these results are still only preliminary, it seems that the "remote chromosphere" model, which can qualitatively explain the presence of Si^{3+} and C^{3+}, fails to explain the profiles of these lines.

It has been shown in Sect. 3 that the "deep chromosphere" model is also consistent with the presence of Si^{3+} and C^{3+} in the wind of AB Aur. A good thermalization of the ionizing radiation is ensured at the relatively low temperature needed to ionize carbon to its 3rd ionization stage, when Saha's equation is used with the range of electron densities typical of the models described in Catala et al. (1984). Would the O VI or N V lines be observed in AB Aur, this model would not be consistent any more. The higher temperatures needed to explain the presence of O^{5+} and N^{4+} would prevent the thermalization of the ionizing radiation. Therefore, this type of model would not explain the superionization observed in some O stars. In the case of AB Aur, the calculation of the C IV resonance lines with this model leads to absorption lines, and a reasonable fit of the observed profile can be obtained (Catala, 1984). We also know that a good fit of the profile of the Mg II resonance lines can be obtained with this model (Catala et al., 1984). Therefore, this model seems more adapted to the case of AB Aur than the "remote chromosphere" model.

Additional observations are also consistent with this model.

1. Observations of the He I 5876 Å line, of the hydrogen P14 to P16 lines, and of the Ca II infrared triplet, all of them in emission, can be qualitatively interpreted in terms of a chromosphere at $T \sim 15{,}000$–$18{,}000$ K, located deep enough in the wind to ensure for example a good coupling of the source function in the He I 5876 Å line with the temperature (Felenbok et al., 1983).

2. Observations of an emission in the core of the Ca II K line is another evidence of the existence of a chromosphere located at a relatively great depth in the wind of AB Aur (Praderie et al., 1982). Detailed calculations of the Ca II K line formation in a model including a deep, extended and expanding chromosphere consistent with the results of Catala (1983) and Catala et al. (1984) are in progress and the preliminary results are encouraging.

3. The Hα line exhibits a P Cygni profile with an intense emission component (Felenbok et al., 1983). Preliminary results of a detailed computation of this line in this type of model, by using the ETLA code, tend to show that a good fit can be obtained. The results of these computations will be presented in a further publication.

At this point of the analysis, we can then conclude that the observation of Si IV and C IV resonance lines in AB Aur, as well as the other observations of this star, are consistent with a model including a deep and extended chromosphere where the temperature reaches 15,000–18,000 K. It is not our point here to speculate on possible mechanisms of production of such a temperature rise.

Acknowledgements. We gratefully thank F. Praderie for suggesting this work and for helpful comments and stimulating discussions. Many thanks also to the referee, who made several important remarks and suggested significant improvements of the paper.

Postscript

In the papers by Catala et al. (1984) and Catala (1984), the "remote chromosphere" is implicitely assumed to be located far away from the stellar core. Thanks to the remarks of the referee on the present paper, we realize that this assumption is unsupported and, as pointed out in this paper, the Si^{3+} and C^{3+} ions can be present in a region where the temperature is of about 10^5 K, even if this region is located at the base of the wind.

References

Castor, J.I.: 1979, *IAU Symp.* **83**, p. 169
Catala, C.: 1983, 3rd cycle thesis, Paris 7 University
Catala, C., Kunasz, P.B., Praderie, F.: 1984, *Astron. Astrophys.* **134**, 402
Catala, C.: 1984, Proc. 4th European Conf., Rome, May 1984, ESA SP218, p. 227
Doazan, V.: 1982, in B *stars with and without emission lines*, NASA SP456
Herbig, G.H.: 1960, *Astrophys. J. Suppl.* **4**, 337
Feigelson, E.D., De Campli, W.M.: 1981, *Astrophys. J.* **243**, L89
Felenbok, P., Praderie, F., Talavera, A: 1983, *Astron. Astrophys.* **128**, 74
Lamers, H.J.G.L.M., Snow, T.P.: 1978, *Astrophys. J.* **219**, 504
Lucy, L.B.: 1982, *Astrophys. J.* **255**, 278
Mihalas, D.: 1978, in *Stellar Atmospheres*, 2nd edition
Mihalas, D., Kunasz, P.B.: 1978, *Astrophys. J.* **219**, 635
Molaro, P., Morossi, C., Ramella, M., Franco, M.: 1983, *Astron. Astrophys.* **127**, L3
Olson, G.L., Castor, J.I.: 1981, *Astrophys. J.* **244**, 179
Praderie, F., Talavera, A., Felenbok, P., Czarny, J., Boesgaard, A.M.: 1982, *Astrophys. J.* **254**, 658

Praderie, F., Simon, T., Boesgaard, A.M., Felenbok, P., Catala, C., Czarny, J., Talavera, A., Le Contel, J.M., Morel, P., Sareyan, J.P., Valtier, J.C.: 1983, 2nd France-Japan Seminar, Paris, ed. J.C. Pecker and Y. Uchida, p. 132

Strom, S.E., Strom, K.M., Yost, J., Carrasco, L., Grasdalen, G.L.: 1972, *Astrophys. J.* **173**, 353

Strom, S.E., Strom, K.M., Grasdalen, G.L.: 1975, *Ann. Rev. Astron. Astrophys.* **13**, 187

Strömgren, B.: 1948, *Astrophys. J.* **108**, 242

Underhill, A.B.: 1980, *Astrophys. J.* **235**, L149

Underhill, A.B.: 1982, in B *stars with and without emission lines*, NASA SP456

THE WIND AND CHROMOSPHERE OF THE HERBIG Ae STAR AB AUR AS SEEN BY IUE

C. Catala

Observatoire de Paris-Meudon, France

ABSTRACT

The Herbig Ae variable AB Aur (spectral type A0) exhibits a line spectrum characteristic of a stellar wind. The results of a detailed quantitative interpretation of the MgII resonance lines (λλ 2796,2802 Å) are summarized and preliminary results of a quantitative interpretation of the CIV resonance line at 1548 Å are presented.

These results show the presence of a deep and extended chromosphere in the wind of AB Aur, where the temperature reaches 18,000 K.

Constraints on the structure of the wind are derived. The mass loss rate is found to lie between 4 10^{-11} and 7 10^{-9} $M_\odot$ yr^{-1}.

A pure thermal Doppler broadening is not sufficient to explain the profile of the MgII and CIV lines, and an additional broadening mechanism must be envisaged.

Keywords: pre-main-sequence stars, stellar winds, stellar chromospheres, line formation

1. INTRODUCTION

The irregular variable AB Aur (A0ep) belongs to the class of Herbig Ae stars, which are widely believed to be pre-main-sequence (PMS) stars (Refs. 8, 17, 18), and can be considered as higher mass (2-5 $M_\odot$) counterparts of T Tauri stars. Most of the Herbig Ae stars exhibit a line spectrum characteristic of a stellar wind and chromospheric activity (Refs. 14, 19, 7). Since nothing is known about the mechanisms of wind production and of chromospheric heating in such stars, the first step towards the comprehension of the physical processes at work must be a determination of the structure of their atmospheres. This can be done by a semi-empirical modelling of the outer layers of these stars.

AB Aur is the brightest Herbig Ae star in the northern hemisphere and a large number of high resolution spectroscopic observations of this star are available (Refs. 14, 6). A semi-empirical modelling of its outer layers is then possible by the interpretation of the lines formed in these layers. Since most of the other Herbig Ae stars show the same spectral features as AB Aur (Refs. 19, 7), this star can be considered as representative of a part of its class. In AB Aur, one of the best evidences for the presence of a wind is the P Cygni profile of the MgII resonance lines (Ref. 14) and the SiIV and CIV resonance lines in absorption constitute a strong argument for the existence of a chromospheric region (Ref. 5).

A detailed interpretation of the MgII resonance lines of AB Aur has already been published (Ref. 4, hereinafter paper I). This work led to the derivation of constraints on the wind and chromosphere structure. These results are summarized in the present paper. Preliminary results of the quantitative interpretation of the CIV resonance lines are then presented. This interpretation leads to tighter constraints on the conditions in the chromosphere of AB Aur.

2. INTERPRETATION OF THE MgII RESONANCE LINES

The MgII resonance lines in AB Aur, which can be seen in Ref. 14, show a type IV P Cygni profile according to Beals' classification (Ref. 1). In paper I, detailed computations of these lines in a spherical and expanding atmosphere have been performed and have been applied to the case of AB Aur. A brief summary of this work is given here. For more detail, the reader is referred to paper I.

2.1 The model

The type of model that has been considered in paper I for interpreting the MgII resonance lines consists in a spherical expanding envelope surrounding a "classical" photosphere represented by a model of Kurucz (Ref. 9) for T_{eff}=10,000 K and log g=4. This representation is supported by the observation of the Paschen continuum, of the Balmer jump and of the wings of Hδ, which are all well fitted by this model.

The observed maximum blue-shift in the absorption component of the MgII resonance lines on the spectrum presented in Ref. 14 is V_s=380 $km.s^{-1}$, while neutral sodium D lines show P Cygni profiles with absorption components blue-shifted by 130 $km.s^{-1}$ (Ref. 6). Since the NaI D lines are necessarily formed at greater distances from the stellar core than the MgII resonance lines, these observations indicate that the wind is decelerated after it has reached its maximum velocity, somewhere in the MgII resonance line formation region or further out. There is no argument to decide where this deceleration occurs. In paper I, it has been assumed to be located after the MgII

Proc. 4th European IUE Conference, 15 – 18 *May* 1984, *Rome, Italy*, *ESA SP-218* (*July* 1984)

line formation region, which is consistent with all the observations at our disposal.

It has been shown in paper I that the presence of C^{3+} and Si^{3+} can be explained by two kinds of models. The first one is the "remote chromosphere" model, in which the ionization balance for $C^{2+} \rightleftarrows C^{3+}$ and $Si^{2+} \rightleftarrows Si^{3+}$ is a coronal equilibrium. In this model, a temperature rise up to 10^5 K occurs in a region located outwards of the so-called "dethermalizing layer", defined as the layer where the ionizing radiation (which is in the far UV for the ions considered) begins to depart from the local Planck function. This layer is typically located at about 12-15 stellar radii from the stellar core. The second model is the "deep chromosphere" model, in which a temperature rise occurs below the "dethermalizing layer". In this case, the maximum temperature reached in the chromosphere is not higher than 15,000-20,000 K. These two kinds of models are reviewed in Ref. 5.

2.2 Solution of the transfer equation

The non-LTE line transfer problem in the extended and expanding atmosphere of AB Aur has been solved by using the comoving frame method developed by Mihalas et al. (Refs. 10-13). The choice of this method is imposed because of the simultaneous presence of regions of high and low velocity. It is justified since the velocity law has been assumed monotonic in the whole MgII line formation region. The ion Mg^+ has been considered as a two-level atom and complete redistribution has been assumed. The intrinsic line profile has been taken as a Voigt profile, with a damping parameter $a=5\ 10^{-3}$.

2.3 Results

2.3.1 Chromosphere. The interpretation of the MgII resonance lines in AB Aur has shown the presence of a deep and extended chromosphere, where the temperature reaches values between 15,000 and 20,000 K. In the models without chromosphere or with a "remote" chromosphere, the red photospheric wing in absorption formed at the bottom of the wind prevents the formation of an intense red emission component in the emergent profile, as the one observed. When a "deep" chromosphere is present near the base of the wind, the ion Mg^+ is depleted, and the red photospheric wing in absorption disappears. The base of the chromosphere of AB Aur is located at $\tau_{2800}=10^{-2}$-10^{-3}, which is deeper than the solar chromosphere (τ_{2800} is the continuum optical depth at 2800 Å). The extension of the chromosphere of AB Aur has been shown to be larger than one stellar radius, which is far greater than in the solar case.

2.3.2 Mass loss rate. The results of this work showed that the mass loss rate of AB Aur should lie between $4\ 10^{-11}$ and $7\ 10^{-9}$ $M_\odot\ yr^{-1}$. These values are low when compared to the mass loss rates derived for T Tauri stars (10^{-7} $M_\odot\ yr^{-1}$), but still far higher than the solar mass loss rate. Since Herbig Ae stars are believed to be more evolved than T Tauri stars, this tends to suggest that the mass loss rates for PMS stars are related to their evolution stage.

2.3.3 Doppler broadening. The width of the Doppler core of the intrinsic line profile (denoted v_D in the following) is an essential parameter of the calculations. It has been found that $v_D=45$ km.s^{-1}. This value is supersonic (the sound speed is about 10 km.s^{-1}). The Doppler random velocity is then completely dominated by its non-thermal component. As we will see below, the same kind of conclusion can be drawn for the CIV resonance lines. We will come back on this phenomenon in section 3.2.2.

3. INTERPRETATION OF THE CIV RESONANCE LINES

The MgII resonance lines are formed over a very extended region (from the photosphere up to 50 stellar radii). Hence, from their interpretation, we can only get an information "integrated" over the whole envelope. This is the reason why the constraints on the structure of the wind of AB Aur derived in paper I are not very tight. On the other hand, in the "deep chromosphere" model, the CIV and SiIV resonance lines are formed in a very localized area, and we can expect to derive precise information on this area, the chromosphere, by their interpretation. The detailed calculation of the CIV or SiIV resonance lines will provide a powerful test for the kind of models derived from the interpretation of the MgII resonance lines, and will help to tighten the constraints that have already been set on the structure of the chromosphere. Because the SiIV resonance lines and the CIV λ 1550 Å line are contaminated by the presence of reseau marks and of blends with FeIII and FeII lines, we have chosen to compute the CIV λ 1548 Å line, which is contaminated only on its red boundary by a blend with the CIV λ 1550 Å line. The interpretation of this line is still under progress. The results presented below are only preliminary.

For the non-LTE computation of this line, we have applied the same treatment as for the MgII resonance lines. The C^{3+} ion has been considered as a two-level atom, which is justified, since the ground level and the first excited level are far less energetic than the other excited levels. All the atomic quantities concerning the transition are given in Table 1.

Table 1. Atomic data for CIV λ 1548.19 Å

Quantity	f_{12}	g_1	g_2	Ω_{21}	$\Gamma_{rad}(s^{-1})$	$\Gamma_e(s^{-1})$
Value	0.19	2	4	3.3	$2.65\ 10^8$	$9.4\ 10^7$

Notes to Table 1: f_{12}: oscillator strength,
g_1 and g_2: statistical weights,
Ω_{21}: collisional strength,
Γ_{rad}: radiative damping coefficient
Γ_e: electronic damping coefficient for $n_e=10^{14}$ cm^{-3}

The collisional strength has been computed for typical values of the temperature, by using collisional cross-sections taken from Ref. 20. The electronic damping coefficient has been taken from Ref. 2. All the other quantities have been taken from Ref. 21. We have used the standard solar abundance ($C/H=3.72\ 10^{-4}$) for carbon. The carbon ionization equilibrium has been treated in the same way as in paper I, that is to say by writing Saha's equation below the dethermalizing layers (see section 2.1 for definition) and Strömgren's equation above them. For the calculations with the "remote chromosphere" models, a treatment of the coronal equilibrium has also been introduced (see paper I and Ref. 5 for more detail). The sources of continuum opacity considered are the same as in paper I. All the models have been constructed by adding expanding layers around a classical photospheric model (model of Kurucz, $T_{eff}=10^4$ K,

log g=4). For each model, the mass loss rate has been computed so that $\tau_{2800} = 2/3$ at the photosphere. Our models are then consistent with those used in paper I.

3.1 Results with the "remote chromosphere" models

Although the "remote chromosphere" model has been shown in paper I to be inconsistent with the profile of the MgII resonance lines, it is interesting to see if the CIV lines observed in AB Aur could be formed in a hot region located far away from the stellar core. The results could then be applied to other observations. In this type of models, the C^{3+} ionization equilibrium is a coronal equilibrium, and the temperature has to rise up to 10^5 K for the C^{3+} to be present.

Figure 1 shows the result obtained with model R1, described in Table 2. This profile is typical of all the results obtained with "remote chromosphere" models.

Table 2. Description of the models

Model n°	velocity law	chromosphere pos. Δ_1 (stellar radii)	chromosphere ext. Δ_2 (stellar radii)	chromosphere T_{max} (K)	$\dot{M}$ $M_\odot.yr^{-1}$	v_D $km.s^{-1}$
R1	v_1	15	10	10^5	$1.1\ 10^{-9}$	45
D1	v_2	0.08	1.5	18000	$1.1\ 10^{-9}$	45
D2	v_3	0.08	1.5	18000	$1.9\ 10^{-9}$	100

Notes to Table 2: Δ_1 and Δ_2 have the same definition as in paper I.
The different velocity laws are shown in Table 3.

Table 3. Velocity laws

r/R_{ph}	V ($km.s^{-1}$)		
	v_1	v_2	v_3
1	0.001	0.001	0.001
1.1	3	3	5
1.2	200	6	50
1.3	250	9	100
1.5	280	100	114
2	300	250	150
50	300		

Notes to Table 3: R_{ph} is the photospheric radius. The velocity laws are piecewise linear functions of r/R_{ph}.

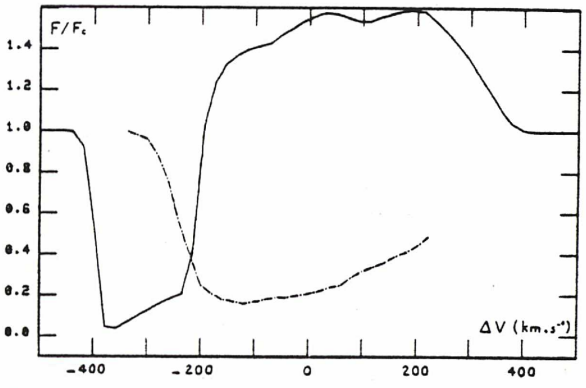

Figure 1. The CIV λ 1548 Å line profile computed with model R1 (full line) compared with the observed profile taken from Ref. 5 and truncated on its red side because of the blend with the 1550 Å line (dashed line).

In the "remote chromosphere" models, the chromospheric region has to be very extended, otherwise the column density of CIV is not sufficient to give rise to a deep absorption line. The emitting region (lateral parts of the envelope) is then very extended and is responsible for the broad and intense emission component seen in Figure 1. The emission component seen in Figure 1 cannot be cancelled by a blend with the absorption component of the CIV λ 1550 Å line. The same conclusion can be reached with all the other "remote chromosphere" models that have been run. We can then conclude that it is definitely impossible to explain the CIV resonance lines with this kind of model.

3.2 Results with the "deep chromosphere" models

The "deep chromosphere" models are very different from the "remote chromosphere" models. First, the C^{3+} ionization equilibrium is dominated by radiative processes and the ionizing radiation is thermalized. As shown in paper I and in Ref. 5, a temperature of 15,000-20,000 K is then sufficient to explain the presence of C^{3+}. Second, the chromosphere is located in a deep region of the wind where the density is high and has not to be very extended to give rise to a deep absorption component for the CIV lines. We can then expect that the emission component of the CIV lines will be weak in this type of models.

3.2.1 Results with v_D=45 $km.s^{-1}$. As a first step, it is natural to compute the CIV λ 1548 Å line in a "deep chromosphere" model, by using the value of the Doppler broadening derived in paper I from the interpretation of the MgII resonance lines, namely v_D=45 $km.s^{-1}$. A typical result (obtained with model D1 of Table 2) is shown in Figure 2. As can be seen on this figure, the absorption component obtained is deep, but not enough, and despite the small extension of the emitting region, an emission component (F_{max}/F_c=1.32) appears on the red side of the line.

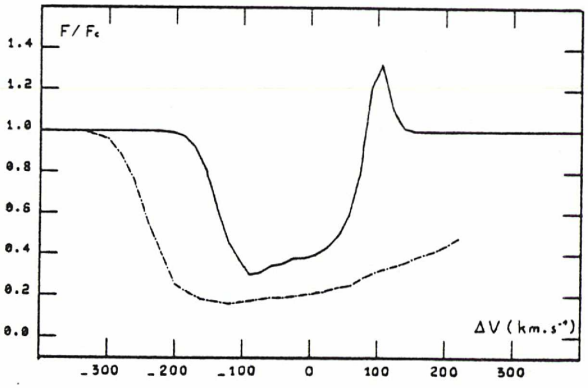

Figure 2 Same as Figure 1, but for model D1

All the possibilities for deepening the absorption component and cancelling the emission component at the same time, with v_D=45 $km.s^{-1}$ and within the limits derived for the model in paper I, have been explored, without success:

i) When the temperature is increased in the chromosphere, the proportion of C^{3+} increases, and the absorption component gets more saturated, but on the other hand, the emission component is enhanced.

ii) The same result is obtained by increasing the extension of the chromosphere.

iii) With a deeper and less extended chromosphere, we expect to get more saturation in the absorption component and a less intense emission component, but within the limit imposed by the absence of an excess emission in the Balmer continuum ($\Delta_1=0.04.R_{ph}$, see paper I), it has been impossible to reproduce the observed profile.

iv) The last possibility is to choose a velocity law with a low gradient at the base of the wind. In this way, we expect to get an almost saturated absorption component near the line center ($\Delta V \sim 0$). But the lower the velocity gradient at the base of the wind, the lower the mass loss rate, as shown in paper I, and we know from the interpretation of MgII lines that $\dot{M}$ lies between 4 10^{-11} and 7 10^{-9} $M_\odot.yr^{-1}$. Moreover, preliminary results of a detailed calculation of the Balmer lines show that $\dot{M} > 10^{-9}$ $M_\odot$ yr^{-1}. This shows that the velocity gradient of the velocity law v_2 used in model D1 is very close to the lower limit.

v) Different combinations of the solutions envisaged above have been tried (for example, a higher temperature together with a less extended chromosphere), but none of them gave satisfactory results.

We can then conclude that it is not possible to explain the CIV resonance lines with a "deep chromosphere" model if the Doppler broadening is $v_D=45$ km.s^{-1}.

3.2.2 Results with $v_D=100$ km.s^{-1}. At first sight, increasing the Doppler broadening to higher values may seem "ad hoc". But this assumption of a high Doppler random velocity can be supported by recent observations of the spectroscopic variability of AB Aur. Praderie et al. (Refs. 15, 16) have observed that this star is spectroscopically variable on several time scales. Their data suggest that the MgII resonance lines are varying with a periodicity equal to the expected rotation period (1.7 days). The interpretation they give of these phenomena is the alternance on the line of sight of fast and slow streams, which could give rise to 3D structures rotating with the star. The difference in velocity between the fast and the slow streams would be of the order of the one measured on the maximum blue-shift of the MgII line absorption component, namely $\Delta V \sim 100$ km.s^{-1}. This kind of structure reminds the 3D structure of the solar wind, in which the same alternance of fast and slow streams is observed (Ref. 3). In the solar wind, these structures are stable over large distances (10 A.U.). But we can reasonably envisage that these structures are not so long-lived in the envelope of AB Aur, because of the great differences in density, in rotation velocity, and may be in magnetic field strength between the wind of AB Aur and the solar wind. We would then be in a case where these structures are stable in the CIV line formation region and then disappear further out in the wind. Let us now turn back to the signification of our Doppler random velocity v_D. In the formalism used for solving the transfer equation, one assumes implicitely that all the random motions in the atmosphere are present on the microscopic scales. Actually, this is equivalent to a situation where inhomogeneous motions are present on scales smaller than the characteristic scale for the line transfer. Because of the velocity gradient in the CIV line formation region, the scale for the line transfer is large, typically greater than one stellar radius, while the scale of the alternance between fast and slow streams is necessarily smaller than one stellar radius. This could justify the use of high values for v_D in the computation of the CIV λ 1548 Å line. Further out in the wind, these structures are likely to dissipate towards smaller scales, creating turbulence, and the conservation of the flux of the turbulent energy leads to smaller values for v_D in the outer parts of the MgII line formation region. Of course, this is only a speculation for the moment, and this kind of model must be carefully checked and tested.

Figure 3 shows the result obtained with the model D2, by using $v_D=100$ km.s^{-1}. The major effect of a large value for v_D is to broaden the absorption component both towards the blue and the red. The emission component then disappears almost entirely. As can be seen on this figure, the computed profile fits reasonably well the observed profile, and the difference at the red boundary of the profile can be attributed to a blend with the blue part of the CIV λ 1550 Å line. This result, together with the results obtained with $v_D=45$ km.s^{-1}, quantitatively supports the ideas developed in the precedent paragraph.

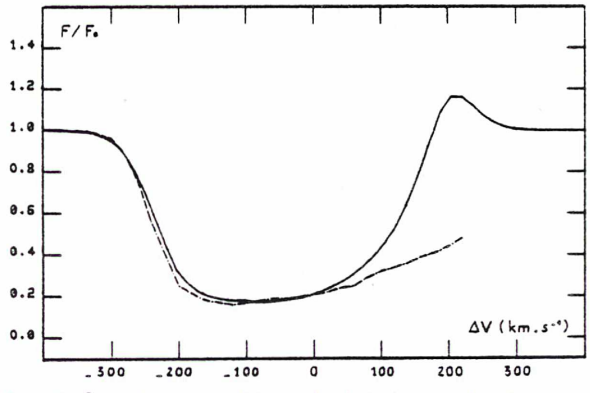

Figure 3. Same as Figure 1, but for model D2.

3.2.3 Constraints on the structure of the chromosphere. By assuming $v_D=100$ km.s^{-1}, it is possible to derive tight constraints on the structure of the CIV line formation region, namely the chromosphere. This requires a lot of modelling, and is under progress. We just give here very preliminary results.

Nothing can be derived on the mass loss rate through the calculation of the CIV λ 1548 Å line. The fraction of C^{3+} is indeed proportional to n_e^{-1} (from Saha's equation), so the C^{3+} density is proportional to $n_e^{-1}.\rho$, which is almost independant of $\dot{M}$ (ρ is the density of the wind, related to $\dot{M}$). The mass loss rate has then no effect on the CIV line profile.

The maximum temperature of model D2 is 18,000 K. Several tests tend to show that a maximum temperature of 19,000 K leads to intense emission components on the red side of the profile. It can then be concluded that $T_{max} < 19{,}000$ K. A more precise determination of T_{max} is under progress.

For the same reason, we find that 1.5 stellar radii is the upper limit for the extension of the chromosphere. From the interpretation of the MgII lines, a lower limit of one stellar radius had been determined. Further work is needed to find constraints on the maximum depth reached by the chromosphere, but we know already that it cannot

be deeper than 1.04 R_{ph}, because of the absence of an excess emission in the Balmer continuum.

Finally, we deduce from the computations that the velocity gradient must be low near the base of the wind (between 1 and 1.1 stellar radii) in order to get a deep absorption component extending to the line center, and that the maximum velocity reached in the chromosphere is around 150 km.s^{-1}, when v_D=100 km.s^{-1}. The global picture is then a velocity law accelerating gently near the photosphere, then more steeply to reach 150 km.s^{-1} at 2 stellar radii, then 300 km.s^{-1} in the outermost parts of the MgII line formation region, and then decelerating down to 150 km.s^{-1} further out as can be deduced from the observation of sodium lines (see paper I).

CONCLUSION

The results of the interpretation of the MgII resonance lines and preliminary results of the calculation of the CIV resonance lines in AB Aur can be summarized as follows:

The stellar photosphere is surrounded by a deep and extended chromosphere. The maximum temperature reached in this chromosphere is around 18,000 K. Its extension is greater than 1 stellar radius and smaller than 1.5 stellar radii.

The mass loss rate has been found to lie between 4 10^{-11} and 7 10^{-9} $M_\odot.yr^{-1}$.

The wind has been shown to accelerate gently near the photosphere, then reach 150 km.s^{-1} within 2 stellar radii, which corresponds approximately to the upper boundary of the chromosphere. Further out, the velocity reaches 300 km.s^{-1}, and then decreases down to at least 150 km.s^{-1} in the most remote parts of the envelope.

The Doppler broadening of the intrinsic profile has been found to be 45 km.s^{-1} for the MgII lines and 100 km.s^{-1} for the CIV lines, which can be interpreted in terms of a 3D structure including fast and slow streams at the bottom of the wind.

Clearly, some more modelling is required for a better understanding of the structure of this envelope. In particular, the computation of the Balmer lines, which is under progress, will give us more precise information on the mass loss rate. Moreover, further observations are needed to test the model of alternate fast and slow streams that has been briefly envisaged here.

ACKNOWLEDGEMENTS

The author greatly acknowledges fruitful discussions with F. Praderie, A. Mangeney, M. Leroy and R. Grappin. Many thanks to P.B. Kunasz who placed his comoving frame numerical code at our disposal.

REFERENCES

1. Beals C.S. 1951, Publ. Dominion Astrophys. Obs. 9, 1.

2. Bogen P. 1972, Zeit. für Naturforsch. 27A, 210.

3. Burlaga L.F. 1983, J. Geophys. Res. 88, 6085.

4. Catala C., Kunasz P.B., Praderie F. 1984, Astron. Astrophys., in press.

5. Catala C., Talavera A. 1984, Astron. Astrophys., submitted.

6. Felenbok P., Praderie F., Talavera A. 1983, Astron. Astrophys. 128, 74.

7. Finkenzeller U., Mundt R. 1984, Astron. Astrophys. Suppl. 55, 109.

8. Herbig G.H. 1960, Astrophys. J. Suppl. 4, 337.

9. Kurucz R.L. 1979, Astrophys. J. Suppl. 40, 1.

10. Mihalas D., Kunasz P.B., Hummer D.G. 1975, Astrophys. J. 202, 465.

11. Mihalas D., Kunasz P.B., Hummer D.G. 1976, Astrophys. J. 203, 647.

12. Mihalas D., Kunasz P.B., Hummer D.G. 1976, Astrophys. J. 206, 515.

13. Mihalas D., Kunasz P.B., Hummer D.G. 1976, Astrophys. J. 210, 419.

14. Praderie F., Talavera A., Felenbok P., Czarny J., Boesgaard A.M. 1982, Astrophys. J. 254, 658.

15. Praderie F., Simon T., Boesgaard A.M., Felenbok P., Catala C., Czarny J., Talavera A., Le Contel J.M., Morel P., Sareyan J.P., Valtier, J.C. 1983, 2nd France-Japan Seminar, Paris, eds. J.C. Pecker, Y Uchida, p. 132.

16. Praderie F., Catala C., Czarny J., Felenbok P. 1984, Workshop on Space Research Prospect in Stellar Activity and Variability, Meudon, eds. F. Praderie, A. Mangeney, in press.

17. Strom S.E., Strom K.M., Yost J., Carrasco L., Grasdalen G.L. 1972, Astrophys. J. 173, 353.

18. Strom S.E., Strom K.M., Grasdalen G.L. 1975, Ann. Rev. Astron. Astrophys. 13, 187.

19. Talavera A., Catala C., Crivellari L., Czarny J., Felenbok P., Praderie F. 1982, Proc. 3rd European IUE Conf., Madrid, ESA SP176, p.99.

20. Taylor P.O., Gregory D., Dunn G.H., Phaneuf R.A., Crandall D.H. 1977, Phys. Rev. Letters 39, 1256.

21. Wiese W.L., Smith M.W., Miles B.M. 1969, Atomic Transition Probabilities vol. I, NSRDS-NBS22.

ANNEXE G

Line formation in the winds of Herbig Ae/Be stars. The CIV resonance lines

Claude Catala

Observatoire de Paris, Section de Meudon
Unité de Recherche Associée au CNRS 264
92195 Meudon Principal Cedex France

and

High Altitude Observatory, National Center for Atmospheric Research*
PO Box 3000, Boulder CO 80307 USA

(*) The National Center for Atmospheric Research is sponsored by the National Science Foundation

Received :

Thesaurus codes: 12.01.1; 19.24.1; 19.48.1; 19.58.1

Main Journal. Subdivision: Stellar Atmospheres.

SUMMARY

We present the results of a detailed computation of the C IV resonance lines in the pre-main sequence Herbig Ae star AB Aur. We have used the equivalent-two-level-atom approach to solve the radiative transfer and statistical equilibrium equations for the multi-level atomic structure of the C III - C IV - C V system. The radiative transfer equation is solved in the co-moving frame of the flow.

Intense absorption lines are obtained with a model that includes a moderate temperature (17000 K), expanding chromosphere. The semi-empirical model built for AB Aur from previous analysis can therefore explain the observed shape of the C IV resonance lines.

The present analysis allows new constraints to be placed on the structure of AB Aur's chromosphere. Its maximum temperature is between 16000 and 18000 K, and 2.5 stellar radii constitutes an upper limit for its extension.

Key words : Lines: formation - Stars: chromospheres - Stars: mass loss - Stars: pre-main sequence

1 - INTRODUCTION

The Herbig Ae/Be stars are commonly believed to be pre-main sequence (PMS) objects of intermediate mass (Herbig, 1960 ; Strom et al., 1972 ; Cohen and Kuhi, 1979 ; Finkenzeller and Mundt, 1984). Among other properties, these PMS stars show definite signs of stellar winds and chromospheres (Praderie et al., 1982 ; Catala et al., 1986a). No ab initio theoretical model has yet been proposed to account for the winds and chromospheres of these stars. Clearly, one of the first steps to take in order to understand these atmospheres is to determine their structure semi-empirically as accurately as possible. Major progress has been made in this direction, due to the quantitative interpretation of several lines in the spectra of these stars.

AB Aur (A0Vep, m_v = 7.2), the brightest Herbig Ae star in the Northern hemisphere, has been shown to be representative of its class (Catala et al., 1986a), and has been extensively studied. A semi-empirical model based on the assumption of a non-rotating, steady-state, spherically symmetric wind has been built for this star. The interpretation of the Mg II resonance lines (Catala et al., 1984) and of the Hα line (Catala and Kunasz, 1987, hereafter CK) have placed tight constraints on the model. This work demonstrated the existence of an expanding chromosphere with temperatures in the range 15000 - 18000 K, and supported a mass loss rate estimate of 1 - 1.8 x 10^{-8} $M_\odot$ yr^{-1}.

Catala and Talavera (1984, hereafter CT) have observed the C IV resonance lines in AB Aur, with the International Ultraviolet Explorer (IUE). These lines appear purely in absorption. They are rather intense (although not saturated), and wide, suggesting that they are formed in expanding regions of the atmosphere. Catala et al. (1987) have obtained a time series for the same lines and, although the maximum blueward displacement of these lines is quite variable, they have the same shape as the ones presented in CT. The mere presence of the C IV resonance lines implies the existence of heated layers in the wind of this A0 star. The most common interpretation of these lines in A or B stars involves a region at $\sim 10^5$ K, where a coronal equilibrium (balance between collisional ionizations and radiative recombinations) prevails for the ionization of C III (see e.g. Doazan, 1982).

An alternative solution was presented by CT, following an idea

originally due to Castor (1979). This second model assumes that the ionizing radiation for the C III - C IV transition is thermalized in a 15000 - 18000 K chromosphere. In that case, radiative ionizations and recombinations control the C III - C IV transition, and the C III - C IV equilibrium is well described by Saha equation. C IV may then exist in sufficient quantities at such moderate temperatures. Making this basic assumption, Catala (1984) computed the profile of the C IV λ 1548 Å line, considering the ion as a two-level atomic system, and approximating the C III - C IV ionization equilibrium by Saha formula. This computation yielded absorption lines for C IV, similar to the observed profile.

Clearly, the major uncertainty in this past work concerns the assumption of thermalized ionizing radiation. A more complete calculation has now been performed, where this assumption is dropped, and where the radiative transfer problem is solved for the transitions of the C III - C IV - C V atomic structure, consistently with the opacities of a set of background species. The present paper is a report of the results of these calculations.

Recent work demonstrated that the wind of AB Aur features important departures from spherical symmetry (Praderie et al., 1986 ; Catala et al., 1986b). The rotational modulation observed in the Mg II resonance lines and in the Ca II K line has been interpreted as the alternation of fast and slow streams in the line of sight as the star rotates. The same kind of behavior has also been detected for the C IV resonance lines (Catala et al., 1987). Although these observations make the use of spherically symmetric models questionable, a great amount of information can be gained on the average structure of the atmosphere by interpreting line profiles with these models. This is true in particular for the red emission components of P Cygni profiles, which are formed in regions of large volume so that the effects of departures from spherical symmetry are smoothed out. On the other hand, absorption components formed in the regions of the atmosphere that are projected onto the stellar disk are expected to be extremely sensitive to the passage of inhomogeneities in the line of sight. In other words, it would not make sense to attempt a detailed interpretation of a line that appears purely in absorption by using a spherically symmetric model. Therefore, in the present paper, we will not try to fit the observed profile, but simply show that intense C IV absorption lines can be expected from an expanding chromosphere at 15000 - 18000 K surrounding and AOV star. This will prove that the semi-

empirical model built from the interpretation of other lines is consistent with the presence of the C IV resonance lines in absorption.

In Section 2, we discuss the atmospheric and atomic models used in the calculations. A brief summary is given of the equivalent-two-level-atom (ETLA) approach used to solve the radiative transfer problem in the co-moving frame. In Section 3, we present the results of the computations and a discussion of their significance. Finally, a summary and general conclusions are given in Section 4.

2 - NUMERICAL TECHNIQUES

2-1 Atmospheric model :

The atmospheric models used in the present analysis have been constructed in the same way as described in Catala et al. (1984) and in CK. The reader is referred to these two papers for details. Let us briefly recall here the principal characteristics of these models.

All of them include hydrostatic layers at the base of the wind, as suggested by several observations (CK). The density and the temperature in these layers are taken from a radiative equilibrium, LTE model for T_{eff} = 10000 K and log g = 4 (Kurucz, 1979). "Back-warming" effects due to the presence of the wind have been neglected. Although they might be important for the detailed structure of the photosphere, they do not affect the C IV resonance lines, whose region of formation lies well above the photosphere. The velocity in the wind is monotonically increasing outward, and is given as a piecewise linear function of the distance from the star's center (r). The mass loss rate is determined so that the continuum optical depth at 2800 Å is 2/3 at the photospheric radius. This choice makes the models easily comparable to the ones used in previous works (Catala et al., 1984; CK). The density in the wind is derived from the velocity law and the mass loss rate through the equation of mass conservation. The temperature decreases outward in the photospheric layers, where it is given by the Kurucz model, until it reaches a given minimum value. Above this layer is the chromosphere, where the temperature increases to a maximum value then decreases again. In the chromosphere, the temperature has a gaussian variation with r and is characterized by four parameters T_{max}, Δ_1, Δ_2, T_0, controlling respectively the maximum temperature, the position and extension of the chromosphere, and the temperature outside the chromosphere (see CK for details). Finally, as in Catala et al. (1984) and CK, a large Doppler random velocity was introduced in the models.

Whereas the models used in CK for the computations of the hydrogen lines extended to 70 stellar radii (R_*), including a huge post-chromospheric region, we can afford in our model to ignore the outermost layers, because of the depletion of C IV in this cool region. We can also reasonably assume that the regions of the atmosphere outside the chromosphere have negligible influence on the formation of the C IV

resonance lines. Therefore, the wind models we consider in this paper extend only up to the outer boundary of the chromosphere (typically $2R_*$).

2-2 Atomic model :

Three ionization stages have been introduced in these computations. A total of 6 levels have been taken into account, 3 for C III, 2 for C IV, and 1 for C V. All the relevant atomic data concerning these levels are presented in Table 1.

The two levels involved in the C IV resonance transition ($2s\ ^2S$, $2p\ ^2P°$) are well decoupled from the rest of the C IV atomic structure. We can therefore neglect the other energy levels of this ion. Considering only 3 levels for C III constitutes a poorer approximation, but is still sufficient for the purpose of showing that one obtains intense absorption lines for C IV with our models.

This atomic structure involves 3 bound-bound transitions, and 5 bound-free transitions. Table 2 lists the oscillator strengths for the bound-bound transitions, taken from Wiese and Glennon (1972). Note that in the co-moving frame calculations, we have ignored the fine structure of the excited levels of C III and C IV, and considered the multiplets as single transitions. In the last step of the profile computation, however, which consists of solving the transfer equation in the observer's frame (see Sect. 2-3), we have computed only the bluest line of the C IV resonance doublet, without taking into account the blend with the second line. The collisional excitation and ionization rates, as well as the photoionization cross-sections have been provided by L. Anderson (private communication). Brief information on these data can be found in Anderson (1985). Auto-ionization and dielectronic recombinations have been neglected. Since they may be important for an ion like C III at the temperatures considered here, they should be included for a more detailed modelling of the C IV resonance lines. These calculations are differed to a further paper. We have adopted a carbon abundance of 3.72×10^{-4}.

The intrinsic profiles of the lines have been assumed to be gaussian, with width determined by the Doppler random velocity specified in the atmospheric model. Complete redistribution has also been assumed in the course of this work. These two assumptions, while questionable in

principle for resonance lines such as the ones treated here, are justified by the limited goal of our analysis.

The background opacity and emissivity sources include 10 levels for H, 10 levels for He, 20 levels for He^+, and a total of 24 levels for C, N, O, Ne, Si, and their ions. All the background species are assumed to be in LTE, with normal abundances. The cross-sections of the background opacity sources are detailed in the appendix of CK, and the ones for metals have been taken from Henry (1970).

2-3 Numerical solution of the transfer equation :

Once the atmospheric and atomic models are specified, our task is to solve the simultaneous equations of radiative transfer and statistical equilibrium for the level populations of C III, C IV, C V and then to compute the emergent flux profile of the C IV λ 1548 Å line. This is achieved by a two-step procedure, fully described in CK. Only a brief summary of the method is given below.

The first step consists of solving the coupled set of statistical equilibrium and radiative transfer equations, using the ETLA method in its co-moving frame formulation, as developed by Mihalas and Kunasz (1978). The choice of the co-moving frame is dictated by the large macroscopic velocity present in our models. In the ETLA method, each transition is isolated from the rest of the atomic structure and treated as a non-LTE two-level problem (with the rates involving the other levels considered fixed), in an overall iteration scheme.

The second step is the calculation of the emergent profile, carried out in the observer's frame, using the level populations obtained after convergence of the co-moving frame ETLA scheme.

The convergence of the ETLA iteration scheme turned out to be very fast in this particular problem. Typically, four overall iterations were sufficient to reach convergence to within less than a percent.

3 - RESULTS AND DISCUSSION

3-1 Reference model :

As already stated, no emphasis will be put on a detailed comparison between the computed and observed C IV line profiles, since these lines are very sensitive to the inhomogeneous structure of the wind, which has not been included in the model. The goal of this work is simply to show that an intense absorption line is to be expected from the model proposed in previous studies (Catala et al., 1984; CK). Therefore, we will use model # 1 of CK as reference for the present work (we call it C1 in the present paper). This model leads to the best fit of the H_α line profile, and includes all of the structural constraints previously derived. Table 3 gives a description of this model, as well as of the other models examined in this study. Details of the velocity law V_1 used in these models can be found in CK.

3-1-1 C IV λ 1548 Å line profile :

Figure 1 shows the λ 1548 Å line profile obtained with model C1. The line appears in absorption, and is as deep as the observed one (see CT and Catala et al., 1987). We note that it has the same global shape as the one obtained by Catala (1984) which had been computed under the assumption of thermalized ionizing radiation (see Sect. 1).

A small amount of emission is present on the red side of the line. This emission is due to the combination of two effects: first, a small chromospheric emission, induced by a rise of the line source function and broadened by the the high Doppler random velocity; second, a volume emission due to the extension of the line formation region. This small red emission component is not observed, either in the λ 1548 Å or in the λ 1550 Å line. Its absence from both lines can be accounted for by the moderate S/N ratio obtained with IUE. Therefore, we conclude that model C1 is consistent with the absence of any emission component in the observed profile.

Because of the velocity law and the value of the Doppler random velocity of model C1, the maximum blueward displacement of the computed line is v_s (C IV) = -150 km s^{-1}. The observation by CT gives v_s (C IV) = -260 km s^{-1}, and the time series obtained by Catala et al. (1987) yields

values ranging from -300 to -390 km s^{-1}. This discrepancy between computed and observed profiles can possibly be overcome by increasing the velocity gradient in the chromosphere, or, as suggested by Catala (1984), by introducing a variable Doppler random velocity, with high values at the base of the wind, and lower values in the post-chromospheric region. We see little interest, however, in pursuing the present study that far, since attempting to fit a variable profile with a single spherically symmetric model would clearly constitute an overinterpretation of the computations. The only conclusion we want to draw here is that model C1, which has already been shown to be consistent with other observations (CK), succeeds in explaining the presence of the C IV resonance lines in absorption in AB Aur.

3-1-2 Ionizing radiation :

The analysis presented in CT and in Catala (1984) assumes that the radiation ionizing C III into C IV is thermalized in the chromosphere, and this assumption has been dropped in the present study. In order to understand the basic processes responsible for the formation of the C IV resonance lines, it is interesting to examine the ionizing radiation field and to check if indeed it is thermalized in the chromosphere. Figure 2 shows the departure of the mean intensity J_ν from the local Planck function B_ν slightly shortward of the C III - C IV discontinuity. We note that this departure is less than a percent, except near the outer boundary of the chromosphere, where it becomes significant.

The ionization of He I from its ground state is the main source of opacity in the chromosphere, except at the temperature maximum, where metals, in particular O II, contribute significantly to the opacity. We have run a test case with all the metal opacities set to zero, and checked that the ionizing radiation was still thermalized to within 10 %. The C IV line in this test case shows very little difference with the one of model C1. The He I opacity alone turns out to be sufficient to ensure thermalization of the ionizing radiation in the chromosphere.

In the present calculations, we have assumed that the background species populations are in LTE. This assumption might be a source of uncertainty. It is not excluded that strong departures from LTE might depopulate the ground state of He I such that the radiation shortward of the C III - C IV discontinuity would not be thermalized, although this hypothesis is based on no physical ground. Solving the radiative transfer

for a complex structure such as He I - He II, in presence of a velocity field, is not a trivial problem, and, to the best of our knowledge, has not yet been attempted. Until such a full calculation is carried out, we cannot know if non-LTE effects would tend to increase or decrease the background opacity. Nevertheless, a test case has been run, in which the Helium and metal populations were decreased by a factor of 10, without changing significantly the results. This test suggested that the assumption of LTE for the background species is not crucial for our purpose.

3-1-3 Rates and populations :

Using our results, we can readily check a conclusion given in CT, namely that in a moderate temperature chromosphere, the ionization balance between C III and C IV is entirely controlled by the radiative processes. Figure 3 shows the collisional and radiative ionization and recombination rates for the bound-free transition between the ground states of C III and C IV. The radiative rates dominate the ionization as well as the recombination in the chromosphere. Moreover, the contribution of stimulated recombinations is very small compared to the spontaneous recombinations. Thus, the C III - C IV equilibrium is a balance between photoionization and spontaneous radiative recombinations.

Figure 4 shows the population of C III and C IV in the chromosphere (sums of populations of the different levels considered fo each ion). The ratio n(CIV)/n(CIII) ranges from 4×10^{-5} to 4×10^{-4} in the hottest parts of the chromosphere. It is interesting to note that such a small fraction of C IV can produce an absorption line like the one displayed in Fig. 1, due to the large abundance of the carbon element.

3-2 New constraints on the physical structure :

Although there is no point in attempting a detailed comparison between computed and observed profiles, as argued above, two features of the C IV resonance lines can help us to place new constraints on the physical structure of the wind and chromosphere of AB Aur. Owing to the time series observed by Catala et al (1987), including 5 spectra obtained at different phases of the star's rotation, and to the other past observations of the C IV lines by IUE (1 in CT, 2 in the archives, see CT for the IUE image numbers), we know that these lines never show any

emission component on their red side, and that the absorption component always reaches $F_{abs}/F_c \sim 0.2$, where F_{abs} is the minimum flux in the absorption component and F_c the flux in the adjacent continuum. Other characteristic quantities, such as the line equivalent width or the maximum blueward displacement, are highly variable, and cannot be used for deriving constraints on the physical structure in the framework of a spherically symmetric model.

Table 4 shows the maximum absorption F_{abs}/F_c and the maximum emission F_{em}/F_c obtained with models C1-C8 in the C IV λ 1548 Å line.

As mentioned above (see Sect. 3-1-1), the red emission component appearing on the computed profile is due to both a "real" chromospheric emission, and to a volume emission. An increase in the temperature leads to an enhancement of the line source function, and thus yields a more intense emission component, through the first effect. Model C2, with T_{max} = 18000 K, yields F_{em}/F_c =1.4, while model C3 (T_{max} = 19000 K) yields F_{em}/F_c = 3.8.

Increasing the extension of the chromosphere also leads to a more intense emission component, through the second effect. A chromosphere with a 2 R_* extension (model C5) gives an emission component with F_{em}/F_c = 1.2. However, model C6, with a chromospheric extension of 1 R_*, leads to an emission component of about the same intensity as model C1, suggesting that all of the emission is due to the first effect in this regime.

The maximum depth reached by the absorption component is controlled by the amount of C IV in the line of sight, which depends mainly on both the chromosphere's temperature and extension. Model C4, with T_{max} = 16000 K, and model C6, with a chromospheric extension of 1 R_*, both give F_{abs}/F_c = 0.6. We have noticed that the mass loss rate $\dot{M}$ has no influence on the line profile. The line profile obtained with model C9 ($\dot{M}$ = 1.8 x 10^{-8} $M_\odot$ yr^{-1}) is not appreciably different from the one obtained with model C1 ($\dot{M}$ = 1.1 x 10^{-8} $M_\odot$ yr^{-1}). The ratio n(CIV)/n(CIII) is indeed very well approximated by Saha equation, and therefore inversely proportional to the electron density. This dependence of n(CIV)/n(CIII) on $\dot{M}$ is compensated by the proportionality of the carbon total number density to the mass loss rate.

The described dependence of the two noticeable features in the C IV lines on the parameters of our models allows us to derive constraints on these parameters. The ratio of the oscillator strenghs of the two C IV

resonance lines is only 2. Therefore, the presence of the red emission component of model C2, with $F_{em}/F_c = 1.4$, would be easily detected on the red side of the C IV λ 1550 Å line by IUE. Because, as we have seen above, the contribution of the volume emission to this red emission component becomes negligible when Δ_2 is less than 1.5 R_*, there is no hope of decreasing its intensity by decreasing the extension of the chromosphere. Therefore, we conclude that an upper limit for the temperature reached in the chromosphere is 18000 K.

Model C7, with T_{max} = 16000 K and Δ_2 = 2.5 R_*, still gives a fair amount of red emission ($F_{em}/F_c = 1.15$), mainly due to volume emission, and leads to a weak absorption component, reaching only $F_{abs}/F_c = 0.6$. This result suggests that 16000 K is a comfortable lower limit for T_{max}, and that an upper limit for the extension of the chromosphere is 2.5 R_*.

The parameter v_D (Doppler random velocity) is arbitrary in our formulation, but is needed to represent intrinsic broadening processes that cannot be described more accurately (see CK). All of the constraints derived above have been obtained by assuming that the Doppler random velocity in the chromosphere is 45 km s^{-1} - a value derived previously from the analysis of the Mg II resonance lines (Catala et al., 1984). Catala (1984), however, has suggested the possibility that this Doppler random velocity could be larger in the chromosphere. A higher value of v_D could be introduced to take into account high turbulent velocities, or samll scale inhomogeneities, possibly induced by the alternation of slow and fast streams detected by Praderie et al. (1986) and Catala et al. (1986b). The effect of a higher value for v_D would be to broaden the absorption component both toward the blue and toward the red, and to decrease the intensity of the emission component (Catala, 1984). Since this emission component plays a major role in the above analysis, the constraints on the temperature and the extension of the chromosphere would then have to be loosened.

4 - CONCLUSION

We have shown that a moderate temperature chromosphere (T_{max} = 17000 K) leads to intense C IV resonance lines in absorption in the spectrum of a Herbig Ae star. Therefore, there is no need to invoke high temperatures ($\sim 10^5$ K) to explain the presence of these lines in the observed spectrum of AB Aur.

A full computation of the C III - C IV - C V system, also including background opacity sources like H, He, C, N, O, Si and their ions, has confirmed the preliminary conclusions presented in CT and Catala (1984) : in a chromosphere at 17000 K, surrounding an AOV stellar photosphere, the radiation ionizing C III into C IV is thermalized and the ionization balance is entirely radiative.

The semi-empirical model derived for AB Aur from previous studies (Catala et al., 1984 ; CK), and including an expanding chromosphere at 17000 K, leads to intense C IV resonance lines in absorption, similar to the observed ones.

Although a detailed comparison of the computed and observed profiles is impossible, due to the presence of strong inhomogeneities in the wind of this star, several new constraints have been placed on the structure of the chromosphere: its maximum temperature is between 16000 and 18000 K, and its extension is smaller than 2.5 R_*.

It is unlikely that the same kind of moderate temperature rise can explain the superionization observed in O and early B stars (Snow and Morton, 1976). The temperature needed for obtaining species like O VI for example are probably too high to allow thermalization of the ionizing radiation. On the other hand, a moderate temperature chromosphere could possibly explain the C IV lines observed in absorption in the spectra of some Be stars (Doazan, 1982).

Even though it might be easier to theoretically account for the presence of heated layers at 17000 K than at 10^5 K, a full hydrodynamical model of the winds and chromospheres of Herbig Ae/Be stars is still to be built. We believe that the numerous constraints on the physical structure derived in the present paper and in the course of previous work (Catala et al., 1984 ; Catala, 1984 ; CK) will be very efficient tools to test the hydrodynamical models that will be proposed in the future.

ACKNOWLEDGEMENTS

I acknowledge fruitful discussions with D. Hummer, P. Kunasz, B. Lites and F.Praderie. I am especially grateful to L. Anderson for providing me with up-to-date atomic data on C III and C IV. I thank the "Conseil Scientifique du Centre de Calcul Vectoriel pour la Recherche", for the allocation of part of the computing time necessary for this study. This work, initiated at Meudon Observatory, was completed while I was a short-term visitor at the High Altitude Observatory. I wish to thank HAO for its kind invitation. Finally, I thank B. Lites and F. Praderie for their critical reading of the manuscript, and C. Morrow for putting this paper in acceptable English.

REFERENCES

Anderson, L.S.: 1985, Astrophys. J. **298**,848

Castor, J.I.: 1979 IAU Symp. **83**, p.169

Catala, C., Kunasz, P.B., Praderie, F.: 1984, Astron. Astrophys. **134**,402

Catala, C., Talavera, A.: 1984 (CT), Astron. Astrophys. **140**,421

Catala, C.: 1984, Proc. 4th European IUE Conf., Rome, ESA SP218, p.227

Catala C., Czarny, J., Felenbok, P., Praderie,F.: 1986a, Astron. Astrophys. **154**,103

Catala, C., Felenbok, P., Czarny, J., Talavera, A., Boesgaard, A.M.: 1986b, Astrophys. J. **308**,791

Catala, C. Kunasz, P.B.: 1987 (CK), Astron. Astrophys. **174**,158

Catala, C., Praderie, F., Felenbok, P.: 1987, Astron. Astrophys., in press

Cohen, M., Kuhi, L.V.: 1979, Astrophys. J. Suppl. **41**,743

Doazan, V.: 1982, in "B stars with and without emission lines", NASA SP456

Finkenzeller, U., Mundt, R.: 1984, Astron. Astrophys. **55**,109

Henry, R.J.W.: 1970, Astrophys. J. **161**,1153

Herbig, G.H.: 1960, Astrophys. J. Suppl. **4**,337

Kurucz, R.L.: 1979, Astrophys. J. Suppl. **40**,1

Mihalas, D., Kunasz, P.B.: 1978, Astrophys J. **219**,635

Praderie, F., Talavera, A., Felenbok, P., Czarny, J.,Boesgaard, A.M.: 1982, Astrophys. J. **254**, 658

Praderie, F., Simon, T., Catala, C., Boesgaard, A.M.: 1986, Astrophys. J. **303**,311

Snow, T.P., Morton, D.C.: 1976, Astrophys. J. Suppl. **32**,429

Strom, S.E., Strom, K.M., Yost, J., Carrasco, L., Grasdalen, G.L.: 1972, Astrophys. J. **173**,353

Wiese, W.L., Glennon, B.M.: 1972, in "American Institute of Physics Handbook" (New-York : McGraw-Hill)

FIGURE CAPTIONS

Fig. 1: The C IV λ 1548 Å line profile computed with model C1 (reference model). The maximum temperature of the chromosphere in model C1 is 17000 K. Note that the line is almost purely in absorption, and intense.

Fig. 2: Departure from thermalization of the ionizing radiation for the C III - C IV ground states transition, and for model C1. The radiation field J_ν and the local Planck function B_ν are at $\nu = 1.1669 \times 10^{16} s^{-1}$, which is slightly shortward of the transition discontinuity. The boundaries of the figure in the $\text{Log}\tau_{5000}$ scale correspond to the limits of the chromosphere. Note that the radiation field is thermalized to within a percent in most of the chromosphere. Near the outer boundary of the chromosphere, the Planck function decreases strongly, much faster than the radiation field. The arrow points to the location where the optical depth at -20 km s^{-1} from the line center is unity.

Fig. 3: Radiative and collisional rates for ionization and recombination, for the C III - CIV ground states transition, and for the chromosphere of model C1. Note that radiative rates dominate this transition. The arrow has the same meaning as in Fig. 2.

Fig. 4: C III and C IV populations in the chromosphere of model C1, computed as the sum of the populations of the different levels considered for each ion. The arrow has the same meaning as in Fig. 2.

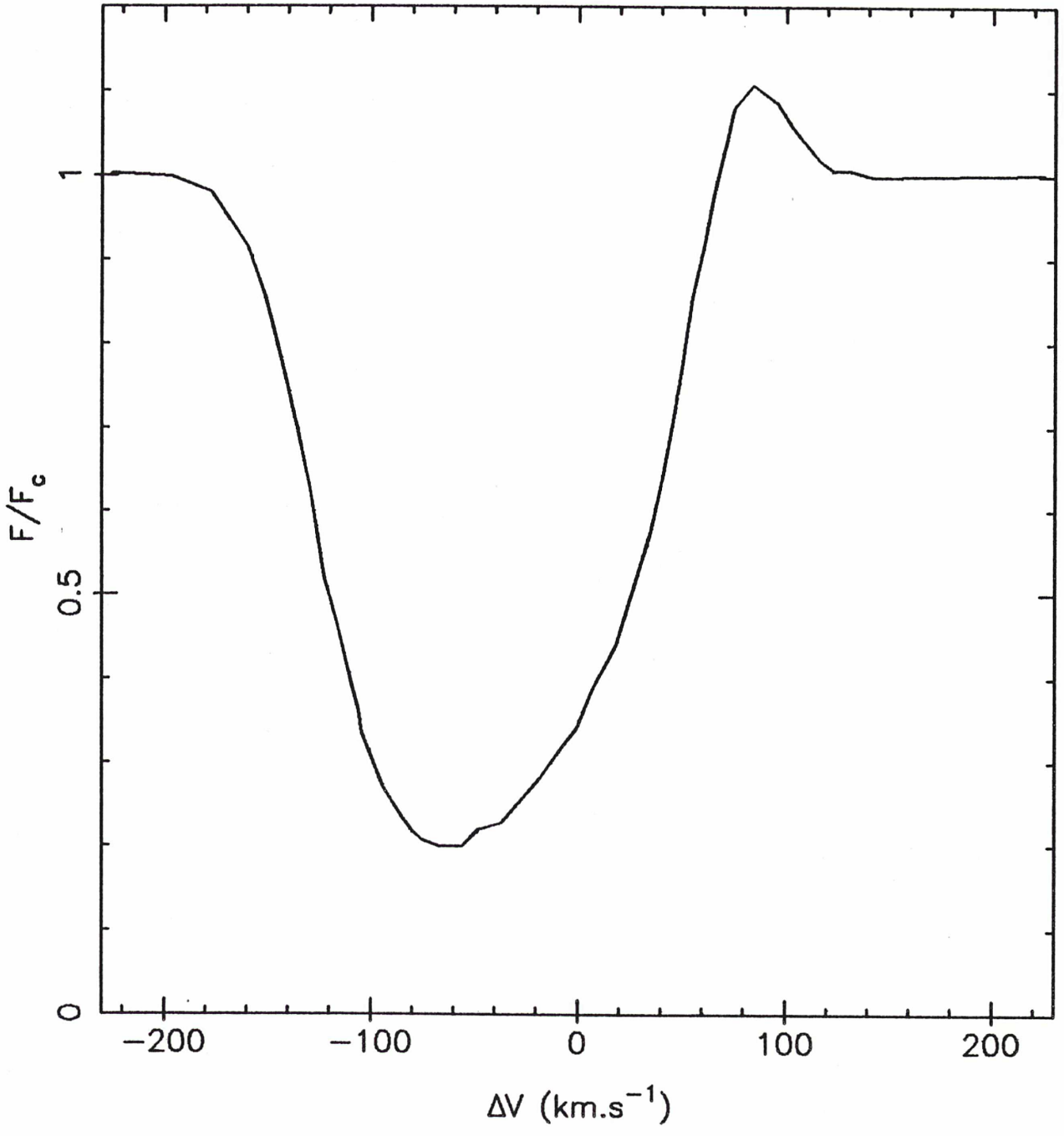
F/F$_c$
0
0.5
1
−200
−100
0
100
200
ΔV (km.s^{-1})

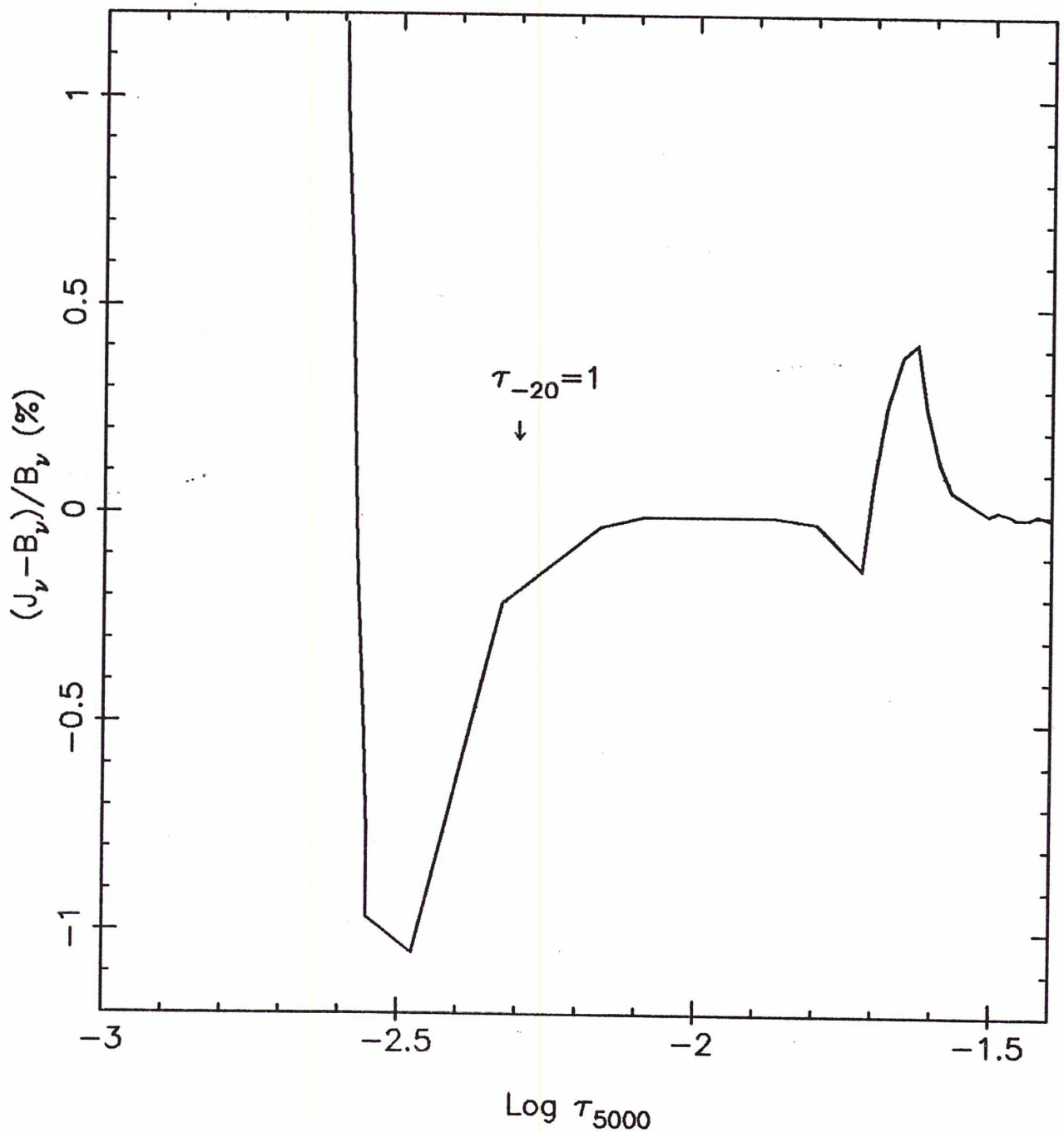
1
0.5
0
−0.5
−1
$(J_\nu - B_\nu)/B_\nu$ (%)
$\tau_{-20}=1$
−3
−2.5
−2
−1.5
Log τ_{5000}

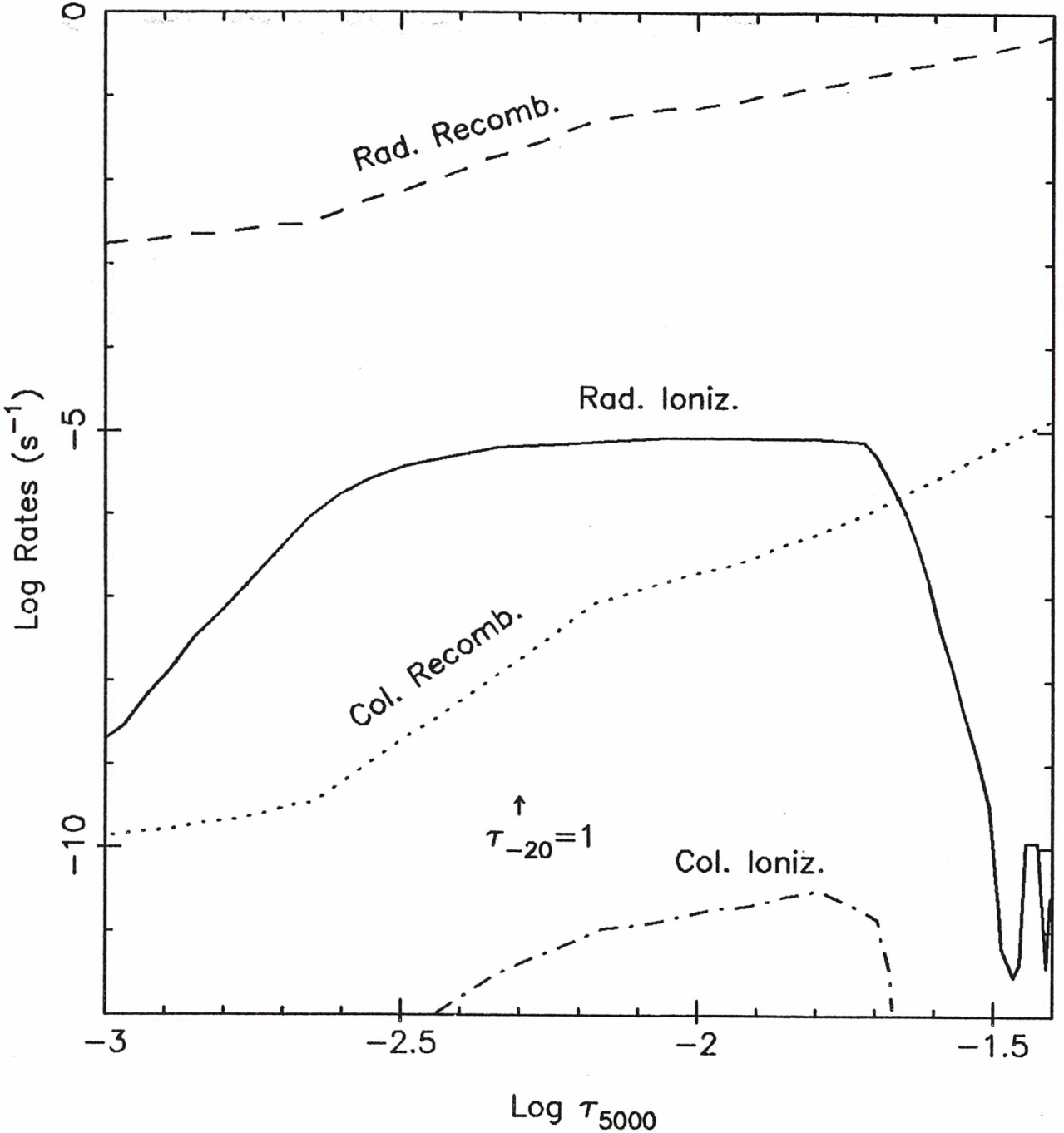
0
−5
−10
Log Rates (s^{-1})
Rad. Recomb.
Rad. Ioniz.
Col. Recomb.
τ_{-20}=1
Col. Ioniz.
−3
−2.5
−2
−1.5
Log τ_{5000}

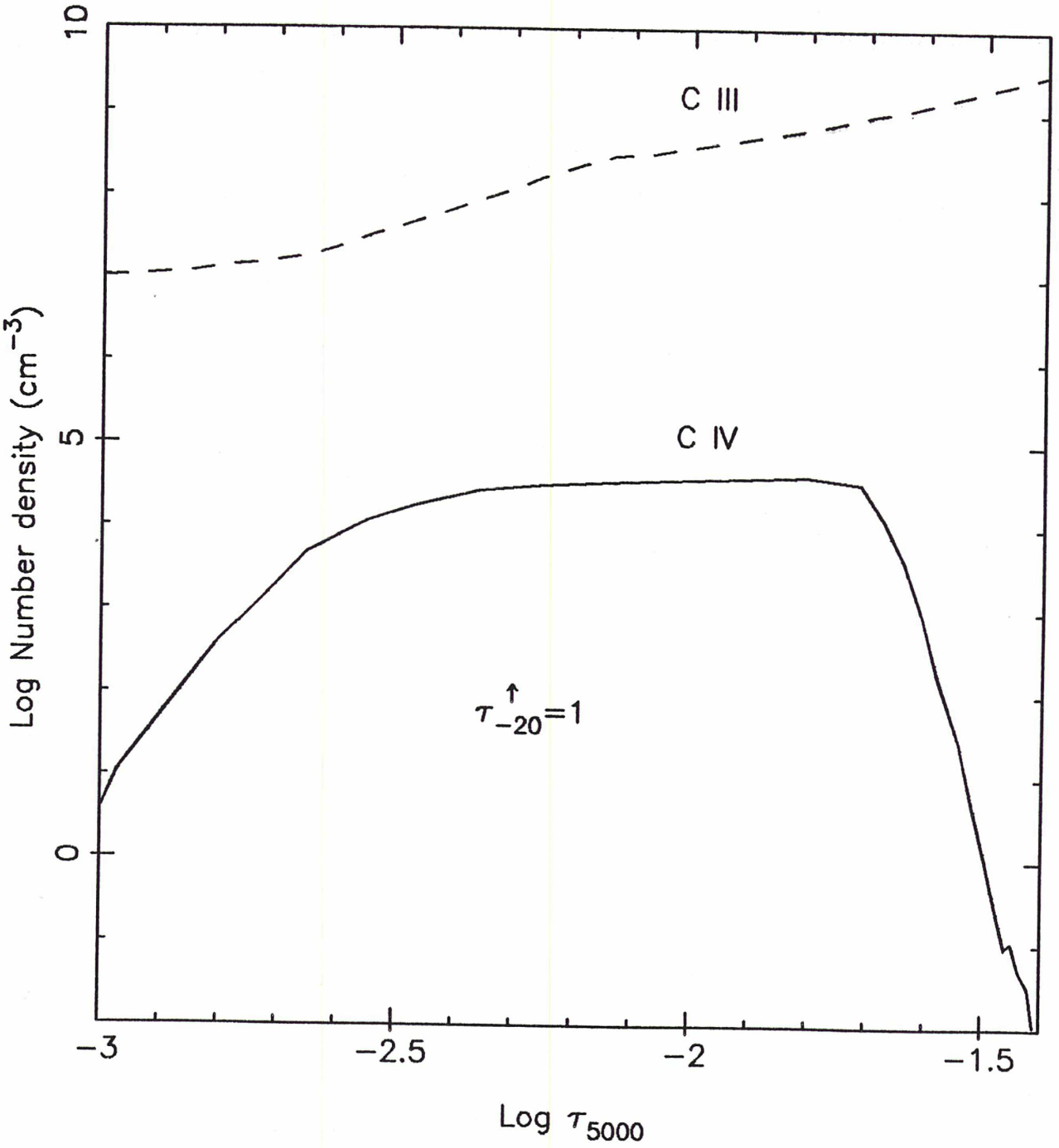
10
5
0
C III
C IV
$\tau_{-20}=1$
Log Number density (cm^{-3})
−3
−2.5
−2
−1.5
Log τ_{5000}

Table 1 - Energy Levels

E is the energy level and E_I is the ionization energy from this level.

#	Level	Stat. Weight	$E\,(\mathrm{cm}^{-1})$	$E_I\,(\mathrm{cm}^{-1})$
1	CIII $2s^2\,{}^1S$	1	0	386159.70
2	CIII $2s\,2p\;{}^3P^o$	9	52401.64	333758.06
3	CIII $2p^2\,{}^1P^o$	3	102352.04	283807.66
4	CIV $2s\;{}^2S$	2	386159.70	520177.80
5	CIV $2p\;{}^2P^o$	6	450697.55	455639.95
6	CV $1s^2\,{}^1S$	1	906337.50	0

Table 2 - Oscillator Strengths

Transition	f
CIII ${}^1S$ - ${}^3P^o$	0
CIII ${}^1S$ - ${}^1P^o$	0.73
CIV ${}^2S$ - ${}^2P^o$	0.285

Table 3 - Models

Δ_1 and Δ_2 are in Stellar radii
$\dot{M}$ is in $M_\odot\ yr^{-1}$ and v_D in $km\ s^{-1}$
See CK for the significance of the parameters.

Model No.	Velocity Law	Chromosphere			T_{min}	T_0	$\dot{M}$	v_D
		Δ_1	Δ_2	T_{max}				
C_1 = model 1 of CK	V_1	0.08	1.5	17000	7100	3000	1.1×10^{-8}	45
C_2	V_1	0.08	1.5	18000	7100	3000	1.1×10^{-8}	45
C_3	V_1	0.08	1.5	19000	7100	3000	1.1×10^{-8}	45
C_4	V_1	0.08	1.5	16000	7100	3000	1.1×10^{-8}	45
C_5	V_1	0.08	2.0	17000	7100	3000	1.1×10^{-8}	45
C_6	V_1	0.08	1.0	17000	7100	3000	1.1×10^{-8}	45
C_7	V_1	0.08	2.5	16000	7100	3000	1.1×10^{-8}	45
C_8	V_1	0.08	1	18000	7100	3000	1.1×10^{-8}	45
C_9	V_1 modified*	0.08	1.5	17000	7100	3000	1.8×10^{-8}	45

*V_1 has been modified at the base to account for the change in $\dot{M}$.

Table 4 - Maximum Absorption and Emission in the C IV λ 1548 Å Line

Model n^o	T_{max}	Δ_2	F_{abs}/F_c	F_{em}/F_c
C_1	17000	1.5	0.2	1.10
C_2	18000	1.5	0.1	1.38
C_3	19000	1.5	0.1	3.80
C_4	16000	1.5	0.6	1.05
C_5	17000	2.0	0.2	1.18
C_6	17000	1.0	0.6	1.08
C_7	16000	2.5	0.6	1.15
C_8	18000	1.0	0.1	1.20

CHAPITRE III

ACTIVITE

1 - Généralités:

Le problème de l'activité stellaire est un des problèmes les plus passionnants de l'astrophysique moderne. C'est en effet par l'activité que se manifestent des phénomènes présumément magnétiques ayant leur source dans les intérieurs stellaires, intérieurs que nous pensions bien connaître il y a une vingtaine d'années. L'étude de l'activité stellaire a apporté une foule de nouvelles questions sur l'état dynamique à grande échelle dans les intérieurs, qui sont loin d'être élucidées à l'heure actuelle.

Presque toutes les étoiles de type plus tardif que F0 où l'activité a été recherchée en ont montré des signes très nets. Par analogie avec le cas du soleil, il est naturel de spéculer que l'activité dans ces étoiles tardives est reliée au champ magnétique. Une hypothèse supplémentaire consiste à dire que le champ magnétique est d'origine dynamo, c'est-à-dire qu'il est généré par le couplage entre la rotation de l'étoile et les mouvements turbulents dans la zone convective. Cette hypothèse est étayée dans le cas des étoiles autres que le soleil par plusieurs travaux observationnels montrant des corrélations entre indices d'activité et nombre de Rossby (relié de façon simple au nombre dynamo: $R_0^{-2} \propto N_D$). Nous avons déjà parlé de ces travaux au chapitre I.

Par contre, aucun phénomène d'activité (au sens où nous l'avons définie au chapitre I) n'a été mis en évidence pour des étoiles de type moins tardif que F0, à part dans quelques cas très rares. Ce résultat peut être considéré comme un des succès de la théorie dynamo et de la théorie des intérieurs stellaires, cette dernière ne prévoyant que des zones convectives extrêmement minces pour les étoiles de type moins tardif que F0.

Les ABHs occupent une place de choix par rapport à ce problème. Elles sont de type spectral A et B; si l'on en croit les modèles d'évolution pré-séquence principale, elles ont des âges de l'ordre de 10^6 ans, et ne possèdent pas de zones convectives importantes (voir par exemple Gilliland, 1986). Si l'on s'en tient à l'état actuel des théories et si l'on suppose que l'activité est reliée à l'effet dynamo de type solaire à travers tout le diagramme HR, on conclut que les ABHs ne devraient pas présenter de phénomène d'activité et

qu'entamer des recherches dans ce sens constituerait manifestement une perte de temps. La curiosité et l'esprit critique étant le propre du chercheur, nous nous sommes néanmoins lancés dans cette direction, et bien nous en a pris car, comme nous allons le voir dans ce chapitre, nous avons mis en évidence des phénomènes d'activité dans ces ABHs qui n'étaient pas censées en avoir.

Avant d'entrer dans le vif du sujet, rappelons qu'il est important de faire la distinction entre activité et chauffage chromosphérique. L'assimilation de ces deux notions a toujours été faite par analogie avec le soleil, où l'activité se manifeste entre autres par une structuration horizontale au niveau de la chromosphère et où activité et chauffage chromosphérique ont leur origine dans la même région, la zone convective (voir par exemple Noyes, 1986). Avec les ABHs, nous avançons en terrain inconnu, et nous ne savons pas si l'activité et le chauffage chromosphérique se manifestent ou ont leur origine au même endroit. C'est pourquoi nous nous sommes efforcés de ne pas mélanger ces deux concepts.

Les résultats présentés dans ce chapitre sont le fruit d'un travail de collaboration entre de nombreuses personnes. Le rôle de l'auteur dans cette collaboration a été une participation aux observations, et la mise au point et l'utilisation des techniques de recherche de périodes décrites dans les Annexes H et I. Enfin, l'auteur du présent mémoire a joué un rôle prépondérant dans la construction du modèle décrit plus bas.

2 - Modulation rotationnelle dans AB Aur. Un modèle qualitatif:

La variabilité spectroscopique d'AB Aur sur des échelles de temps de l'ordre de la journée est connue depuis 1980. Praderie et al. (1982) ont publié des spectres obtenus en Octobre 1980, montrant des variations du profil de la raie K de Ca II d'une nuit sur l'autre. L'origine de ces variations n'était pas claire à l'époque, et la nécessité d'obtenir une série d'observations aussi continue et aussi longue que possible s'imposait pour résoudre ce problème.

Les observations d'objets célestes en continu sont très difficiles du fait de la rotation de la Terre, et il n'existe que trois possibilités pour les mener à bien. L'observation à partir du pôle a soulevé beaucoup d'enthousiasme après les résultats obtenus par Grec et al. (1980) sur les modes p du soleil, au pôle Sud. Cependant, l'observation d'étoiles au pôle Sud pendant l'hiver austral pose des problèmes techniques et humains considérables,

et n'a pas été tentée jusqu'à présent. Un projet de station astronomique semi-automatique existe pourtant (projet EVE), mais n'a pas dépassé le stade de la conception pour l'instant. Une étude sommaire des conditions météorologiques dans la région du pôle Nord (Spitzberg) a montré que des observations en continu n'y étaient pas envisageables (étude menée en partie par l'auteur, et présentée dans Felenbok et Guérin, 1984).

Les deux autres possibilités sont l'observation multi-site et l'observation depuis l'espace. Toutes deux ont fait leurs preuves dans le passé, et présentent leurs avantages et leurs inconvénients. L'inconvénient majeur des observations multi-site réside dans le fait que la probabilité de réussite est inférieure au produit des probabilités de beau temps dans chacun des sites, quantité qui décroit très vite avec le nombre de sites. Une autre difficulté, si l'on veut utiliser des observatoires de mission déjà existants, est d'obtenir du temps de télescope pour la même période sur les différents instruments. L'avantage des observations multi-site est la possibilité d'utiliser des infrastructures existantes, résultant dans un coût modéré des opérations. Les observations depuis l'espace sont celles offrant le plus d'avantages. Outre les problèmes de mauvais temps, les difficultés de coordination disparaissent, puisqu'un seul instrument utilisé depuis l'espace suffit en principe. L'inconvénient de cette solution réside bien sûr dans son coût. Il n'existe que très peu de satellites d'observation astronomique. En pratique, les observations spectroscopiques depuis l'espace ne sont possibles qu'avec le satellite IUE, jusqu'au lancement du Télescope Spatial (1988?). La demande sur IUE est telle qu'il est bien difficile d'obtenir une allocation permettant une série continue d'observations de plusieurs jours.

En Octobre 1982, a eu lieu une grande campagne multi-site d'observation d'AB Aur, à la fois en spectroscopie et en photométrie. Trente-neuf spectres de la raie K de Ca II ont été obtenus au CFH et à l'OHP (télescope de 152 cm), pendant 6 nuits, alors que 29 images IUE à haute résolution, dans la gamme des grandes longueurs d'onde, étaient enregistrées, sur une durée de 40 heures environ. Au même moment, des observations photométriques à 3500 Å étaient effectuées à Grenade (Espagne) et à San Pedro Martir (Mexique). L'équipe des observateurs comprenait J. Czarny, A. Talavera et A.M. Boesgaard au CFH, P. Felenbok et l'auteur de ce mémoire à l'OHP, F. Praderie à la station IUE de l'ESA, T. Simon à celle de la NASA, J.M. Le Contel et P. Morel à Grenade, J.P. Sareyan et J.C. Valtier à San Pedro Martir. Les résultats de ces observations sont présentés dans les Annexes H et I. L'Annexe H traite des raies UV de Mg II et de Fe II, ainsi que des résultats des observations photométriques, tandis que l'Annexe I traite de la raie K de Ca

II.

Ces observations furent complétées deux ans plus tard par une nouvelle campagne mettant en jeu IUE, avec lequel nous avons obtenu 22 spectres haute résolution, grandes longueurs d'onde, de façon discontinue sur une durée totale de 150 heures, l'OHP, où le ciel a été couvert pendant presque toute la durée des opérations, et l'Observatoire de Van Vleck (Connecticut), où la variabilité photométrique d'AB Aur a été suivie pendant une fraction de la durée totale de la campagne. Pour cette deuxième campagne d'observations d'AB Aur, la composition de l'équipe était la suivante: J. Czarny et J. Guérin à l'OHP, l'auteur du présent mémoire à la station IUE de l'ESA, T. Simon à celle de la NASA, et W. Herbst à Van Vleck. Ces observations supplémentaires sont également décrites dans l'Annexe H.

Le résultat fondamental de l'analyse de ces données est la modulation de la vitesse terminale des raies de résonance de Mg II, avec une période de 45 heures, ainsi que la modulation de l'aile bleue de la raie K de Ca II, avec une période de 32 heures. La modulation des raies de Mg II est visible sur les deux séries de spectres. Cependant, la série d'Octobre 1982 ne couvrant que 40 heures, on comprend bien la nécessité d'une confirmation de la période par une série complémentaire couvrant plusieurs cycles, même discontinue. Aucune variation n'a été décelée dans les raies de Fe II dans la série d'Octobre 1982, et ces mêmes raies, si elles sont variables en Novembre 1984, ne montrent aucune périodicité dans ces variations.

L'interprétation la plus naturelle des variations périodiques des raies de Mg II et de Ca II est une modulation des phénomènes observés par la rotation de l'étoile, ou de son atmosphère étendue. Il est en général très difficile de mesurer la projection de la vitesse de rotation (v sin i) d'une étoile pré-séquence principale de type A ou B. On ne dispose en effet que d'une seule bonne raie photosphérique pour le faire, la raie de Mg II à 4481 Å. On trouve dans la littérature deux valeurs assez différentes pour le v sin i d'AB Aur. Davis et al. (1983) donnent v sin i = 75 km s^{-1}, ce qui conduit à une période de rotation à la photosphère P_{rot} = 40 sin i heures, si on suppose R_*=1.75 10^{11} cm (valeur utilisée au chapitre II), tandis que Finkenzeller (1985) trouve v sin i = 140 ± 30 km s^{-1}, c'est-à-dire P_{rot} = (25±5) sini heures. Si l'on ne veut pas remettre en question la qualité des observations et des méthodes ayant conduit à ces résultats, il faut donc admettre que la raie de Mg II à 4481 Å est variable, et donc qu'elle n'est pas élargie par la rotation seule. Dans ce cas, les vsini trouvés ne sont que des limites supérieures, conduisant à des limites

inférieures pour les périodes de rotation. Malgré ce problème, la similitude entre les périodes des modulations trouvées et la vitesse probable de rotation d'AB Aur est frappante. C'est pourquoi l'interprétation de ces modulations, présentée dans les Annexes H et I, fait intervenir la rotation d'AB Aur.

Le modèle qualitatif construit dans les Annexes H et I explique la modulation rotationnelle des raies de Mg II et de Ca II par l'alternance sur la ligne de visée de jets lents et rapides dans le vent d'AB Aur. Cette alternance rappelle celle observée dans le vent solaire (voir par exemple Burlaga, 1984; Hundhausen, 1985), imposée par la structure du champ magnétique à la surface du soleil, les jets rapides correspondant aux régions de lignes de champ ouvertes, et les jets lents aux régions de lignes de champ fermées. Dans le cas d'AB Aur, si la distribution des jets lents et rapides est irrégulière, par exemple favorisant en jets rapides une moitié de la surface par rapport à l'autre, on s'attend à une modulation avec la période de rotation de l'étoile. Si la distribution est plus régulière, avec par exemple n jets régulièrement répartis en longitude, on s'attend par contre à une modulation avec une période $P = P_{rot} / n$, où P_{rot} est la période de rotation de l'étoile. Cette hypothèse n'a pas été considérée dans les Annexes H et I, car elle impliquerait une vitesse de rotation incompatible avec les mesures de v sini.

Le problème majeur de cette interprétation réside dans la différence entre les deux périodes trouvées pour les raies de Mg II (45±6 heures) et la raie K de Ca II (32±4 heures) En effet, si la modulation est due à la rotation d'une structure "attachée" à la surface de l'étoile, seule la période de rotation de la surface de l'étoile doit apparaitre dans les données. Les variations, correspondant au passage d'une onde de densité sur la ligne de visée, devraient donc présenter la même période pour les deux raies.

Une explication à ce phénomène est proposée dans l'Annexe I, toujours inspirée de ce qu'on connait du vent solaire. Dans l'héliosphère, l'interaction entre les jets lents et rapides donne naissance à deux chocs (direct et inverse), qui tendent à éroder les structures et à les faire disparaître, entre 1 et 2 UA. Dans les conditions radicalement différentes présentes dans le vent d'AB Aur (densité, taux de rotation), ces chocs pourraient apparaître beaucoup plus près de la surface de l'étoile, si bien que les structures ne seraient stables que sur quelques rayons stellaires. Or, la raie K de Ca II est formée à la base du vent, donc dans la région de stabilité des structures en corotation, tandis que le bord violet des raies de Mg II (quantité modulée) se forme à environ $5R_*$, et donc peut-être dans une région où les structures ont déjà disparu. Les variations des raies de Mg II seraient donc dues au passage

sur la ligne de visée d'inhomogénéités lors de la rotation de l'atmosphère étendue elle-même, dont la période de rotation à $5R_*$ est bien sûr plus grande que la période de rotation de la surface de l'étoile. Dans le même ordre d'idée, on pourrait penser que la région de formation des raies de Fe II (qui ne varient pas en même temps que celles de Mg II) se situe encore au-delà, à une distance où la période de rotation de l'atmosphère étendue est trop longue pour être visible dans nos données, ou bien où les inhomogénéités ont disparu à cause de la rotation différentielle de l'atmosphère. Dans ce modèle, la période de rotation de l'étoile est donc de 32 heures, et celle de l'atmosphère à environ $5R_*$ est de 45 heures.

Une nouvelle série d'observations a été effectuée en Janvier 1986, avec IUE, en vue de confirmer la variabilité des raies de Mg II et de rechercher celle des raies de résonance de C IV. A cause des temps de pose nécessaires pour l'observation des raies de C IV (presque un "shift" entier de IUE pour chaque image), cinq spectres seulement ont été obtenus dans chaque série de raies. Les résultats de ces observations sont détaillés dans l'Annexe J. On y montre que les raies de C IV varient également de façon spectaculaire. Il est hors de question de déterminer une période à l'aide de 5 points seulement, et l'Annexe J se contente de présenter plusieurs scénarios compatibles avec les observations. Il en ressort que le modèle qualitatif bâti dans les Annexes H et I est cohérent avec ces nouvelles observations.

Enfin, nous avons également observé à plusieurs reprises les variations de la raie Hα de cette étoile. Ces observations, qui ne sont pas entièrement dépouillées à l'heure actuelle, feront l'objet d'une publication future.

En conclusion, l'ensemble de ces observations nous a permis de mettre en évidence une structure en jets du vent d'AB Aur, contrôlée par une structure azimuthale à la surface de l'étoile. Ceci montre l'existence d'une activité, au sens où nous l'avons définie, pour cette étoile. Si on pousse plus loin l'analogie avec le soleil et avec l'activité des étoiles de type tardif, on peut supposer que les jets lents et rapides sont contrôlés par la structure du champ magnétique. Nous n'avons cependant aucune preuve directe de l'existence d'un champ magnétique dans AB Aur. Les techniques connues de mesure des champs magnétiques ne s'accomodent pas des faibles magnitudes et des taux de rotation élevés des ABHs.

Rappelons enfin que le modèle présenté ci-dessus et dans les Annexes H, I et J n'est que qualitatif. L'estimation de la distance à laquelle se forment les chocs (Annexe I)

s'appuie sur un raisonnement entièrement cinématique, inspiré de Mullan (1984). Cependant, on peut aisément prévoir que les interactions dynamiques entre les jets vont jouer un rôle important dans la physique des chocs directs et inverses (voir chapitre IV). Ce modèle doit donc être considéré comme très préliminaire, et comme guide pour un modèle plus réaliste et plus quantitatif que nous avons commencé à bâtir (voir chapitre IV).

3 - Recherche de modulation rotationnelle dans d'autres ABHs:

Au point où nous en sommes, la question se pose de savoir si AB Aur est un élément très singulier de la classe des ABHs, ou si le phénomène d'activité que nous avons découvert est général pour l'ensemble de ces étoiles. Pour répondre à cette question, nous devons rechercher l'existence de modulation rotationnelle dans d'autres ABHs. Nous allons nous heurter aux problèmes pratiques signalés au début du paragraphe précédent. D'autre part, AB Aur étant une des ABHs les plus brillantes, les autres candidats à la modulation rotationnelle seront plus difficiles à observer (temps de pose plus longs). Malgré ces problèmes, plusieurs tentatives ont été effectuées dans le courant de l'année 1986, et ce sont les résultats préliminaires de ces observations que nous décrivons dans ce paragraphe.

3-1 HD250550:

Cette étoile a le type spectral A0 et une magnitude visuelle m_V=9.1 (voir Annexe B). Dans l'Annexe B, nous avons vu que sa raie Hα présentait des variations importantes sur une échelle de temps de quelques mois. Il est possible que ces variations soient reliées à un phénomène d'activité semblable à celui observé pour AB Aur. D'autre part, une estimation de son taux de rotation conduit à v sin i = 110 km s^{-1} (Finkenzeller, 1985). Cette étoile est donc un excellent candidat pour la recherche d'une modulation rotationnelle.

En février 1986, a eu lieu une campagne multi-site d'observations de cette étoile. Les instruments utilisés étaient:

- le spectrographe Coudé du TCFH (observateurs: M. Dreux et l'auteur de ce mémoire)
- le spectrographe Cassegrain du télescope de 2.5 m "Isaak Newton" aux Canaries (P. Felenbok et A. Talavera)
- le spectrographe à fibre "Isis" au 1.93 m de l'OHP (J. Czarny et J. Guérin)

Le but de cette campagne était d'observer la raie K de Ca II de HD250550, avec

la meilleure couverture temporelle possible. La météo, hélas, ne fut pas de notre bord, et nous avons essuyé un échec cuisant. Seuls, quelques spectres ont été obtenus aux Canaries et à Hawaii.

Ces quelques spectres sont néanmoins suffisants pour montrer que la raie K de Ca II est très variable sur des échelles de temps très courtes. En particulier, deux spectres obtenus au CFH à deux heures d'intervalle montrent des variations spectaculaires du profil de cette raie. Ces deux spectres sont présentés sur la figure III-1.

Fig. III-1 HD250550 Ca II K

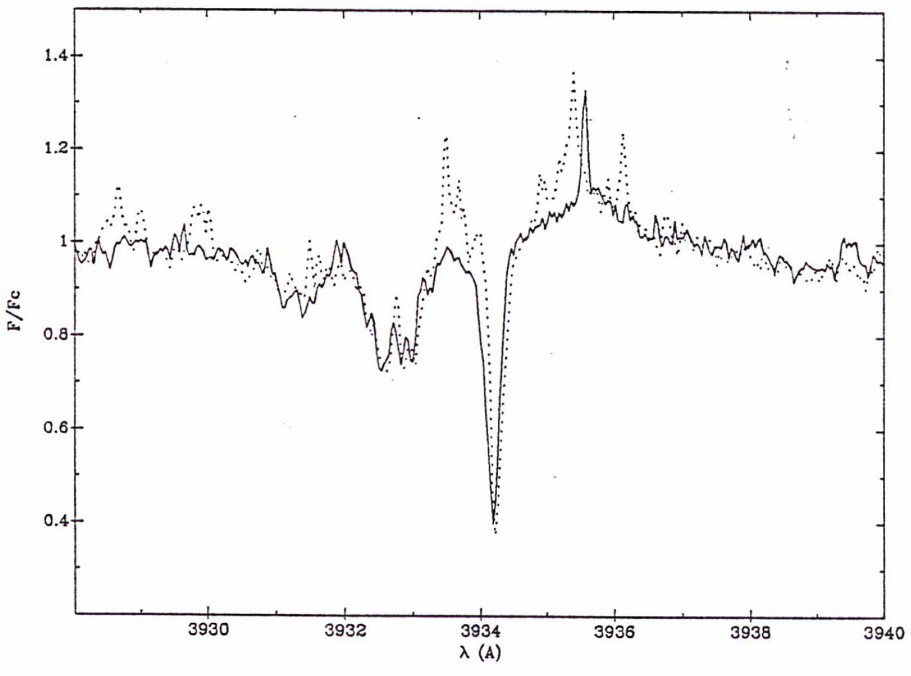

On constate que la composante principale de la raie a varié énormément entre les deux poses. Par conséquent, cette étoile apparait plus que jamais comme un très bon candidat pour ce genre d'étude, et doit retenir notre attention pour les observations à venir.

3-2 BD +46°3471:

C'est une étoile de type spectral A4 et de magnitude visuelle m_V=10.1 (voir Annexe B). Finkenzeller (1985) estime son taux de rotation à v sin i = 150 km s^{-1}. Il s'agit

donc là d'un autre bon candidat pour notre recherche d'activité.

Une autre campagne multi-site d'observations a été tentée en Juillet 1986, pour la raie Hα de cette étoile. Elle ne faisait intervenir que deux instruments:

- le spectrographe coudé "Hamilton" au télescope de 120 pouces de l'Observatoire de Lick (observateurs: U. Finkenzeller et l'auteur de ce mémoire)
- le spectrographe à fibre "Isis" au 1.93 m de l'OHP (P. Felenbok et J. Guérin)

La raie K de Ca II n'a pas été choisie pour cette observation, en dépit des résultats excellents obtenus pour AB Aur, à cause de l'impossibilité d'observer cette raie à l'OHP pour une étoile aussi faible. Dû à la faible différence de longitude entre les deux sites, la couverture temporelle obtenue n'était pas excellente, mais suffisante cependant pour nous permettre de détecter le phénomène recherché, le cas échéant. Quarante-trois spectres ont été obtenus, vingt-sept à Lick, 16 à l'OHP. Les spectres obtenus à Lick ont été dépouillés à Berkeley et au JILA de Boulder (Colorado), et ceux de l'OHP ont été dépouillés à Meudon. L'ensemble des données a été homogénéisé à Meudon.

Nous avons détecté dans le courant de ces observations (5 nuits) certaines variations de la raie Hα, qui apparaît purement en émission. La figure III-2 montre les deux spectres les plus différents de cette série. On constate une variation maximale de l'ordre de 10% de l'émission dans la raie.

FIG III-2

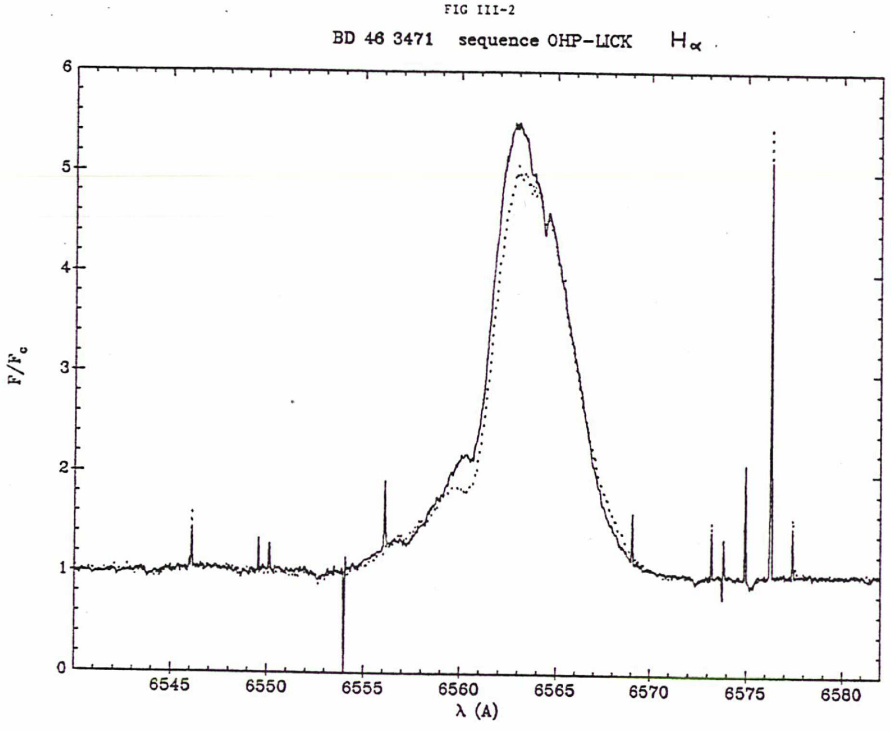

Nous avons recherché une période dans les variations de l'aile bleue de la raie (où elles sont les plus intenses). Pour cela, un polynôme de degré 2 a été ajusté à l'aile bleue, et nous avons calculé le spectre de puissance des 3 coefficients correspondants, par la méthode décrite dans l'Annexe I. Après déconvolution par le spectre de puissance de la fenêtre d'observation, aucune période ne subsiste clairement. Ceci indique que les variations observées ne sont pas reliées à la rotation de l'étoile.

Ce résultat peut s'interpréter de plusieurs façons. Tout d'abord, et c'est l'explication la plus immédiate (mais pas nécessairement la plus probable), il est possible que BD +46°3471 ne soit pas active, auquel cas le phénomène d'activité ne serait pas général pour les ABHs. Il resterait cependant à expliquer la variabilité observée sur la figure III-2, ainsi que les fortes variations long terme du profil de la raie Hα dans cette étoile, visibles par la comparaison du profil présenté dans l'Annexe B et celui de la figure III-2. Une autre possibilité serait l'existence d'un cycle d'activité pour les ABHs, auquel cas nous aurions surpris BD +46°3471 dans une phase calme en Juillet 1986. Seules des observations ultérieures pourraient nous permettre de répondre à cette question. Enfin, il est possible que nous ayons fait un mauvais choix en sélectionnant la raie Hα pour cette étude. Cette raie se forme en effet assez loin de l'étoile (voir Annexe D), et si on considère un modèle semblable à celui bâti pour AB Aur (voir Annexes H, I, J et paragraphe III-2), il n'est pas exclu qu'aucune structure liée à la rotation ne soit présente dans sa région de formation. De nouvelles observations dans la raie K de Ca II devraient apporter une réponse à cette question. Pour toutes ces raisons, BD +46°3471 reste un bon candidat pour de futures observations.

3-3 HD163296:

Cette étoile est un peu particulière, en ce sens qu'elle ne remplit pas un des critères de Herbig: en effet, elle n'est associée à aucune nébulosité. Cependant, son excès infrarouge important (Finkenzeller et Mundt, 1984) et son taux de rotation élevé v sin i = 120 km s^{-1} (Finkenzeller, 1985) suggèrent son appartenance à la classe des ABHs. De plus, la variabilité spectaculaire de sa raie Hα sur une échelle de temps de quelques mois (Thé et al., 1985c) en fait un bon candidat pour une recherche d'activité.

HD163296 a donc fait l'objet de la troisième campagne d'observations menée en 1986, utilisant les instruments suivants:

- IUE, mode haute dispersion, grandes longueurs d'onde (observateurs: F. Praderie et

H.R.E. Tjin-A-Djié à la station de l'ESA, T. Simon et l'auteur de ce mémoire à la station de la NASA)

- CAT de l'ESO, au Chili (A. Talavera)

Le but principal de ces observations était une recherche de période pour les variations des raies de Mg II à 2800 Å, éventuellement confirmée par les observations des raies Hα et Ca II K prévues au CAT. En tout, 39 images IUE ont été obtenues sur les 10 jours de la campagne, ainsi que 12 spectres dans la région de la raie K de Ca II, et 5 spectres dans la région de Hα. Les données IUE ont été dépouillées à Meudon par F. Praderie et l'auteur de ce mémoire, grâce au logiciel développé par J. Borsenberger, et les données "sol" ont été dépouillées en partie à La Silla (Chili), et en partie à la station ESA de IUE, par A. Talavera. Ces données sont en cours d'exploitation, et seront publiées prochainement.

Nous avons mis en évidence une variation spectaculaire des raies de résonance de Mg II, sur une échelle de temps de quelques heures. La figure III-3 montre le profil du doublet de résonance de Mg II pour deux des spectres de la série. La variation de ce profil y apparait clairement. Le même genre de variations spectaculaires est également évident sur le profil de la raie K de Ca II et sur celui de la raie Hα.

Fig. III-3 HD163296 Mg II

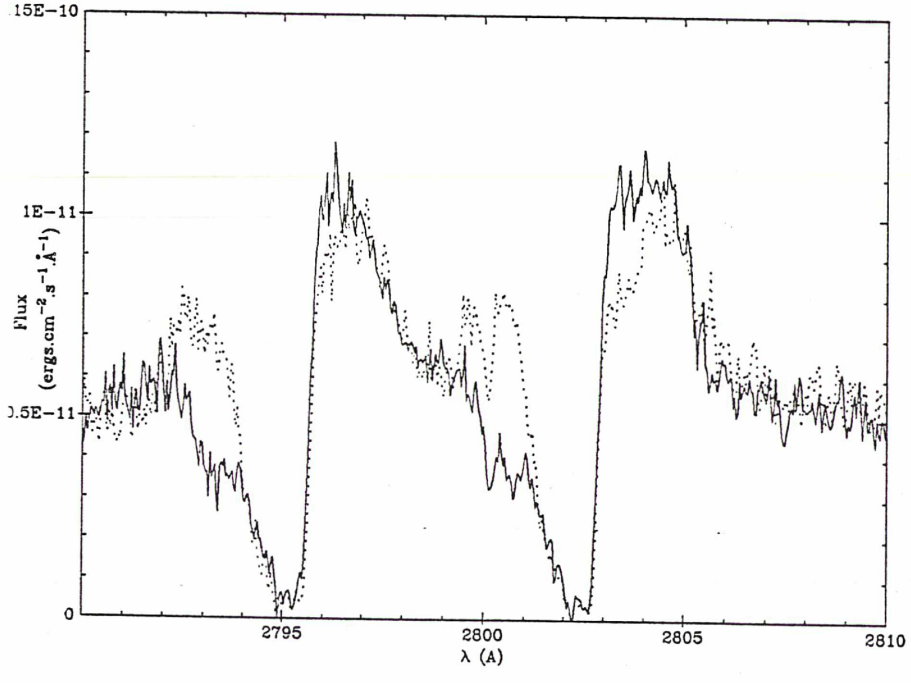

L'étude quantitative de ces variations n'en est pour l'instant qu'à un stade préliminaire. Pour les raies de Mg II, nous avons entamé une analyse semblable à celle présentée dans l'Annexe I. Deux périodes apparaissent clairement dans le spectre de puissance obtenu. La première, p=130 heures, est trop proche de la durée totale des observations (230 heures), et peut très bien provenir de la présence d'un évènement particulier (éjection, par exemple). La deuxième, p=32 heures, pourrait être le signe d'une modulation rotationnelle. Cependant, un long travail de vérification est encore à fournir pour confirmer ces résultats, et ceux-ci doivent donc être considérés comme préliminaires.

Pour la raie K de Ca II, une étude préliminaire a également montré que les variations observées sont compatibles avec une période de 32 heures. Avec 12 spectres seulement, il est impossible de faire mieux que vérifier la compatibilité des données avec telle ou telle période. Quant aux observations de la raie Hα, elles ne sont pas encore entièrement dépouillées.

Quoi qu'il en soit, HD163296 est le meilleur candidat que nous ayons pour l'existence du phénomène d'activité (AB Aur mise à part). Nous nous sommes donc engagés dans l'analyse détaillée des données déjà obtenues et, afin de consolider la détermination de la période de variations des raies de Mg II, nous réobserverons cette étoile dans le courant de cette année.

4 - Conclusion:

Nous avons donc mis en évidence un phénomène d'activité dans une ABH (AB Aur), nous avons de bonnes indications de la présence du même phénomène dans une autre (HD163296), et nous disposons d'un troisième excellent candidat pour ce genre de recherche (HD250550). Ces résultats suggèrent donc que l'activité est un phénomène peut-être assez répandu dans la classe des ABHs, et pour le moins présent.

Les ABHs sont les seules étoiles pour lesquelles on ait mis en évidence une modulation du vent. Dans tous les autres cas où une modulation a été détectée, elle était directement due à des phénomènes ayant lieu à la surface de l'étoile (taches ou plages), y compris pour les étoiles T Tauri. Pour ces dernières cependant, des phénomènes de variabilité à court terme de raies formées dans leurs vents ont été observés (Worden et al., 1981; Mundt et Giampapa, 1982), mais la périodicité de ces variations n'a pas été

démontrée.

Quelle peut être l'origine d'une structure non radiale comme celle du vent d'AB Aur? La première idée qui vient à l'esprit est que, comme dans le cas du soleil, un champ magnétique structuré existe à la surface de l'étoile et force à son tour la structure du vent en jets lents et jets rapides, les jets lents sortant de régions à boucles de champ fermées et les jets rapides de régions à boucles de champ ouvertes.

Dans cette hypothèse, quelle est l'origine du champ magnétique? Comme nous l'avons vu au paragraphe III-1, on suppose en général que l'activité des étoiles tardives est due à un champ magnétique généré par l'effet dynamo. Or, la dynamo de type solaire suppose l'existence d'une zone convective, qui n'est pas censée être présente dans des étoiles comme les ABHs. On peut envisager trois "solutions" à ce problème, aucune d'entre elles n'ayant fait à ce jour l'objet d'une étude détaillée.

On peut tout d'abord suspecter le placement de ces étoiles sur les trajets théoriques d'évolution pré-séquence principale. La classification spectrale et la détermination des luminosités bolométriques des étoiles pré-séquence principale n'est pas une tâche facile, et il est toujours possible que les masses et les âges des ABHs pour lesquelles nous avons détecté de l'activité aient été surestimés. Dans ce cas, on pourrait envisager l'existence de zones convectives épaisses (>0.1 R_*) pour ces étoiles, en accord avec les théories actuelles d'évolution pré-séquence principale.

D'autre part, les ABHs peuvent avoir un champ magnétique entretenu par une dynamo non solaire: pour que l'effet α puisse être efficace, il faut qu'il existe un champ de vitesse d'hélicité non nulle dans les couches internes de l'étoile. Un tel champ de vitesse pourrait être la conséquence d'instabilités liées à la rotation différentielle. Signalons que l'existence d'instabilités liées à la rotation différentielle dans les zones radiatives a été envisagée comme explication des anomalies d'abondance dans plusieurs types d'étoiles (Zahn, 1987).

La troisième possibilité consiste à supposer que le champ magnétique n'est pas généré par l'effet dynamo, mais provient soit du champ magnétique uniforme présent dans la nébuleuse protostellaire, et "amplifié" lors de la contraction de l'étoile, soit d'un champ magnétique généré par dynamo lors d'une phase antérieure de l'évolution de l'étoile. Les ABHs sont en effet peut-être assez jeunes pour que ce champ magnétique primordial ou antérieur n'ait pas eu le temps d'être dissipé. Le temps de dissipation $\tau_D \approx 4\pi\sigma R_*^2/c^2$, où σ est la conductivité électrique (estimée à $2\ 10^8\ s^{-1}$ à 10^4 K), est en effet de l'ordre de

10^{11} ans. Un mécanisme identique a été proposé par Uchida (1986) pour les étoiles O et B. Le problème est de savoir si le champ magnétique peut survivre à l'étape convective de la phase pré-séquence principale, pendant laquelle la résistivité turbulente joue un rôle essentiel, résultant dans une forte dissipation magnétique.

Rappelons enfin que nous n'avons pas de preuve directe de l'existence de champs magnétiques dans les ABHs. La structure non radiale du vent que nous avons détectée a peut-être une autre cause. Par exemple, elle pourrait être due à des inhomogénéités de température à la surface de l'étoile qui auraient à leur tour une influence sur le mécanisme de production du vent. Des instabilités liées à la rotation pourraient encore être à l'origine de ces inhomogénéités.

THE ASTROPHYSICAL JOURNAL, 303:311–326, 1986 April 1

SHORT-TERM SPECTRAL VARIABILITY IN AB AURIGAE: CLUES FOR ACTIVITY IN HERBIG Ae STARS. I. THE ULTRAVIOLET LINES OF Mg II AND Fe II[1]

FRANÇOISE PRADERIE,[2] THEODORE SIMON,[3] CLAUDE CATALA,[2] AND ANN MERCHANT BOESGAARD[3]
Received 1985 June 21; accepted 1985 September 25

ABSTRACT

The Herbig Ae star AB Aur was monitored with the *IUE* satellite in the long-wavelength, high-resolution mode, first during 40 consecutive hours in 1982 and second intermittently over a span of 150 hr in 1984. The Mg II λ2795 wind profile and a number of Fe II ultraviolet lines were studied for variability during the two epochs.

We find temporal variations in the Mg II blue wing velocity by 30%–50% at both epochs. The intensity of the blue absorption wing is variable, but the redshifted emission part of the line is much less so. By contrast, the Fe II spectrum was constant in all respects in 1982, but variable in 1984. The Fe II absorption lines in 1982 show two narrow components displaced shortward of a main absorption. The location and intensity of the components is very stable in 1982, but the profiles are variable in 1984. There was no evidence that AB Aur varied photometrically at either epoch.

An analysis of the Mg II blue wing velocity versus time shows that the variability can be fitted with a sine curve of period 45 ± 6 hr, which we interpret to be the stellar rotation period. The period found is indeed very close to the rotation period of the star, as estimated from its projected rotation velocity and radius.

The observed rotational modulation of the blue wing velocity of Mg II λ2795 in the wind of AB Aur is the first direct evidence of a nonaxisymmetric wind in an A-type pre–main-sequence object. A qualitative model for the expanding envelope is proposed, with recurrent corotating fast and slow streams, a model analogous to the solar wind in the inner heliosphere. At variance with the Sun, the stellar wind is cool and dense enough in the portions of the envelope in which the observed variable parts of the Mg II line profile originate that optical and UV lines can trace its variable structure. The constancy of the Fe II spectrum in 1982 and its variability in 1984 are accounted for if these lines are formed farther out than the Mg II region, in a remote part of the envelope where the corotating streams in the wind have merged and pressure waves have interacted and dominate the structure.

As a consequence of our analysis, we argue that if rotation is the central parameter in explaining the observed short-term variations in the wind of AB Aur, the set of phenomena described could be magnetic in origin.

Subject headings: stars: emission-line — stars: individual — stars: winds — ultraviolet: spectra

I. INTRODUCTION

Among pre–main-sequence stars, those of intermediate mass (3–5 $M_\odot$) constitute the group of Herbig Ae–Be stars (Herbig 1960; Strom *et al.* 1972; Finkenzeller and Mundt 1984). The location of such stars in the Hertzsprung-Russell diagram has been established by Strom *et al.* (1972) and by Cohen and Kuhi (1979), whose work suggests that the Herbig stars represent a prolongation of T Tauri stars toward higher effective temperature. One of these stars, AB Aur (HD 31293, A0ep), was chosen for this study mainly because it is bright enough ($V = 7.2$) to be observed at high spectral resolution in the ultraviolet with *IUE*.

Like the T Tauri stars, the pre–main-sequence Ae–Be stars exhibit irregular variability in both visible light and line spectrum. Let us focus here on spectral variability. The characteristic time scales for the appearance and disappearance of both absorption and emission features in the hydrogen Balmer lines range from months to years (Merrill and Burwell 1933; Sanford and Merrill 1958; Finkenzeller 1983). These changes do not seem to be periodic. Similar long-term changes have been found in the Mg II and Fe II resonance lines of AB Aur (Praderie *et al.* 1984*a*). Changes of profile shape from day to day were also discovered in the Ca II K line (Praderie *et al.* 1982), which led us to suggest a flarelike activity in this star, as had already been proposed for T Tauri stars (Worden *et al.* 1981; Mundt and Giampapa 1982). Although Garrison and Anderson (1977) reported a P Cygni profile in Hα, which they attributed to a wind, it has been shown since then that AB Aur also exhibits definite signs of a chromosphere (Praderie *et al.* 1982; Felenbok, Praderie, and Talavera 1983; Catala, Kunasz, and Praderie 1984; Catala and Talavera 1984). Other stars of the same group also show spectroscopic evidence for winds and chromospheres, whether observed in the space ultraviolet (Talavera *et al.* 1982) or in the visible and near infrared (Catala *et al.* 1985*a*). Since chromospheric activity is variable with a primary time scale related to the star's rotation period in solar-type dwarfs (Vaughan *et al.* 1981; Boesgaard and Simon 1984), it also seemed promising to search for rotational modulation in Herbig stars. Such periodic variability, if present, would then provide a strong argument in favor of a common origin for chromospheric activity in pre–main-sequence stars and in stars on the main sequence; moreover, by analogy with the Sun, this

[1] Based on observations by the *International Ultraviolet Explorer* (*IUE*) collected at the Goddard Space Flight Center (NASA) and Villafranca del Castillo (ESA).

[2] Département de Recherches Spatiales et Unité de Recherche Associée au CNRS n° 264, Observatoire de Paris, Section de Meudon.

[3] Institute for Astronomy, University of Hawaii.

TABLE 1

PROPERTIES OF THE HERBIG Ae STAR AB AURIGAE

$\log (L/L_\odot)$	$M/M_\odot$	$R/R_\odot$	$T_{\rm eff}$ (K)	$\log g$	$v_{\rm esc}$ (km s^{-1})	d (pc)
1.83[a]	2.5	2.7	10.000	4.4[a]	590	150[a]
2.0[b]	3.0	3.3	...	...	590	160[b]

NOTE.—$T_{\rm eff}$ = 11,000 K would give $R/R_\odot$ = 2.5, value used in Fig. 2.
[a] Strom *et al.* 1972.
[b] Cohen and Kuhi 1979.

would favor control of the observed activity by surface magnetic fields.

The characteristics of AB Aur are summarized in Table 1. AB Aur was chosen for this study also because an estimate of its projected rotational velocity $v \sin i$ was at hand: Praderie *et al.* (1982) obtained $v \sin i \leq 90$ km s^{-1}. If we adopt $R/R_\odot = 3 \pm 0.3$ from Table 1, then the photospheric rotation period is $P \geq 41 \pm 4$ hr for an inclination i of 90°. With more recent determinations of $v \sin i$ (75 km s^{-1}, Davis, Strom, and Strom 1983; 140 ± 30 km s^{-1}, Finkenzeller 1985), one obtains $P \leq 48 \pm 5$ hr and $P \leq 26 \pm 8$ hr respectively, irrespective of $\sin i$. The rather discrepant values of $v \sin i$ can be explained first by the choice of the line used: the Ca II K line is not a bona fide photospheric line in AB Aur, and only an upper limit of $v \sin i$ could be reached by Praderie *et al.* (1982) in spite of spectra with 0.095 Å resolution. Other authors used the Mg II λ4481 line. The difference between Davis, Strom, and Strom (spectra with 0.3 Å resolution) and Finkenzeller (spectra with 0.8 Å resolution) is probably due to the differences in the analytical methods the authors used for deriving $v \sin i$. In any case, these short values of the rotation period make AB Aur well suited for a variability study with *IUE*.

In this paper we report the results of two observing programs in which we monitored AB Aur with the high-resolution, long-wave spectrographs of *IUE*. During the first, in 1982, we observed AB Aur with continuous coverage over one complete rotation cycle, and in the second, in 1984, we made observations at selected rotational phases in 3.5 cycles over a time span of 150 hr. Preliminary results for the 1982 observations have been presented by Simon, Boesgaard, and Praderie (1982), Praderie *et al.* (1983), Praderie *et al.* (1984*b*). The observations and data reduction are described in § II. The ultraviolet and visible continuum, the hourly spectral variability in Mg II, and the behavior of the Fe II resonance lines, are presented respectively in §§ III, IV, and V. The significance of Mg II short-term variability on the one hand, and of Fe II constancy or variability on the other hand, is discussed in § VI, as well as the consequences for the models of the envelope of AB Aur. The last section discusses various implications of our results for activity phenomena in Herbig stars.

II. OBSERVATIONS AND DATA REDUCTION

We obtained continuous phase coverage of AB Aur with the *IUE* satellite from 1982 October 25 to 27 in contiguous NASA and ESA shifts over a time span of 40 consecutive hours, then from 1984 November 5 to 11 we observed at selected rotational phases in several cycles involving again NASA and ESA time, over a total span of 150 hr. We observed in high-resolution (HR) mode (0.2 Å) with the LWR camera (2000–3500 Å) in 1982 and with the LWP camera in 1984. We obtained a total of 29 large-aperture spectra in 1982 and 22 spectra in 1984. A log of all the HR observations is given in Table 2. The exposure times were chosen to give well-exposed Mg II resonance line (λ2800) profiles, both in their absorption and in their emission parts. The spectra were also suitable for the study of Fe II UV multiplets 1, 2, 3, 62, 63, and 64, among others.

In alternating sequence with the HR spectra, we obtained large-aperture, low-resolution (~6 Å) SWP (1150–2000 Å) spectra, 28 in 1982 and 17 in 1984. The exposure time for these SWP images was 3 minutes.

TABLE 2

LOG OF HIGH-RESOLUTION *IUE* OBSERVATIONS OF AB AURIGAE

A. LWR

Number	Image[a]	1982 October UT (midexposure)	Exposure Time (minutes)
1.....	14485 G	25.944	30
2.....	14486 G	25.996	40
3.....	14487 G	26.050	45
4.....	14488 G	26.108	50
5.....	14489 G	26.166	45
6.....	14490 G	26.222	45
7.....	14491 G	26.278	45
8.....	14492 G	26.336	45
9.....	14493 G	26.392	45
10.....	14494 G	26.449	45
11.....	14495 G	26.505	45
12.....	14496 G	26.562	45
13.....	14497 V	26.625	45
14.....	14498 V	26.681	45
15.....	14499 V	26.747	45
16.....	14500 V	26.802	45
17.....	14501 V	26.859	45
18.....	14502 V	26.916	45
19.....	14503 G	26.975	45
20.....	14504 G	27.030	45
21.....	14505 G	27.088	45
22.....	14506 G	27.143	45
23.....	14507 G	27.200	45
24.....	14508 G	27.257	45
25.....	14509 G	27.313	45
26.....	14510 G	27.368	45
27.....	14511 G	27.429	45
28.....	14512 G	27.485	45
29.....	14513 G	27.541	45

B. LWP

Number	Image[a]	1984 November UT (midexposure)	Exposure Time (minutes)
1.....	4733 V	5.506	38
2.....	4736 V	6.509	33
3.....	4737 V	6.560	30
4.....	4747 V	7.723	30
5.....	4753 V	8.621	30
6.....	4754 V	8.668	30
7.....	4755 V	8.720	30
8.....	4757 G	9.197	30
9.....	4758 G	9.247	30
10.....	4759 G	9.288	30
11.....	4764 V	9.612	21
12.....	4765 V	9.664	30
13.....	4766 V	9.712	30
14.....	4768 G	10.172	30
15.....	4769 G	10.230	30
16.....	4770 G	10.206	30
17.....	4774 V	10.606	30
18.....	4775 V	10.654	30
19.....	4776 V	10.701	30
20.....	4784 V	11.682	30
21.....	4785 V	11.733	30
22.....	4786 V	11.774	25

[a] G, observations from Goddard; V, observations from Villafranca.

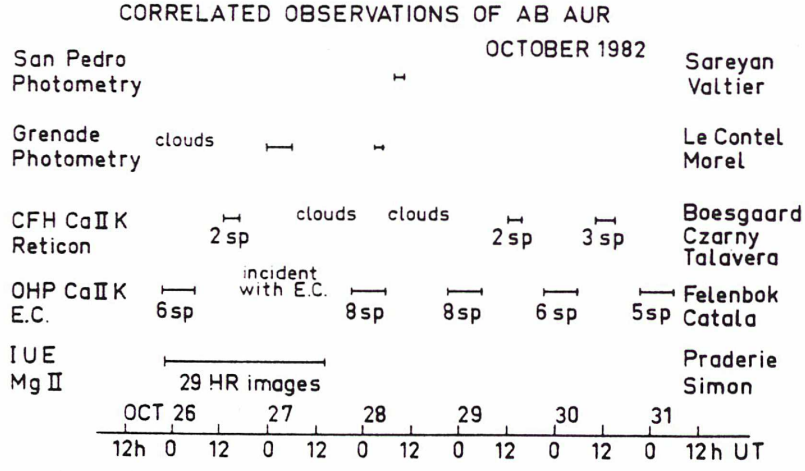

FIG. 1.—Time line of 1982 October observations. E.C., electronic camera; HR, high resolution.

A coordinated campaign of ground-based observations was organized in 1982 involving the Canada-France-Hawaii 3.60 m telescope (CFHT) and the 1.50 m at Observatoire de Haute-Provence; these instruments were used at coudé focus. Two photometric telescopes, the 0.6 m at Pico de la Veleta, near Granada (Spain), and the 1 m at San Pedro Martir (Mexico), also took part in the observations (see Fig. 1). Preliminary results of the whole campaign were presented by Praderie *et al.* (1983). During the 1984 observations, photometric observations were carried out at our request by W. Herbst at Van Vleck Observatory.

We reduced the *IUE* HR echelle spectra from the 3d file of the Guest Observer (G.O.) tape by means of software developed at the Paris-Meudon Observatory by J. Borsenberger. The ripple correction was performed following Ake (1982) for the LWR spectra and following Cassatella (1984) for the LWP spectra. In overlapping wavelength regions of adjacent orders of the echelle spectrum, a weighted average of intensity was formed (weighted by the relative photometric response of each order). The spectra were absolutely calibrated using the flux calibrations provided by Holm *et al.* (1982) for the LWR and by Cassatella (1984) for the LWP cameras. The spectra were also examined at the *IUE* regional data center of the NASA/Goddard Space Flight Center, using standard reduction software available there, and these independent reductions gave virtually identical results. For consistency we present here the reductions carried out at Meudon.

In the echelle spectra, the wavelength scale on the G.O. tape was adjusted to fit the Mg I presumably interstellar line present in the spectrum of AB Aur ($\lambda_0 = 2852.13$ Å). From a study of interstellar lines in the visible, Felenbok, Praderie, and Talavera (1983) showed that the interstellar lines have a LSR velocity of 6.3 ± 0.3 km s^{-1}, a value identical to within the uncertainties with the velocity of the associated molecular cloud. A similar result was obtained for other Herbig Ae–Be stars by Finkenzeller and Jankovics (1984), who also showed that there are no systematic motions of these stars relative to their associated molecular clouds.

The Mg II and Fe II line spectrum was studied both in absolute flux units and in reduced units (i.e., normalized to the continuum). In order to define the continuum level, we compared the HR spectra of AB Aur with an *IUE* spectrum (LWR 2915) of η Leo (A0 Ib), a star with narrow lines ($v \sin i = 20$ km s^{-1}), no detectable wind profiles (Praderie, Talavera, and Lamers 1980), and a well-developed Fe II spectrum. The continuum windows were chosen to represent high-intensity points in η Leo and to be fairly remote from regions where in AB Aur we suspect there are weak, variable Fe II emission lines (see § V below). The wavelengths of these continuum windows are given in Table 3. The continuum level at each window was fixed interactively by eye from examination of the spectra on a graphics terminal.

The low-resolution (LR) SWP spectra were analyzed at Paris-Meudon Observatory by means of software which corrects the data for halation effects and scattered light along the grating dispersion (Crivellari and Morossi 1982), and also with software available at the *IUE* GSFC regional data analysis facility.

III. THE ULTRAVIOLET AND VISIBLE CONTINUUM

As we noted earlier, AB Aur displays a number of characteristic time scales for variability. In this section and in the following ones, all our available data will be presented and analyzed. We first consider the continuum, then the UV Mg II and Fe II lines.

In 1982, we obtained 28 LR SWP spectra of AB Aur in intervals between HR long-wavelength spectra. We have coadded these spectra, and Figure 2 shows the resulting spectrum from 1250 to 2000 Å. In individual spectra we measured the integrated flux in 100 Å bins. No definite sign of photometric variability can be detected beyond what is expected for the photometric reproducibility of *IUE*. In particular, the spectral resolution is too low to discern subtle changes in the C IV resonance lines which Catala and Talavera (1984) noted from three HR images. In 1984, 17 *IUE* LR short-wavelength spectra were obtained, reduced, and averaged in the same

TABLE 3

LOCATION OF THE CONTINUUM WINDOWS IN THE ULTRAVIOLET SPECTRUM OF AB AURIGAE

Multiplets	Wavelengths (Å)
Mg II (1, 3)	2758.0, 2844.0
Fe II (2, 3)	2350.5, 2401.0
Fe II (64, 2)	2401.0, 2579.5
Fe II (1)	2579.5, 2678.0
Fe II (62, 63, 263, 283)	2678.0, 2758.0
Fe II (60, 78, 216, 217)	2844.0, 2975.0

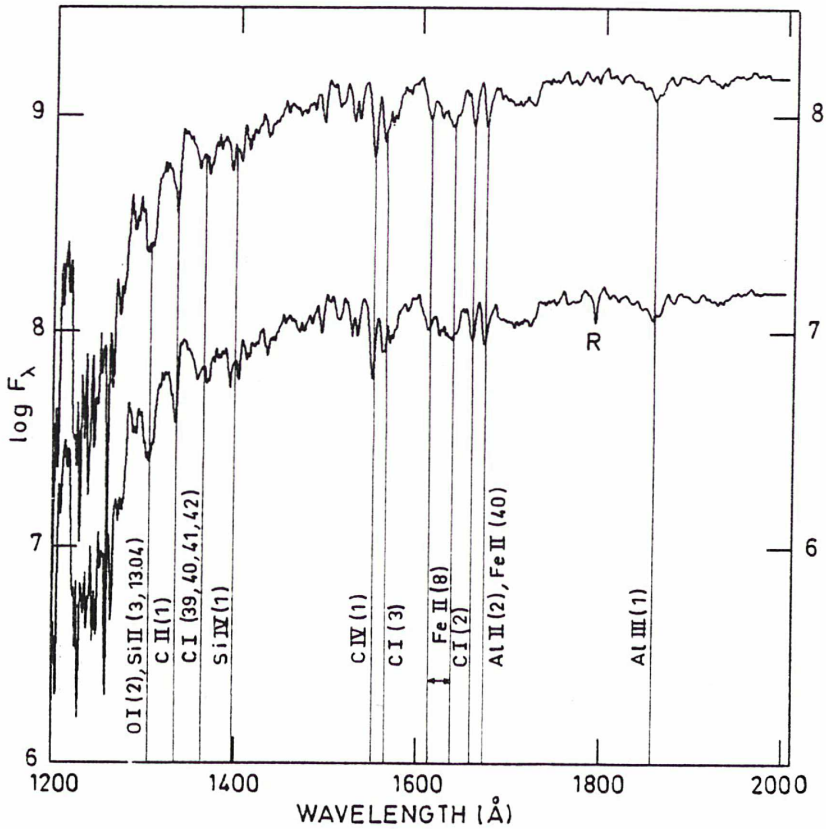

FIG. 2.—(*lower curve*) Average of 28 spectra obtained with the SWP camera of *IUE* in 1982 October. (*upper curve*) Average of 17 SWP spectra obtained in 1984 November. Plotted here is the flux F_λ at the surface of the star dereddened for $E(B-V) = 0.18$, as derived from the scaling factor $2R_*/d$, with $R_* = 2.5\ R_\odot$, $d = 160$ pc. F_λ is in ergs cm^{-2} s^{-1} Å^{-1}. "R" indicates a reseau mark. The 1984 November spectrum is shifted upward by one decade in log F_λ (*right-hand scale*).

manner as for 1982 October (Fig. 2). No difference exists between the two average curves (the standard deviation averaged between 1400 and 1900 Å is 0.004 mag).

We also searched for possible continuum variations in the vicinity of the Mg II λ2800 lines. From the 29 LWR images of 1982, we obtain a standard deviation for the continuum intensity of 3.5% for a ~1 Å bin around 2758 Å and 4.6% for a ~1 Å bin around 2844 Å. We attribute this scatter entirely to our procedure of visually locating the continuum. As for the short-wavelength region, a coadded spectrum was produced in the Mg II and Fe II region. Again, no variation of the continuum was detected above a limit of ±8%, which is the photometric accuracy of *IUE* that was established through a careful study of the reproducibility of *IUE* spectra in HR, long-wavelength spectra by Franco *et al.* (1984).

The continuum in the vicinity of the Mg II resonance lines was also studied in the HR spectra of 1984. At 2758 Å, the continuum level is constant to within 3.8% (s.d.), while at 2844 Å, it does not vary by more than 3.7% (s.d.), these results being derived from the 18 images taken with the same exposure time (30 minutes) and the other images being excellently compatible with the quoted deviations.

The Balmer continuum ($\lambda \approx 3500$ Å, 100 Å width bandpass) did not vary by more than 0.02 mag during the sparse observations performed on 1982 October 26–28 (Praderie *et al.* 1983). A series of *IUE* measures of the FES (fine error sensor) counts was also available in 1982 October, from which the V magnitude of the star can be derived given its $B-V$ color ($B-V = 0.14$). Over the span of the observations, the color-corrected V_{FES} was stable to $\sigma = 0.02$ mag.

At our request, AB Aur was observed by W. Herbst at the 60 cm telescope at Van Vleck Observatory on 1984 November 3, 7, 8, and 15 in the Johnson/Cousins filters U, B, V, R, and I. The star was found to be constant relative to the comparison star BD +30°746 to within 0.02 mag in V. The $B-V$, $V-R$, and $R-I$ colors did not vary ($\sigma = 0.02$), while $U-B$ had a slightly larger dispersion ($\sigma = 0.03$ mag). In 1984 November the *IUE*-derived V_{FES} was stable to $\sigma = 0.02$ mag, except on November 8, where the average V increased by 0.08 mag relative to the value obtained on the other days. This fading of the star was not noticed by Herbst in his ground-based observations. However, Herbst did not observe at exactly the same time. Also, we did not see a change in the UV continuum in the SWP images on that day. Hence this departure might be instrumental in origin.

From this study we therefore conclude that the UV continuum, the Balmer continuum at 3500 Å (observed in 1982), and the Balmer and Paschen continua (observed in 1984) did not vary during our observing campaigns.

IV. THE Mg II RESONANCE LINES

The Mg II (λ2795.523 and λ2802.698) resonance lines of many Herbig Ae stars exhibit P Cygni type IV profiles (Beals 1951), which indicate the presence of a wind (Praderie *et al.* 1982; Catala 1984*b*). The blue-shifted absorption part of the profile is almost or totally saturated. The emission part of the

line is intense. Since the broad lines of the doublet are blended together in AB Aur, it is preferable to study the absorption in Mg II λ2795 and the emission in Mg II λ2802. The blue wing velocity V_s(Mg II) measured at the level of the continuum in the λ2795 line corresponds to the largest velocity shift observed in the spectrum; it is larger than V_s(C IV) = 260 km s^{-1} (Catala and Talavera 1984), larger than or equal to the blue trough velocity in Hα, V_s(Hα) = 300 km s^{-1} (Felenbok, Praderie, and Talavera 1983), and larger than any blueshift observed in the Ca II K line profile (130 km s^{-1}). Note that one should strictly compare velocities measured at the same time, because all the lines mentioned vary in AB Aur. It therefore appears reasonable to call V_s a "terminal velocity" for the Mg II line-forming region, even though the wind may be decelerated at larger radial distances (Felenbok, Praderie, and Talavera 1983; Finkenzeller and Mundt 1984). The values measured for V_s were obtained from spectra plotted in reduced units, and V_s determined in the wavelength scale referred to the Mg II interstellar lines, as indicated in Figure 3. To extrapolate from the absorption part of the λ2795 profile up to the continuum, we gave more weight to the portion of the blue wing with reduced intensity between 0.2 and 0.6, since this segment of the λ2795 profile is equally well defined on all the available spectra. Since the definition of the Mg II interstellar lines is not equally clear on each image, we used several images having prominent features as templates. We then proceeded onward from these images by adjusting the other spectra so as to coincide along the steep portions of the line profile connecting the absorption and emission components.

It is worth pointing out here that the Mg II interstellar lines, as well as other similar lines originating from the 0 eV level in UV multiplets of Mn II and Fe II, have measured separations, as read from the routinely extracted wavelengths, equal to the laboratory values to within ±0.04 Å. However, these lines are blueshifted with respect to the Mg I λ2852.13 line, to which we have locked our wavelength scale, by 39 km s^{-1} in the 1982 October and 1984 November spectra. It is not possible without further study to decide which lines are interstellar in origin. This point does not really matter here, since our analysis depends only on *relative* variations of V_s.

We searched for variability in three spectral features: (1) V_s, (2) the intensity at wavelengths located in the blue wing of Mg II λ2795, and (3) the emission equivalent width W_{em}(λ2802).

a) Variability in Mg II *Terminal Velocity*

Inspection of the Mg II lines, either in absolute flux units or in reduced units, immediately reveals that V_s(Mg II) varies with time. Figures 4 and 5 illustrate this phenomenon, which is best seen in Mg II λ2795.

The variation of V_s versus time from our 1982 observations is presented in Figure 6*a*. The extreme values of V_s are 495 and 370 km s^{-1}. The measurement error in V_s, which includes positioning of the continuum and of the interstellar lines, is estimated to be ±20 km s^{-1}. The average value of the measured V_s during the 40 hr of observation is $\langle V_s \rangle$ = 418 ± 37 (s.d.) km s^{-1}.[4]

The variability exhibited in Figure 6*a* shows an increase in the blue wing velocity of 2795 Å to 500 km s^{-1}, then a decrease to 370 km s^{-1} with a monotonic trend of overall sinusoidal aspect. These data are therefore compatible with a cyclic variation with period ~45 hr, a value which is consistent with the estimated upper limits of the photospheric rotation period reported in § I.

Confirmation is indeed obtained from observations carried out over several rotation cycles, as is shown by our 1984 November data. Again the hourly variation of V_s(Mg II) is quite obvious (Fig. 6*b*). The extreme values are 315 and 495 km s^{-1}, which differ by 180 km s^{-1} or 57%. The average value of the measured V_s over the 150 hr of observation is $\langle V_s \rangle$ =

[4] The difference between those values and preliminary results published in Praderie *et al.* (1983, 1984*b*) is due to a different position of the continuum level once we realized that the previous continuum windows, chosen at 2770 and 2831 Å, are perturbed by weak emission lines, as explained in § V.

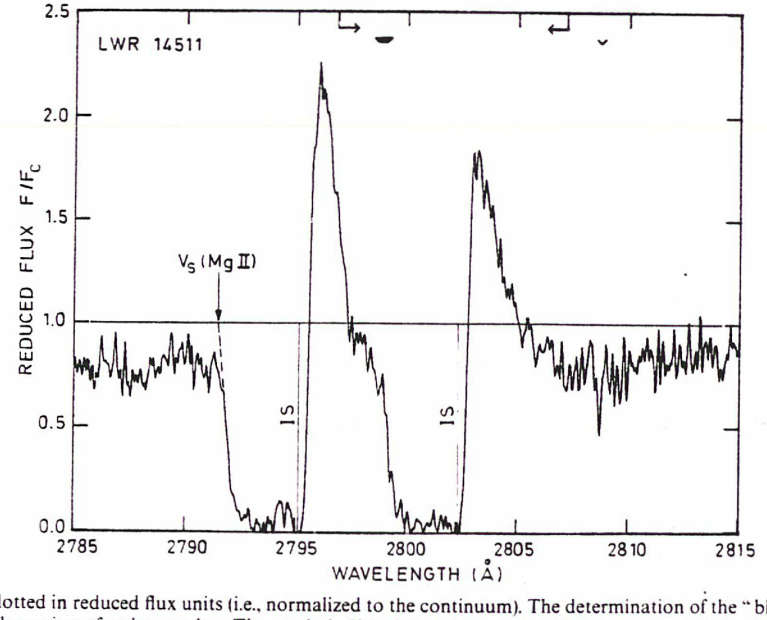

FIG. 3.—Mg II resonance lines plotted in reduced flux units (i.e., normalized to the continuum). The determination of the "blue wing" or "terminal" velocity V_s is depicted. The two arrows indicate the region of order overlap. The symbols *V* and ◇ denote respectively a reseau mark (or bright spot) and extrapolated intensity transfer function. The interstellar features are indicated by "IS."

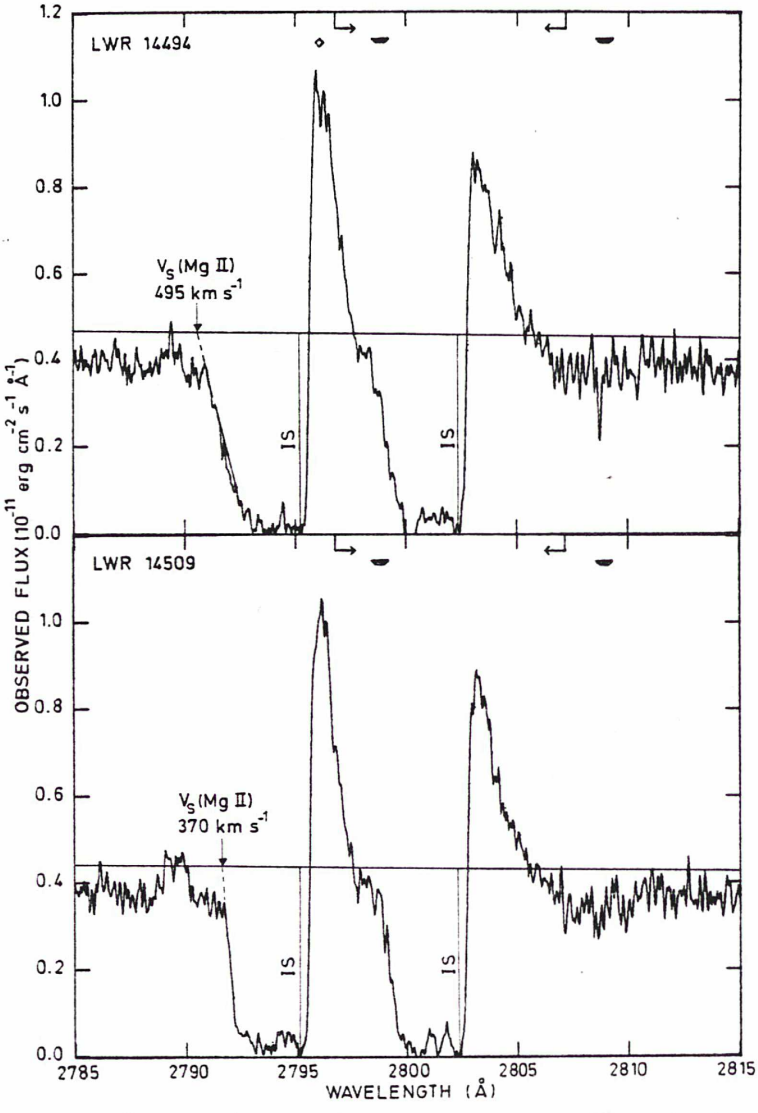

FIG. 4.—Echelle spectra of the Mg II resonance lines plotted in absolute flux units at Earth. Note the difference in V_s between the two images (LWR 14494 and 14509).

400 ± 63 (s.d.) km s^{-1}. One notes that the dispersion over the average of the measurements $\langle V_s \rangle$ is larger than in 1982 October, and that the average value is lower by 18 km s^{-1}. However, ignoring at this point the fact that V_s is variable with time, the 1982 and 1984 $\langle V_s \rangle$ values are perfectly compatible.

Figure 6*b* does not at first sight give clear proof of a cyclic variation such as is immediately apparent in Figure 6*a*. Therefore, a systematic procedure for period determination was applied to the 1984 November data. It is always a delicate matter to search for periods in data affected by gaps, which is the case of our 1984 November time series of observations. However, if a period exists, it should not only be obvious to the eye over one cycle, as is the case in 1982 October, but also should fit several cycles, as observed in 1984 November.

We therefore tried to fit the 1984 November data with a sine curve using the following procedure. The method followed was to fix the period of the sinusoid and to perform a least-squares fit to the data with the amplitude and the phase of the sinusoid as parameters, and then to let the period vary. For each trial period, we computed the residual $R = \sum_{i=1}^{N} [Y_i - F(x_i)]^2 / \sum_{i=1}^{N} Y_i^2$, where N is the number of observations, Y_i are the observed quantities (V_s), and $F(x_i)$ are the values of the fitting function at the points x_i which represent the midexposure times of our spectra. When applied to the whole set of data for 1984 November, this procedure did not yield any minimum for R. However, Figure 6*b* strongly suggests that the six largest values of V_s obtained on November 9 and 10 (LWP 4764–4770) might correspond to an isolated event that is superposed on a smoother variation. This event lasted for at least 15 hr, but less than 32 hr. Fifteen hours is the time needed for the wind to travel a distance of 12 R_*, so that we can interpret it as an outburst of short duration at its source that is observed all along its passage across the region of formation of the Mg II resonance lines. It can then be considered as a "flarelike" phenomenon of the kind we already observed in the Ca II K line and in the Balmer lines in 1980 October (Praderie *et al.* 1982). Consequently, in a second attempt we omitted these six points and tried again to fit the data with a

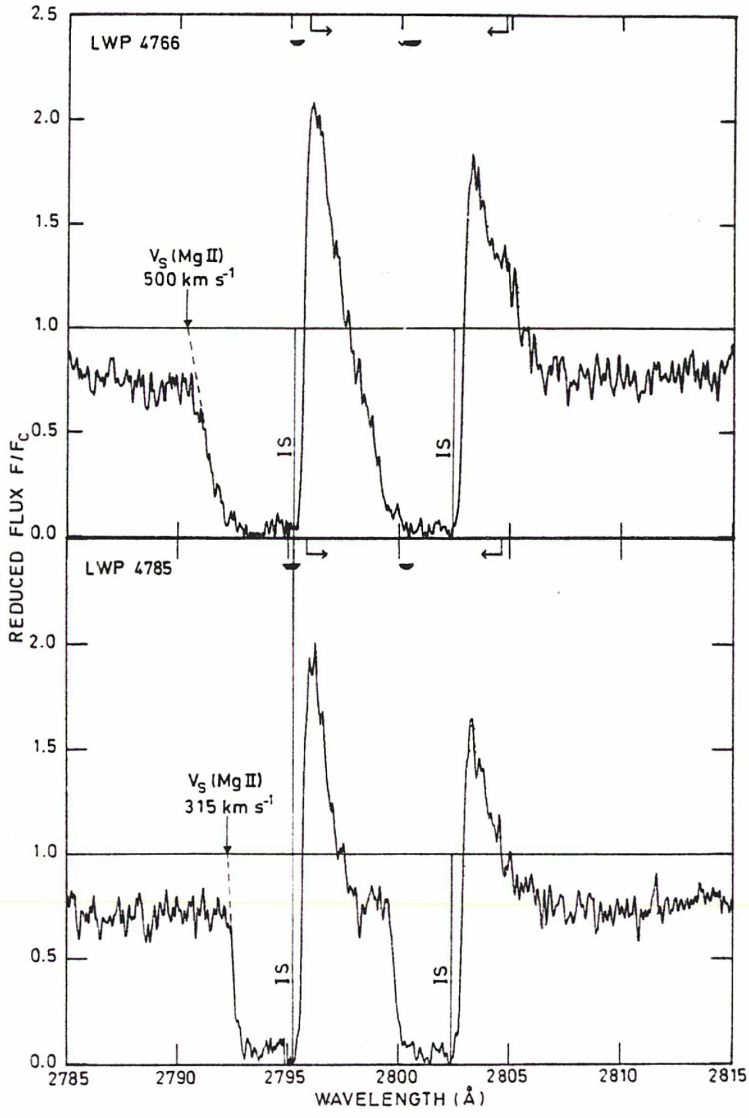

FIG. 5.—Mg II resonance lines spectral region in reduced flux units. The two images (LWP 4766 and 4785) show large differences in profiles and V_s values.

sinusoid. This procedure reduces the sample of available data points from 22 to 16. Figure 7 shows a plot of R as a function of the assumed period of the sinusoid; there is now a clear minimum, which gives confidence that the periodic time behavior of the observed values cannot be doubted. Figure 6*b* displays the result of the best fit. These two figures suggest that the 1984 data are consistent with a sinusoidal variation of period 45 ± 6 hr, plus an individual event that lasted for at least 15 hr.

The same fitting procedure was followed for the 1982 October data. For these data, we obtain a very wide minimum for R, simply because the total duration of the observations is of the order of the assumed period. Nevertheless, Figure 6*a*, which displays the result of fitting the sine curve with a period of 45 hr, shows that the 1982 October data are consistent with this period. In what follows, we explicitly assume that the period we have found is the rotation period P in the formation region of V_s(Mg II).

It is quite remarkable that we observed a stationary phenomenon, namely, that after 2 yr the spectroscopic tracer of the star's rotation, V_s(Mg II), exhibits the same time variability with the same period. As for the amplitude of the sine curve fit, it is not conserved, and is larger in 1984 November (142 km s^{-1} instead of 92 km s^{-1}). It is not possible with the available data to check the phase stability of the phenomenon; we are forced to conclude that there is a persistence over time of the existence of active sites or active longitudes, which, when they cross the visible disk, modulate some observable features.

b) Variability of Mg II λ2795 *Absorption Wing Intensity*

A general variability criterion has been used to search for variability in intensity. For each wavelength region, extending over about 100 Å, a point by point average of each set of spectra (separately for 1982 and 1984) was performed and the standard deviation $\sigma(\lambda)$ computed. An average of $\sigma(\lambda)$ over wavelength, $\langle\sigma\rangle$, was then obtained. We deduce that the spectrum is variable if, at a given λ, $\sigma(\lambda) \geq 3\langle\sigma\rangle$. The application of the criterion is subject to a careful analysis of the $\sigma(\lambda)$ curve in order to eliminate such camera artifacts as bright spots and reseau marks.

For the Mg II λ2795 line, the intensity in the absorption part

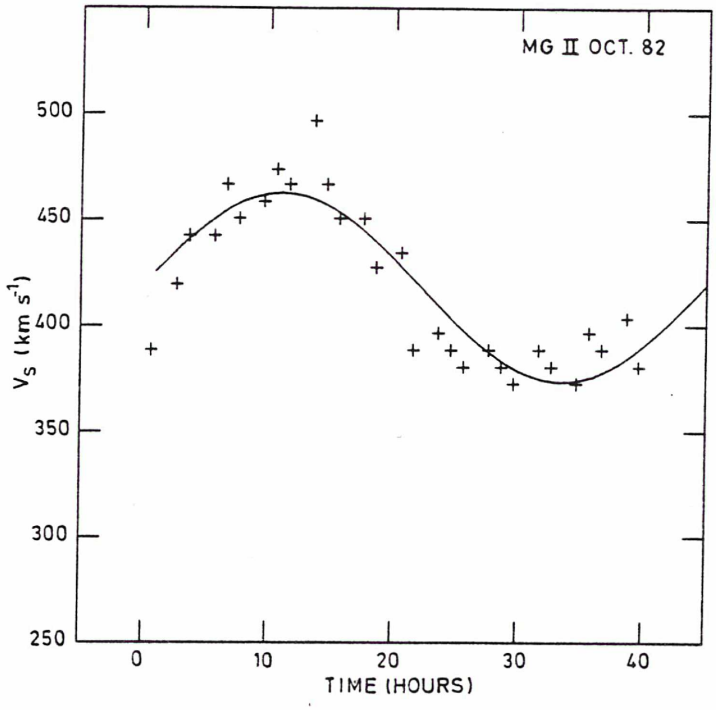

FIG. 6a

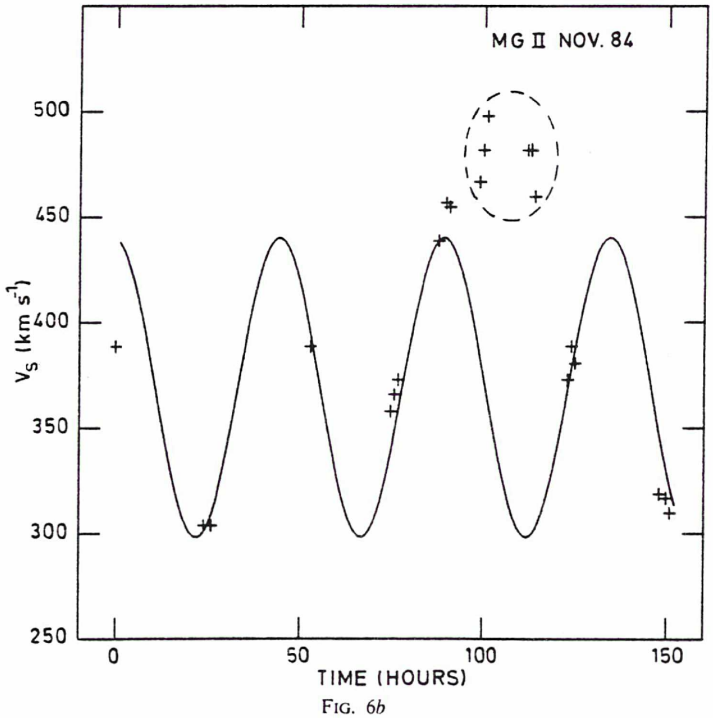

FIG. 6b

FIG. 6.—(*a*) Variations of the Mg II "terminal velocity" over 40 hr in 1982 October. A sine curve with a period of 45 hr is plotted for comparison with observations (*plusses*). (*b*) Variations of the Mg II "terminal velocity" over 150 hr in 1984 November. The sine curve fit excludes the six encircled points, which are attributed to a flarelike event. The measurement error for V_s is ± 20 km s^{-1}.

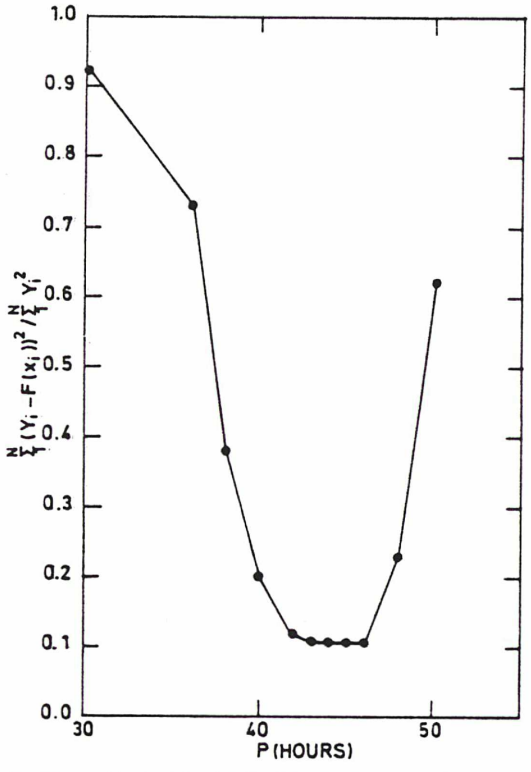

FIG. 7.—The residual of the sine fit to the observed set of data $V_s(t)$ for 1984 November vs. period P.

was studied in the blue wing, from about $V_s/2$ to larger values in Doppler shift up to V_s. This region is devoid of artifacts. On our 1982 spectra, we find $\sigma(\lambda) \geq 3\langle\sigma\rangle$ in this whole spectral region, $\langle\sigma\rangle$ being computed over a 100 Å wide region. The blue wing of the λ2795 line is therefore variable in intensity for expansion velocities between $V_s/2$ and V_s. Other parts of the profile, though, do not vary in 1982. In 1984, the variations are so obvious that we did not perform the same analysis (see Fig. 5).

c) *Search for Variability in the Emission Parts of the* Mg II *Line Profiles*

Spectral variability could also be present in the emission equivalent width and in the peak emission intensity observed in Mg II $\lambda\lambda$2795 and 2802. All four quantities vary in a random way over the 40 hr of observations in 1982 October; however, none satisfies the criterion that in a given image the deviation measured be larger than 3 σ. The most significant results are related to the emission part of Mg II λ2802, which suffers no blending with the λ2795 line. The average value of $W_{em}(\lambda 2802)$ is 980 $\pm$ 120 (s.d.) mÅ.[5] We note that inaccuracies in positioning the continuum and the effects of order averaging both affect $W_{em}(\lambda 2802)$, the error being estimated at 110 mÅ. A comparison of the spectra in absolute units confirms the lack of emission intensity variations, while the variations in V_s are quite obvious in the same visual examination.

The Mg II λ2802 emission is more variable in 1984 November than in 1982 October. Over the 150 hours of observation, the peak to peak variation of $W_{em}(\lambda 2802)$ is a factor of 1.45, although the average value of 973 mÅ is very close to that of 1982 October. However, the standard deviation is now 216 mÅ, larger than the estimated error of measurement (110 mÅ). We find no correlation between $W_{em}(\lambda 2802)$ and V_s(Mg II); there is a tendency for the emission to be broader when $W_{em}(\lambda 2802)$ is larger, which occurs in particular for the eight images LWP 4764–4775.

To summarize this section on Mg II variability, we find that the blueshifted absorption part of the Mg II line profile varies systematically in terminal velocity and intensity over a time scale of 45 hr, which we interpret as the rotation period, while the redshifted emission component of the profile is less variable. In the first instance, the variability is the result of changes in the structure of the envelope localized on the line of sight to the stellar core, while most likely the variability in the emission part of Mg II lines, formed by a volume integration over the envelope, is smoothed out by uncorrelated (or correlated) local variations throughout the envelope.

V. THE Fe II SPECTRUM

The Fe II spectrum is intense in AB Aur. As already described (Praderie *et al.* 1982; Talavera *et al.* 1982), most of the Fe II lines are in absorption, and the resonance lines show no sign of P Cygni structure, i.e., no emission is located redward of the rest wavelengths. Some aspects of their long-term variability are presented in Praderie *et al.* (1984*a*).

In the 1982 October spectra, the strongest absorption lines of UV multiplets (1, 2, 3, 32, 33, 34, 35, 62, 63, and 64), when not too blended, are separated into three components. The most intense component is the shortward one, which is well separated from the others (Fig. 8), while the longward one is located at the rest wavelength in the Mg II/Fe II interstellar line system. The Doppler shifts of the two blueshifted components ($\Delta\lambda_1$, $\Delta\lambda_2$) relative to the undisplaced component have been measured on all possible unblended Fe II lines and on all 29 available spectra. The shifts remain constant over the 40 hr of observation and correspond to well-defined velocity shifts of $V_1 = 56$ km s^{-1} and $V_2 = 150$ km s^{-1}. Because of this constancy, we show in Figure 8 average spectra in the regions of UV multiplets 1, 62, and 63. Since the two extra blueshifted components appear in subordinate lines, as well as in resonance ones, at velocities very different from the interstellar one measured in other lines, these components must be intrinsic to the star rather than interstellar in origin.

The appearance of the Fe II spectrum in 1982 October is different from what we have observed at other epochs (Praderie *et al.* 1984*a*), when one could find either simple asymmetric lines (in 1981 January) or broad but unsplit, almost square line profiles (in 1983 January). In 1984 January the Fe II lines are again split into three components of nearly equal intensity, and their shapes evolve still more in 1984 November. Significantly, the velocities determined for the Fe II components are smaller than V_s(Mg II), and this is the case in all other images examined in the long-term variability study of Praderie *et al.* (1984*a*).

That the Fe II resonance lines exhibit no P Cygni structure, while the Mg II resonance lines and Hα do, can be attributed to one or several of the following reasons. (1) The spectral region where the Fe II lines are located is crowded by absorption lines, and those suffice to prevent the Fe II scattered photons from producing emission. (2) The wind region where the Fe II lines originate is farther out than the Mg II– and Hα–forming layers. There, the spherically symmetric approximation for the shape

[5] The present value of $W_{em}(\lambda 2802)$ differs from a preliminary result (Praderie *et al.* 1983) which was determined from a different choice of the continuum normalization.

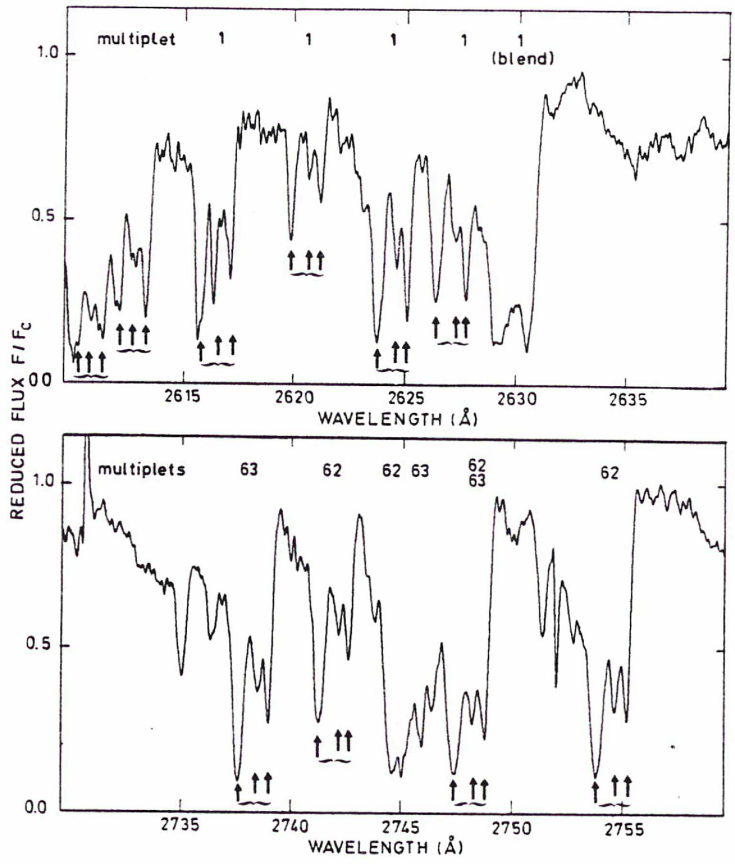

FIG. 8.—Average spectrum (29 spectra coadded) in two Fe II regions observed in 1982 October: Mult. UV 1 and Mult. UV 62–63. In this figure only, the wavelength scale is in the Mg II/Fe II interstellar lines system.

of the envelope is no longer valid. This latter assumption will be reinforced by the variability study which follows. (3) The scattered Fe II photons are destroyed by cold dust. This mechanism, already suggested by Kunasz and Praderie (1981) to explain the absence of emission in the Mg II wind profile in α Cyg (A2 Ib), is more efficient in a young star like AB Aur, where dust is indeed detected through an IR excess and through the 9.7 μm silicate emission (Allen 1973; Cohen 1980). Again it would suggest that Fe II is formed at large distances from the stellar photosphere, at places where the expanding gas envelope contains dust grains. However, the Fe II lines of the Herbig star HD 250550 exhibit the same shape (Talavera *et al.* 1982), while this star presents no silicate bump nor any $B-V$ excess. (4) The atomic structure of Fe II is very complex and could allow depopulation of the upper levels of the concerned lines via other transitions.

Isolated emission lines also occur in the Fe II spectrum of AB Aur, as was first noted by Talavera (private communication). These lines belong to UV multiplets 60, 61, 78, 216, 217, 234, 277, and 282. We have noted above that in our preliminary study (Praderie *et al.* 1983) the λ2831.56 line of multiplet 217 and λ2771.18 of multiplet 282 were identified as high-intensity points to locate the continuum. This explains the differences between values of V_s(Mg II) and $W_{em}(\lambda 2802)$ given here and those published earlier. A list of the Fe II emission lines in the spectrum of AB Aur appears in Table 4. Some of the multiplets are intercombination ones. All share the property that their lower energy level is not directly connected to the ground configuration (a^6D) of Fe II. Further work on these emission lines will be published elsewhere (Talavera, in preparation).

As we did for Mg II, we looked for evidence of variability in several features of the Fe II spectrum: (1) velocity in the least blended lines, (2) the intensity of the absorption components, (3) the peak intensity of the emission lines, and (4) the integrated strengths of the emission lines. All the spectra were treated in reduced units, with continuum windows located as indicated in Table 3.

TABLE 4

EMISSION LINES IN THE ULTRAVIOLET Fe II SPECTRUM OF AB AURIGAE

λ (Å)	Multiplet	Configuration
2771.184.....	282	$b^2G-y^4H^o$
2779.302.....	234	$b^2H-z^2G^o$
2783.690.....	234	$b^2H-z^2G^o$
2831.562.....	217	$b^2P-z^2D^o$
2835.716.....	216	$b^2P-z^4G^o$
2880.750.....	61	$a^4D-z^6P^o$
2926.584.....	60	$a^4D-z^6F^o$
2944.399.....	78	$a^4P-z^4P^o$
2947.658.....	78	$a^4P-z^4P^o$
2949.178.....	277	$b^2G-z^2F^o$
2953.774.....	60	$a^4D-z^6F^o$

In 1982, no detectable variation exists in the blue wing velocity. For instance, the average value of V_s for Fe II λ2727.5 is 210 km s^{-1}, with an rms dispersion of 6.5 km s^{-1}.

The intensity at maximum absorption of the pair of blue-shifted components for Fe II $\lambda\lambda$2617.6, 2621.7 (mult. 1), 2714.4, 2727.5, 2739.5 (mult. 63), 2743.2, and 2755.7 (mult. 62) showed only a random pattern over the 40 hr of observation in 1982, although the variation often exceeds the $\pm 8\%$ statistical uncertainties established by Franco *et al.* (1984) in their study of the Mg II resonance lines of solar-type stars. However, no periodic variation can be recognized in the absorption intensity fluctuations of the Fe II lines in our 1982 spectra of AB Aur.

The general variability criterion discussed earlier was applied to three spectral regions containing the Fe II absorption lines (2340–2415, 2540–2640, and 2700–2980 Å). Namely, a $\sigma(\lambda)/\langle\sigma\rangle$ curve was produced for each region for the entire set of available images from 1982. An example is given in Figure 9. All details in this figure where $\sigma(\lambda) \geq 2\langle\sigma\rangle$ were analyzed, and all could be identified with artifacts due to the camera or exclusively to one of the images (radiation hits). In particular, we found no local maxima in $\sigma(\lambda)$ at the rest wavelengths of the Fe II absorption components, maxima which would have indicated variability in the intensity of the Fe II absorption components.

We therefore conclude that no short-term intensity variations in excess of *IUE*'s photometric precision are present in the Fe II UV absorption lines in the 29 images obtained over the 40 hr of observation in 1982.

The emission lines of multiplets 60 and 78 were also examined for variability by means of the variability criterion described above. No significant variation was found in the peak intensities in the 1982 spectra.

Fluctuations in the equivalent widths of Fe II emission lines W_{em} were detected. They are fairly intense in the case of the λ2926.6 line (mult. 60). However, we estimate the error $\Delta W_{em}/W_{em} \approx 0.30$, and so we find that in 1982 only five points of 29 lie outside the error range, which we judge to be totally insignificant.

It therefore appears that in 1982 the Fe II line spectrum in the star AB Aur behaves very differently from the Mg II spectrum. The Fe II absorption lines are very constant in blue wing velocity, in separation of the components, and in intensity. The Fe II emission lines do not exhibit conspicuous *organized*

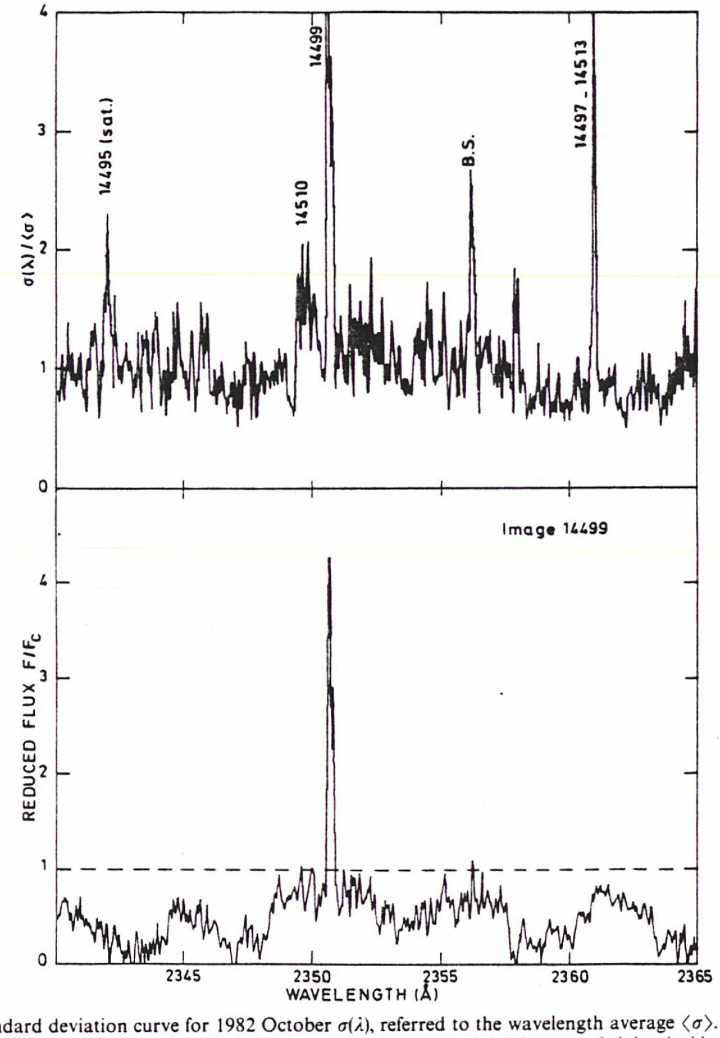

FIG. 9.—(*a*) An example of the standard deviation curve for 1982 October $\sigma(\lambda)$, referred to the wavelength average $\langle\sigma\rangle$. The $\sigma(\lambda)$ is computed for 29 individual images between 2340 and 2365 Å. Camera artifacts are identified by LWR image number, e.g., "B.S." denotes a bright pixel in the LWR camera. (*b*) An example of the effect of an artifact in image LWR 14499 on structure in the $\sigma(\lambda)/\langle\sigma\rangle$ curve. The other deviating points can all be similarly analyzed.

intensity variations either. By contrast, the blue absorption in the Mg II resonance lines exhibits periodic variations in velocity and intensity, while the Mg II emission is not distinctly variable.

In 1984, the aspect of the Fe II lines is very different from that observed in 1982. The lines are no longer split into three components; their absorption core is broad and deep. While we had to apply refined methods to finally conclude that the Fe II spectrum is not variable from the 1982 data, the variations in 1984 are so conspicuous over our series of 22 images that they were immediately obvious.

Figure 10 displays an example of this variability in the region of Fe II multiplets 62 and 63. The variations are particularly easy to see near Fe II λ2755.73 (mult. 62). On the upper panel of Figure 10, note that Fe II λ2753.29 (mult. 235) is clearly distinct from Fe II λ2755.73, and so is the case on images LWR 4733–4747. A detailed examination of the whole set of 1984 November data showed that a blueshifted absorption component appeared in all the lines of multiplets 1, 62, and 63 on LWP 4753. On Figure 10 (*lower panel*), for instance, this component in Fe II λ2755.73 has become mixed with Fe II λ2753.29. The width of this component increased continuously, then decreased from LWP 4774 on, and eventually the component disappeared on LWP 4784. In the region of Fe II λ2755.73, then, the multiplet 235 line is back to its well-separated state relative to Fe II λ2755.73. The total duration of this blue component was 3 days. No such variation was observed in the emission lines of multiplets 60, 61, and 78. Finally, there is no correlation at all between the "flarelike" phenomenon seen in the Mg II lines (§ IV*a*) and any feature in the Fe II lines.

VI. SIGNIFICANCE OF THE TIME VARIABILITY OF Mg II AND Fe II

The observations of AB Aur can be examined successively within the framework of two models. The first is a spherically symmetric representation of the wind of AB Aur, which is useful in studying the overall formation of various spectral characteristics. The second model is nonspherically symmetric and is suggested by new information deduced from variability studies. In such a laterally inhomogeneous model, the different aspects of the projected stellar disk seen by an observer, which result from the star's rotation, are responsible for the variability.

We first point out that no organized hourly profile variation, such as that which we have found for the Mg II "terminal velocity" V_s of AB Aur, has been reported in any other star of type A, whether dwarf or supergiant, pre–main-sequence or main-sequence. In hotter stars profile fluctuations have been observed in wind-sensitive lines: York *et al.* (1977) reported intensity variations in O VI in O-type stars on time scales of 1–6 hr; Slettebak and Snow (1978) found short-term irregular variability in the Si IV, Mg II, and Hα lines of the Be star γ Cas. These authors did not recognize the stellar rotation period nor

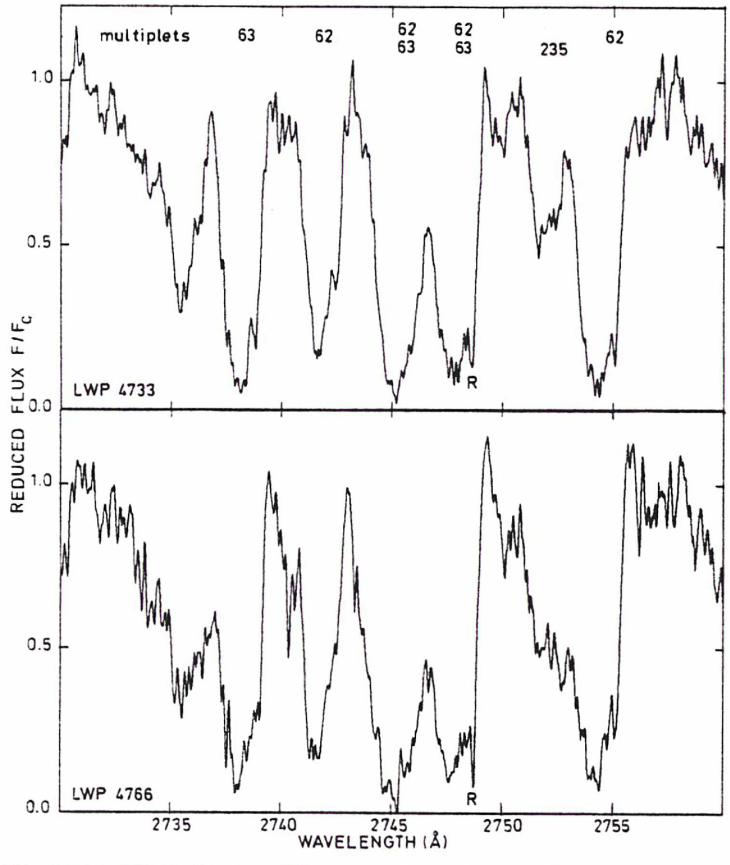

FIG. 10.—One of the Fe II regions of Fig. 8 (Mult. UV 62–63) at two different epochs within the 1984 November run, chosen to exhibit the short-term variability of Fe II as described in text.

any other period in their data.[6] High temporal resolution profile variability in B and Be stars (Smith *et al.* 1984; Baade 1984) constitutes a very new step in the study of pulsational motions of hot star atmospheres.

AB Aur is spectroscopically very different from an ordinary dwarf A star, as indicated by the P Cygni profile of Mg II. Since one cannot envisage on the basis of available data that AB Aur is a binary (Finkenzeller 1983), we are left with a variability phenomenon which may be restricted to pre–main-sequence stars, of which, among the hottest ones, only AB Aur has thus far been studied in sufficient detail. We found that a time scale very similar to the rotation period plays a role in modulating the terminal velocity of the Mg II λ2795 line, and this leads naturally to an interpretation in terms of rotation.

The Mg II line formation in AB Aur has been studied for a spherically symmetric expanding medium, with a monotonic velocity law increasing from small values at the photosphere to $V_\infty \approx 300$ km s^{-1} at $\sim 20\ R_*$ (Catala, Kunasz, and Praderie 1984). The Mg II line profile has been computed in a two-level atom NLTE approximation. In this representation of the envelope of AB Aur, the absorption part of the Mg II profile is sensitive to all velocities up to V_∞, and the strength of the emission intensity depends strongly on the presence of a chromosphere, which acts on the one hand to raise the line source function and on the other to fix the ionization fraction of Mg II in the lower portions of the expanding envelope. This chromosphere extends from 1 to 2.5 R_*, and its temperature reaches 15,000–18,000 K, a range of values confirmed by a recent study of the C IV resonance lines in this star (Catala and Talavera 1984; Catala 1984*a*).

The sinusoidal variation of V_s(Mg II) we have observed at two different epochs reflects a phenomenon that is best observed along the line of sight to the stellar core and one that is not averaged out by volume integration effects, as is the case of an emission feature such as $W_{em}(\lambda 2802)$. Furthermore, the intensity in the blue absorption wing of the λ2795 line is variable for Doppler shifts ranging from $\sim V_s/2$ up to V_s. Therefore the variability in the envelope must extend over at least the corresponding radial distances if $V(r)$ is taken as a unique, monotonic function of distance. However, the mere existence of such variability, and of a periodic one, is incompatible with a spherically symmetric model of the star's envelope and suggests that the envelope of AB Aur needs to be represented by a nonuniform expanding model.

It is attractive to interpret the time variability of V_s(Mg II) shown in Figure 6 as the effect of large-scale perturbations in the stellar wind (Praderie *et al.* 1984*a*; Catala 1984*a*). As in the Sun, if the wind is structured in fast and slow streams of material, their passage across the line of sight produces for a remote observer a periodic pattern of variability as the star rotates and drives the envelope in corotation. In this picture, the envelope must be dense and cool enough that spectroscopically observable effects can be observed, unlike the case of the tenuous and hot solar wind. When fast streams (or one fast stream) face the observer, then V_s(Mg II) attains large values; when slow streams (or one slow stream) cross the visible disk, then V_s is at its smallest values. A similar, solar wind–inspired model has been elaborated by Mullan (1984) for the winds of hot stars, hybrid stars, and cool supergiants, but with a different purpose than to explain variability.

In the Sun, the origin of such streams is in the coronal holes for the fast ones, and in active regions (or at active longitudes) for the slow ones. Due to the solar rotation, the streams that emerge radially from the surface corotate and form a spiral structure; this structure keeps its individuality up to a large distance from the Sun in the interplanetary medium (10 AU). At greater distances, the streams are eroded and finally merge; hence, a more ordered configuration is restored (e.g., Burlaga 1984).

In Mullan's (1984) model, the fast streams overtake the slow ones in a region which corotates with the star. The radial distance to this "corotating interactive region" depends strongly on the longitude dependence of the velocity within the fast streams. Since we do not know anything about this dependence in AB Aur, we cannot determine at which distance the streams begin to merge. If this happens beyond the region contributing the most to the observed variations of V_s(Mg II), these variations give us a real measure of the velocity difference between fast and slow streams. If not, the bluest parts of the Mg II lines are formed in a region where the streams have begun to merge, and we see only smoothed variations. The azimuthal and latitudinal coverage of the stellar disk by the fast and slow streams must be substantial since we see (Fig. 6*a*) a continuous variation of V_s(Mg II), by contrast with short-lived but periodically distributed enhancements in V_s.

In the case of AB Aur, one then wonders if a structured expansion of the solar wind type extends throughout the wind or if it is characteristic of only a range of radial distances in the envelope. The observations of the UV Fe II lines are of interest here. In a spherical wind model, the expansion velocities in Fe II (either the blue wing velocity or the Doppler shifts of the components) can correspond either to the acceleration zone near the stellar surface or to the remote decelerating part of the wind, which gives rise to the blueshifted absorption in Na I D lines at $V = 130$ km s^{-1} (Felenbok, Praderie, and Talavera 1983; Finkenzeller and Mundt 1984). The first alternative can be eliminated, because otherwise we could not understand why the Mg II absorption lines are variable while at the same time the Fe II lines are so constant in all respects in 1982. Note that the blue wing velocity in Fe II at that epoch, 210 km s^{-1}, is only slightly larger than half of V_s(Mg II), namely $\sim$200 km s^{-1}. The difference is too small to support an overlap in the regions where Fe II and the variable parts of the Mg II profile, i.e., $V \geq V_s$(Mg II)/2, are formed. We believe it is more reasonable to assume that the Fe II lines originate in the cool decelerating part of the wind, above the Mg II–forming region. It cannot be assumed that the well-identified fast and slow streams existing in the Mg II–forming part of the wind keep their individuality in regions as remote as those where the Fe II lines form; otherwise again we should observe a periodic variability in the Fe II lines, and never a phase of constancy. These facts suggest that, as in the Sun, the fast and slow streams eventually merge, after a destruction of the ordered spiral configuration present at radial distances closer to the star.

How can we reconcile such a picture with the two contrasting characteristics of the Fe II lines in AB Aur as observed in 1982 and 1984, namely, (1) the existence of discrete velocity components, which are almost always present over several years (see Praderie *et al.* 1984*a*), and (2) the constancy of the Fe II spectrum in 1982 and its variability in 1984? The components correspond either to a velocity plateau at well-defined

[6] This work was completed when we received the paper by Brown, Shore, and Sonneborn (1985) on the helium-weak star HR 1063, in which the C IV resonance lines vary on the same time scale as the magnetic field, i.e., with the rotation period.

values of V or to a density enhancement (shell). The first occurrence seems unlikely, at least in the sense suggested by Mullan (1984): the velocity plateau which exists between consecutive fast and slow streams in a solar wind–type model would demand, if it existed in AB Aur, that a variability of Fe II accompany the Mg II variability in 1982 as the star rotates. This was not observed. The second alternative, i.e., the formation of shells at $r \geq 20\ R_*$ in the Fe II–forming region, would be compatible with the erosion of streams into pressure waves, directly observed in the heliosphere behind the region of corotating fast and slow streams (Burlaga 1984). In the case of AB Aur, to understand the time behavior of the Fe II lines one would need a stable configuration of such compression regions across the line of sight over 40 hr to interpret the 1982 data, while different "annuli" of these pressure waves would pass in front of the observer over 150 hr in 1984, accounting for the appearance and disappearance of components in the UV Fe II lines.

In the absence of the detailed radiative transfer computation of the Fe II lines, which should in particular explain why those UV lines do not show a classical P Cygni structure, we propose that the Fe II lines are formed in a nonuniform region $20\ R_*$ or farther from the star, a region structured by pressure waves rather than by fast and slow streams, and contributing little to the formation of the bluest parts of the Mg II line.

Deeper in the envelope at radial distances corresponding to velocities smaller than about $V_s/2$, the lines which can be used to probe the wind include the Ca II and C IV resonance lines. The C IV lines have been analyzed by Catala and Talavera (1984), but the variability of C IV has not yet been studied in detail. The Ca II lines were observed in 1982 October. Their variability over five nights is pronounced, and a period can be extracted from the series of 39 available spectra (Catala *et al.* 1985*b*, Paper II of this series). The Ca II data are discussed in this forthcoming paper, and further properties of the wind model assessed.

If the structure of the wind of a very young star such as AB Aur shares some common characteristics with that of the solar wind, if rotation accounts for the variability observed in some of the lines, and if the large-scale structure present in the wind persists over several rotations, as suggested by the Mg II data, we may have indirect proof of the presence of a magnetic field. As in the Sun, the field may alternate between closed loop structures and open field configurations. The regions corresponding to closed loops would be the seat of the Ca II K emission component and of all other chromospheric lines (Ca II IR triplet, He I λ5876; see Felenbok, Praderie, and Talavera 1983). Consequently, we expect other chromospheric lines to be variable on a short time scale, as is the case for Ca II. "Coronal hole"–type regions with open magnetic field lines might extend into the envelope and be the source of the fast streams observed in the Mg II lines. Since short-term periodic variability in Mg II extends over at least 150 hr in 1984 November (Fig. 6*b*), this means that these regions, as in the Sun, persist on the stellar surface at the same location over more than three rotation periods. All these phenomena can be called "activity," whether present as rotational modulation in emission features or in radial velocities. Similarly, what we have called by extension "flarelike events" are shorter time scale ($\tau \ll P_{rot}$) phenomena which manifest themselves either by a reinforcement in emission intensity, or by a sudden increase in velocity, or by the abrupt appearance of a short-lived absorption component.

The suggested model differs in one major respect from the solar wind: the temperature of the flow must be low (5000–10,000 K) in the region where the variable parts of the Mg II line profiles and the Fe II lines are formed. When we refer to "coronal hole"–type regions as the source of the recurrent fast streams in the wind, this designation is used only for the purpose of analogy, because no plasma at $T \approx 10^5$–10^6 K has yet been observed in AB Aur (Feigelson and De Campli 1981). Whether the star actually has a corona, and also what mechanism can accelerate the winds of Herbig stars in general, is unknown. Our proposed model is purely phenomenological.

The ultraviolet Fe II spectrum such as is observed in AB Aur has no counterpart in solar-type stars and makes this star more similar to hot stars, such as Be stars, or O and B stars. High-speed (Lamers, Gathier, and Snow 1982) and low-velocity (Gry, Lamers, and Vidal-Madjar 1984) absorption components are present in the resonance lines in a number of O and B stars where the origin of these components is still debated. In AB Aur, the short-term (this paper) and long-term (Praderie *et al.* 1984*a*) variability of Fe II can be qualitatively reconciled with a "remote heliosphere"–type model, as proposed here, implying the formation of pressure waves, but at densities large enough that optical and UV effects can be observed in the spectrum. We also point out that AB Aur shares some similarity with T Tauri stars, although not on the same time scale. Mundt (1984) reports that in a number of T Tauri stars, the blueshifted absorption components observed in the Na I D lines (but not in Fe II) seems to be constant in intensity and velocity, while Hα is variable. But these results refer to periods of order months or years; more closely spaced observations are needed in T Tauri stars before pushing a comparison further.

VII. CONCLUSIONS: ACTIVE PHENOMENA IN HERBIG Ae STARS?

The Herbig Ae stars are located at the junction of hot stars and of cool stars in the H-R diagram (Strom *et al.* 1972; Cohen and Kuhi 1979). One of them, AB Aur, better studied than the others, exhibits short-term spectral variability, which calls for an inhomogeneous structure of its expanding envelope. We have shown that, in AB Aur as in cool solar-type dwarfs, rotation modulates its observed features, here the Mg II terminal velocity. Also, like hot stars, AB Aur shows a prominent system of variable, narrow absorption components which are found not only in Fe II, but also in Ca II K (Simon, Boesgaard, and Praderie 1982; Praderie *et al.* 1983; Catala *et al.* 1985*b*).

In this paper, we have labeled as "activity" the rotationally modulated variability observed in AB Aur and presented a solar wind–inspired model, although cool, for its expanding envelope. We have also suggested that such a model can encompass the formation of Fe II components. Let us consider now whether such a model can be envisaged without posing difficulties for an intermediate-mass star as young as 10^6 yr (Cohen and Kuhi 1979).

As compared to many other young stars, AB Aur is a fairly rapid rotator: its $v \sin i$ of 75 km s^{-1} contrasts with those of T Tauri stars, which in the case where axial rotation rates have been determined are slow rotators ($v \sin i$ typically ≤ 25 km s^{-1}; see Vogel and Kuhi 1981), as well as three-fourths of the G stars in the young Orion Ic cluster ($v \sin i \approx 12$ km s^{-1}; Smith, Beckers, and Barden 1983). However, rotation rates have yet to be measured for the T Tauri stars with the most intense emission lines, and there exists a component of rapid rotators among the G stars in the Orion Ic cluster whose $v \sin i$ reaches 200 km s^{-1}.

The rotation/activity connection remains an open question in T Tauri stars. According to Vogel and Kuhi (1981), there is little correlation between activity level and rotation rate in T Tauri stars. Rotational modulation of chromospheric or coronal emission features has not been reported, except for fragmentary evidence in RU Lup (Boesgaard 1984). Periodic light variations have recently been discovered in some weak-emission T Tauri stars (Schaefer 1983; Rydgren and Vrba 1983; Vrba *et al.* 1985) and attributed to rotational modulation by large spots on stars which happen to be rapid rotators (e.g., $P = 1.9$ days for V410 Tau). In AB Aur, though, no light variations are observed simultaneous with the spectral variability we report here, to the level of 0.02 mag. For AB Aur we do not need spots such as those invoked (Rydgren and Vrba 1983; Herbst, Holtzman, and Klasky 1983) to account for the episodic variations observed in some cooler Ae irregular variables; or photometric techniques do not detect spots in hotter stars because of smaller contrast relative to the photosphere; or simply those spots do not develop in the hotter of the Herbig stars, as suggested by Finkenzeller and Mundt (1984, their Fig. 4).

The hypothesis that activity phenomena are of magnetic origin in T Tauri stars receives more and more attention. Their high levels of activity and the difficulty of providing the energy required to drive such activity, except by external causes such as accretion, led Gershberg (1982) to conjecture that strong magnetic fields in T Tauri stars on the one hand are responsible for the patchy aspect of the stellar surface ("spots," which at that time had not yet been observationally confirmed), and on the other hand modify the normal regime of radiation output over spots. For Gershberg, the magnetic field is most likely fossil, but it could also be dynamo-generated, thereby providing the common link between activity in T Tauri, UV Ceti, and other active stars.

Recently, Simon, Herbig, and Boesgaard (1985) have established the time decay of activity among main-sequence F–G stars with ages between $t = 10^8$ and $10^{9.5}$ yr. They find that ultraviolet activity "saturates" in a plateau for the youngest main-sequence stars, while the T Tauri stars lie one to three orders of magnitude above this plateau. Introducing the Rossby number (Ro $= P/\tau_c$, with τ_c = turnover time for convective elements at a significant depth in the convective zone), they show that this parameter correlates well with all activity signatures, as was earlier demonstrated by Noyes *et al.* (1984) for Ca II, Mangeney and Praderie (1984) for X-rays, and by Vilhu (1984). They also note that T Tauri stars should be characterized by either long τ_c or very short P. This picture explicitly assumes that the magnetic field responsible for activity phenomena is generated with the stars' subphotospheric convective envelopes.

AB Aur brings a new element in this chain. Since the star is of type A and is located near the main sequence in the H-R diagram, the activity signatures have evolved relative to what they are in solar-type pre–main-sequence stars, but, as recalled above, one finds definite emission lines as well as wind profiles. As we stated earlier, there is no paradox in calling the observed variability of V_s(Mg II) an indication of activity, inasmuch as this variability is related to the rotation period, and we have conjectured that rotation, and hence a dynamo-generated magnetic field, controls the observed activity phenomena. However, a question arises of whether there exists a deep enough convective zone in the Ae stars to insure that an effective dynamo mechanism can operate. We argue (1) that the evolutionary tracks toward the main sequence are not in the ultimate state of refinement, especially for the massive and intermediate-mass pre–main-sequence stars; and (2) that if Mangeney and Praderie (1984) are right in their correlation between X-ray luminosity and the Rossby number all along the main sequence, then there is no fundamental distinction between the activity of solar-type and hot stars. An ad hoc and less appealing alternative is that the magnetic field is fossil in young pre–main-sequence A-type stars like AB Aur.

Let us point out that AB Aur, like the T Tauri stars studied by Vogel and Kuhi (1981) and the Orion Ic G stars (Smith, Beckers, and Barden 1983), does not obey the relationship for decay of activity (expressed, for instance, by the rotation rate Ω) versus age t established by Skumanich (1972). If this $t^{-1/2}$ relationship is applicable to stars as massive as 3 $M_\odot$, and if it applies to young stars, the rotation period of AB Aur should be $\sim$9 hr (assuming $t = 10^6$ yr), instead of 45 hr found here. This large discrepancy with Skumanich's relation points toward the Herbig stars belonging above the "saturated" plateau of activity versus age, as is the case for the T Tauri and Orion Ic stars. It most likely contains the key to the global problem of magnetic field generation and magnetic field plus wind braking in these very young stars.

We are grateful to the *IUE* project scientist, Dr. Yoji Kondo, and to the staff of the GSFC and VILSPA *IUE* stations, and especially A. Talavera, for their efficient assistance. E. Legrand and P. Bénard contributed to the study of the Fe II lines during a stay at Meudon Observatory in spring 1984, and we thank them for their thorough work. We acknowledge fruitful discussions with P. Felenbok, J. Czarny, and A. Talavera, who participated in the coordinated campaign 1982, as well as J. M. le Contel, J. C. Valtier, J. P. Sareyan, and P. Morel. We also thank W. Herbst, who kindly undertook photometric observations of AB Aur during the 1984 *IUE* observations. F. P. and C. C. had inspiring discussions with A. Mangeney. T. S. gratefully acknowledges the support of NASA grant NAG 5-146.

REFERENCES

Ake, T. B. 1982, *IUE NASA Newsletter*, No. 19, p. 37.
Allen, D. A. 1973, *M.N.R.A.S.*, **161**, 145.
Baade, D. 1984, *Astr. Ap.*, **135**, 101.
Beals, C. S. 1951, *Publ. Dom. Ap. Obs. Victoria*, **9**, 1.
Boesgaard, A. M. 1984, *A.J.*, **89**, 1635.
Boesgaard, A. M., and Simon, T. 1984, *Ap. J.*, **277**, 241.
Brown, D. N., Shore, S. N., and Sonneborn, G. 1985, *A.J.*, **90**, 1354.
Burlaga, L. F. 1984, *Space Sci. Rev.*, **39**, 255.
Cassatella, A. 1984, private communication.
Catala, C. 1984*a*, in *Proc. 4th European IUE Conf.* (Rome) (ESA SP, No. 218), p. 227.
———. 1984*b*, in *Proc. Colloquium on nearby Molecular Clouds, 8th European IAU Regional Meeting* (Toulouse), ed. G. Serra (Springer Lecture Notes in Phys., No. 237), p. 198).
Catala, C., Czarny, J., Felenbok, P., and Praderie, F. 1985*a*, *Astr. Ap.*, in press.
Catala, C., Felenbok, P., Czarny, J., Talavera, A., and Boesgaard, A. 1985*b*, *Ap. J.*, submitted.
Catala, C., Kunasz, P. B., and Praderie, F. 1984, *Astr. Ap.*, **134**, 402.
Catala, C., and Talavera, A. 1984, *Astr. Ap.*, **140**, 421.
Cohen, M. 1980, *M.N.R.A.S.*, **191**, 499.
Cohen, M., and Kuhi, L. V. 1979, *Ap. J. Suppl.*, **41**, 743.
Crivellari, L., and Morossi, C. 1982, *Astr. Ap.*, **106**, 332.
Davis, R., Strom, K. M., and Strom, S. E. 1983, *A.J.*, **88**, 1644.
Feigelson, E. D., and De Campli, W. M. 1981, *Ap. J. (Letters)*, **243**, L89.
Felenbok, P., Praderie, F., and Talavera, A. 1983, *Astr. Ap.*, **128**, 74.
Finkenzeller, U. 1983, *Astr. Ap.*, **124**, 157.
———. 1985, *Astr. Ap.*, **151**, 340.
Finkenzeller, U., and Jankovics, I. 1984, *Astr. Ap. Suppl.*, **57**, 285.

Finkenzeller, U., and Mundt, R. 1984, *Astr. Ap. Suppl.*, **55**, 109.
Franco, M. L., Crivellari, L., Molaro, P., Vladilo, G., Ramella, M., Morossi, C., Allochio, C., and Beckman, J. E. 1984, *Astr. Ap. Suppl.*, **58**, 693.
Garrison, L. M., and Anderson, C. M. 1977, *Ap. J.*, **218**, 438.
Gershberg, R. E. 1982, *Astr. Nach.*, **303**, 251.
Gry, C., Lamers, H. J. G. L. M., and Vidal-Madjar, A. 1984, *Astr. Ap.*, **137**, 29.
Herbig, G. H. 1960, *Ap. J. Suppl.*, **4**, 337.
Herbst, W., Holtzman, J. A., and Klasky, R. S. 1983, *A.J.*, **88**, 1648.
Holm, A., Bohlin, R. C., Cassatella, A., Ponz, D. P., and Schiffer, F. H. 1982, *Astr. Ap.*, **112**, 341.
Kunasz, P. B., and Praderie, F. 1981, *Ap. J.*, **247**, 949.
Lamers, H. J. G. L. M., Gathier, R., and Snow, T. P. 1982, *Ap. J.*, **158**, 186.
Mangeney, A., and Praderie, F. 1984, *Astr. Ap.*, **130**, 143.
Merrill, P. W., and Burwell, C. G. 1933, *Ap. J.*, **77**, 103.
Mullan, D. J. 1984, *Ap. J.*, **283**, 303.
Mundt, R. 1984, *Ap. J.*, **280**, 749.
Mundt, R., and Giampapa, M. S. 1982, *Ap. J.*, **256**, 156.
Noyes, R. W., Hartmann, L., Baliunas, S. L., Duncan, D. K., and Vaughan, A. H. 1984, *Ap. J.*, **279**, 763.
Praderie, F., Catala, C., Czarny, J., and Felenbok, P. 1984*a*, in *Space Research Prospects in Stellar Activity and Variability*, ed. A. Mangeney and F. Praderie (Meudon: Paris Obs.), p. 265.
Praderie, F., Simon, T., Boesgaard, A. M., Felenbok, P., Catala, C., Czarny, J., and Talavera, A. 1984*b*, in *Proc. NASA Workshop on The Origin of Radiative Heating/Momentum in Hot Stars*, ed. A. B. Underhill and A. G. Michalitsianos (NASA Conf. Pub., No. 2358), p. 81.
Praderie, F., *et al.* 1983, in *Proc. 2d France Japan Seminar on Active Phenomena in the Outer Atmosphere of the Sun and Stars*, ed. J. C. Pecker and Y. Uchida (Paris: Paris Obs.), p. 132.
Praderie, F., Talavera, A., Felenbok, P., Czarny, J., and Boesgaard, A. M. 1982, *Ap. J.*, **254**, 658.
Praderie, F., Talavera, A., and Lamers, H. J. G. L. M. 1980, *Astr. Ap.*, **86**, 271.
Rydgren, A. E., and Vrba, F. J. 1983, *Ap. J.*, **267**, 191.
Sanford, R. F., and Merrill, P. W. 1958, *Pub. A.S.P.*, **70**, 602.
Schaefer, B. E. 1983, *Ap. J. (Letters)*, **266**, L45.
Simon, T., Boesgaard, A. M., and Praderie, F. 1982, *Bull. AAS*, **14**, 879.
Simon, T., Herbig, G., and Boesgaard, A. M. 1985, *Ap. J.*, **293**, 551.
Skumanich, A. 1972, *Ap. J.*, **171**, 565.
Slettebak, A., and Snow, T. P., Jr. 1978, *Ap. J. (Letters)*, **224**, L127.
Smith, M. A., Beckers, J. M., and Barden, S. C. 1983, *Ap. J.*, **271**, 237.
Smith, M. A., Fitch, W. S., Africano, J. L., Goodrich, B. D., Halbedel, W., Palmer, L. H., and Henry, G. W. 1984, *Ap. J.*, **282**, 226.
Strom, S. E., Strom, K. M., Yost, J., Carrasco, L., and Grasdalen, G. 1972, *Ap. J.*, **173**, 353.
Talavera, A., Catala, C., Crivellari, L., Czarny, J., Felenbok, P., and Praderie, F. 1982, in *Proc. 3d European IUE Conf.* (Madrid) (ESA SP, No. 176), p. 99.
Vaughan, A. H., Baliunas, S. L., Middlekoop, F., Hartmann, L., Mihalas, D., Noyes, R. W., and Preston, G. W. 1981, *Ap. J.*, **250**, 276.
Vilhu, O. 1984, *Astr. Ap.*, **133**, 117.
Vogel, S. N., and Kuhi, L. V. 1981, *Ap. J.*, **245**, 960.
Vrba, F. J., Rydgren, A. E., Zak, D. S., and Schmelz, J. T. 1985, *A.J.*, **90**, 326.
Worden, S. P., Schneeberger, T. J., Kuhn, J. R., and Africano, J. L. 1981, *Ap. J.*, **244**, 520.
York, D. G., Vidal-Madjar, A., Laurent, C., and Bonnet, R. 1977, *Ap. J. (Letters)*, **213**, L61.

F. PRADERIE and C. CATALA: Département de Recherche Spatiale, Observatoire de Paris, Section de Meudon, F 92195 Meudon Principal Cedex, France

T. SIMON and A. MERCHANT BOESGAARD: Institute for Astronomy, University of Hawaii, 2680 Woodlawn Drive, Honolulu, HI 96822

THE ASTROPHYSICAL JOURNAL, 308:791–804, 1986 September 15

SHORT-TERM SPECTRAL VARIABILITY IN AB AURIGAE: CLUES FOR ACTIVITY IN HERBIG Ae STARS. II. THE Ca II K LINE

CLAUDE CATALA,[1,2] PAUL FELENBOK,[1,3] AND JEAN CZARNY[3,4]
Observatoire de Paris, Section de Meudon
ANTONIO TALAVERA[4]
Astronomy Division ESTEC, Villafranca Tracking Station
AND
ANN MERCHANT BOESGAARD[4]
Institute for Astronomy, University of Hawaii
Received 1985 October 28; accepted 1986 March 11

ABSTRACT

The Herbig Ae star AB Aur (A0ep) was monitored with the Canada-France-Hawaii 3.6 m and the Observatoire de Haute-Provence 1.52 m telescopes in the Ca II K line, for six nights in 1982 October. Some of the 39 recorded spectra were simultaneous with ultraviolet spectra obtained with *IUE* during a round-the-clock observation described in Paper I of this series.

We find that the Ca II K line is variable and modulated with a period of 32 ± 4 hours, corresponding to the estimated rotation period of the star. We also report the appearance on some of the spectra of blueshifted absorption components and of a small emission component near the core of the stellar line. In addition, a redshifted emission component appears on most of the spectra. The Ca II H line and the Hε line, observed at the Canada-France-Hawaii telescope, are also variable and their variations seem correlated with that of the Ca II K line.

We interpret the 32 hour period found in the Ca II K stellar line as due to a rotational modulation. The qualitative model of fast and slow streams alternating along the line of sight, presented in Paper I, is analyzed in more detail, and we interpret the difference between the 45 hour period found in the Mg II data (Paper I) and the 32 hour period in the Ca II data as due to a differential rotation in the envelope of the star. The existence of this differential rotation allows us to estimate upper limits for the magnetic field and the Alfvén radius in the envelope of AB Aur, as well as for the rate of angular-momentum loss. It is concluded that this angular-momentum loss might play a major role in the evolution of the star.

The blueshifted absorption components can be the results of puffs in some of the streams leaving the star's surface, or they can be formed in the so-called corotating interaction regions, where the fast and the slow streams merge. The core emission component is interpreted as due to motions near the stellar pole, and the redshifted emission component simply as due to the extension of the line emitting region.

Subject headings: stars: emission-line — stars: individual — stars: rotation — stars: spectrum variables

I. INTRODUCTION

In the 25 years since Herbig's pioneering work (Herbig 1960), his original conjectures that the Herbig Ae/Be stars are pre–main-sequence (PMS) objects of intermediate mass (2–7 $M_\odot$) and higher mass counterparts of T Tauri stars have been confirmed (Strom *et al.* 1972; Cohen and Kuhi 1979; Finkenzeller and Mundt 1984).

The Herbig Ae/Be stars can be divided into three subclasses, according to their Hα profiles: double-peak emission, single-peak emission, or P Cygni profile (Finkenzeller and Mundt 1984). It has been shown recently that the stars of the "P Cygni" subclass exhibit striking similarities in several other lines, which suggests a similar structure for their envelopes (Catala *et al.* 1986). Thanks to this similarity, AB Aur, the brightest member of the P Cygni subclass, can be considered as representative of the whole subclass. Quantitative interpretations of Mg II and C IV resonance lines in AB Aur (Catala, Kunasz, and Praderie 1984; Catala 1984; Catala and Talavera 1984) and of the first lines of the hydrogen Balmer series (Catala and Kunasz 1986) were carried out under the assumptions of spherical symmetry and stationarity and led to a model including a stellar wind and a deep expanding chromosphere at the base of the wind.

However, the short-term spectral line variability which has been observed for T Tauri stars (Schneeberger, Worden, and Wilkerson 1979; Mundt and Giampapa 1982; Boesgaard 1984) and for Herbig Ae/Be stars (Praderie *et al.* 1982; Finkenzeller 1983; Praderie *et al.* 1984; Thé *et al.* 1985) strongly suggests that their winds might be neither spherically symmetric nor stationary, but that strong inhomogeneities could be present in their envelopes. Understanding the causes of this variability is not only interesting in itself, but will also provide information about the physical processes at work in these atmospheres. It is then important to study in more detail the short-term variability in PMS stars.

Being the brightest Herbig Ae star of the northern hemisphere, AB Aur (HD 31293, A0ep, $m_V = 7.2$) has been chosen

[1] Visiting Astronomer, Observatoire de Haute-Provence, operated by the Centre National de la Recherche Scientifique of France.
[2] Unité de Recherche Associée au CNRS 264.
[3] Unité de Recherche Associée au CNRS 812.
[4] Visiting Astronomer, Canada-France-Hawaii Telescope, operated by the National Research Council of Canada, the Centre National de la Recherche Scientifique of France, and the University of Hawaii.

for a detailed study of its short-term variability. An important observation campaign, involving the *International Ultraviolet Explorer* (*IUE*), the Canada-France-Hawaii 3.6 m telescope, the 1.52 m telescope at the Observatoire de Haute-Provence (OHP), France, and two photometric telescopes (0.6 m at Pico de la Veleta, Spain, and 1 m at San Pedro Martir, Mexico), was carried out in 1982 October. Its goal was to monitor the star for 40 hours in the ultraviolet range and for five nights in the Ca II line and photometrically, with a certain time interval of total simultaneity between the *IUE* and the ground-based observations. Preliminary results of the whole campaign have been presented in Praderie *et al.* (1984). In addition to the 1982 October campaign, the star has been observed intermittently in the UV range for 150 hours in 1984 November with *IUE*. The detailed results of the two sets of *IUE* observations have been presented and discussed in Praderie *et al.* (1986, hereafter Paper I), along with the results of the photometric monitoring. The striking conclusion of Paper I is that the maximum blueward shift of the Mg II resonance lines, called V_s(Mg II), varies periodically with a period of 45 hours, which can be interpreted as a rotational modulation, since available estimates of the projected rotation velocity (v sin i), combined with estimates of the stellar radius, lead to a rotation period of the same order of magnitude.

In Paper I, a model involving an alternation of slow and fast streams rotating with the star has been suggested to account for such a modulation. The proposed model for AB Aur is directly inspired by the structures well known in the solar wind (Burlaga 1983, 1984). Indirect evidence of the presence of surface inhomogeneities can be seen in this alternation of slow and fast streams.

The present paper aims at describing and discussing the results of the Ca II K line observations during the 1982 October campaign. The total span of these observations was 130 hours, i.e., about three or four rotation cycles. We can then expect to derive valuable information from a careful analysis of these data. Moreover, since the Ca II line is formed in a very localized region, at the base of the wind (Catala *et al.* 1986), while the blue edge of the Mg II resonance lines is formed farther out (Paper I; Catala, Kunasz, and Praderie 1984), we can also expect to investigate a possible radial dependence of the modulation.

Section II describes the telescopes and the instrumentation used, as well as the reduction techniques. The procedure followed to analyze the line variations is detailed in § III. In § IV the results are discussed and compared with those derived from the Mg II data, in the framework of the model proposed in Paper I. A summary of the results and general conclusions are given in § V.

II. OBSERVATIONS

The observations of the Ca II K line of AB Aur during the 1982 October campaign were made using the coudé equipment of the Canada-France-Hawaii 3.6 m telescope at Mauna Kea and of the OHP 1.52 m telescope. The log of these observations is given in Table 1. Only six spectra were recorded at the Canada-France-Hawaii Telescope (CFHT) owing to poor weather, while 33 spectra have been obtained at OHP.

At the CFH 3.6 m telescope, the detector was a cooled RL 1872 f/30 Reticon with 15 μm × 750 μm pixels. Some special optical features of the coudé spectrograph include a specially coated blue-sensitive mirror train, an image slicer coated for the blue, and a mosaic grating consisting of four Bausch and Lomb 830 groove mm^{-1} gratings. A region of about 68 Å was covered with a spectral resolution of 0.12 Å. Three of the spectra obtained at CFHT are contaminated by a periodic pattern (4 pixel period) because of an inefficient operation of the Reticon cooling system. This pattern has been removed from the data by filtering the highest frequencies. This filtering results in a loss of resolution, and the filtered spectra are not as good as the unaffected ones, but their quality is still acceptable. All reduction techniques have been fully described in previous papers (Felenbok, Praderie, and Talavera 1983; Boesgaard and Tripicco 1986).

At the OHP 1.52 m telescope, the detector was an electronographic Lallemand camera, equipped with a S-11 photocathode. We used the echelle spectrograph in its multiorder configuration, with a Carpenter prism to separate the orders. Because of the smaller size of the telescope, the nonoptimization of the optical surfaces to the blue wavelengths, the poor transmission of the OHP atmosphere at these wavelengths, and the lower sensitivity of the detector, the OHP spectra are considerably noisier than the CFH ones: the mean signal-to-noise ratio obtained at CFHT is 110, while the mean signal-to-noise ratio obtained at OHP is only 20. Moreover, in order to keep a good temporal resolution which was our main purpose, the exposure times could not be too much increased. For these reasons, only a small amount of information can be extracted from the OHP individual spectra. However, their interest lies in their great number, and, as will be shown below, many results can be obtained from this series. All the OHP spectra were scanned with a PDS microdensitometer at the Institut d'Optique (Orsay, France). This scanning resulted in a two-dimensional image for each spectrum, on which the order containing the Ca II K line covered several rows. After a correction for the curvature of the order, the different rows composing this order were averaged. Then the data reduction procedure was the same as the one used for the Reticon spectra. The scanned OHP spectra cover a region of about 48 Å, with a spectral resolution of 0.22 Å.

For the CFHT observations, comparison spectra obtained on the same night as the stellar spectra have been used to provide wavelength scale and reference points. At OHP, the comparison spectra were recorded on the same plates as the stellar spectra.

The hydrogen Balmer lines have very extended wings in AB Aur, and the Ca II K line lies in the blue edge of the wing of Hϵ. The fluxes of the Ca II K spectra have been divided by the local continuum flux, defined by two points close to the Ca II K line, at 3920 and 3950 Å. We have thus removed any influence of possible Hϵ variations on the Ca II line.

III. DATA ANALYSIS

a) Overview of Line Profiles Based on the CFHT Spectra

Since the three best CFHT spectra (those unaffected by the contamination described in § II) have higher spectral resolution and higher signal-to-noise ratios, we present those profiles and analysis and use them as guidance for the interpretation of the longer series from OHP. Figure 1 shows the complete spectral region of the three best CFHT Reticon spectra revealing the Ca II K line and the complex profile of the Hϵ and Ca II H lines. Variations are clearly present in the strength and shape of both Ca II and Hϵ. The presence of absorption and emission components can be seen clearly. Table 2 contains the information on the various measurements made on the spectra

TABLE 1

LOG OF THE Ca II K OBSERVATIONS OF AB AUR

Date 1982 October	UT Midexposure	Telescope (cm)	Exposure Time (minutes)	Sequence Number in Figs 3 and 4	Observers[a]
25.....	22	152	60	1	
25.....	2318	152	70	1	
26.....	0025	152	60	1	
26.....	0130	152	60	1	
26.....	0231	152	60	1	
26.....	0334	152	60	1	
26.....	1019	360	121	2	Boesgaard, Lavery
26.....	1440	360	100	2	Boesgaard, Lavery
27.....	2018	152	83	3	
27.....	2132	152	60	3	
27.....	2234	152	60	3	
27.....	2337	152	60	3	
28.....	0040	152	60	3	
28.....	0132	152	60	3	
28.....	0245	152	60	3	
28.....	0347	152	60	3	
28.....	2002	152	105	4	
28.....	2128	152	60	4	
28.....	2230	152	60	4	
28.....	2333	152	60	4	
29.....	0035	152	60	4	
29.....	0137	152	60	4	
29.....	0239	152	60	4	
29.....	0348	152	72	4	
29.....	1234	360	60	5	Czarny, Talavera
29.....	2054	152	70	6	
29.....	2202	152	76	6	
29.....	2303	152	75	6	
30.....	0038	152	73	6	
30.....	0155	152	76	6	
30.....	0321	152	90	6	
30.....	1026	360	84	7	Czarny, Talavera
30.....	1209	360	63	7	Czarny, Talavera
30.....	1325	360	64	7	Czarny, Talavera
30.....	2125	152	90	8	
30.....	2257	152	90	8	
31.....	0032	152	90	8	
31.....	0221	152	88	8	
31.....	0346	152	73	8	

[a] Where no names are listed, observers were Catala and Felenbok.

of equivalent widths (W_λ), residual intensity (F/F_c), full width at half-maximum intensity (FWHM), and radial velocity in the geocentric frame (V_r) as measured at FWHM. Corrections of 19 and 10 km s^{-1} must be applied to these V_r values to convert them into, respectively, the heliocentric frame and the local standard of rest.

A very narrow absorption feature appears on all the CFHT spectra, at the position of both Ca II K and Ca II H lines. The width of this component is not larger than the instrumental width, and it can then be considered as interstellar (IS). The presence of this IS component has already been reported by Praderie *et al.* (1982) and Felenbok, Praderie, and Talavera (1983).

The Ca II K stellar line shows a range of variations of a factor of 2.5 in W_λ with values in the range 0.180–0.470 Å; it is the weakest on 1982 October 30, where the core appears to be partly filled in with emission. The effect of the variation due to the amount of emission in the core can be seen also in the F/F_c measurement. Also affected is the apparent width of the feature when that measurement is made at the half-intensity point, inasmuch as the half-intensity level is controlled by the amount of core emission; therefore, when the Ca II K absorption is weakest, the FWHM is largest. In addition, the velocity of the line bisector at the half-intensity level (V_r) is also affected by the variations in the emission and is redshifted most when the emission is strongest, i.e., the absorption is weakest (October 30). Thus we see that the variations in the measurable parameters of the Ca II K line are strongly influenced by the difference in the emission in the core.

While the Ca II K line is primarily photospheric absorption seen against the continuum, the Ca II H line is seen as an emission feature against the deep phosospheric absorption wing of Hϵ. One convenient way to compare the amount of emission in the two Ca II lines is to measure the residual intensity of the stellar line at the wavelength position where the IS features are, ignoring the IS absorption components themselves. We note that these values of F/F_c vary in phase for the two Ca II lines (Fig. 2*a*). There is a caveat relevant to the measurements of the line residual intensities: the IS Ca II K feature should always absorb the same proportion of flux. In fact, this proportion is the same on October 26 and 29 spectra, but is 6% weaker on October 30 spectrum. This difference is

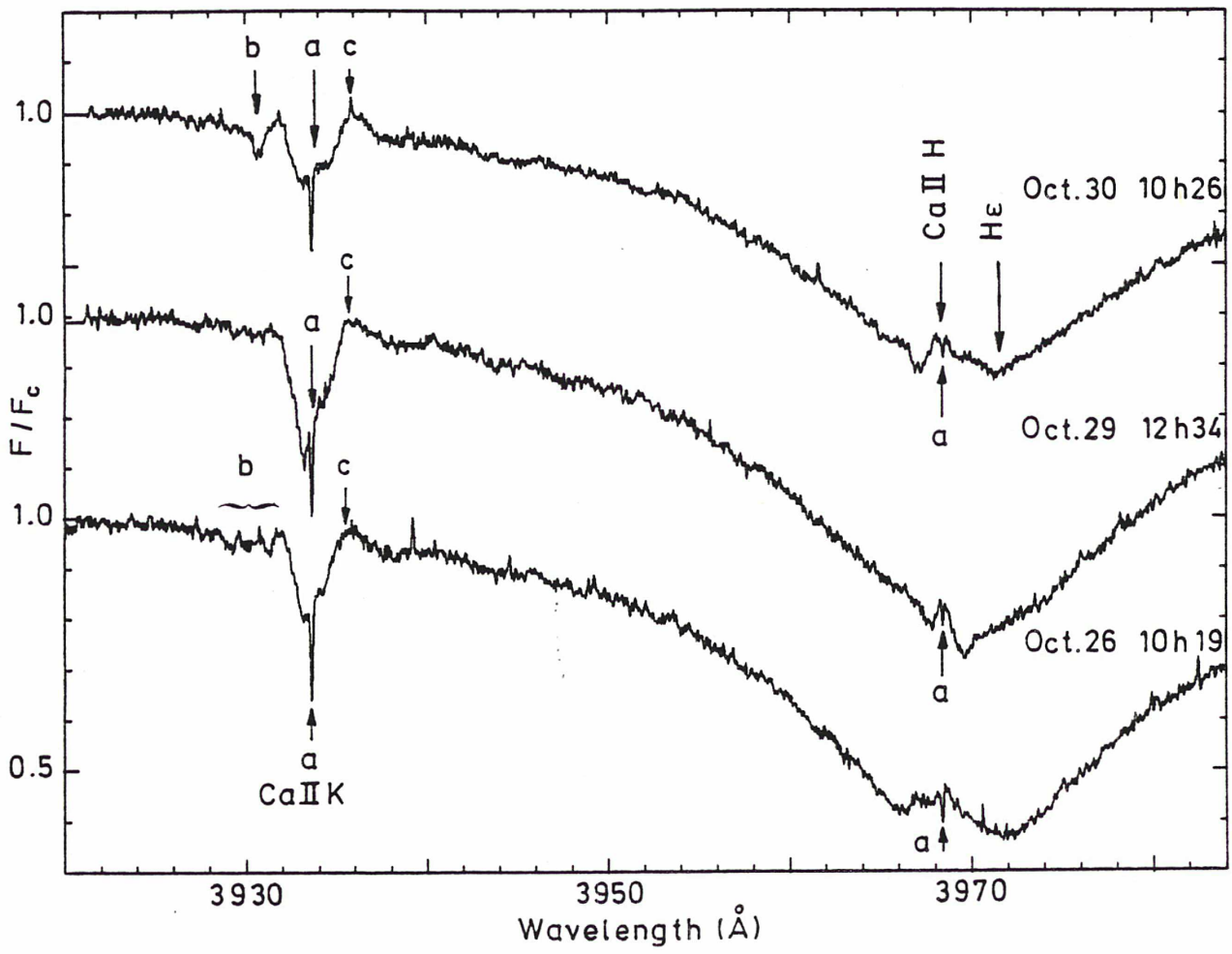

FIG. 1.—The three best CFHT spectra of the Ca II K, Ca II H, and Hε lines. The dates and universal times at midexposure are indicated. The spectra are in reduced units, and the wavelength scale is geocentric. (*a*) Interstellar component. (*b*) Blueshifted absorption components. (*c*) Redshifted emission.

TABLE 2

MEASURED PARAMETERS OF THE CFHT SPECTRA

FEATURE	PARAMETER	1982 Oct 26	1982 Oct 29	1982 Oct 30
Main Ca II K line absorption	W_λ (Å)	0.249	0.466	0.184
	FWHM (Å)	1.58	1.73	2.19
	F/F_c	0.83	0.73	0.89
	V_r (km s^{-1})	0	−4	+13
Redward Ca II K emission	W_λ (Å)	0.041	0.043	0.053
	FWHM (Å)	1.15	1.18	1.15
	F/F_c	1.04	1.04	1.05
	V_r (km s^{-1})	+189	+194	+192
Ca II K absorption components	W_λ (Å)	0.013, 0.013, 0.018	...	0.040
	FWHM (Å)	0.14, 0.24, 0.17	...	0.58
	F/F_c	0.97, 0.97, 0.96	...	0.94
	V_r (km s^{-1})	−170, −253, −330	...	−217
Ca II K core emission[a]	F/F_c	0.86	0.79	0.91
Ca II H core emission[a]	F/F_c	0.47	0.43	0.56
Hε at centerline[b]	F/F_c	0.40	0.37	0.51
Hε absorption component	V_r (km s^{-1})	−327	−196	−222

[a] Measured at the wavelength of the IS feature at the F/F_c level as if there were no IS absorption.
[b] Centerline found from reflecting the line profile around its bisector to achieve best match in the wing.

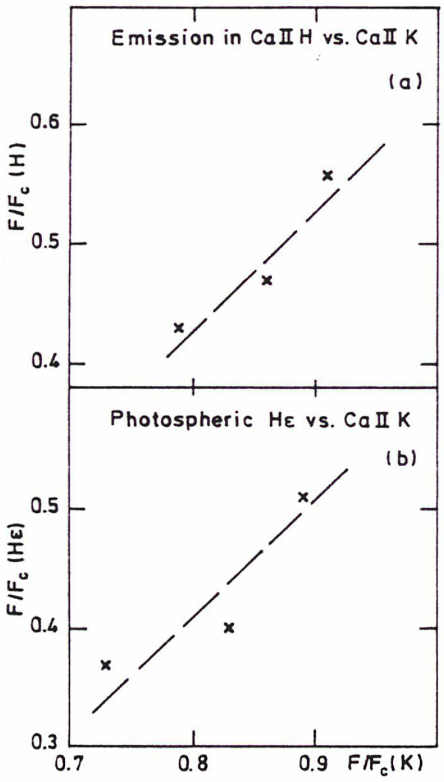

FIG. 2.—Residual intensity measurements in Ca II H and K and Hε for the three best CFHT spectra. (*a*) Comparison of the reduced intensity of the core emission component in Ca II H and Ca II K. The residuals are measured at the wavelength of the interstellar feature, ignoring the interstellar component itself; a smooth line has been drawn at the top of that feature in order to represent the stellar profile. (*b*) Photospheric Hε compared with Ca II K. The Hε residual was measured at the centerline determined by the best match of the Hε wings. The Ca II K residual corresponds to the deepest point in the K line absorption.

probably due to the Reticon temperature rise mentioned in § II, which could have begun at the end of the October 30 1026 UT exposure.

On all three CFHT spectra a redshifted emission feature is clearly visible. This feature is remarkably constant in strength and position. Individual measurements are given in Table 2. Such a feature was not present in another series of observations obtained in 1980 October (Praderie *et al.* 1982).

Three narrow blueshifted absorption components are present at Ca II K on 1982 October 26. The FWHM values are about 15 km s^{-1}, and the absorption is only about 3%–4% of the continuum, with equivalent widths of about 15 mÅ. These components have blueshifts of −170, −253, and −330 km s^{-1}. On that same spectrum, there is an absorption component at the highest Ca II K blueshift in the Hε profile. It has a V_r value of −327 km s^{-1} from the Hε centerline defined by matching the wings of the line. In the Hε profile, there is a hint of the middle component (−253 km s^{-1} at Ca II K) just shortward of the interstellar Ca II H narrow absorption in the Hε core. This is reminiscent of the 1980 October series, where on one night there was a strong blueshifted component appearing at Ca II K and in all the Balmer lines that were observed on those spectrograms.

The 1982 October 26 CFHT spectrum was taken simultaneously with two of the *IUE* spectra described in Paper I. We note that the maximum blueshift in the Ca II K components on this spectrum (−311 km s^{-1} in the heliocentric frame) is lower than the maximum blueshift in the Mg II resonance lines observed by *IUE* exactly at the same time (−450 km s^{-1} in the heliocentric frame). Since the Ca II K line is formed closer to the star than the blue edge of the Mg II lines (Catala *et al.* 1986), and since the problems of variability are overcome by the simultaneity of the observations, we have here a further proof that the wind of AB Aur is accelerated outward, at least up to the region where the blue edge of the Mg II lines is formed (> 5 stellar radii).

There are no obvious blueward absorption components at Ca II on October 29, but a single, stronger feature emerges on the October 30 spectrum. Its equivalent width of 40 mÅ is comparable to the sum of the three absorptions on October 26, as is its FWHM of 44 km s^{-1} similar to the sum of the earlier three. This feature has a velocity of −217 km s^{-1}, which is remarkably similar to that of the Hε component at −222 km s^{-1} on the same spectrum.

Finally, the amount of absorption in the main Ca II K feature and the Hε feature also seem to vary together, and both are weakest on the October 30 spectrum (Fig. 2*b*).

b) General Behavior of the Ca II K *Line*

In addition to the results described in the previous section, a great amount of information can be gained by the analysis of the long time series taken at both CFHT and OHP. Figure 3 gives a general view of the Ca II K line series, observed from October 26 to October 31. The three best CFHT spectra are presented in this figure. They correspond to three different nights. The OHP spectra have been added together on a one-night basis, so that each OHP spectrum displayed in Figure 3 represents an average over one night. The spectra are normalized to the continuum level. The difference in the Earth velocity with respect to the Sun, projected onto the line of sight, between the beginning and the end of the observation interval, is only 2 km s^{-1}. Several very interesting features appear on this figure.

The Ca II K line exhibits an asymmetric profile variable in several respects: intensity, shape, and position. The global position of the stellar line can be easily appreciated in Figure 3 thanks to the immobile IS component. Because of the low resolution and the low signal-to-noise ratio of the OHP spectra, this component does not appear clearly on some of them. The same type of Ca II K line variability in intensity, shape, and position was reported by Praderie *et al.* (1982), on the basis of five spectra obtained on five consecutive nights. We further note variations of larger amplitude on a longer time scale for the intensity in the line: the residual intensity at the bottom of the line was about 0.55 in 1980 October and about 0.85 in 1982 October.

The general behavior of the Ca II K line with time is better seen in Figure 4, which shows isointensity curves in the wavelength-time plane. The lower threshold has been taken as 0.89, i.e., the points where $F/F_c \leq 0.89$ are white in Figure 4. This threshold is the one leading to the most obvious contrast in the variations. The gaps in the observations are represented by white rows, but their real duration has not been taken into account. Figure 4 shows that the global position of the Ca II stellar line is moving back and forth in the geocentric frame all along the observation interval. We can also guess "by eye" a possible periodic behavior for this motion. However, it seems that the blue and the red boundaries of the line do not behave

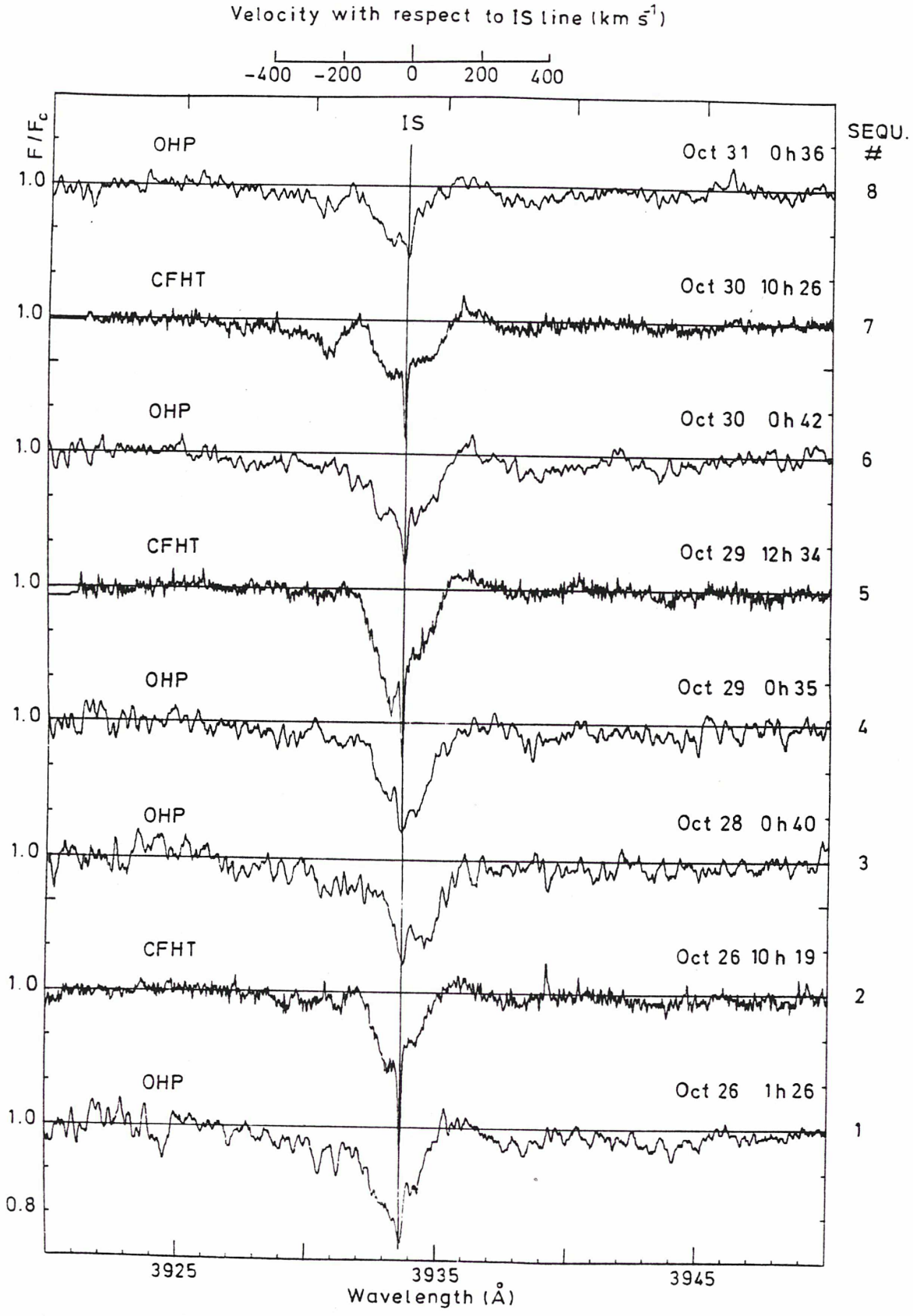

FIG. 3.—General view of the Ca II K line series. The OHP spectra have been co-added on a one-night basis. All the spectra are in reduced units, and the wavelength scale is geocentric. The date and universal time at midexposure are indicated for each spectrum. The interstellar component appears very clearly on the CFHT spectra. Note the asymmetry of the stellar line and its variations with respect to the interstellar component.

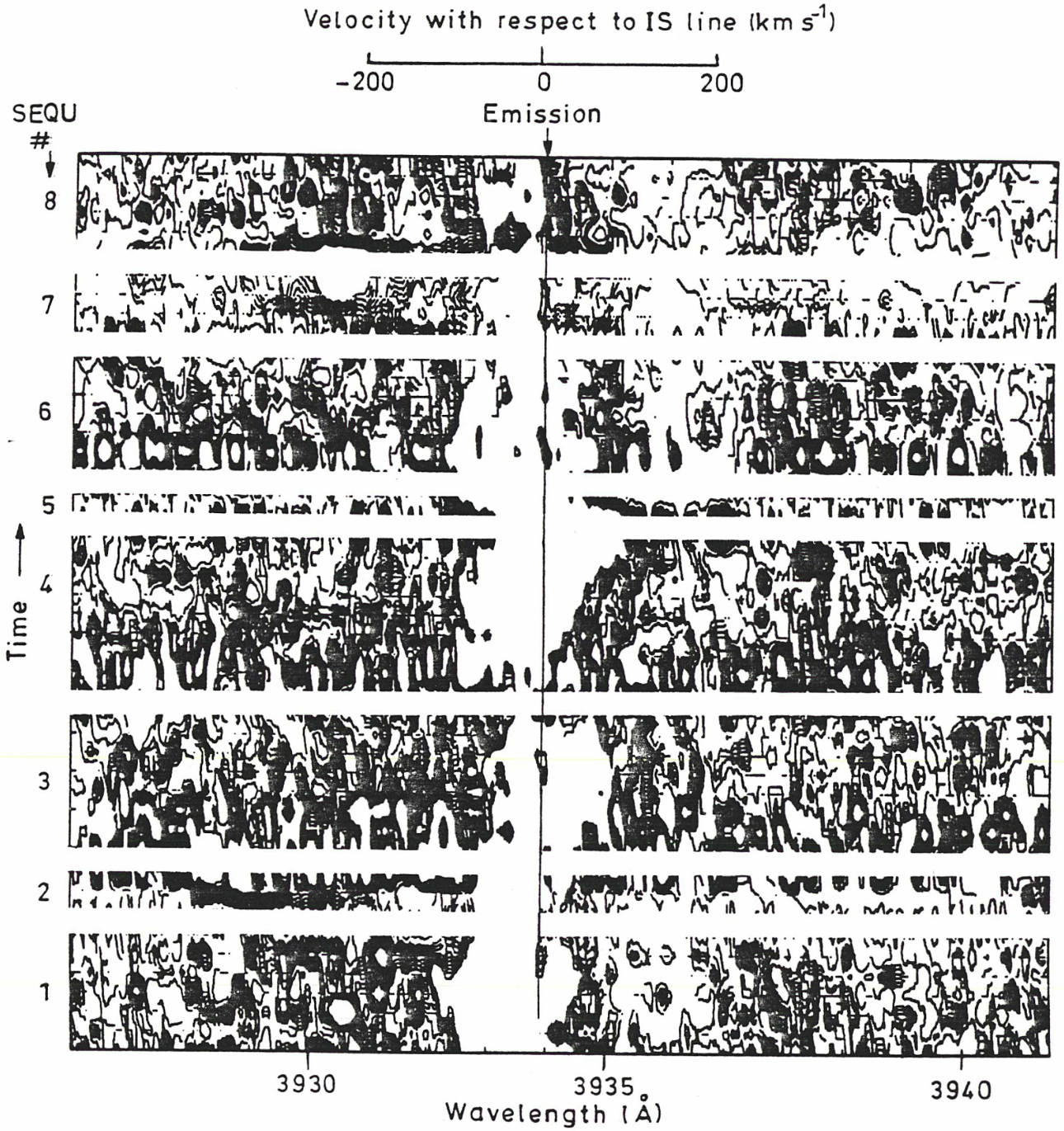

FIG. 4.—Time variation of the stellar Ca II K line. This figure represents isointensity curves in the wavelength-time plane. The lower threshold is 0.89, and the spectra are in reduced units. The wavelength scale is geocentric. On the time axis, no care has been taken to represent the real duration of the gaps between the observations. Note the striking variation of the stellar line, and its suggested periodicity. Note also the sporadic presence near the line core of an emission component, which does not seem to be affected by the general motion of the line.

exactly in the same way, i.e., that the line is not simply moving without changing shape. The variations of the blue and the red sides do not show the same characteristic. For example, between October 28 2002 UT and October 29 0348 UT (sequence 4), the blue side remains more or less at the same wavelength, while the red side is moving toward the red. This is not surprising, since the two sides are formed in different regions in the stellar atmosphere, because of the expansion. A more detailed analysis of these variations will be presented in § III*c*.

In addition to the blue absorption components appearing in the CFHT spectra described in § III*a*, one or several absorption components show up on some of the other spectra. These components are shown in Figure 5, where the corresponding individual spectra are displayed.

We also note the presence in 14 spectra of a small emission

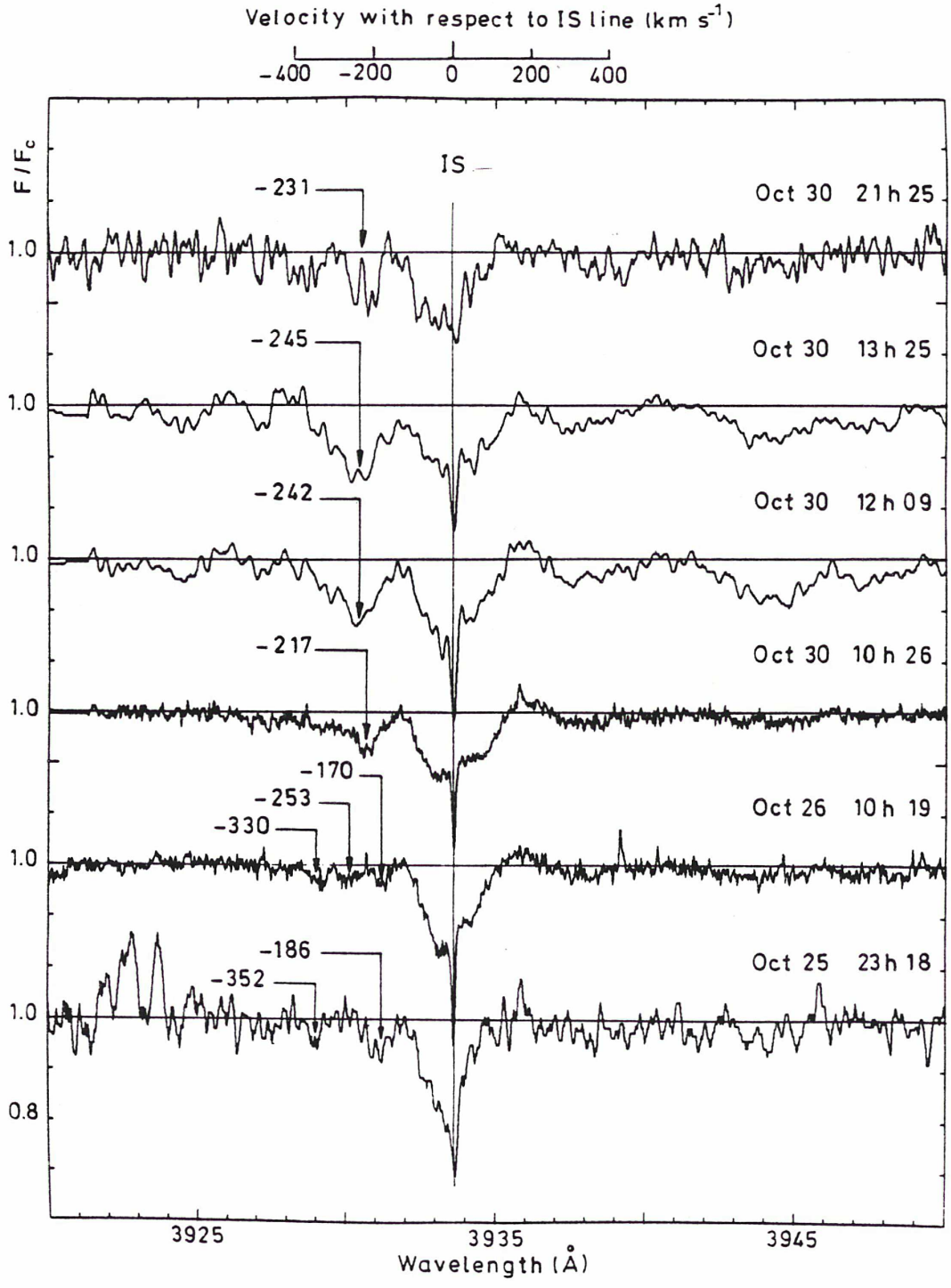

FIG. 5.—Individual spectra showing blueshifted absorption components. The spectra are in reduced units. The wavelength scale is geocentric, but the velocities indicated on the figure are with respect to the interstellar line.

component near the core of the stellar line, redshifted by 25 ± 4 km s^{-1} with respect to the interstellar component. This red emission component is easily seen in Figure 4. The striking feature is that it is not affected at all by the general motion of the stellar line: this emission component remains exactly at the same velocity all along the observation interval (to within 4 km s^{-1}). We have found no regularity in its appearance and disappearance. A similar emission component had also been noted in 1980 October by Praderie *et al.* (1982), but the latter was blueshifted. We will come back to the possible interpretation of this feature in § IV.

Finally, the red wing emission component described in § III*a*, located at about 190 km s^{-1}, appears in most of the spectra, always at the same velocity. We note that it appears in all the spectra with high signal-to-noise ratio and that the signal-to-noise ratio of some of the OHP spectra is too low for

us to state unambiguously the absence or the presence of such a component. We are then tempted to say that it could be present at each time step in 1982 October. But clearly, further observations are needed to reinforce this conclusion.

c) *Periodicity of the* Ca II K *Line Variations*

Since Figure 4 suggests a possible periodic behavior of the data, we have carried out a quantitative treatment in order to extract a period, if there is one. This analysis has been performed over the whole set of individual spectra (39). We first had to choose a quantity characterizing the line at each time step. This quantity had to be sensitive to the variations that we can see in Figure 4. The residual intensity at the bottom of the line, for example, is a bad choice, because it is affected by the presence of the interstellar component, which is thought not to vary. Since the Ca II K line is probably formed at the base of the wind of AB Aur, the red boundary of the line can be affected by an emission component formed in the lateral parts of the envelope, possibly over a large solid angle. Thus, the red boundary of the line, formed in a region "integrating" the variations, is expected to show only smoothed variability. The blue boundary of the line is formed in the region of the atmosphere projected on the stellar disk. This region encompasses only a small solid angle, so it is expected to exhibit the most obvious variations. We have thus chosen to analyze in detail the blue boundary of the stellar line and have determined for each individual spectrum the wavelength in the blue wing of the line where the reduced intensity is 0.89 (this is the value corresponding to the lower threshold used in Fig. 4). This has given us a series of 39 values, $\lambda_b(t_i)$, for which we have carried out a Fourier analysis.

This analysis consisted of a deconvolution of the Fourier power spectrum of our data, $\lambda_b(t_i)$ with the Fourier power spectrum of the observation window (a function equal to unity when observations are available and to zero when they are not). The deconvolution was performed by an overrelaxed iterative procedure imposing at each step the positiveness of the resulting function. This method of deconvolution has been adapted by L. Celnikier (1985, private communication) from Jansson (1970), Jansson, Hunt, and Plyler (1970), and Schafer, Mersereau, and Richards (1981). The result of these computations is shown in Figure 6. A peak, corresponding to a period of 32 hours, clearly comes out from the noise. The error of ± 8 hours on the period has been derived from the theoretical error in the frequency corresponding to the finiteness of the observation interval. This 32 hour peak also appears as the most intense one in the Fourier power spectrum of our data before deconvolution, and does not appear in the Fourier power spectrum of the observation window. The other peaks in the deconvolved power spectrum correspond to periods of 63, 13, and 10 hours. Although the 13 and 10 hour peaks are not very intense, they might correspond to a real behavior of the Ca II K line. However, they are very close to the 12 hour period obviously present in the observation window, and therefore highly suspect. As to the 63 hour peak, taking into account the fact that the total span of the monitoring was only about twice this value, and given the important noise in our data, we believe it not to be of stellar origin.

In order to test the significance of this result, we have verified that mixing the observation dates and times in a random way within the observation window led to nothing but noise after the Fourier transform and the deconvolution. We have also verified that this procedure could properly recover the period

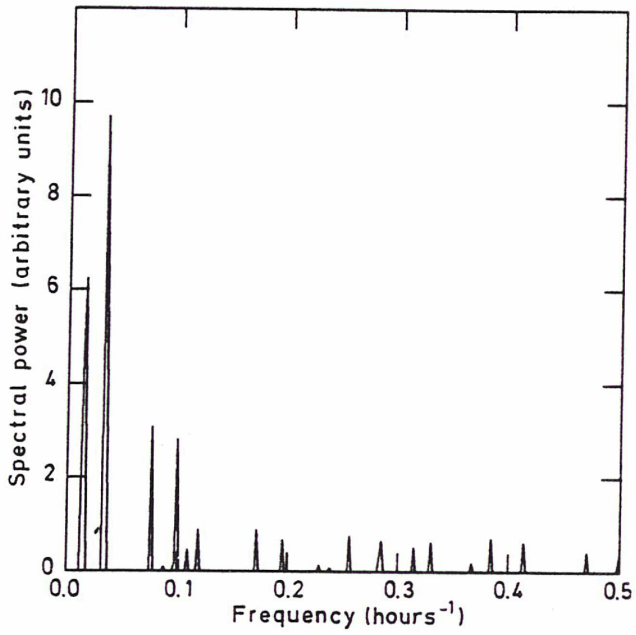

FIG. 6.—Power spectrum of the data $\lambda_b(t)$ (see text for a description of the analysis procedure). The highest peak corresponds to a period of 32 ± 8 hours.

of a sine wave function replacing the data within the observation window.

However, since the period found corresponds to a very low frequency, there is a risk that our Fourier power spectrum might be affected by aliasing problems. Therefore, we have also applied to our data $\lambda_b(t_i)$ the analysis used in the treatment of the Mg II lines in Paper I: we have fitted the data with a sine wave function of a given period, with the amplitude and the phase as parameters, and let the period vary. For each fit, we have computed the residual $R = \sum [\lambda_b(t_i) - F(t_i)]^2 / \sum \lambda_b^2(t_i)$, where the $F(t_i)$ are the values of the fitting function at the points t_i. A plot of these residuals R as a function of the period is shown in Figure 7. There is a clear minimum of R around the 32 hour period which has been found independently from the Fourier analysis. The position and the width of this minimum yield a period $P = 32 \pm 4$ hours, the error of ± 4 hours being derived from the width of the minimum. Note that the two methods (Fourier transform and fitting) are different, and that it is not surprising that the errors in the period found by the two methods are not the same. We note that in neither of the two analyses is there any indication of the 45 hour period found in Paper I for the Mg II data. Figure 8 displays the result of the fitting for $P = 32$ hours.

As a very final test, we have applied the Fourier analysis described above to the difference between the data $\lambda_b(t_i)$ and the values of the sine wave function giving the best fit. As expected, the result no longer shows the peak at 32 hours. The close agreement of the results obtained by two independent methods proves beyond any doubt that the 32 hour modulation period of the Ca II K line is a real, stellar phenomenon.

IV. DISCUSSION: A NONSPHERICALLY SYMMETRIC MODEL WITH DIFFERENTIAL ROTATION

a) *Periodic Variation of the Stellar Line*

One explanation that could be given for the periodic variation of the Ca II K stellar line would be that AB Aur is a

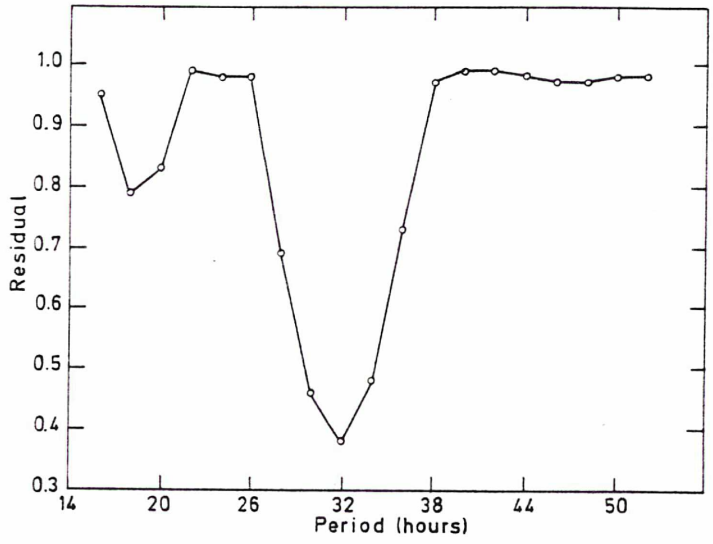

FIG. 7.—Residual of the sine wave fitting of the observed set of data $\lambda_b(t)$ for 1982 October plotted against period P

member of a binary system, and that the motion of the line corresponds to variations of the radial velocity of the star. However, Finkenzeller (1983) analyzed the system velocity of the star (computed from the Balmer lines) at different dates and did not find any change of more than ± 10 km s^{-1}. Since the amplitude of the variations of the Ca II stellar line is higher (± 20 km s^{-1}; see Fig. 8), and since 21 of the 39 points of our data lie outside ± 10 km s^{-1} around the mean value, we can discard this explanation.

The second possible cause of such a periodic variation is the star's rotation. Estimates of the projected rotational velocity of AB Aur can be found in the literature. Davis, Strom, and Strom (1983) give 75 km s^{-1} from the Mg II λ4481 line, which corresponds to a period $P = 48 \sin i$ hours, assuming a stellar radius of 3 $R_\odot$. However, using the Mg II λ4481 and the He I $\lambda\lambda$4388, 4471 lines, Finkenzeller (1985) finds a value of 140 ± 30 km s^{-1}, quite different from the previous one, and does not try to explain this discrepancy. In any case, the 32 hour period which we have found from our data is not too different from what is expected for the photospheric rotational period of AB Aur. The periodic variation of the Ca II stellar line could then be interpreted as a rotational modulation, as has been done in Paper I for the periodic behavior of the Mg II lines. The model proposed in Paper I is an alternation along the line of sight of slow and fast streams, similar to the streams observed in the solar wind. The same kind of model has also been proposed to explain several features observed in hot stars, hybrid stars, and cool supergiants (Mullan 1984). Such a model could be considered for the explanation of the 32 hour period observed in the Ca II K line, but we must carefully investigate all the implications of our results on this model. These implications are surveyed in the following sections of this paper. However, it is clear that at the present state, this model is only tentative and that additional quantitative analysis as well as further observations are needed to test several qualitative interpretations presented below.

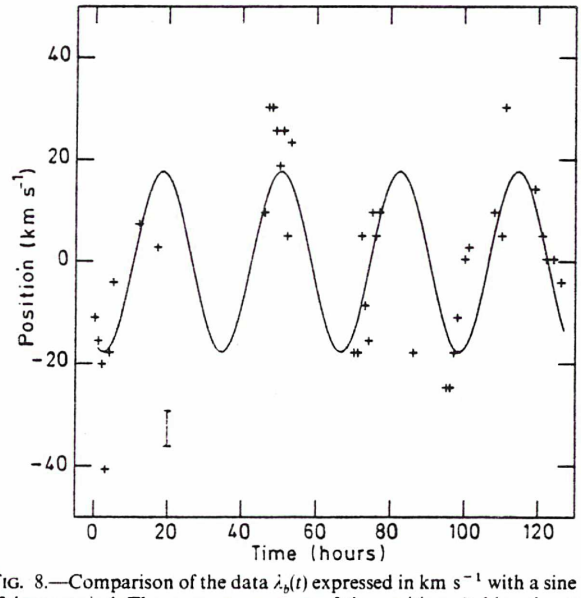

FIG. 8.—Comparison of the data $\lambda_b(t)$ expressed in km s^{-1} with a sine curve of 32 hour period. The average accuracy of the positions (taking the noise of the spectra into account) is given.

b) Stream Structure in the Stellar Wind

The variations of the Mg II resonance lines analyzed in Paper I have led to a qualitative model wherein these lines are modulated by the rotation of a stream structure originating from the inhomogeneous base of the wind. The observation of the Ca II K modulation, and most of all the difference between the 45 hour period in the Mg II data and the 32 hour period in the Ca II K data, allow us to take a second step in the building up of this qualitative model. In the following, we discuss this period difference and refine our view of the inhomogeneous wind of AB Aur. However, the model presented in Paper I and refined in the present paper remains qualitative.

The difference between the two periods is puzzling, because the stream structure must be rotating at the same angular velocity as the star itself, up to the distance where the streams merge. We must keep it very clear that the rotation of this stream structure is not a mass motion, but a kind of density wave rotating at the angular velocity of the stellar photosphere. As a consequence, any line formed in the region where

the stream structure is stable should be modulated with the period of rotation of the stellar photosphere.

A first possibility to explain the period difference between the Mg II and Ca II data is to consider that the stream structure is not stationary. The nonstationarity of this structure would result in a distortion of the streams, which could lead to different apparent periods for lines formed in different regions of the wind, or observed at different times. The similarity of the periods found from the Mg II data of 1982 October and 1984 November (Paper I) argues against this explanation. However, the period of the 1982 October data is less well determined, because the observation spanned only one cycle. Therefore this explanation cannot be so simply discarded.

A second possibility is that the blue edges of the Mg II resonance lines form in a region where the streams have already merged, whereas the Ca II K line forms inside the stream structure. Let us first discuss the regions of formation of the two lines.

Line computations in spherically symmetric models are a good tool for determining the regions of formation of the lines. Catala, Kunasz, and Praderie (1984) have shown that the Mg II resonance lines of AB Aur are formed over a very extended region, from the photosphere up to radial distance $r = 50R_*$, where R_* is the stellar radius. However, their study and the one of Catala (1984) show that the blue edges of these lines, whose velocity has been denoted V_s(Mg II) in Paper I, form at more than $5R_*$. The 45 hour period derived in Paper I for V_s(Mg II) then has its origin in a region of the envelope relatively far from the stellar surface.

No detailed computation of the Ca II K line has yet been performed for that kind of envelope, but Catala *et al.* (1986) have shown that it is very likely to form in a more compact region, at the base of the wind. We then conclude that the 32 hour period derived from the Ca II data corresponds to a phenomenon occurring very close to the stellar surface. We should note at this point that the correlation found between the behavior of the Ca II and K lines and the Hϵ line cores (§ III*a*) indicates that these three line cores are formed in the same region of the star's envelope.

Since the regions of formation of the Mg II and the Ca II lines are different, it is possible that the Ca II K line is formed in the part of the wind where the stream structure is stable, while the Mg II lines are formed in the region where the streams have merged. In this case, the Ca II K line is modulated by the rotation of the structure (which is not a mass motion), i.e., with the period of rotation of the star, and V_s(Mg II) is modulated with the period of rotation of the envelope (which is a mass motion) at the distance of formation of the blue edges of the Mg II lines. Let us examine this second possibility in more detail.

First of all, we must wonder whether the streams can merge before the region of formation of the blue edges of the Mg II resonance lines. Following Mullan (1984), we can write that the structures begin to merge when the fast streams overtake their adjacent slow streams. Mullan (1984) has estimated the distance to these corotating interaction regions (CIRs) by assuming that the longitudinal dependence of the velocity at the base of a fast stream is a linear ramp. If we replace this assumption by a more general one involving a power-law dependence on the longitude ϕ, we can write

$$V_f(\phi) = V_0 + \frac{(V_{\max} - V_0)}{W}\,\phi^n\,, \qquad (1)$$

where $V_f(\phi)$ is the velocity of the fast stream at longitude ϕ, V_0 the velocity of the adjacent slow stream, $V_{\max}$ the maximum velocity in the fast stream, W the longitudinal half-width of the fast stream, and n an exponent describing the longitudinal dependence of the velocity within the fast stream. We can calculate the distance r_i to the CIR, i.e., the region where the fast stream begins to overtake the slow one. We find

$$\begin{aligned} r_i &= R_* && \text{if } n < 1,\\ r_i &= R_*\left[1 + W\left(\frac{V_0}{V_{\rm rot}}\right)\left(\frac{V_0}{V_{\max} - V_0}\right)\right] && \text{if } n = 1,\\ r_i &= R_*\left\{1 + \frac{n}{n-1}\,W\left(\frac{V_0}{V_{\rm rot}}\right)\left[\frac{(n-1)V_0}{V_{\max} - V_0}\right]^{1/n}\right\} && \text{if } n > 1, \end{aligned} \qquad (2)$$

where $V_{\rm rot}$ and R_* are respectively the rotation velocity and the radius of the star. These results show that the interaction regions can occur very close to the stellar surface. Assuming, for example, that $W = 10°$, and taking $V_0 = 300$ km s^{-1}, $V_{\max} - V_0 = 150$ km s^{-1}, $V_{\rm rot} = 100$ km s^{-1} (velocities consistent with Mg II data), we find that the maximum value for r_i (obtained for $n = 2$) is $2.5R_*$. Note that if the velocity rises sharply near the boundaries of the fast streams ($n < 1$), the CIRs start at the star's surface.

In the solar wind, a pair of forward and reverse shocks form at the beginning of the CIR and erode them (Burlaga 1984). We can easily extrapolate this phenomenon to the case of the wind of AB Aur. In order to obtain a crude estimate of the radial size of the CIRs, and to find the distance at which the streams have completely merged, we can write that the shocks are likely to destroy the structures after the time necessary for the sound to cross the interaction region, i.e., $t = r_i W/c_s$, where c_s is the sound velocity. Here we have assumed that the longitudinal width of a stream is the same all over the envelope. During that time, the wind has traveled a distance $r = V_{\rm exp}\,t$, where $V_{\rm exp}$ is the "mean" expansion velocity of the wind. The structure can then be destroyed at small distances from the star's surface if the longitudinal width of the streams is small and if the interaction regions start close to the stellar surface. By assuming, for example, that $r_i = R_*$ (which occurs if the longitudinal dependence of the velocity is very sharp at the boundary between fast and slow streams), a full width of 10° for the fast streams, a sound velocity of 10 km s^{-1} (corresponding to a temperature of 10,000 K), and a "mean" velocity in the stream of 450 km s^{-1}, we find that the streams have merged within $4R_*$, which is definitely closer to the star than the region where the variations of V_s(Mg II) originate. Even after the streams have merged, we can imagine the existence of longitudinal inhomogeneities in radial velocity, produced by the inhomogeneous feeding of the medium by the streams themselves, which could last for several stellar radii before being swept off by the differential rotation of the envelope. We can then interpret the modulation of the Mg II data as due to the rotation of these inhomogeneities, whereas the Ca II K line is modulated by the rotation of the stream structure in the inner region. The period of modulation of the Mg II data (45 hours) would then be the period of rotation of the envelope itself at $5R_*$, and the period of modulation of the Ca II data (32 hours) would be the period of rotation of the stream structure, equal to the photospheric rotation period of the star. The relatively small difference between the rotation at the star's surface and at $5R_*$ shows that the radial dependence of the rotation angular velocity in

the envelope is indeed not very strong, so that the inhomogeneities modulating the Mg II lines can survive up to rather great distances. As a conclusion, if we accept this point of view, we must envisage that besides the rotation of the stream structure, the envelope itself is rotating, with a rotation angular velocity decreasing with increasing distance. The difference between the 32 hour period of the Ca II data and the 45 hour period of the Mg II data gives a rough measure of the radial dependence of the rotation in the envelope of AB Aur. Hence, the analysis of our Ca II K series has made more precise the qualitative model proposed in Paper I. However, the link between the different regions of the wind is still to be investigated from a theoretical point of view. In particular, it is not clear where pressure waves without streams, like those observed in the solar wind (Burlaga 1983, 1984), which have been considered in Paper I to explain the behavior of the Fe II lines, become the preponderant feature in the wind.

Given these values of the angular velocities (corresponding to a period of 32 hours at the photosphere and of 45 hours at 5 stellar radii), we notice that the rotational velocity $V_{\rm rot}$ increases with radial distance at least near the base of the envelope. From the 45 hour period, we find that the rotational velocity at $5R_*$ is about 300 km s^{-1}. This high value of the rotational velocity could explain the existence of a type III P Cygni profile for the Hα line of this star (Mihalas and Conti 1980; Catala *et al.* 1986).

If we keep following the analogy between the wind of AB Aur and the solar wind, the existence of a stream structure in its wind suggests the presence of a magnetic field at the surface of AB Aur. The latter must force the base of the envelope to corotate up to the Alfvén radius (the radius at which the flow velocity equals the Alfvén velocity). It is possible to derive from our data a rough upper limit for the magnetic field in the envelope of AB Aur. We first note that because the angular velocity of the envelope at $5R_*$ is lower than the angular velocity at the stellar surface, the flow velocity must become greater than the Alfvén velocity at a distance which is less than $5R_*$. Then, the Alfvén velocity is smaller than V_s(Mg II), which yields

$$B^2 \leq \dot{M} V_s(\text{Mg II})/r_A^2 , \quad (3)$$

and, since $r_A \geq R_*$,

$$B^2 \leq \dot{M} V_s(\text{Mg II})/R_*^2 . \quad (4)$$

Taking $10^{-7}\ M_\odot$ yr^{-1} as a comfortable upper limit for $\dot{M}$ (Catala, Kunasz, and Praderie 1984), V_s(Mg II) = 450 km s^{-1}, and $R_* = 3.0\ R_\odot$, we find $B \leq 80$ G.

If we assume further that beyond the Alfvén radius the envelope rotates with a Keplerian rotation velocity, and again that the variations of the Mg II lines originate at $5R_*$ we obtain an estimate of the Alfvén radius r_A from the 45 hour period. We find $r_A = 3.8R_*$. However, it is very likely that the kinematic viscosity and the magnetic field itself, even beyond the Alfvén radius, produce a speeding up of the rotation velocity with respect to a pure Keplerian law. Therefore, our estimate of the Alfvén radius is only an upper limit. However, we must keep in mind that the existence of a magnetic field at the surface of AB Aur is not definitely established, but only suggested by an analogy with the solar wind.

The upper limit for the Alfvén radius can lead to an upper limit for the angular-momentum loss in the envelope of AB Aur. The angular-momentum loss indeed can be estimated as

$$\dot{J} \sim \dot{M} r_A^2 \Omega , \quad (5)$$

where Ω is the angular velocity at the Alfvén radius. If we take the same upper limit for $\dot{M}$ as previously ($10^{-7}\ M_\odot$ yr^{-1}), and $\Omega = 5 \times 10^{-5}$ radians s^{-1} (corresponding to a 32 hour period), we find $\dot{J} \leq 10^{38}$ g cm^2 s^{-2}. An estimate of the angular momentum of the star is given by

$$J \sim M R_*^2 \Omega , \quad (6)$$

where M is the stellar mass and R_* the photospheric radius. Assuming a stellar mass of 2.5 $M_\odot$, we find $J \sim 10^{52}$ g cm^2 s^{-1}. In order to estimate the effect of the angular momentum loss on the evolution of the star, we may compare J and $\dot{J}\tau$, where τ is the estimated age of the star, which is 10^6 years (Cohen and Kuhi 1979). We find that the corresponding upper limit $\dot{J}\tau \leq 10^{51}$ g cm^2 s^{-1} is not very different from J, which shows that the angular-momentum loss might play a decisive role in the evolution of the star.

An important question is raised by the relatively small amplitude of the Ca II variations ($\sim \pm 20$ km s^{-1}), when compared with the one of the Mg II variations ($\sim \pm 45$ km s^{-1} in 1982 and ± 70 km s^{-1} in 1984). This is difficult to understand in the framework of Mullan's (1984) model. If the Mg II variations originate beyond the beginning of the CIR, in a region where the streams have merged, the amplitude of the Mg II variations is necessarily smaller than the real velocity difference between fast and slow streams. Since the Ca II K line is formed closer to the star than the Mg II resonance lines, the amplitude of the Ca II variations should be at least equal to that of the Mg II variations, if the velocity difference between fast and slow streams was constant along with radial distance. Our observations then suggest that such is not the case, and that there must exist an important gradient of velocity difference between fast and slow streams (difference increasing with r), as well as a gradient of velocity within a single stream.

Finally, since the Ca II K line is formed close to the star surface, inside the stream structure, the 32 hour period that we have found is equal to the star's photospheric rotation period. It is then possible to give a rough estimate of the inclination angle of the rotation axis of the star with respect to the line of sight toward the Earth. If we assume again $R_* = 3.0\ R_\odot$ and if we adopt the value $v \sin i = 75$ km s^{-1} (Davis, Strom, and Strom 1983), we find $i = 41° \pm 6°$. If the value of Finkenzeller (1985) is adopted ($v \sin i = 140 \pm 30$ km s^{-1}), we find $i = 73° \pm 17°$.

c) Blueshifted Absorption Components

We have seen in §§ III*a* and III*b* that one or several discrete blueshifted absorption components appear in some of our Ca II spectra. What is the origin of these components?

One interpretation involves sporadic outbursts in the wind. In order to explain the high velocity of the observed components, we can envisage the occurrence of "puffs" in some of the streams, that is to say, strong enhancements of the wind density at the base of the streams, with short durations, which then travel through the envelope. Because of this high density, components could be formed in these particular streams at greater distances than the rest of the Ca II K line, and therefore at a higher velocity. The density enhancements would cross the region of formation of the Ca II K line in 2 or 3 hours: for example, at a velocity of 350 km s^{-1} (corresponding to the bluest component seen in Fig. 5), the wind travels more than 2 R_* during that time, which we believe can correspond to the size of the region of formation of the Ca II K line in presence of an enhanced density (its size in "normal" condition is likely to

be smaller than this). Since the exposure times we have used are not very small compared with the time required for such density enhancements to cross the line formation region, and since there must exist a velocity gradient at the base of the wind, the components are likely to change their velocity during the exposure, which would explain the important width of some of them. An outburst has also been suggested in Paper I to explain a "flarelike" phenomenon seen in the Mg II lines.

However, two major difficulties arise with this interpretation. First, in order to understand the presence of several components on the same spectrum, we must imagine several outbursts very close in time within the same stream, or in different streams very close to one another. Such a situation could seem unlikely. Second, we should see from time to time components formed at the very base of the wind, therefore at very low velocities. They should then appear "inside" the stellar line, and this is not observed for the Ca II K line. One way to prevent their existence is to envisage a very strong velocity gradient at the base of the streams where the outbursts occur (which is almost equivalent to saying that the bursts themselves start at large ejection velocities), followed by a region of low velocity gradient. The outburst material would then spend very little time at low velocities, and we would see them only at high velocities. Another way to prevent the existence of components "inside" the Ca II K stellar line is to assume that the physical conditions at the base of the outbursts (temperature, density) are too different from those of the average medium for the Ca II K line to be formed.

Another interpretation of these absorption components involves the CIRs discussed in § IV*b*. Mullan (1984) has proposed that the narrow components observed in hot stars could be formed in the CIRs. Such an explanation could apply in our case. It is well known that the CIRs of the solar wind are bounded by a pair of forward and reverse shocks, that there is a broad velocity plateau between the shocks, and that the density can be considerably higher (5 times) in the CIRs than in the "average" wind (Burlaga 1983, 1984). If these CIRs are located beyond the region of formation of the stellar line, they could give rise to high-velocity absorption components, because of their high density. Since the radial distance at which a CIR begins depends on the velocity differential between fast and slow streams (see eq. [2]), and since we can imagine the existence of several fast streams of different velocities close to one another, there could exist several CIRs at different radial distances along the same line of sight. This could explain why we happened to observe several components on the same spectrum.

In this interpretation, the component should appear and disappear periodically, with the star rotation period, because the CIRs rotate at the same angular density as the star. Although our data are not sufficient to show such a periodic behavior, we note that there are exactly three rotational cycles between the spectrum of October 26 1019 UT, showing three absorption components, and the spectrum of October 30 1026 UT, exhibiting a single absorption component whose equivalent width and FWHM are the sum of the three absorption components in the October 26 spectrum, as if these three components had merged into one single component after 3 cycles. Since this absorption component still appears on the two following spectra, the passage of the corresponding CIR on the line of sight would have lasted for at least 3 hours, showing that its longitudinal extent should have been at least 25°. Here again, further observations are needed to analyze this interesting phenomenon.

d) The Sporadic Core Emission Component

The emission component appearing from time to time near the line core, without apparent regularity, is very puzzling. This emission component is without a doubt the sign of enhanced chromospheric activity, occurring very close to the photosphere. The sporadic and nonperiodic appearance, always at the same wavelength, of this emission component formed close to a rotating star, can be explained only by the existence of an intermittent phenomenon near the visible pole of the star, which is the only region of the stellar surface not affected by the rotation. In our 1982 October series, this component is redshifted, so it must be associated with sporadic accretion on to the stellar pole. This interesting feature then shows that, besides the longitudinal departures from spherical symmetry, which we can see from the rotational modulation of different lines, the atmosphere of AB Aur is also asymmetric in the latitudinal direction. A more detailed observational study of the time behavior of such a component would be of great interest. Moreover, an accretion of matter onto the stellar pole must lead to a shock at the stellar surface, and we can expect an X-ray emission from this shock. Assuming that the density at the stellar photosphere is 10^{-9} g cm^{-3} (typical for an A0 V star) and that most of the energy dissipated in the shock is used in the X-ray emission, and using the velocity of the core emission component with respect to the IS line as an estimate of the projected velocity of the infalling matter, we find that the corresponding X-ray luminosity is $L_X = \alpha \times 2.3 \times 10^{33}/\cos^2 i$ ergs s^{-1}, where α is the fraction of the stellar surface fed by the accretion. Our knowledge of the inclination angle i is poor, because of the poor determination of $v \sin i$. However, we have seen in § IV*b* that $35° \leq i \leq 90°$, so $L_X \geq \alpha \times 10^{33}$ ergs s^{-1}. The value of α is unknown, but reasonable values around 0.1–0.01 would definitely ensure detectability by the *Einstein* satellite. Feigelson and DeCampli (1981) give an upper limit of 3×10^{29} ergs s^{-1} for the soft X-ray luminosity of AB Aur. Sanders, Cassinelli, and Anderson (1982) also report nondetection of AB Aur's X-ray emission. These nondetections could be due to the sporadic aspect of the described phenomenon. In this context, an X-ray monitoring of this star, simultaneous with a monitoring of the Ca II K line, would be very useful.

e) The Red Wing Emission Component

As already stated, a broad and redward displaced emission component appears on most of our spectra and is possibly present in all of them. This red emission was not present in the 1980 October series (Praderie *et al.* 1982). This component could indicate high-velocity infalling material, but it could also simply be formed in the lateral parts of the Ca II K formation region. Catala, Kunasz, and Praderie (1984) indeed have shown that the emission part of a P Cygni profile must be redshifted if the line is optically thick. The amount of this redshift depends mainly on the broadening of the intrinsic line profile. The constancy of the position of this component (§§ III*a* and III*b*) would then indicate that this broadening does not vary at this time scale. Let us recall here that this broadening can be attributed to turbulent motions or to disorganized motions on small spatial scales (Catala, Kunasz, and Praderie 1984; Catala *et al.* 1986; Catala 1984). However, in the absence of a detailed computation of Ca II lines with spherically symmetric models, it is not possible to say whether such an explanation makes sense. In particular, it has to be shown that the extent of the region of formation of the Ca II K line is large enough to give rise to the observed emission component.

V. SUMMARY AND CONCLUSION

The basic results presented in this paper can be summarized as follows:

The Ca II K line of AB Aur presents a periodic behavior over 5 days in 1982 October, with a period of 32 hours. We propose to explain this behavior by a rotational modulation of the line. Besides this general behavior, absorption and emission components appear from time to time.

The periodicity of the stellar Ca II K line confirms the model proposed in Paper I from Mg II resonance line observations, consisting of an alternation of fast and slow streams in the wind of AB Aur. There is a clear difference between the 32 hour period derived from the Ca II data and the 45 hour period derived in Paper I from the Mg II resonance lines. This difference can be explained either by a nonstationary stream structure or by a model in which the Mg II variations originate in a region where the streams have merged, whereas the Ca II K line forms inside the stream structure. In the second model, the Mg II lines are modulated by the rotation of the envelope itself (which is a mass motion) and the Ca II K line is modulated by the rotation of the stream structure (which is not a mass motion). In the framework of this model, we are able to estimate the radial dependence of the rotation in the envelope. This would be the first evidence for a differential rotation observed in an expanding envelope.

We propose to interpret the blueshifted absorption components appearing on some of the spectra as due to sporadic outbursts, or to the presence of "corotating interaction regions," as has been proposed for the blueshifted components in hot stars (Mullan 1984). The core emission component can be explained by sporadic accretion onto the stellar pole.

The model presented in Paper I and refined in the present paper is still very qualitative; its exploration on a more quantitative basis is totally beyond the scope of the present paper.

Since in the solar wind the alternation of fast and slow streams is a consequence of the magnetic structure at the surface of the Sun, all the results presented in Paper I and in the present paper might also indicate the presence of magnetic fields in AB Aur. The study of spectral line variability would then appear as a very important step in the investigation of magnetic fields in PMS stars.

We can then speculate that there might be a relationship between the rotation and the existence of a magnetic field, such as is expected if the magnetic field is generated by a dynamo effect. Our knowledge of convection zones in PMS stars is too poor to allow us to speculate theoretically on the efficiency of the dynamo effect in such stars. The very existence of activity phenomena in PMS A stars might be an indirect indication of the presence of convection zones quite different from those of main-sequence A stars. An answer to this question would be found if we could observe the same kind of rotational modulation in other Herbig Ae stars. For example, a correlation between the level of activity or variability and the rotation velocity could be searched for. Such a correlation would tell us whether the magnetic field is of dynamo origin.

We are very grateful to F. Praderie, who assumed a leadership role in this program of observations. We acknowledge fruitful discussions with L. Celnikier, A. Mangeney, F. Praderie, T. Simon, and J. L. Steinberg. Special thanks are due to L. Celnikier and A. Mangeney for their help concerning the Fourier analysis of our data. This work is part of a joint effort to understand the variability of AB Aur, and we thank the people who participated in the 1982 October campaign: J. M. le Contel, P. Morel, F. Praderie, J. P. Sareyan, T. Simon, and J. C. Valtier. We are grateful to R. J. Lavery and to the staffs of CFHT and OHP for their assistance during the observations. Part of the work in Hawaii was supported by NSF grant AST82-16192 to A. M. B.

REFERENCES

Boesgaard, A. M. 1984, *A.J.*, **89**, 1635.
Boesgaard, A. M., and Tripicco, M. J. 1986, *Ap. J.*, **303**, 724.
Burlaga, L. F. 1983, *J. Geophys. Res.*, **88**, 6085.
———. 1984, *Space Sci. Rev.*, **39**, 255.
Catala, C. 1984, in *Proc. Fourth European IUE Conf.* (Rome) (ESA SP 218), p. 227.
Catala, C., Czarny, J., Felenbok, P., and Praderie, F. 1986, *Astr. Ap.*, **154**, 103.
Catala, C., and Kunasz, P. B. 1986, in preparation.
Catala, C., Kunasz, P. B., and Praderie, F. 1984, *Astr. Ap.*, **134**, 402.
Catala, C., and Talavera, A. 1984, *Astr. Ap.*, **140**, 421.
Cohen, M., and Kuhi, L. V. 1979, *Ap. J. Suppl.*, **41**, 743.
Davis, R., Strom, K. M., and Strom, S. E. 1983, *A.J.*, **88**, 1644.
Feigelson, E. D., and DeCampli, W. M. 1981, *Ap. J. (Letters)*, **243**, L89.
Felenbok, P., Praderie, F., and Talavera, A. 1983, *Astr. Ap.*, **128**, 74.
Finkenzeller, U. 1983, *Astr. Ap.*, **124**, 157.
———. 1985, *Astr. Ap.*, **151**, 340.
Finkenzeller, U., and Mundt, R. 1984, *Astr. Ap. Suppl.*, **55**, 109.
Herbig, G. H. 1960, *Ap. J. Suppl.*, **4**, 337.
Jansson, P. A. 1970, *J. Opt. Soc. Am.*, **60**, 184.
Jansson, P. A., Hunt, R. H., and Plyler, E. K. 1970, *J. Opt. Soc. Am.*, **60**, 596.
Mihalas, D., and Conti, P. S. 1980, *Ap. J.*, **235**, 515.
Mullan, D. J. 1984, *Ap. J.*, **283**, 303.
Mundt, R., and Giampapa, M. S. 1982, *Ap. J.*, **256**, 156.
Praderie, F., *et al.* 1984, in *Proc. France-Japan Seminar on Active Phenomena in the Outer Atmosphere of the Sun and Stars*, ed. J.-C. Pecker and Y. Uchida (Meudon: Observatoire de Paris), p. 132.
Praderie, F., Simon, T., Catala, C., and Boesgaard, A. M. 1986, *Ap. J.*, **303**, 311 (Paper I).
Praderie, F., Talavera, A., Felenbok, P., Czarny, J., and Boesgaard, A. M. 1982, *Ap. J.*, **254**, 658.
Sanders, W. T., Cassinelli, J. P., and Anderson, C. M. 1982, *Bull. AAS*, **14**, 629.
Schafer, R. W., Mersereau, R. M., and Richards, M. A. 1981, *Proc. IEEE*, **69**, 432.
Schneeberger, J. T., Worden, S. P., and Wilkerson, M. S. 1979, *Ap. J. Suppl.*, **41**, 369.
Strom, S. E., Strom, K. M., Yost, J., Carrasco, L., and Grasdalen, G. 1972, *Ap. J.*, **173**, 353.
Thé, P. S., Tjin-A-Djie, H. R. E., Praderie, F., Catala, C., and Felenbok, P. 1985, *Messenger*, No. 41, p. 8.

A. MERCHANT BOESGAARD: Institute for Astronomy, University of Hawaii, 2680 Woodlawn Drive, Honolulu, HI 96822

C. CATALA, P. FELENBOK, and J. CZARNY: Observatoire de Paris, Section de Meudon, 92195 Meudon Principal Cédex, France

A. TALAVERA: Astronomy Division ESTEC, Villafranca Tracking Station, P.O. Box 54065, Madrid, Spain

Astron. Astrophys. 182, 115–119 (1987)

ASTRONOMY AND ASTROPHYSICS

Research Note

Rotational modulation of the wind of the PMS star AB Aur: new observations in C IV and Mg II★

C. Catala★★, F. Praderie★★, and P. Felenbok★★★

Observatoire de Paris, Section de Meudon, F-92195 Meudon Principal Cedex, France

Received January 15, accepted January 30, 1987

Summary. In continuation of a time monitoring program devoted to short term spectral variability in Herbig pre-main-sequence stars, we present new results obtained for the star AB Aur. On a one day time scale, the variability of the blue edge velocity of the Mg II 2795 Å line is confirmed, and that of the C IV 1548 Å line established. Since our observations cover only 6 days and since the phase coverage is not tight enough, the new data can only support the periodic variability of V_s found previously. Periods between 40 and 50 hr are possible. Scenarios for the wind model of AB Aur are discussed.

Key words: stars: pre-main sequence; stars: chromospheres; stars: mass loss

1. Introduction

Short term spectral variations have been recently discovered for AB Aur (HD 31293), a representant of the intermediate mass pre-main sequence (PMS) Herbig Ae/Be stars (Praderie et al., 1986, Paper I; Catala et al., 1986, Paper II). These two papers show that the Mg II resonance lines and the Ca II K line are modulated by the stellar rotation, bringing a new piece to the puzzle of the activity in these PMS stars. This rotational modulation has indeed been interpreted by an alternation on the line of sight of fast and slow streams, similar to the structures observed in the solar wind (e.g. Burlaga, 1984). If we follow the analogy with the sun, this behavior constitutes an argument in favor of a magnetic origin for the activity in these stars.

Moreover, a clear difference has been found between the periods derived for the Mg II lines (45 ± 6 hr), and for the Ca II K line (32 ± 4 hr). This difference has been attributed to the radial dependence of the rotation in the envelope of the star. Observations of the C IV resonance lines can bring important constraints to this model. Being formed in the extended chromosphere, a region intermediate between the regions of formation of the Ca II K line (photosphere and lower chromosphere) and of the blue edge of the Mg II lines (post-chromospheric region), they will allow us to probe in more detail the behavior of the fast-and-slow-stream structure in the wind of AB Aur. Moreover, the quasi-simultaneous observation of the Mg II lines can provide information about eventual phase differences in the variations of the two sets of lines formed in different parts of the envelope.

Section 2 presents the observations of the C IV and the Mg II resonance lines obtained in 1986 January with the International Ultraviolet Explorer (IUE). Section 3 discusses the periodic behavior of this set of observations. A discussion of the possible consequences of these results on the already existing model is presented in Sect. 4. Finally, a summary and general conclusions are given in Sect. 5.

2. Observations and data reduction

Due to the long exposure time necessary for the high resolution observation of the C IV lines, only 5 spectra in each of the IUE wavelength ranges could be obtained during the 5 shifts allocated. The log of the observations is given in Table 1.

The IUE echelle spectra were reduced with the FASMII software, developed at Paris-Meudon Observatory (Borsenberger, 1985). This software performs a very accurate background removal, and is also able to reconstruct the flux in saturated parts of the spectra. The continuum level was determined at 1543 Å and 1583.5 Å for the C IV lines and at 2758 Å and 2844 Å for the

Table 1. Log of observations of AB Aur (January 1986)

	Image	T_{exp} (min)	UT (days) mid exp.	Station
SWP	27536	900	16.627	VILSPA + GSFC
	27545	353	18.494	VILSPA
(region	27548	390	19.491	VILSPA
of	27549	374	20.486	VILSPA
C IV)	27552	370	21.489	VILSPA
LWP	7514	30	16.958	GSFC
	7524	30	18.354	VILSPA
(region	7531	38	19.348	VILSPA
of	7538	40	20.335	VILSPA
Mg II)	7543	40	21.341	VILSPA

Send offprint requests to: C. Catala

★ Based on observations obtained with the International Ultraviolet Explorer at the Villafranca del Castillo ESA station

★ Unité de Recherche Associée au CNRS 264

★★ Unité de Recherche Associée au CNRS 812

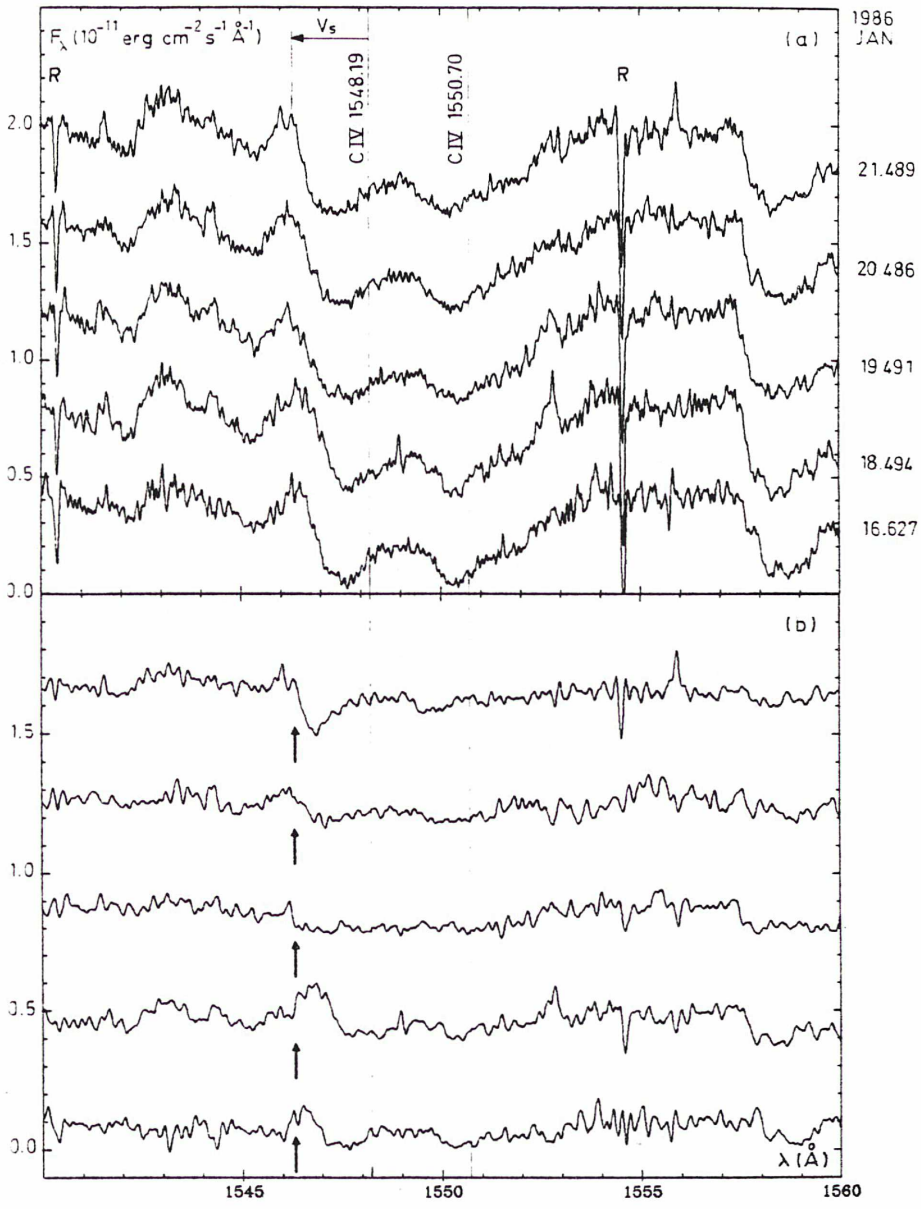

Fig. 1a. The region of the C IV resonance doublet in 1986 January. The flux scale (flux at earth) corresponds to the bottom spectrum. Upper spectra are displaced from each other by $0.4\,10^{-11}$ erg cm^{-2} s^{-1} Å^{-1}

Fig. 1b. Difference between the spectra and the mean spectrum in the C IV doublet region. The flux scale (the same as in Fig. 1a) corresponds to the bottom spectrum. Upper spectra are displaced from each other by $0.4\,10^{-11}$ erg cm^{-2} s^{-1} Å^{-1}. The arrows point to the region of the spectrum where the measurement of V_s has been made. Note the important variations from spectrum to spectrum in this region

Mg II lines. The blue edge velocity V_s was measured at the continuum level on the spectra in reduced units, as in previous papers. For both sets of lines, we have used the bluest component for measuring V_s. All spectra were placed on a common reference scale, based on the C I 1656.93 Å interstellar line for the C IV spectra, and on the Mg I 2852.13 Å interstellar line for the Mg II spectra. The error on V_s, mainly due to the location of the continuum and to that of the interstellar lines, is ± 25 km s^{-1}.

Figures 1a and 2a show the C IV and Mg II resonance doublets for the whole series of observations. Figures 1b and 2b present the differences between the spectra and the mean spectrum. The short term variability of both sets of lines is obvious from these figures. The average value of V_s(C IV) is 348 $\pm$ 37 (s.d.) km s^{-1}, and the one of V_s(Mg II) is 350 $\pm$ 30 (s.d.) km s^{-1}. We note that both values are very similar.

3. Data analysis

Because of the small number of observations obtained during this campaign, we cannot hope to unambiguously extract a period of variation from our data. Therefore, our goal is only to check the consistency of these data with the already established rotational modulation of AB Aur's envelope, and to see how this new set of observations fits in the already existing qualitative model. The analysis carried out is then very simple: we compare the data points with a set of sine-waves of different periods and different amplitudes, and decide in each case, on a visual basis, if the candidate sine-wave is consistent with the observations. Although probably non-systematic, this procedure is powerful enough to allow us to find several solutions, which are presented in Table 2 and Fig. 3. We note that 32 hr (period derived from the Ca II K

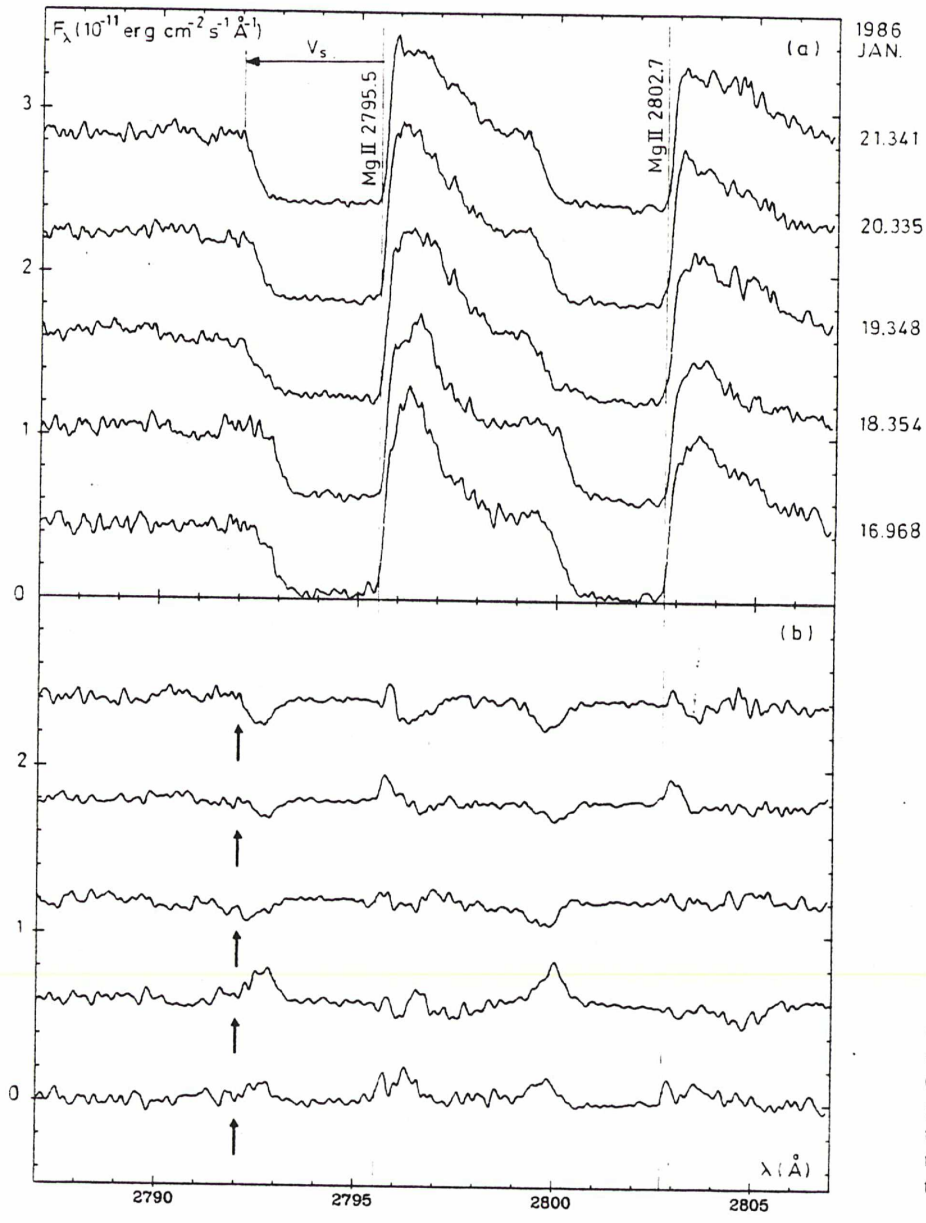

Fig. 2a. The region of the Mg II resonance doublet in 1986 January. The flux scale corresponds to the bottom spectrum. Upper spectra are displaced from each other by $0.6\,10^{-11}$ erg cm^{-2} s^{-1} Å^{-1}.

Fig. 2b. Difference between the spectra and the mean spectrum in the Mg II doublet region. The flux scale (the same as in **a**) corresponds to the bottom spectrum. Upper spectra are displaced from each other by $0.6\,10^{-11}$ erg cm^{-2} s^{-1} Å^{-1}. The arrows point to the region of the spectrum where the measurement of V_s has been made. Note the important variations from spectrum in this region

Table 2. Possible periodic variations of the Mg II and C IV lines

Lines	Period (h)	Total amplitude (km s^{-1})
C IV	38–40	150
	44–46	180
Mg II	38–40	150 (in phase with C IV variation)
	50	180

variations in Paper II) is not among the possible periods. As to the 45 hour period derived from the Mg II variations in Paper I, it is consistent with the C IV variations, but only marginally consistent with the Mg II variations in our new data.

4. Discussion

In this section, we examine the consequences of these new observations on the existing non-axisymmetric model. Let us first briefly describe this model.

The basic picture envisaged to explain the Mg II and Ca II spectral variations involves a laterally heterogeneous wind, consisting of an alternation of fast and slow streams. This structure gives rise to a pattern rotating at the same angular velocity as the star's photosphere. Due to the interactions of streams, forward and reverse shocks are produced at the interface between two adjacent streams. These shocks erode the structures, which are thus stable only up to a certain distance from the photosphere. The onset of the stream interaction is discussed by Mullan (1984) on the basis of a completely kinematical model. However, dynamic interaction between the streams is likely to occur as soon as they leave the star's surface, and probably plays an important role in controlling the onset of the shocks (Siscoe, 1976; Hund-

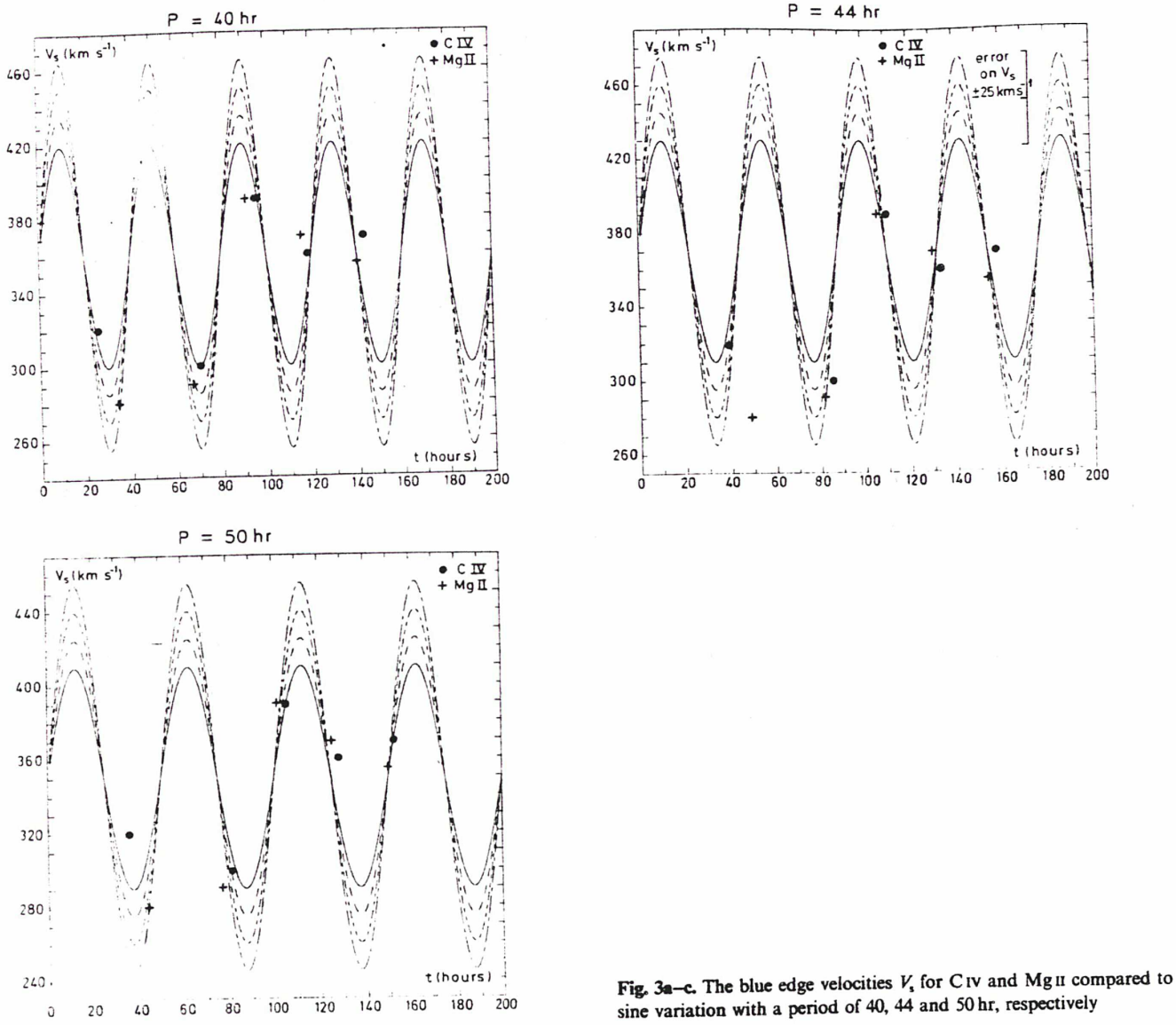

Fig. 3a–c. The blue edge velocities V_s for C IV and Mg II compared to a sine variation with a period of 40, 44 and 50 hr, respectively

hausen, 1985). As a consequence, the location of the shocks, and therefore the extent of the region where the corotating structures are stable, is a function of the longitudinal distribution of the radial velocity in the wind, the rotation velocity, the temperature and the magnetic field.

It has been proposed in Paper II that the Ca II K variations could originate in the region where the structures are stable, and therefore be modulated with the star's rotation period. On the other hand, the Mg II variations could originate in a region located beyond this stability region and therefore be modulated by inhomogeneities rotating with the envelope itself, with a different period.

From the results of the present analysis, we conclude that three scenarios are possible in the framework of this model:

i) The C IV and Mg II lines vary in phase with a period of 38–40 hr. In this case, since the period is longer than the 32 hr period assumed for the star's rotation, the blue edges of the C IV and Mg II lines are formed after the structures have been eroded by the shocks, and their modulation is due to the rotation of the envelope. In this scenario, the structures are eroded as close to the photosphere as $1.5R_*$, where the blue edge of the C IV lines is formed (Catala and Talavera, 1984; Catala, 1984; Catala, 1987). The fact that the C IV and Mg II lines vary in phase suggests that the major contribution to the formation of the blue edge of the Mg II lines comes from a region close to the outer boundary of the chromosphere. The difference between the 38–40 hour period envisaged here and the 45 hr period found in the 1984 Nov. data indicates a variation of the position of this region of formation, possibly linked to a variation of the average velocity of the wind. It is indeed possible that the maximum velocity in the flow V_{max} was reached only at some distance from the chromosphere in 1984 Nov. (a distance of $4R_*$ from the photosphere has been proposed in Paper I), and that the 45 hr period found for this date indicated the envelope rotation period at this distance. By contrast, V_{max} was reached much closer to the chromosphere in 1986 Jan., with the 38–40 hr period giving an estimate of the envelope

rotation period at the outer boundary of the chromosphere ($1.5R_*$ from the photosphere). If this scenario corresponds to reality, the present data will then provide a third point in the measurement of the envelope rotation as a function of radius.

ii) The C IV lines vary with a period of 38–40 hr or 44–46 hr, whereas the Mg II lines vary with a period of 50 hr. In this case, the C IV and Mg II variations originate in different regions of the envelope. The C IV blue edge is still formed at the outer boundary of the chromosphere, and the two possible periods we find indicate that the structures have been eroded before this region. On the other hand, the 50 hr period for the Mg II variations indicates that the main contribution to the blue edge of these lines originates further away, even at a greater distance than in 1984 Nov.

iii) The Mg II lines vary with a period of 38–40 hr or 50 hr, whereas the C IV lines vary in a more complex way (i.e. not sinusoidal), but with a periodicity of 32 hr. We envisage this case because of the complex behavior exhibited by the Ca II K line variations in 1982 Oct. (Paper II, Fig. 8). If the C IV lines have the same type of complex behavior, they could be modulated with a 32 hr period without us being able to recognize this period in our present data. Because the Mg II lines have shown in the past much more regular variations (Paper I), a periodicity of 32 hr can be more easily ruled out for these lines than for the C IV lines. In this scenario, the corotating structures are stable in the region of formation of the blue edge of the C IV lines, i.e. at the outer boundary of the chromosphere ($1.5R_*$ from the photosphere). They are eroded only further away, between this region and the region of formation of the blue edge of the Mg II lines. The C IV lines, formed in the region of stability of the corotating structures, are then modulated with the period of rotation of the star.

These three scenarios are quite different from each other. Our inability to decide for any of them is a consequence of the paucity of our observational data. Additional observations over a longer time span are clearly needed to rule out one or two of these scenarios.

5. Conclusion

The intermittent observations of the Mg II and the C IV resonance lines in AB Aur during 117 hours in 1986 January have confirmed the variability of the Mg II lines and shown the short term variability of the C IV lines. Unlike previous observations of the Mg II and Ca II variations, the data presented here are too few to allow us to ascertain unambiguously the periodicity of the variations.

However, these data are useful for placing constraints on the model which has been proposed to explain the previously observed rotational modulation of the Mg II and Ca II lines. In the framework of this model, three possible scenarios have been proposed, each of them leading to a different extent for the stability of the corotating region.

The point which would now need further strenghtening and clarification is the relation between the pattern in fast and slow streams, and the likely correlated occurrence of magnetic regions with open or closed field lines on the stellar surface. At present, no magnetic field is detected on AB Aur, nor in any of the similar pre-main sequence stars, and it is not clear if a magnetic field would be of primordial or of dynamo origin.

Acknowledgements. We are grateful to the staffs of the GSFC and VILSPA IUE stations for their efficient assistance. We thank Dr. M. Grewing who, as a referee, suggested improvements of the paper which increased its clarity.

References

Borsenberger, J: 1985, *ESA Newsletter* **24**, 24
Burlaga, L.F: 1984, *Space Sci. Rev.* **39**, 255
Catala, C., Talavera, A.: 1984, *Astron. Astrophys.* **140**, 421
Catala, C.: 1984, *Proc. 4th European IUE Conf.*, Rome, ESA SP218, p. 227
Catala, C., Felenbok, P., Czarny, J., Talavera, A., Boesgaard, A.M.: 1986, *Astrophys. J.* **308**, 791 (Paper II)
Catala, C.: 1987, (in preparation) *Astron. Astrophys.* (submitted)
Hundhausen, A.J: 1985, in *Collisionless Shocks in the Heliosphere: A Tutorial Review*, Washington, Am. Geophys. Union, p. 37
Mullan, D.J: 1984, *Astrophys. J.* **283**, 303
Praderie F., Simon, T., Catala, C., Boesgaard, A.M.: 1986, *Astrophys. J.* **303**, 311 (Paper I)
Siscoe, G.L: 1976, *J. Geophys. Res.* **81**, 6235

CHAPITRE IV

VERS UNE DESCRIPTION QUANTITATIVE A TROIS DIMENSIONS DES VENTS NON AXISYMETRIQUES

1 - Généralités:

Après l'analyse semi-empirique des ABHs présentée au chapitre II et la découverte de leurs phénomènes d'activité (chapitre III), deux directions de recherche s'offrent à nous sur le plan théorique:

i) l'étude des mécanismes de production du vent et de chauffage de la chromosphère adéquats pour les ABHs: cette étude peut se faire dans un premier temps par la construction de modèles à symétrie sphérique, donc à une dimension.

ii) la modélisation des structures en jets dans les vents de ces étoiles et l'étude de l'interaction entre les jets: ceci nécessite par contre des calculs à deux ou trois dimensions.

Les deux problèmes ne sont pas indépendants, mais on peut cependant tenter de les résoudre indépendamment dans un premier temps. Pour cela, il suffit d'ignorer l'existence des structures non radiales dans le problème i), et de paramétrer les termes d'apport de quantité de mouvement et d'énergie dans le problème ii).

La suite de ce chapitre est consacrée à une introduction succinte au deuxième problème. Il s'agit en fait d'un problème qui dépasse largement le cadre de l'étude des ABHs, puisque ces structures en jets que nous nous proposons d'étudier sont présentes dans de nombreux types d'étoiles (Mullan, 1984), et en particulier dans le vent solaire. Ce travail en est encore au stade purement prospectif, et aucun résultat précis n'est présenté dans ce chapitre.

2 - Nécessité d'un modèle dynamique:

Mullan (1984) traite le problème de l'interaction entre jets lents et jets rapides de façon entièrement cinématique. C'est ainsi par exemple qu'il considère qu'il y a formation d'un choc lorsque les particules d'un jet rapide rattrapent celles d'un jet lent. Avec cette hypothèse, il est aisé de décrire la phénoménologie des chocs directs et inverses en fonction des seuls paramètres cinématiques (principalement v_{exp}, vitesse d'expansion du flot, et v_{rot}, vitesse de rotation de l'étoile) des vents qu'il considère. Dans l'Annexe I, nous avons également utilisé cette hypothèse pour discuter la région de formation des chocs directs et

inverses dans le vent d'AB Aur.

Cependant, cette approche néglige toute interaction dynamique entre les jets, laquelle peut avoir une importance considérable. Il y a en effet interaction entre les jets avant que les particules du jet rapide ne rattrapent celles du jet lent, due simplement à la compression en avant du jet rapide. D'autre part, les chocs ne se forment pas nécessairement à l'endroit où le jet rapide rattrape le jet lent. Par exemple, si deux jets sont directement adjacents à la base du vent, le modèle cinématique de Mullan (1984) prévoit la formation des chocs dès la surface de l'étoile. Or, on voit intuitivement que les chocs vont se former lorsque la projection de la vitesse relative des deux jets sur la normale à leur interface sera supérieure à la vitesse locale de propagation des ondes (vitesse du son ou vitesse d'Alfvèn, suivant l'importance du champ magnétique). Ceci ne se produit pas nécessairement à la surface de l'étoile.

On comprend donc qu'un modèle dynamique est indispensable pour décrire proprement l'interaction entre les jets lents et les jets rapides dans le vent des ABHs. Weber et Davis (1967), puis Sakuraï (1985) ont développé des modèles dynamiques à plusieurs dimensions pour décrire le vent solaire en tenant compte du champ magnétique et de la rotation du soleil. Cependant, ces modèles ne prennent pas en compte la structure en jets du vent solaire et ne peuvent nous servir ici que de point de départ pour une étude plus complète.

3 - Modèle stationnaire à deux ou trois dimensions:

Un modèle analytique extrêmement simplifié de l'interaction dynamique entre les jets dans le vent solaire a été construit par Siscoe (1976). Ce modèle est probablement adaptable à d'autres cas que le vent solaire sans grande difficulté. Néanmoins, d'autres modèles, beaucoup plus sophistiqués, ont été bâtis depuis lors, et il est sans doute plus rentable de chercher à adapter au cas des ABHs ces modèles plus complets.

Pizzo (1982) a développé des modèles numériques de jets stationnaires à 3 dimensions pour le vent solaire. Ces modèles sont également adaptables au cas des ABHs. Une collaboration a été engagée à cette fin entre V. Pizzo, K. MacGregor (tous deux de HAO, Boulder, Colorado) et l'auteur de ce mémoire. L'inconvénient de la méthode de Pizzo (1982) est qu'on doit impérativement se placer dans la région supersonique ou superalfvénique (si le champ magnétique est important) du vent et spécifier tous les champs du problème (vecteur vitesse, vecteur champ magnétique, température, densité) à la limite inférieure du domaine d'intégration. Or, pour une étoile comme AB Aur, on peut prévoir que l'interaction entre les jets va être importante dès la surface de l'étoile, car le rapport

v_{rot}/v_{exp} est assez élevé. On risque donc de laisser de côté des phénomènes intéressants se produisant près de la surface de l'étoile. Il semble donc nécessaire de développer un modèle plus sophistiqué que celui de Pizzo (1982).

4 - Modèle non stationnaire à deux ou trois dimensions:

Construire un tel modèle consiste à résoudre les équations II-4 à II-6, complétées éventuellement par des termes dus au champ magnétique, force de Lorentz dans l'équation II-5 et chauffage Joule dans l'équation II-6, ainsi que par l'équation d'évolution du champ magnétique. Le système doit aussi être complété par la donnée d'une série de conditions aux limites (une pour chaque caractéristique entrant à chaque limite) et d'un état initial. Le milieu étant compressible, des chocs vont pouvoir se développer dans la solution. Comme nous l'avons signalé, les chocs jouent d'ailleurs un rôle prépondérant dans la physique des phénomènes que nous voudrions étudier. Il s'agit donc là d'un problème considérable, jamais résolu, et ce travail, dont nous commençons à peine à jeter les bases, doit être considéré comme une entreprise à très long terme.

A priori, deux méthodes numériques sont envisageables pour aborder ce problème. La première est la méthode dite aux différences finies, de loin la mieux connue et la plus employée dans les problèmes aux dérivées partielles (voir par exemple Ritchmyer et Morton, 1967). La deuxième est la méthode pseudo-spectrale, moins connue, mais prenant de plus en plus d'importance de nos jours (voir Gottlieb et Orszag, 1977). Dans le but de déterminer quelle méthode est la mieux adaptée à notre cas, nous avons entrepris de les comparer sur des problèmes simples à une dimension. Nous donnons ci-dessous les principaux avantages et inconvénients des méthodes pseudo-spectrales utilisant des polynômes de Tchébichev.

Les méthodes pseudo-spectrales présentent trois avantages principaux par rapport aux méthodes aux différences finies. Tout d'abord, elles ont une précision d'ordre infini, c'est-à-dire par exemple que la projection d'une fonction sur une base de N polynômes de Tchébichev tend vers la fonction plus vite que toute puissance de N. Cette propriété permet d'atteindre une certaine précision avec une grille beaucoup moins fine qu'avec une méthode aux différences finies. Ceci n'est vrai en toute rigueur que pour une fonction infiniment dérivable. La précision est d'ordre fini pour une fonction qui ne l'est pas.

Le deuxième avantage des méthodes pseudo-spectrales est qu'elles n'obligent pas à donner des conditions aux limites "supplémentaires" comme les méthodes aux différences finies d'ordre élevé. Avec une méthode pseudo-spectrale, il suffit d'imposer le nombre de conditions aux limites requis par la nature du problème (une par caractéristique entrante

pour un problème hyperbolique comme le nôtre). Les méthodes aux différences finies, par contre, impliquent la donnée d'un nombre fixe de conditions aux limites, imposé par le schéma numérique, et nous obligent à écrire des relations de compatibilité qui ne sont pas toujours triviales (voir Nakagawa et Steinolfson, 1976; Nakagawa et al., 1987).

Enfin, l'expérience nous a montré que les méthodes pseudo-spectrales sont en général très sensibles à la façon dont sont posées les conditions aux limites, ce qui peut être considéré comme un avantage. C'est-à-dire qu'un problème mal posé (surspécifié par exemple) rendra spectaculairement instable une méthode pseudo-spectrale, alors qu'une solution plausible, donc dangereuse, peut être obtenue avec une méthode aux différences finies.

L'inconvénient majeur des méthodes pseudo-spectrales utilisant des polynômes de Tchébichev est relié à la forme particulière de la grille de collocation utilisée (voir Gottlieb et Orszag, 1977, pour la définition d'une grille de collocation). L'intervalle entre deux points de la grille est en effet très petit aux frontières de l'intervalle de calcul, et diminue comme N^{-2} lorsqu'on augmente le nombre de polynômes de base. La condition de Courant correspondante est donc très sévère. Il existe des schémas temporels implicites qui permettent en principe de s'affranchir de la condition de Courant, mais utiliser un pas de temps supérieur à celui de la condition de Courant a pour conséquence une distorsion des ondes sonores ou MHD. Or nous savons que ces ondes joue un rôle important dans notre problème, et nous ne pouvons donc pas nous permettre de violer la condition de Courant. La forme de la grille de collocation reste donc pour nous un inconvénient sérieux des méthodes pseudo-spectrales utilisant des polynômes de Tchébichev.

L'analyse détaillée de ces méthodes sur des problèmes simples à une dimension (tube à chocs, par exemple) est en cours. Nous avons déjà pu montrer qu'on peut aisément traiter des problèmes avec chocs avec ces méthodes, à condition d'introduire une viscosité artificielle dans les équations. Ainsi, le problème d'un tube à chocs avec un rapport de pression de 10 a pu être traité avec seulement 33 polynômes de Tchébichev. D'autre part, nous avons étudié en détail la stabilité de divers schémas temporels vis-à-vis de la forme exacte des conditions aux limites. Un long chemin reste cependant à parcourir avant même de choisir quelle méthode employer dans notre problème complexe de vent stellaire à trois dimensions.

CHAPITRE V

CONCLUSION

Cette thèse représente environ six années de travail sur les ABHs et les phénomènes qui leur sont reliés. En 1981, on connaissait l'existence des ABHs, ainsi que leur nature pré-séquence principale, mais on ignorait presque tout de la structure de leurs atmosphères, si ce n'est qu'elles devaient être étendues. Notre travail a permis de combler cette importante lacune.

Grâce à la modélisation semi-empirique utilisant de nombreuses observations, nous avons pu placer des contraintes précises sur la structure des atmosphères de ces étoiles. C'est ainsi que, par exemple, nous avons mis en évidence l'existence de leurs chromosphères, dont nous avons déterminé les paramètres.

Nous avons également montré l'existence de phénomènes d'activité dans les ABHs. L'origine exacte de cette activité est encore inconnue, mais on peut prévoir qu'elle va poser des problèmes fondamentaux dans le domaine de l'évolution pré-séquence principale.

Nous estimons qu'il est temps de se lancer dans une nouvelle phase de l'étude des ABHs. Il s'agit d'une part de comprendre les mécanismes de production de leurs vents et de chauffage de leurs chromosphères, et d'autre part de modéliser quantitativement les structures par lesquelles se manifeste leur activité.

Les ABHs occupent une position très importante dans le diagramme HR, et leur étude est absolument indispensable si nous voulons comprendre les phénomènes de vents, de chromosphères et d'activité. Avec les résultats présentés dans ce mémoire, l'étude théorique de ces phénomènes dans les ABHs peut démarrer sur des bases saines.

REFERENCES

Abbott, D.C.: 1982, *Astrophys. J.* **259**,282

Abbott, D.C., Lucy, L.B.: 1985, *Astrophys. J.* **288**,679

Boesgaard, A.M., Simon, T.: 1984, *Astrophys. J.* **277**,241

Böhm-Vitense, E., Dettmann, T.: 1980, *Astrophys. J.* **236**,560

Bouvier, J., Bertout, C., Benz, W., Mayor, M.: 1986, *Astron. Astrophys.* **165**,110

Bouvier, J.: 1987, thèse de doctorat, Université Paris 7

Burlaga, L.F.: 1983, *J. Geophys. Res.* **88**,6085

Burlaga, L.F.: 1984, *Space Sci. Rev.* **39**,225

Calvet, N., Albarran, J.: 1984, *Rev. Mexicana Astron. Astrof.* **9**,35

Calvet, N., Basri, G., Kuhi, L.V.: 1984, *Astrophys. J.* **277**,725

Carpenter, K.G., Brown, A., Stencel, R.E.: 1985, *Astrophys. J.* **289**,676

Cassinelli, J.P.:1979, *Ann. Rev. Astron. Astrophys.* **17**,275

Cassinelli, J.P., Olson, G.L.: 1979, *Astrophys. J.* **229**,304

Cassinelli, J.P.: 1984, dans *"The Origin of Nonradiative Heating/Momentum in Hot Stars"*, eds. A.B. Underhill, A.G. Michalitsianos, NASA CP2358, p.2

Castor, J.I., Abbott, D.C., Klein, R.I.: 1975, *Astrophys. J.* **195**,157

Catala, C.: 1983a, *Astron. Astrophys.* **125**,313

Catala, C.: 1983b, thèse de troisième cycle, Université Paris 7

Cayrel, R.: 1963, *Comp. Rend. Acad. Sci. Paris* **257**,3309

Cayrel, R.: 1964, *SAO Spec. Rep.* **167**,169

Cohen, M.: 1973, *Monthly Not. Roy. Astron. Soc.* **161**,105

Cohen, M.: 1975, *Monthly Not. Roy. Astron. Soc.* **173**,279

Cohen, M., Kuhi, L.V.: 1979, *Astrophys. J. Suppl.* **41**,743

Cohen, M.: 1980, *Monthly Not. Roy. Astron. Soc.* **191**,499

Davis, R., Strom, K.M., Strom, S.E.: 1983, *Astron. J.* **88**,1644

Doazan, V.: 1982, dans *"B stars with and without emission lines"*, NASA SP 456

Dumont, S., Heidmann, N., Kuhi, L.V., Thomas, R.N.: 1973, *Astron. Astrophys.* **29**,199

Feigelson, E.D., De Campli, W.M.: 1981, *Astrophys. J.* **243**,L89

Felenbok, P., Praderie, F., Talavera, A.: 1983, *Astron. Astrophys.* **128**,74

Felenbok, P., Guérin, J.: 1984, dans *"Space Research Prospects in Stellar Activity and Variability"*, Observatoire de Paris. Meudon, eds. A. Mangeney et F. Praderie, p.359

Finkenzeller, U., Mundt, R.: 1984, *Astron. Astrophys. Suppl.* **55**,109

Finkenzeller, U., Jankovics, I.: 1984, *Astron. Astrophys. Suppl.* **57**,285

Finkenzeller, U.: 1985, *Astron. Astrophys.* **151**,340

Finkenzeller, U., Basri, G.S.: 1987, *Astron. Astrophys.*, sous presse

Freire, R., Czarny, J., Felenbok, P., Praderie, F.: 1978, *Astron. Astrophys.* **68**,89

Friend, D.B., MacGregor, K.B.: 1984, *Astrophys. J.* **282**,591

Gilliland, R.L.: 1986, *Astrophys. J.* **300**,339

Gondoin, P.: 1986, *Astron. Astrophys.* **160**,73

Gottlieb, D., Orszag, S.: 1977, *"Numerical Analysis of Spectral Methods. Theory and Applications"*, CBMS-NSF, Regional Conf. Series in Applied Mathematics

Grec, G., Fossat, E., Pomerantz, M.: 1980, *Nature* **288**,541

Guzik, J.A., Willson, L.A.: 1987, *Astrophys. J.*, sous presse

Hartmann, L., MacGregor, K.B.: 1980, *Astrophys. J.* **242**,260

Hartmann, L., Edwards, S., Avrett, E.: 1982, *Astrophys. J.* **261**,279

Herbig, G.H.: 1960, *Astrophys. J. Suppl.* **4**,337

Herbig, G.H.: 1970, *Mém. Roy. Soc. Sci. Liège, Série 5,* **9**,13

Holzer, T.E., MacGregor, K.B.: 1985, dans *"Mass Loss from Red Giants"*, eds. M. Morris et B. Zuckerman, D. Reidel Publishing Company

Hundhausen, A.J.: 1985, dans *"Collisionless Shocks in the Heliosphere: a tutorial Review"*, Washington, Am. Geophys. Union, p.37

Jiang, D.R., Perrier, C., Léna, P.: 1984, *Astron. Astrophys.* **135**,254

Kunasz, P.B., Auer, L.H.: 1987, preprint

Kwok, S.: 1975, *Astrophys. J.* **198**,583

Lamers, H.J.G.L.M., Rogerson, J.B.: 1978, *Astron. Astrophys.* **66**,417

Lamers, H.J.G.L.M., Snow, T.P.: 1978, *Astrophys. J.* **219**,504

Leroy, M., Lafon, J.P.J.: 1982, *Astron. Astrophys.* **106**,345

Linsky, J.L.: 1980, *Ann. Rev. Astron. Astrophys.* **18**,439

Mangeney, A., Praderie, F.: 1984, *Astron. Astrophys.* **130**,143

Mendoza, E.E.: 1966, *Astrophys. J.* **143**,1010

Migozzi, M.C.: 1984, thèse de troisième cycle, Université Paris 7

Mihalas, D., Kunasz, P.B., Hummer, D.G.: 1975, *Astrophys. J.* **202**,465

Mihalas, D., Kunasz, P.B., Hummer, D.G.: 1976a, *Astrophys. J.* **203**,647

Mihalas, D., Kunasz, P.B., Hummer, D.G.: 1976b, *Astrophys. J.* **206**,515

Mihalas, D., Kunasz, P.B., Hummer, D.G.: 1976c, *Astrophys. J.* **210**,419

Mihalas, D., Kunasz, P.B.: 1978, *Astrophys. J.* **219**,635

Mihalas, D., Mihalas, B.: 1984, *"Foundations of Radiation Hydrodynamics"*: Oxford: Oxford University Press

Mullan, D.J.: 1984, *Astrophys. J.* **283**,303

Mundt, R., Giampapa, M.S.: 1982, *Astrophys. J.* **256**,156

Nakagawa, Y., Steinolfson, R.S.: 1976, *Astrophys. J.* **207**,296

Nakagawa, Y., Hu, Y.Q., Wu, S.T.: 1987, *Astron. Astrophys.*, sous presse

Noyes, R.W., Hartmann, L.W., Baliunas, S.L., Duncan, D.K., Vaughan, A.H.: 1984, *Astrophys. J.* **279**,763

Noyes, R.W.: 1986, dans *"Physics of the Sun"*, vol. III, eds. P.A. Sturrock, T.E. Holzer, D.M., Mihalas, R.K. Ulrich, Geophysics and Astrophysics Monographs, D. Reidel Publishing Company

Parker, E.N.: 1958, *Astrophys. J.* **128**,644

Pauldrachs, A., Puls, J., Kudritzki, R.P.: 1986, *Astron. Astrophys.* **164**,86

Pizzo, V.J.: 1982, *J. Geophys. Res.* **87**,4374

Praderie, F.: 1973, dans*"Stellar Chromospheres"*, eds. S.D. Jordan, E.H. Avrett, NASA SP 317, p.79

Praderie, F.: 1977, *Mem. Soc. Astron. Italiana* **553**

Praderie, F.: 1981, dans *"Activity and Outer Atmospheres of the Sun and Stars"*, 11th Advanced Course, Swiss Society of Astronomy and Astrophysics, Saas-Fee, eds. A.O. Benz, Y. Chmielewski, M.C.E. Huber, H. Nussbaumer

Praderie, F., Talavera, A., Felenbok, P., Czarny, J., Boesgaard, A.M.: 1982, *Astrophys. J.* **254**,658

Praderie, F., Crivellari, L.: 1982, *Astron. Astrophys.* **107**,75

Praderie, F., Catala, C., Czarny, J., Felenbok, P.: 1984, dans *"Space Research Prospects in Stellar Activity and Variability"*, Observatoire de Paris, Meudon, eds. A. Mangeney et F. Praderie, p.265

Ritchmyer, R.D., Morton, K.W.: 1967, *"Difference Methods for Initial Value Problems"*,

Interscience New-York

Rodono, M., Byrne, P.B., Neff, J.E., Linsky, J.L., Simon, T., Butler, C.J., Catalano, S., Cutispoto, G., Doyle, J.G., Andrews, A.D., Gibson, D.M.: 1987, *Astron. Astrophys.* **176**,267

Sakuraï, T.: 1985, *Astron. Astrophys.* **152**,121

Simon, T., Herbig, G.H., Boesgaard, A.M.: 1985, *Astrophys. J.* **293**,551

Siscoe, G.L.: 1976, *J. Geophys. Res.* **81**,6231

Stencel, R.E., Linsky, J.L., Brown, A., Jordan, C., Carpenter, K.G., Wing, R.F., Czyzak, S.: 1981, *Monthly Not. Roy. Astron. Soc.* **196**,47P

Strom, S.E, Strom, K.M., Yost, J., Carrasco, L., Grasdalen, G.L.: 1972, *Astrophys. J.* **173**,353

Strömgren, B.: 1948, *Astrophys. J.* **108**,242

Taylor, P.O., Gregory, D., Dunn, G.H., Phaneuf, R.A., Crandall, D.H.: 1977, *Phys. Rev. Letters* **39**,1256

Thé, P.S., Cuypers, H., Tjin-A-Djié, H.R.E., Feinstein, A., Westerlund, B.E.: 1985a, *Astron. Astrophys.* **150**,345

Thé, P.S., Hageman, T., Westerlund, B.E., Tjin-A-Djié, H.R.E.: 1985b, *Astron. Astrophys.* **151**,391

Thé, P.S., Tjin-A-Djié, H.R.E., Catala, C., Praderie, F.: 1985c, *The Messenger* **41**,8

Uchida, Y., 1986: 26th COSPAR, Symp. on Stellar and Solar Activity, *Adv. in Space Sci.*, sous presse

Ulrich, R.K., Knapp, G.R.: 1979, *Astrophys. J. Letters* **230**,L99

Vaughan, A.H., Baliunas, S.L., Middlekoop, F., Hartmann, L., Mihalas, D., Noyes, R.W., Preston, G.W.: 1981, *Astrophys. J.* **250**,276

Vernazza, J., Avrett, E., Loeser, R.: 1981, *Astrophys. J. Suppl.* **45**,635

Weber, E., Davis, L.: 1967, *Astrophys. J.* **148**,217

Weber, S.V.: 1981, *Astrophys. J.* **243**,954

Wiese, W.L., Smith, M.W., Miles, B.M.: 1969, *Atomic Transition Probabilities* vol I, NSRDS-NBS22

Willson, L.A., Bowen, G.H., Struck-Marcell, C.: 1987, *Comments on Astrophysics*, sous presse

Wood, P.R.: 1979, *Astrophys. J.* **227**,220

Worden, S.P., Schneeberger, T.J., Kuhn, J.R., Africano, J.L.: 1981, *Astrophys. J.*

244,520
Zahn, J.P.: 1987, dans *"The Internal Solar Angular Velocity"*, 8th NSO Summer Symposium, Sunspot, New Mexico, eds.: B.R. Durney et S. Sofia, p.201

LISTE DES SYMBOLES UTILISES

(dans l'ordre d'apparition dans le texte)

$R_\odot$	:	rayon solaire = $7\ 10^{10}$ cm
R_*	:	rayon stellaire
T_r	:	température de rayonnement
$\dot{M}$	:	taux de perte de masse
S_ν	:	fonction source à la fréquence ν
S_L	:	fonction source dans la raie
S_c	:	fonction source dans le continu
J_ν	:	intensité moyenne du rayonnement
Φ_ν	:	profil intrinsèque de la raie
B_ν	:	fonction de Planck à la fréquence ν
ε	:	probabilité de destruction des photons (paramètre de thermalisation)
A_{21}	:	taux de désexcitation radiatif
C_{21}	:	taux de désexcitation collisionnel
v_D	:	vitesse Doppler aléatoire
v_{th}	:	vitesse d'agitation thermique
Ω	:	force de choc
n_e	:	densité électronique
T_e	:	température électronique
τ_L	:	profondeur optique dans la raie
τ_c	:	profondeur optique dans le continu
T_{max}	:	température maximum atteinte dans la chromosphère
Δ_2	:	étendue de la chromosphère
ρ	:	densité en masse
$\underset{\sim}{v}$	:	vecteur vitesse
P	:	pression thermique
M_*	:	masse de l'étoile
G	:	constante de la gravitation = $6.672\ 10^{-8}$ dyne $cm^2\ g^{-2}$
r	:	distance au centre de l'étoile
$\underset{\sim}{e}_r$	:	vecteur unitaire dans la direction radiale

$\underset{\sim}{D}$	:	vecteur apport de quantité de mouvement
γ	:	rapport des chaleurs spécifiques = C_p/C_v
Q	:	apport d'énergie (radiative et non radiative)
E^+	:	apport d'énergie non radiative
E^-	:	pertes radiatives
w	:	composante radiale de la vitesse = $\underset{\sim}{v}.\underset{\sim}{e_r}$
v_ϕ	:	composante azimuthale de la vitesse
v_{rot}	:	vitesse de rotation à la surface de l'étoile
F_ν	:	flux de rayonnement à la fréquence ν
c	:	vitesse de la lumière
$\Delta\nu_D$	:	largeur Doppler de la raie en unités de fréquence
σ_L	:	section efficace d'absorption dans la raie (en $cm^2\ g^{-1}$)
L	:	luminosité de l'étoile
v_∞	:	vitesse terminale du vent
χ_ν	:	coefficient d'absorption (cm^{-1}) à la fréquence ν
χ_L	:	coefficient d'absorption dans la raie
$\bar{J}$	=	$\int_{raie}\ \phi_\nu\ J_\nu\, d\nu$
ν_0	:	seuil du continu considéré
E^-_{tot}	:	quantité totale d'énergie perdue par rayonnement
F^-_{tot}	:	flux de densité d'énergie perdue par rayonnement
vsini	:	projection de la vitesse de rotation de l'étoile sur la ligne de visée
P_{rot}	:	période de rotation de l'étoile
N	:	nombre de polynômes dans une décomposition spectrale

Réalisé avec le concours du Service Imprimerie de la 5ème Circonscription
1, Place Aristide-Briand – 92190 Meudon – Tél. 45 34 75 50 – Télex 204135